Les données nucléaires de base pour la simulation : besoin, mesure, modélisation, évaluation et validation

Emmeric Dupont

Habilitation à Diriger des Recherches
Université Paris-Saclay

Les données nucléaires de base pour la simulation : besoin, mesure, modélisation, évaluation et validation

Emmeric Dupont
CEA Paris-Saclay, Irfu/DPhN

Présentée le 28/05/2020

Devant le jury composé de

Pierre Désesquelles	Président
Oscar Cabellos	Rapporteur
Maëlle Kerveno	Rapporteur
Olivier Sérot	Rapporteur
Elsa Merle-Lucotte	Examinatrice
Laurent Tassan-Got	Examinateur

Avant-propos et remerciements

Ce document de synthèse a été préparé en vue d'obtenir une habilitation à diriger des recherches. Il décrit une sélection de travaux scientifiques que j'ai réalisés, encadrés ou auxquels j'ai contribués de manière significative dans le domaine des données nucléaires de base pour la simulation.

Les données nucléaires constituent le fil conducteur de ces activités qui ont permises d'une part l'amélioration de la connaissance en physique nucléaire de basse énergie et d'autre part l'amélioration des données et modèles de réactions nucléaires directement utilisés pour la simulation de systèmes complexes, en particulier les réacteurs nucléaires.

La partie principale du document présente un résumé des travaux de recherche effectués depuis le doctorat. La présentation des travaux se fait essentiellement de manière chronologique en montrant les données nucléaires sous différents angles : besoin, mesure, modélisation, évaluation et validation.

- Le premier chapitre introduit brièvement le concept de données nucléaires.
- Le deuxième chapitre sur l'évaluation et la validation des données présente les activités réalisées dans le cadre du projet international JEFF au sein du Service de Physique des Réacteurs et du Cycle (DEN-SPRC) au CEA Cadarache.
- Le troisième chapitre sur la mesure et la modélisation des données présente les recherches effectuées au sein du Service de Physique Nucléaire (DSM-SPhN) au CEA Saclay, en particulier sur la modélisation des réactions photonucléaires.
- Le quatrième chapitre couvre les travaux réalisés lors d'un détachement à l'Agence de l'OCDE pour l'énergie nucléaire (AEN), notamment les études sur les méthodes d'ajustement pour l'amélioration des données, et la priorisation des besoins.
- Le cinquième chapitre intitulé "le retour aux sources (de neutron)" présente les activités en cours au Département de Physique Nucléaire (ex-SPhN) dans le cadre de la Collaboration n_TOF.
- Le dernier chapitre présente les conclusions et les perspectives.

Les annexes regroupent un bref curriculum vitae incluant les expériences d'encadrement et de coordination, et une liste de mes publications et rapports cités dans le manuscrit.

Tous les travaux présentés ont été réalisés dans un cadre collaboratif, que ce soit avec les collègues des différentes directions du CEA, avec les chercheurs de l'IN2P3 ou avec des collaborateurs étrangers, dans le cadre de projets nationaux (GEDE(PE)ON, NEEDS/NACRE…), Européens (CHANDA, EUFRAT, SANDA…) et internationaux (JEFF, WPEC, CIELO, NRDC/EXFOR…), ainsi que dans le cadre de la Collaboration n_TOF.

Il n'est malheureusement pas possible de citer tous ceux qui ont contribué d'une façon ou d'une autre à cette exploration du domaine des données nucléaires… mais je suis sûr que tous les collaborateurs, collègues, post-docs, doctorants et étudiants avec qui j'ai eu la chance de travailler se reconnaitront : MERCI à tous !!

Je tiens aussi à remercier les membres du jury, Pierre Désesquelles, Elsa Merle-Lucotte, Laurent Tassan-Got, et en particulier les rapporteurs, Maëlle Kerveno, Oscar Cabellos, et Olivier Sérot, pour leur expertise scientifique, leur temps et leur soutien.

Merci également aux correspondants HDR de l'université Paris-Saclay, Réza Ansari et Bruno Espagnon, de m'avoir guidé sur le chemin de la HDR.

Table des matières

1 Introduction – Les données nucléaires

Le terme "données nucléaires" (ou "constantes nucléaires") couvre l'ensemble des données de base essentielles à la simulation d'un système au sein duquel se produisent des réactions nucléaires spontanées ou induites. Ces données sont des constantes de la nature, indépendantes du système étudié (réacteur nucléaire, nucléosynthèse, dispositif médical, etc.). Pour la majorité de ces applications, en particulier quand la précision demandée aux simulations est élevée, il est nécessaire de couvrir un très large spectre de données qui ont été préalablement évaluées et validées.

Pour tous les noyaux et autant de particules incidentes que nécessaire il faut connaitre en fonction de l'énergie toutes les sections efficaces de réaction, ainsi que les multiplicités et les distributions en angle et énergie des produits de réaction. A cela s'ajoute les données de structure nucléaire et de décroissance radioactive. Cet ensemble de données évaluées est compilé dans des bibliothèques de plusieurs centaines à plusieurs milliers de noyaux. Elles sont disponibles dans un format international normalisé afin de faciliter leur diffusion et leur utilisation.

Ces données sont mesurées et mises à jour dans ces bibliothèques car il n'existe pas de "modèle standard" du noyau permettant de prédire de façon réaliste les réactions nucléaires de basse énergie à partir des interactions fondamentales. Il existe en revanche une panoplie de modèles et de paramètres développés à partir de mesures de sections efficaces, distributions secondaires, etc. Ces mesures permettent d'améliorer la qualité des données, à la fois de manière directe en mettant à jour les fichiers, et aussi de manière indirecte via l'amélioration des modèles qui permettent ensuite de compléter les évaluations en interpolant/extrapolant les données manquantes.

Par définition le domaine des données nucléaires est à l'intersection entre la physique nucléaire et ses applications. A ce titre, les recherches en physique nucléaire continuent d'irriguer les applications du nucléaire, en permettant de compléter et d'affiner les mesures pour améliorer les modèles et les fichiers évalués en termes de cohérence, précision et complétude. Cette approche pluridisciplinaire est très développée dans la communauté des données nucléaires et indispensable pour définir les besoins à partir des incertitudes cibles des applications. La collaboration avec les utilisateurs est également essentielle pour valider les données évaluées vis-à-vis de l'application cible et ainsi s'assurer qu'elles répondent bien à leur besoin.

Ce manuscrit présente les travaux de recherche menés dans le domaine des données nucléaires, qui en constituent le fil conducteur. Les résultats présentés dans les chapitres suivants couvrent les domaines de la mesure à l'évaluation des données, en passant par leur modélisation, sans oublier les étapes de validation intégrale et de définition des besoins, toutes deux réalisées en étroite collaboration avec les utilisateurs.

- Le travail d'évaluation des données permet la synthèse entre les informations expérimentales et théoriques disponibles. L'évaluation des données nucléaires du rhodium-103 est présentée dans la section 2.1.1.
- La validation intégrale permet de vérifier que les données évaluées (et leurs incertitudes) répondent au besoin de l'application. La section 2.2 présente deux exemples de contribution à la validation de la bibliothèque JEFF-3.
- Les lois de la physique contenues dans les modèles de réaction nucléaires constituent l'ossature des évaluations. La modélisation des réactions photonucléaires des actinides est abordée dans la section 3.2.1 et l'étude de la fonction force radiative réalisée dans le cadre de la thèse de J. Moreno-Soto est présentée dans la section 5.1.

- Ce sont essentiellement les besoins des applications qui guident le choix des données à améliorer. Une contribution à la quantification du besoin d'amélioration des données et de leur incertitude est présentée dans la section 4.1 sur les méthodes d'ajustement pour l'amélioration des données nucléaires.
- Les données expérimentales constituent la base des données évaluées. La nouvelle mesure du rapport alpha (rapport des sections efficaces de capture et de fission) de l'uranium-233 réalisée dans le cadre de la thèse de M. Bacak est présentée dans la section 5.2.

2 L'évaluation et la validation des données

L'évaluation et la validation des données sont deux étapes incontournables et indissociables pour passer du domaine de la physique nucléaire à celui des applications.

L'évaluation permet la synthèse entre les informations expérimentales et théoriques. Le fichier évalué quant à lui va bien au-delà puisqu'il doit être cohérent et complet afin de couvrir l'ensemble des données caractérisant l'interaction d'un neutron (ou toute autre particule) avec un noyau.

La validation intégrale permet de vérifier que les données évaluées répondent au besoin de l'application en termes de prédiction et de précision.

2.1 L'évaluation

Le processus d'évaluation consiste à combiner toutes les informations expérimentales et théoriques disponibles afin de produire un fichier de données caractérisant le plus souvent l'interaction d'un neutron avec un noyau, c'est à dire les paramètres de résonances, sections efficaces, distributions en angle et énergie des produits de la réaction, et multiplicités le cas échéant.

Parmi les principales réalisations dans ce domaine, on peut citer l'évaluation du rhodium-103 [Dupont 05a], présentée dans le paragraphe suivant, ainsi que les évaluations des isotopes de l'iode [Dupont 05b], et celle du samarium-148 réalisée dans le cadre du stage de R. Torre [Torre 05].

2.1.1 Modélisation et évaluation des données nucléaires du rhodium-103

Le rhodium naturel est composé de rhodium-103 uniquement. C'est un noyau stable dans son état fondamental et de période 56 min dans son état métastable situé à ~40 keV. C'est un des produits de fission les plus important (parmi les cinq premiers) pour les réacteurs nucléaires à spectre thermique ou rapide. C'est également un matériau couramment utilisé dans les mesures par activation en raison des propriétés de son état métastable.

Une nouvelle évaluation de ~0 à 30 MeV a été réalisée pour couvrir à la fois les besoins de simulation des réacteurs nucléaires et ceux des techniques de mesure par activation. L'évaluation couvre les trois domaines d'énergie traditionnellement considérés : c'est-à-dire les régions des résonances résolues (RRR), des résonances non-résolues (URR) et du continuum statistique (CONT). Un soin particulier est apporté à la cohérence des données entre ces trois domaines, particulièrement dans les zones d'énergie où les modèles se recouvrent. La transition entre la modélisation des domaines résolu et non-résolu est contrôlée par des tests statistiques basés sur les distributions des paramètres de résonance.

Les paramètres des premières résonances ont été remesurés précisément auprès de la source de neutrons Gelina (JRC-Geel, Belgique) et intégrés dans l'évaluation finale.

L'ensemble du domaine des résonances résolues des principales évaluations a été analysé pour extraire les paramètres de résonance moyens. Ces derniers ont été utilisés pour modéliser le domaine non-résolu, qui assure la transition avec la région du continuum.

La modélisation du continuum statistique sur la base d'un potentiel optique semi-microscopique (SMOM) a été réalisée en collaboration avec le Service de Physique Nucléaire (SPN) de la DAM-Ile de France. L'utilisation d'un modèle semi-microscopique prédictif couplé au code TALYS a permis une modélisation cohérente et raisonnable de toutes les voies de réaction ouvertes à haute énergie.

Nous avons obtenu un accord satisfaisant entre les paramètres utilisés pour modéliser ces différentes régions en énergie comme illustré dans le tableau suivant pour la voie neutron. Les valeurs de l'espacement moyen (D_0), des fonctions densités neutroniques (S_l) et du rayon de diffusion (R') obtenues dans ce travail sont cohérentes et globalement en accord avec les valeurs issues de la littérature et des fichiers évalués (valeurs qui sont relativement dispersées pour S_1 et S_2 par manque de contraintes expérimentales).

Comparaison des paramètres moyens du système n + ^{103}Rh pour la voie neutron ; toutes les incertitudes indiquées pour "ce travail" sont statistiques

	D_0 (eV)	**S_0** $\times 10^4$	**S_1** $\times 10^4$	**S_2** $\times 10^4$	**R'** (fm)
ce travail (RRR)	26 ± 1	0.55 ± 0.07	—	—	—
ce travail (URR)	26.00	0.58 ± 0.02	4.21 ± 0.04	0.63 ± 0.04	6.51
ce travail (CONT)	25.90	0.46	4.69	0.57	6.47
JEFF-3.0* (URR)	28.24	0.57	5.0	1.0	6.56
JENDL-3.3 (URR)	32.13	0.45	4.21	0.53	6.52
JEF-2.2 (URR)	25.77	0.485	6.33	0.595	6.56
RIPL-2	32 ± 4	0.47 ± 0.06	5.5 ± 0.9	—	—

* JEFF-3.0 = ENDF/B-VI.8

A titre d'illustration, la comparaison avec les données mesurées est présentée dans la figure suivante pour la section efficace ^{103}Rh(n,n')^{103m}Rh. Le même travail de comparaison et d'optimisation des paramètres a été réalisé pour toutes les voies de réaction disposant de données expérimentales.

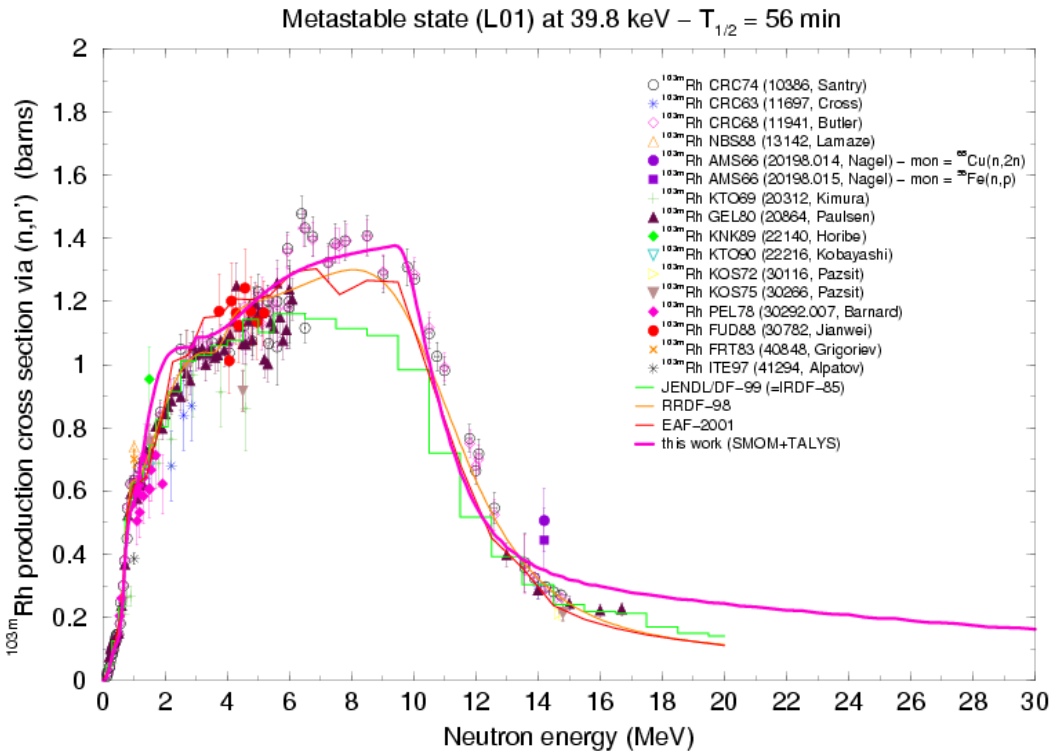

Modélisation de la section efficace de production du rhodium-103 métastable

Les résultats de la modélisation ont été mis au format ENDF et les valeurs intégrales pertinentes pour les applications de type activation et pour les réacteurs à spectre thermique

et rapide ont été comparées aux valeurs de référence utilisées jusqu'à présent dans les simulations.

Cette évaluation a été adoptée dans la bibliothèque JEFF-3.1 [Koning 07] et l'ensemble de sa réalisation est détaillée dans l'article [Dupont 05a] qui suit.

[Dupont 05a]

E. Dupont, et al., Neutron data evaluation and validation of rhodium-103, AIP Conference Proceedings 769, 95 (2005)

http://doi.org/10.1063/1.1944965

Neutron Data Evaluation and Validation of Rhodium-103

E. Dupont*, E. Bauge†, S. Hilaire†, A. Koning** and J.-Ch. Sublet*

*Commissariat à l'Energie Atomique, CEA/DEN–Cadarache, Saint-Paul-lez-Durance, France
†Commissariat à l'Energie Atomique, CEA/DAM–Ile de France, Bruyères-le-Châtel, France
**Nuclear Research & consultancy Group, NRG, Petten, The Netherlands

Abstract. Rhodium-103 is a prominent fission product in nuclear reactors as well as a usual detector in fast neutron activation or dosimetry techniques. The neutron-induced reactions and the energy regions of interest differ significantly depending on the applications. In this paper, a new evaluation spanning the 0-to-30 MeV energy range is described. The quality of the transitions between the various energy intervals was assessed with the help of statistical techniques to test the resonance parameter distributions and the SPRT method to check optical model calculations. The evaluated nuclear data file was verified and processed. The quality of the data was successfully tested against both differential and integral results for activation, thermal and fast reactor applications. This new file should be part of the upcoming JEFF-3.1 library.

INTRODUCTION

Rhodium-103 is a stable $I^\pi = 1/2^-$ odd-even nucleus with a metastable state at 40 keV. Rhodium is one of the major fission products for both thermal and fast fission reactors as well as a common detector for activation measurements. In this paper, we describe a methodology to produce a new evaluated nuclear data file ensuring physics consistency in a broad energy range (0-30 MeV). In order to make sure that this new evaluation answers integral needs, the file is tested for both fission reactors and activation applications.

NEUTRON DATA EVALUATION

One usually distinguishes three main energy ranges in the evaluated nuclear data files, the resolved resonance region (RRR), the unresolved resonance region (URR) and the continuum region (CONT). Although the underlying physics is the same, these regions are modelled using different codes and theories. The quality of the transitions between the above energy ranges can be assessed with the help of statistical techniques and the SPRT method [1] to check optical model calculations.

Resolved Resonance Region (RRR)

This energy region was not evaluated. Neutron transmission and capture measurements have been recently performed at GELINA (IRMM, Belgium) and preliminary resonance parameters were published [2]. Final values of the resonance parameters [3] should be inserted in the evaluated file at a later stage.

Interaction of the rhodium ground state with low energy neutrons forms compound nucleus resonances whose quantum numbers are given in Table 1.

At energy below a few keV, the resonance parameter distributions from various evaluations were simply analysed to check their consistency and extract accurate s-wave average parameters.

The SAMMY/SAMDIST code [4, 5] has been used to display resonance parameter distributions (Wigner, χ^2, Porter-Thomas laws) and cumulative histograms for every J^π spin group of JEFF-3.0 (ENDF/B-VI.8), JENDL-3.3 and JEF-2.2 evaluated files. As an example, Fig. 1 shows the cumulative number of s- and p-wave levels vs. energy for these evaluations. However, raw averaged parameters extracted that way could be biased because of wrong parity assignments and/or missing levels.

To avoid such a bias, the ESTIMA code [6] performs a Bayesian estimation of the parity of a level with a certain reduced neutron width, as well as a fit of the theoretical Porter-Thomas law on the experimental distribution. This method gives results independent of missing levels or wrong parity assignments. Indeed, the s-wave average spacings (D_0) displayed in Table 2 are more consistent between evaluations compared to the raw results shown

TABLE 1. Resonance J^π for the first three partial waves

ℓ	0		1		2	
$I \pm 1/2$	0	1	0	1	0	1
J^π	0^-	1^-	1^+	$0^+, 1^+, 2^+$	2^-	$1^-, 2^-, 3^-$

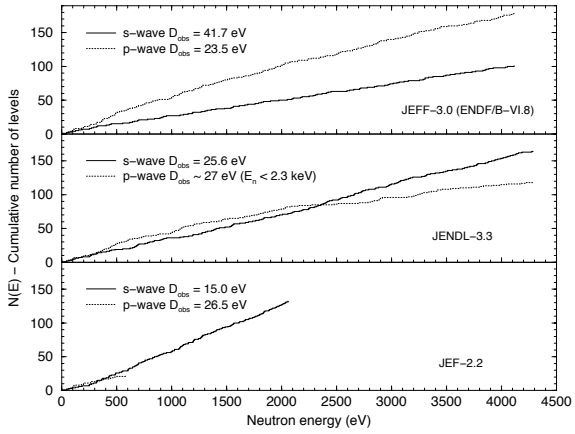

FIGURE 1. Cumulative number of resolved levels vs. energy, the raw average spacing is the inverse of the line slope.

TABLE 2. Estimation of the averaged resonance parameters

Evaluated Library	Wrong Parity	Missing Levels	D_0 (eV)	S_{n0} $\times 10^4$
ENDF/B-VI.8	1 %	33 %	27.5(7)	0.55(7)
JENDL-3.3	15 %	20 %	24.7(4)	0.56(7)
JEF-2.2	57 %	8 %	33.5(6)	0.49(8)

in Fig. 1.

A similar study for the photon channel gives discrepant results because (1) part of the evaluated radiative widths are not adjusted on experimental data but simply assumed equal to a constant default value; (2) the averaged value is strongly dependent on a few unlikely (and uncertain) radiative widths. When one considers only experimental data and its uncertainties, the weighted average value is more reliable [7],

$$\Gamma_{\gamma 0} = 171 \pm 3\ meV.$$

The present study highlights the good quality of ENDF/B-VI.8 [8] which is the most recent evaluation work at low energy and the basis of our resolved resonance region up to 4 keV.

Unresolved Resonance Region (URR)

Although s-wave average parameters deduced from the resolved resonance region are rather accurate, this is less so for $\ell \geq 1$ parameters. In the unresolved resonance range, distant level parameter (R_ℓ^∞), neutron strength function $(S_{n\ell})$ and radiative width $(\Gamma_{\gamma\ell})$ for the lowest partial waves can be adjusted onto experimental data with the SAMMY/FITACS code [4, 9]. In this code, the average spacing (D_ℓ) and the channel radius $(a_{c\ell})$ are not adjustable parameters. The scattering radius (R'_ℓ) is a function of $a_{c\ell}$ and R_ℓ^∞.

TABLE 3. Initial values of the URR average parameters

ℓ	0	1	2
D_ℓ (eV)	26.00	11.97	7.59
$a_{c\ell}$ (fm)	6.53	$a_{c1} = a_{c0}$	$a_{c2} = a_{c0}$
R'_ℓ (fm)	6.52	6.54	6.52
$S_{n\ell} \times 10^4$	0.50 ± 0.03	5.0 ± 0.5	0.50 ± 0.05
$\Gamma_{\gamma\ell}(meV)$	171 ± 3	171 ± 3	$\Gamma_{\gamma 2} = \Gamma_{\gamma 0}$
$S_{\gamma\ell} \times 10^4$	66	143	225

TABLE 4. Final values of the URR average parameters

ℓ	0	1	2
R'_ℓ (fm)	6.51	6.54	6.54
$S_{n\ell} \times 10^4$	0.58 ± 0.02	4.21 ± 0.04	0.63 ± 0.04
$\Gamma_{\gamma\ell}(meV)$	172 ± 2	160 ± 1	$\Gamma_{\gamma 2} = \Gamma_{\gamma 0}$
$S_{\gamma\ell} \times 10^4$	66	134	227

The data input was selected for the first three partial waves $(\ell \leq 2)$ as shown in Table 3. The s-wave parameters were deduced from the previous resonance parameter statistical study. Other parameter values were just prior guesses. The energy and spin-parity of the ^{103}Rh low-lying levels were obtained from reference [10].

The experimental total and capture cross-sections used in this work were selected from the international EXFOR database [11].

Several iterations were necessary to determine the best set of average parameters and normalisation constants describing the whole set of measured data. The final average parameters obtained from the fit are shown in Table 4. The s-wave parameters are consistent with the ones obtained from the resolved resonance region.

Figures 2 and 3 display the calculated total and capture cross-sections (labelled SAMMY/FITACS) together with available experimental data.

Continuum Region (CONT)

Consistent calculation of all open channels above the resonance region is possible with a modern tool associated to a comprehensive parameter library, e.g. TALYS [12]. In this work, the coupled-channels optical model code ECIS [13] was used with a semi-microscopic deformed potential SMOMP [14] to calculate total, reaction and direct inelastic cross-sections as well as neutron and proton transmission coefficients up to 30 MeV. The latter coefficients were finally used within TALYS-0.52 to split the reaction into every open channel using the parameter library information and nuclear reaction models.

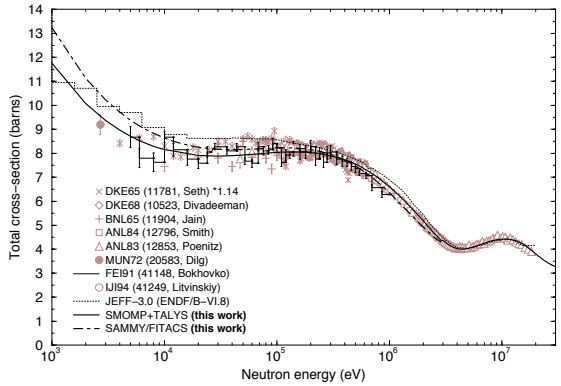

FIGURE 2. Total cross-section – theory vs. experiment

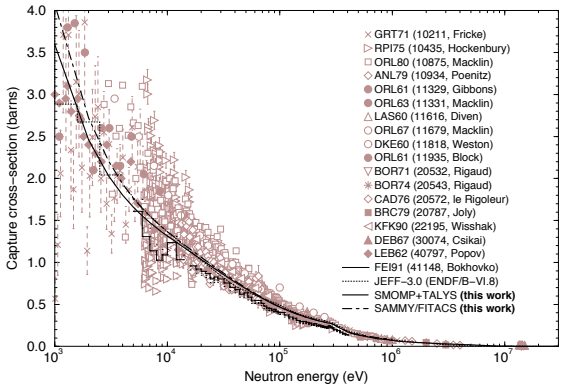

FIGURE 3. Capture cross-section – theory vs. experiment

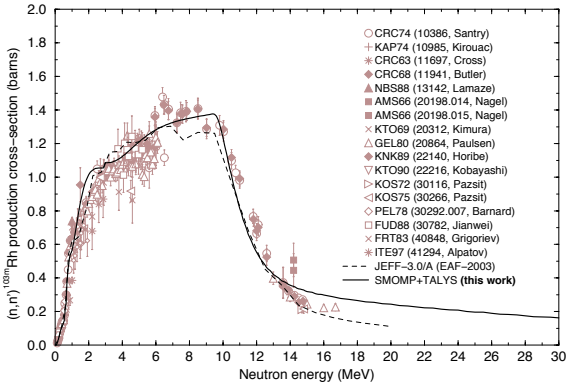

FIGURE 4. ^{103m}Rh production via inelastic scattering

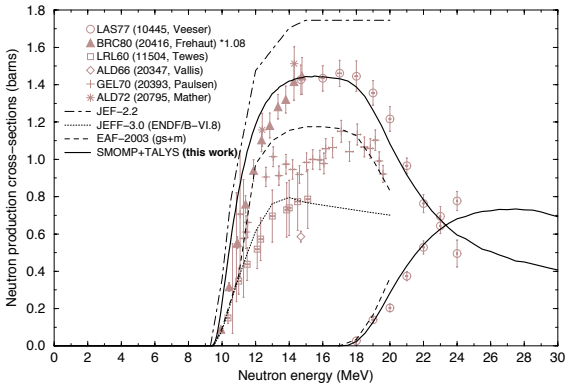

FIGURE 5. $(n,2n)$ and $(n,3n)$ cross-sections

A few model parameters (such as radiative width, level density parameter, spin cut-off, preequilibrium constant) were slightly modified to be consistent with the experimental data and, as much as possible, with the URR evaluation. Table 5 shows the average parameters used for the continuum region modelling.

As an illustration, Fig. 2–5 show some comparisons between part of our results (labelled SMOMP+TALYS) and experimental data [11]. Actually, all results were compared with available evaluations and experimental data, including inelastic scattering on discrete levels, elastic scattering angular distributions, light charged particle emissions and metastable state productions [15].

TABLE 5. Average parameters used in the continuum region

ℓ	0	1	2
D_ℓ (eV)	25.90	11.92	7.56
R'_ℓ (fm)	6.47	—	—
$S_{n\ell}\times 10^4$	0.46	4.69	0.57
$\Gamma_{\gamma\ell}(meV)$	166	$\Gamma_{\gamma 1}=\Gamma_{\gamma 0}$	$\Gamma_{\gamma 2}=\Gamma_{\gamma 0}$
$S_{\gamma\ell}\times 10^4$	64	139	220

Assembly and Verification of the File

The results of the modelling in the unresolved resonance and continuum regions were merged with the JEFF-3.0 (ENDF/B-VI.8) resolved resonance region thanks to SAMMY [4] and TALYS [12] formatting capabilities. The unresolved resonance region format being rather limited, its upper limit was set to the first inelastic threshold at 40 keV. The new evaluated nuclear data file was verified with the ENDF utility codes [16].

NEUTRON DATA VALIDATION

The evaluated nuclear data file was processed with the NJOY [17] and PREPRO [18] code packages. The integral quality of the data was tested against relevant exper-

imental results for thermal and fast reactors as well as activation applications.

Thermal Reactor. Oscillation measurements in the MINERVE French experimental reactor had shown an overestimation of all previously evaluated radiative capture cross-sections [19]. About 95% of the resonance integral comes from the first resonance. An estimation of the impact of the preliminary IRMM resonance parameters [2] is encouraging and should reduce the observed discrepancy between simulation and integral experiment.

Fast Reactor. In the fast energy range, comparisons of one-group cross-sections with reference values are a good test of the integral quality of any evaluation. Table 6 shows a comparison between different evaluated files and gives the standard deviation of these values. The PREPRO code package [18] was used with a micro-flux weighting spectrum adopted from reference [20]. The fast energy capture cross-section is rather well known, which is not the case of the inelastic scattering and $(n,2n)$ cross-sections (see also Fig. 5). In the case of rhodium, the radiative capture is the most important cross-section to verify. Actually, this work gives an average cross-section close to JEF-2.2's, which was adjusted on the STEK integral data [21]. Therefore, one expects satisfactory agreement with integral results when using the present data.

Activation. The EASY package [22] allows differential and integral testing of relevant cross-sections for activation applications. Present data are in good agreement with differential experiments. Further integral tests will check the ^{104}Rh ground and metastable states productions via radiative capture. Compared to JEFF-3.0/A (EAF-2003), the increase of the $^{103}\mathrm{Rh}(n,\gamma)^{104m}\mathrm{Rh}$ cross-section is expected to improve the agreement with integral results.

TABLE 6. Fast-spectrum one-group cross-sections (in barns)

Evaluation	Year	(n,γ)	(n,n')	$(n,2n)$
This work	2004	0.6710	0.4504	1.627×10^{-4}
JEFF-3.0*	1999	0.6702	0.4832	7.875×10^{-5}
CENDL-3	1997	0.6818	0.4244	1.239×10^{-4}
JENDL-3.3†	1994	0.6771	0.4043	1.239×10^{-4}
JEF-2.2	1990	0.6810	0.4006	2.113×10^{-4}
BROND-2.2	1989	0.6535	0.4129	7.875×10^{-5}
Average (b)		0.6724	0.4293	1.299×10^{-4}
RMS		1.6 %	7.4 %	39 %

* adopted from ENDF/B-VI.8
† same as JENDL-3.2

CONCLUSION

A new rhodium-103 evaluation was produced for fission reactors and activation applications. The three usual energy regions were carefully analysed and modelled to ensure physics consistency in the whole evaluated file up to 30 MeV. Special care was devoted to the RRR/URR and URR/CONT region boundaries. Relevant integral quantities for fission reactors and activation applications were calculated and successfully compared to reference values. This new file was proposed for insertion into the next release of the JEFF-3 General Purpose and Activation libraries and adopted in the JEFF-3.1 starter file.

REFERENCES

1. J.-P. Delaroche, *et al.*, "The optical model with particular consideration of the coupled-channels optical model", IAEA-190, p. 251 (1976).
2. E. Berthoumieux, *et al.*, in *ANS/ENS International Winter Meeting*, New Orleans, Louisiana, USA, p. 627 (2003).
3. A. Brusegan, *et al.*, this conference.
4. N. M. Larson, "Updated Users' Guide for SAMMY: Multilevel R-Matrix Fits to Neutron Data Using Bayes' Equations", ORNL/TM-9179/R6 (2003).
5. L. C. Leal, N. M. Larson, "SAMDIST: A Computer Code for Calculating Statistical Distributions for R-Matrix Resonance Parameters", ORNL/TM-13092 (1995).
6. E. Fort, J.-P. Doat, "ESTIMA: A Code to Calculate Average Parameters from Sets of Resolved Resonance Parameters", NEANDC-161'U' (1983).
7. P. Ribon, Ph.D. thesis, CEA-N-1149 (1969).
8. S. Y. Oh, *et al.*, "Neutron cross section evaluations of fission products below the fast energy region", BNL-NCS-67469 (2000).
9. F. H. Fröhner, *Nucl. Sci. Eng.*, **103**, 119–128 (1989).
10. R. B. Firestone, *Table of Isotopes*, vol. 1, John Wiley & Sons, 8^{th} Edition (1998).
11. *Nuclear Reaction Data Centres Network (NRDC, IAEA)*, OECD NEA Data Bank EXFOR retrieval system (2003).
12. A. Koning, *et al.*, this conference.
13. J. Raynal, "ECIS97", Unpublished (1997).
14. E. Bauge, *et al.*, *Phys. Rev. C*, **63**, 024607 (2001).
15. E. Dupont, E. Bauge, "Le point sur la modélisation du système n+^{103}Rh", Unpublished (2003).
16. C. L. Dunford, "ENDF Utility Codes Release 6.13", Brookhaven National Laboratory (2002).
17. R. E. MacFarlane, "NJOY-99.90", Los Alamos National Laboratory (1999).
18. D. E. Cullen, "PREPRO2000 – ENDF/B Pre-processing Codes", IAEA-NDS-39 rev.10 (2000).
19. N. Thiollay, *et al.*, in *Nuclear Criticality Safety, ICNC'99*, Versailles, France, vol. II, p. 612–621 (1999).
20. H. Gruppelaar, "Status of pseudo-fission-product cross-sections for fast reactors", NEA/WPEC-17 (1998).
21. *International Reactor Physics Evaluation Project*, IRPhE/STEK, http://www.nea.fr/abs/html/nea-1714.html.
22. R. Forrest, *et al.*, in *Nuclear Data for Science and Technology*, Tsukuba, Japan, p. 96–99 (2001).

2.2 La validation

La principale raison d'être des fichiers de données évaluées est leur utilisation par des codes de simulation pour prédire le comportement de systèmes complexes. Dans le domaine applicatif, en particulier pour les réacteurs nucléaires, ces simulations doivent être validées par comparaison avec des mesures intégrales.

Les expériences intégrales réalisées en réacteur ou maquette critique impliquent un grand nombre de noyaux et donc de données nucléaires. Dans ce cas il est possible de réaliser des recherches de tendances statistiques sur les ajustements de données permettant de minimiser les écarts entre les résultats des simulations et les mesures intégrales [Dupont 02a] [Romain 02] [Fort 03]. Toutefois cet exercice nécessite de bien connaître l'incertitude des données nucléaires et de résoudre un *problème inverse* qui ne comporte pas de solution unique. Les résultats doivent donc être interprétés avec prudence. Nous reviendrons sur ces méthodes d'ajustements lors de la présentation des travaux du sous-groupe 33 du WPEC (chapitre 4).

La validation la plus courante consiste simplement à réaliser les simulations avec les nouvelles données puis comparer les résultats avec les mesures ou les calculs de référence pour des tests de non régression. L'interprétation des résultats est relativement facile quand il s'agit de valider une seule évaluation mais beaucoup plus complexe dans le cas d'une bibliothèque complète à cause des inévitables compensations d'erreurs dans les simulations. Une étude approfondie via une analyse de sensibilité des paramètres intégraux aux données nucléaires [Dupont 03] est la meilleure façon de comprendre l'origine des écarts calcul-expérience (ou calcul-référence). C'est d'ailleurs un préalable indispensable pour permettre une utilisation raisonnable des méthodes d'ajustement statistique.

2.2.1 Analyse des tendances intégrales en spectres rapides de JEFF-3

Dans le rapport [Dupont 03] qui suit on réalise une validation préliminaire en spectre rapide de la bibliothèque JEFF-3.0 au travers de calculs directs et d'une analyse de sensibilité des paramètres intégraux aux principales données nucléaires.

Les calculs directs portent sur les paramètres intégraux mesurés dans des maquettes critiques chargées soit avec un mélange d'uranium et de plutonium (cœurs Pu), soit avec de l'uranium uniquement (cœurs U). Ces calculs sont réalisés avec les bibliothèques JEF-2.2, JEFF-3.0 et des bibliothèques hybrides constituées d'une nouvelle évaluation JEFF-3.0 insérée dans la bibliothèque JEF-2.2. L'analyse des résultats montre que les changements dans les isotopes majeurs que sont U-235,238 et Pu-239 n'expliquent qu'une partie des différences obtenues en utilisant les bibliothèques complètes JEF-2.2 et JEFF-3.0.

L'analyse de sensibilité est une technique puissante qui permet de lever le voile sur les contributions des autres isotopes sans pour autant réaliser tous les calculs directs que cela impliquerait normalement. L'étude de la sensibilité du facteur de multiplication (k_{eff}) révèle l'importance des données nucléaires représentées dans la figure suivante pour les cœurs Pu. L'écart entre les valeurs de k_{eff} des bibliothèques JEFF-3.0 et JEF-2.2 peut alors simplement être calculé en faisant la somme des produits des coefficients de sensibilités par la différence relative entre les données JEFF-3.0 et JEF-2.2.

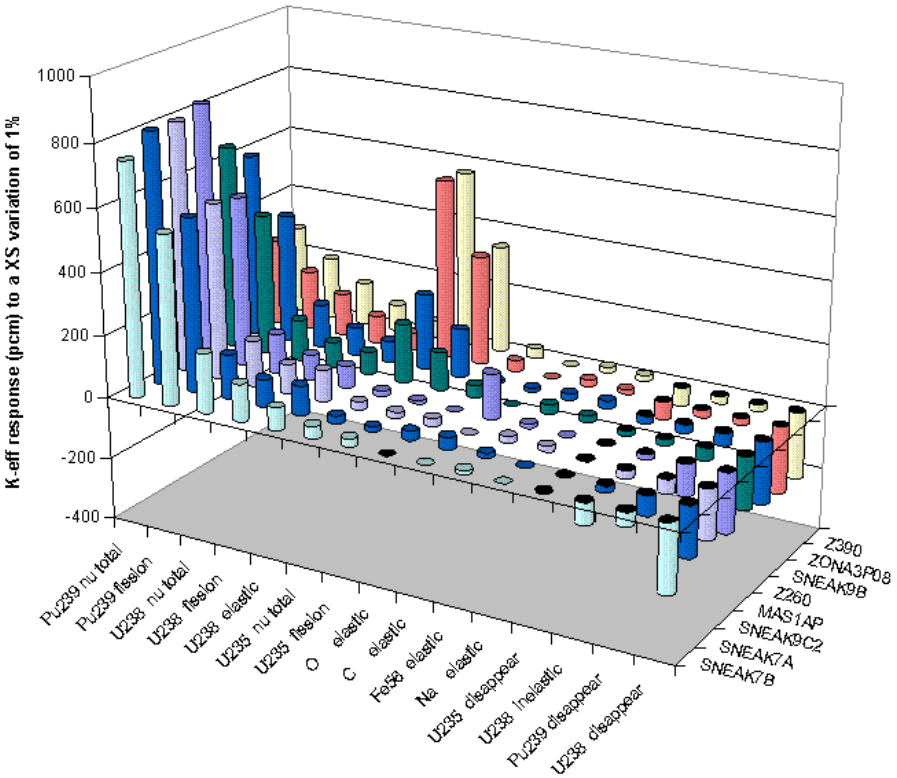

Sensibilité de k_{eff} aux principales données nucléaires (cœurs Pu)

Les principaux enseignements de cette étude sont résumés ci-dessous.

- L'impact de la nouvelle évaluation de U-235 est similaire par calcul direct et par calcul de sensibilité. En fait, les changements majeurs entre JEFF-3.0 et JEF-2.2 pour cette évaluation sont limités aux sections efficaces et à la multiplicité des neutrons de fission (nubar), données qui sont prises en compte dans les calculs de sensibilité. En particulier, il n'y a pas de différence dans les distributions d'énergie des neutrons prompts de fission. Par conséquent, l'analyse de sensibilité réalisée qui consistait à déduire le changement intégral à partir des coefficients de sensibilités et des variations des sections efficaces et du nubar est adéquate.
- Le cas de Pu-239 est a priori plus compliqué en raison de la réévaluation complète de cet isotope dans JEFF-3.0, y compris toutes les distributions secondaires. Cependant, l'approche incrémentale adoptée pour évaluer et valider ce fichier montre que les changements dans le spectre de fission n'ont pas d'impact significatif sur les simulations. Par conséquent, on peut supposer que les différences intégrales observées dans le k_{eff} sont essentiellement dues aux modifications des sections et du nubar.
- En revanche, la présente analyse de sensibilité est insuffisante pour U-238 car les modifications majeures entre les évaluations JEFF-3.0 et JEF-2.2 concernent non seulement les sections efficaces inélastiques et élastiques, mais également les distributions en angle et énergie des neutrons diffusés inélastiquement pour lesquelles nous ne disposons pas de coefficients de sensibilité.

Le rapport [Dupont 03] qui suit détaille les calculs réalisés et permet de mieux comprendre l'impact des diverses améliorations de la bibliothèque JEFF-3.0 qui ont permis de réduire les écarts calcul-expérience des paramètres intégraux. Au-delà de cette validation éclairée, l'analyse des résultats permet également d'identifier les données restant à améliorer, par exemple la section de capture de U-238 qui sera révisée à plusieurs reprises dans les versions suivantes de JEFF : 3.1 (2005), 3.2 (2014), 3.3 (2017).

[Dupont 03]

E. Dupont, Preliminary Analysis of JEFF-3.0/GP Trends in Fast Spectrum Experiments, JEFF internal report JEF/DOC-956 (2003)

Preliminary Analysis of JEFF-3.0/GP Trends in Fast Spectrum Experiments

Emmeric Dupont*

CEA/DEN/DER/SPRC/LEPh, Cadarache, France

Abstract

This document presents the results of integral validation calculations performed with the JEFF-3.0 library processed for the ERANOS-2.0 code system. The selected integral experiments are mainly those performed in the MASURCA facility at CEA-Cadarache as well as a few SNEAK configurations.

1. Introduction

A pre-validation of JEFF-3.0/GP in the same fast spectrum configurations has been done before its official release for specific isotopes and the results have already been reported: ^{239}Pu [1], ^{235,238}U [2], and a few other actinide cross-sections [3]. Following the processing of the whole JEFF-3.0/GP into application libraries (β-version) [4], fast reactor benchmark experiments have been recalculated. These configurations were calculated with the ERANOS-2.0 code system [5]: ECCO for cell calculations and BISTRO for core calculations. When a natural element was present in JEF-2.2 and missing in JEFF-3.0, its isotopic composition was taken from reference [6]. Following these direct calculations, a detailed sensitivity analysis was performed in order to quantitatively assess the contribution of every nuclear data to the observed k_{eff} differences.

2. Direct calculations

2.1. K-effective

Figure 1 shows the results obtained with JEF-2.2 and JEFF-3.0 libraries. Experiments are arbitrarily ranked by order of increasing U-235 atom density in the core. The cores without plutonium (i.e. ^{235}U only) are on the right hand side of the graphs (starting from R390). Generally, the use of the JEFF-3.0 (vs. JEF-2.2) library leads to lower k-effective values. This reactivity effect is large and much welcome for uranium cores whereas it is not so good, though smaller, for other cores.

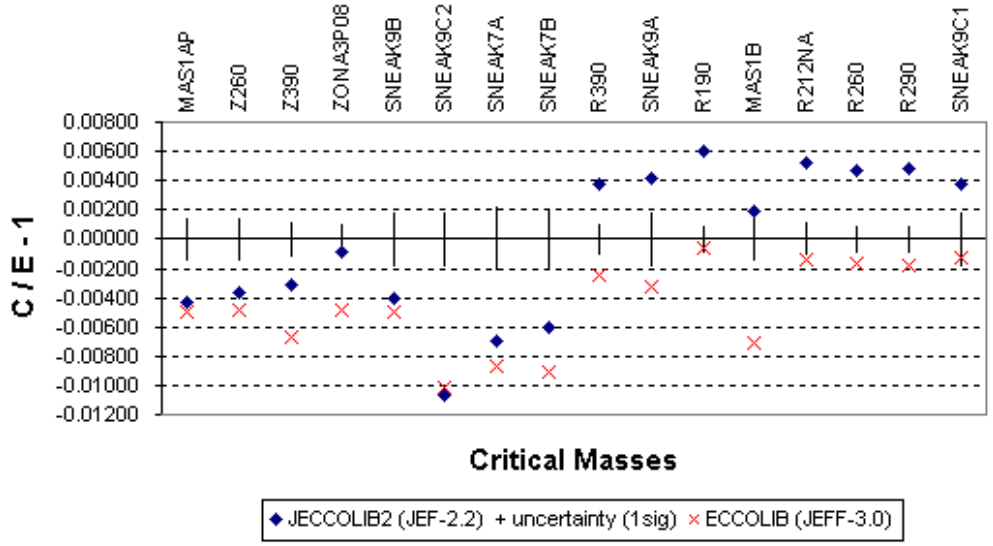

Figure 1 - K-effective calculations with JEF-2.2 and JEFF-3.0 libraries

* emmeric.dupont@cea.fr

For uranium cores (cf. Table 1), critical mass calculations yield lower k-effective values by about 600÷700 pcm, except for MAS1B which is more sensitive (~ 900 pcm) and SNEAK9C1 which is less sensitive (~ 500 pcm). Reference [2] had shown that a JEFF-3.0 ^{235}U substitution into a JEF2-based ECCO library already led to lower k-effective values by ~350 pcm on average (~800 pcm for SNEAK9A and MAS1B). In the same reference [2], a similar test on ^{238}U had shown an average decrease in k-effective value of ~80 pcm for the same uranium cores. Thus, most of the reactivity effect in uranium cores is explained by uranium isotopes alone. The absolute value of the remaining difference (from tens of pcm up to 240 pcm for R290) could be explained by the influence of ^{52}Cr and ^{23}Na isotopes due to large changes in their scattering data.

Table 1 - Contribution of uranium isotopes to k_{eff} differences (direct calculations)

Cores	**k_{eff} (JEFF-3.0) – k_{eff} (JEF-2.2) [pcm]**			
	Δk (library)	**Δk (^{235}U) [2]**	**Δk (^{238}U) [2]**	**Δk(^{235}U)+Δk(^{238}U)**
R390	-623	-455	-121	-576
SNEAK9A	-743	***-740***	-77	-817
R190	-659	-425	-109	-534
MAS1B	***-907***	***-803***	-64	-867
R212Na	-658	-314	-87	-401
R260	-633	-340	-71	-411
R290	-660	-355	-63	-418
SNEAK9C1	***-508***	-297	-72	-369

For "plutonium" cores (which also contain uranium, cf. Table 2), there are rather large reactivity effects (–200 to –400 pcm) for Z390, ZONA3P08, SNEAK7A and SNEAK7B, and smaller ones (~100 pcm) for the remaining cores. Reference [2] had shown that the JEFF-3.0 ^{238}U reactivity effect led to an average decrease in k-effective value by ~150 pcm for all these "plutonium" cores (except SNEAK7B, which contains about twice as many U-238 atoms), and that the ^{235}U effect was especially large (–300 pcm) for Z390 and ZONA3P08. The results shown in Table 2 confirm these trends. On the other hand, reference [1] had shown that reactivity effects due to ^{239}Pu modifications were generally small and of opposite sign compared to the present ones.

Table 2 - Contribution of ^{239}Pu and U isotopes to k_{eff} differences (direct calculations)

Cores	**k_{eff} (JEFF-3.0) – k_{eff} (JEF-2.2) [pcm]**			
	Δk (library)	**Δk (^{235}U) [2]**	**Δk (^{238}U) [2]**	**Δk (^{239}Pu) [1]**
MAS1AP	-64	-14	-142	-19
Z260	-116	-90	-119	122
Z390	***-364***	***-278***	-141	-18
ZONA3P08	***-397***	***-281***	-154	-27
SNEAK9B	-91	-135	-168	33
SNEAK9C2	54	-12	-142	150
SNEAK7A	***-176***	-16	-171	29
SNEAK7B	***-298***	-17	***-386***	77

The difference Δ between Δk(library) and the sum of Δk(isotope) is generally rather small (Δ < 100 pcm). However, as previously stated in the case of uranium cores, there certainly exist other isotopes not taken into account that could have compensating effects. In the case of MAS1AP (Δ = 111 pcm) and SNEAK9B (Δ = 179 pcm), it is clear that the ^{240}Pu and ^{23}Na influences are not negligible.

The effect of the isotopes not explicitly mentioned in the above study (direct calculations) will be discuss in §3.2 (k_{eff}-sensitivity analysis), and illustrated in Appendix 2.

2.2. Bucklings

Figure 2 shows the results obtained with the JEF-2.2 and JEFF-3.0 libraries. The use of the JEFF-3.0 library leads to lower buckling values for uranium cores (on the right hand side of the graph, starting from R390) and has little effect on the other cores. Generally, the calculated values are in much better agreement with experimental results when using the new JEFF-3.0 library.

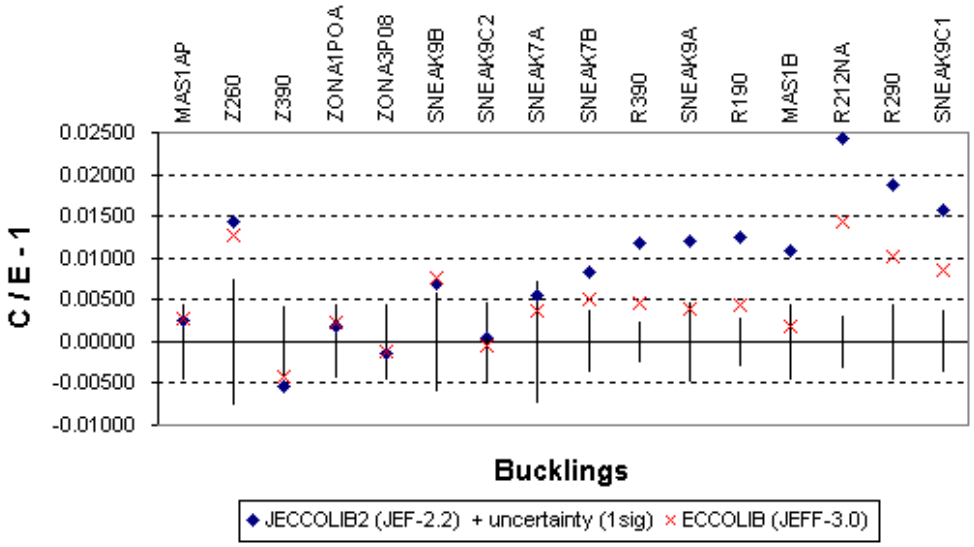

Figure 2 - Buckling calculations with JEF-2.2 and JEFF-3.0 libraries

Those improvements are partly explained by changes in uranium data, as shown in Table 3. However, other isotopes not listed in that table certainly have a significant effect. Indeed, the difference Δ between Δk(library) and the sum of Δk(isotope) from Table 3 is larger than 400 pcm for Z390, ZONA3P08, R212Na, R290, SNEAK9C1.

Table 3 - Contribution of ^{239}Pu and U isotopes to buckling differences (direct calculations)

Cores	Buckling : k_{eff} (JEFF-3.0) – k_{eff} (JEF-2.2) [pcm]			
	Δk (library)	Δk (^{235}U) [2]	Δk (^{238}U) [2]	Δk (^{239}Pu) [1]
MAS1AP	13	-9	-12	-24
Z260	-163	-3	-47	206
Z390	116	-18	-230	-99
ZONA1POA	49	-9	-134	42
ZONA3P08	42	-27	-250	-130
SNEAK9B	61	-14	-134	77
SNEAK9C2	-93	-7	-34	201
SNEAK7A	-186	-10	-38	33
SNEAK7B	***-310***	-15	***-316***	93
R390	***-718***	***-598***	-153	0
SNEAK9A	***-812***	***-828***	-37	0
R190	***-816***	***-424***	-52	0
MAS1B	***-917***	***-880***	66	0
R212Na	***-1011***	***-278***	-2	0
R290	***-869***	***-324***	6	0
SNEAK9C1	***-713***	***-299***	18	0

2.3. Spectral Indices

The following spectral indices are all relative to the ^{235}U fission reaction rate (F25). The standard notation is also used for other reaction rates: F49 (^{239}Pu fission), F28 (^{238}U fission), C28 (^{238}U capture). Since the ^{235}U(n,f) cross section is identical above 2.25 keV (upper limit of the new RRR) in both JEFF-3.0 and JEF-2.2 evaluated files, the interpretation of any variation in these ratios should be easier.

There is no significant change in the F49/F25 spectral index (cf. Figure 3), as already shown in Reference [1].

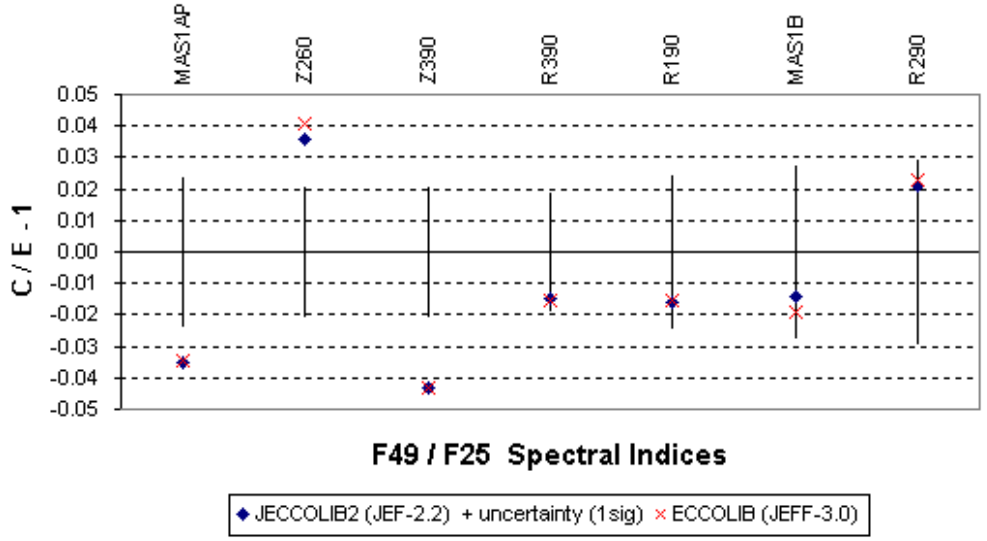

Figure 3 - F49/F25 calculations with JEF-2.2 and JEFF-3.0 libraries

The spectral index F28/F25 (cf. Figure 4) is very sensitive to any change in the reactor spectrum. One had shown in Reference [2] that modifications of the uranium-238 elastic cross section (above inelastic threshold) and inelastic scattering data (cross sections and secondary distributions) led to a constant decrease by about 1.8% of this spectral index for all the studied cores. There is apparently, in JEFF-3.0/GP, one or several compensating effect(s), making the interpretation difficult. Indeed, the effect reported here is generally much smaller or even of opposite sign.

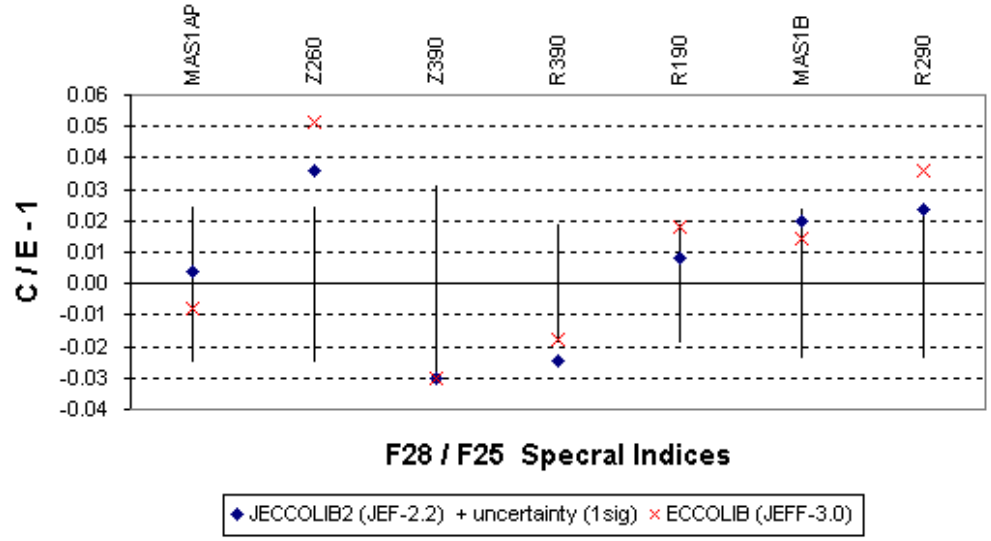

Figure 4 - F28/F25 calculations with JEF-2.2 and JEFF-3.0 libraries

The C28/F25 (cf. Figure 5) spectral index is not significantly affected when using JEFF-3.0/GP data.

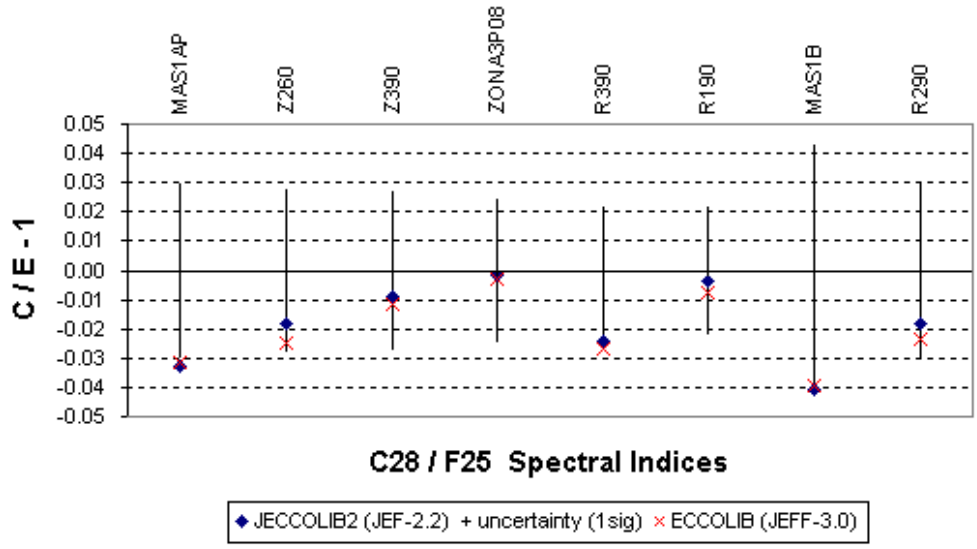

Figure 5 - C28/F25 calculations with JEF-2.2 and JEFF-3.0 libraries

3. Sensitivity analysis

Some of the results obtained with this first JEFF-3.0 ECCO/ERANOS library were qualitatively expected thanks to the validation work already performed on plutonium-239 and uranium isotopes. However, it has been demonstrated in the previous section that a significant part of some integral differences could be interpreted as resulting from the influence of other isotopes.

More quantitatively, the integral variation δI is related to every reaction variations $\delta\sigma_i$ via the associated sensitivity coefficients :

$$\delta I = \sum_i \delta\sigma_i \frac{\partial I}{\partial \sigma_i}(\sigma_i) + R_i^1 ,$$

$$\text{with } R_i^1 = \frac{1}{2}(\delta\sigma_i)^2 \frac{\partial^2 I}{\partial \sigma_i^2}(\sigma_i + \theta\delta\sigma_i) \text{ , } 0 < \theta < 1 .$$

When $\delta\sigma_i \times \frac{\partial^2 I/\partial\sigma_i^2}{\partial I/\partial\sigma_i}(\sigma_i)$ is small enough ($\forall$ i), one can simply use the first order sensitivity $\partial I/\partial\sigma_i$.

In the next sections, the integral quantity will refer to k_{eff} and the nuclear data will be defined as follows (ECCO/ERANOS library definition) :

ν_{tot}	total neutron multiplicity	MT 452 [= MTs 455+456]
(n, f)	fission	MT 18 [= MTs 19+20+21+38]
(n, n)	elastic scattering	MT 2(n) [1]
(n, n'+ y) [2]	pseudo-inelastic scattering	MTs 4(nγ)+22(nα)+23(n3α)+28(np)+29(n2α)+32(nd)+ 33(nt)+34(n^{3}He)+35(nd2α)+36(nt2α)+44(n2p)+45(npα)

[1] in this shortened notation one specifies only the particle(s) in the exit channel for every MT number
[2] "y" stands for Light Charged Particle (LCP) or photon (γ), cf. ENDF-102 manual (Formats and Procedures)

(n, x n'+ y)	neutron production (x > 1)	MTs 11(2nd)+16(2n)+17(3n)+24(2nα)+25(3nα)+ 30(2n2α)+37(4n)+41(2np)+42(3np)
(n, y)	neutron disappearance	MT 101 [= MTs 102(γ)+103(p)+...+116(pt)]

In the present energy range of interest (less than 10 MeV), the last three lumped reactions are more or less equivalent to inelastic scattering (MT4), n,2n (MT16) and radiative capture (MT102).

3.1. Most "k_{eff}-sensitive" nuclear data

Figures 6 and 7 show the k_{eff} response to a 1% variation of every basic nuclear data (only the responses higher than 10 pcm are plotted). For the core configurations under study, the main nuclear data are the following ones (ranked by order of decreasing importance) :

^{239}Pu or ^{235}U	ν_{tot}	– average neutron multiplicity
^{239}Pu or ^{235}U	(n, f)	– fission cross section
^{238}U	(n, γ or LCP)	– neutron disappearance cross section
^{238}U	ν_{tot}	– average neutron multiplicity
^{235}U	(n, γ or LCP)	– neutron disappearance cross section
^{238}U	(n, f)	– fission cross section
^{238}U	(n, n)	– elastic scattering cross section
^{238}U	(n, n')	– inelastic scattering cross section
^{239}Pu	(n, γ or LCP)	– neutron disappearance cross section.

The results can also be rather sensitive to elastic scattering cross sections of sodium, iron, oxygen and carbon, depending on their concentration.

The secondary neutron properties (angle and energy distributions) could not be studied in a similar way because the ERANOS code system does not allow any simple sensitivity calculation to these parameters.

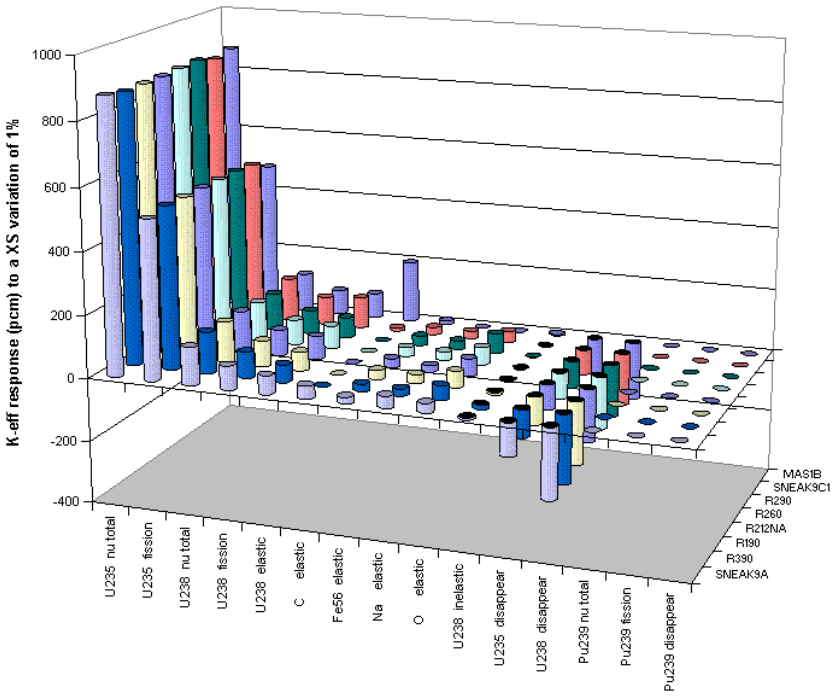

Figure 6 - k_{eff} sensitivities to the main nuclear data (U cores)

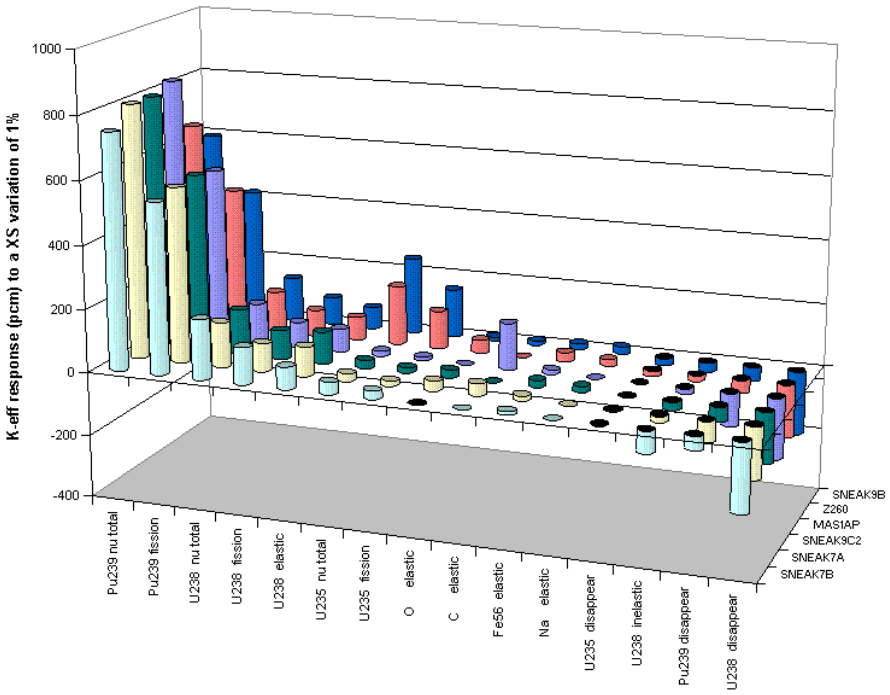

Figure 7 - k_{eff} sensitivities to the main nuclear data (Pu cores)

3.2. Most "k_{eff}-sensitive" nuclear data differences between JEFF-3.0 and JEF-2.2

In the following, we attempt to explain k-effective differences between ERANOS calculations using the "standard" JECCOLIB2 (~JEF-2.2) library and a JEFF-3.0 based ECCO library (β-version). Although some reactions are not part of the previous list, they must be considered because of large differences between the last two versions of JEF(F). On the other hand, some sensitive reactions have no influence on the reactivity differences studied, merely because there are identical in both JEF(F) versions (e.g. fission and disappearance cross sections of uranium-238).

In Appendix 1, one can see the differential nuclear data for which the contribution to the calculated Δk_{eff} is significant, either because the eigenvalue is sensitive to this reaction or because the difference $\Delta\sigma$ between JEFF-3.0 and JEF-2.2 is large (^{52}Cr, ^{27}Al, ^{56}Fe, ^{23}Na, ^{240}Pu and ^{238}U(n,xn) evaluations for instance). One has also plotted the sensitivities of all core configurations in order to give an idea of the essential energy ranges.

The histograms of Appendix 2 illustrate the main contributions to the calculated k-effective of every significant difference between JEFF-3.0 and JEF-2.2 nuclear data. The first graphs correspond to plutonium cores whereas the following ones are for uranium cores.

On each graph of Appendix 2, the results of direct calculations[3] for specific substitutions (Pu239 [1], U235 and U238 [2]) and for the complete nuclear data library switch (cf. §2.1) have been reported in green ("*direct*" bars). The corresponding results from the sensitivity calculations[4] are reported in red ("*sum*" bars).

In every configuration, there is a rather good agreement between U235 trends obtained with direct and sensitivity calculations. Actually, major changes between JEFF-3.0 and JEF-2.2 for this particular evaluation are observed in cross sections and fission neutron multiplicity, there is no difference in

[3] including angular and energy distributions effects
[4] angular and energy distributions are not taken into account

fission neutron energy distributions (MF5/MT18). Therefore, the present sensitivity analysis is adequate.

The case of Pu239 is somehow less adequate due to the complete re-evaluation of this isotope, including all the secondary distributions [7] [8]. However, the iterative approach adopted to evaluate/validate this file has already taught us that the changes in the fission spectrum were not large enough to have any significant impact on the present integral calculations. Therefore, one can reasonably assume that the integral differences observed in k_{eff} are essentially due to changes in cross-sections and ν.

About U238, the present sensitivity analysis is *a priori* inadequate since major changes between JEFF-3.0 and JEF-2.2 evaluations concern not only inelastic and elastic cross sections, but also angle and energy distributions of inelastically scattered neutrons (n,xn data are also different, but their impact is very limited in the present study).

Indeed, the differences observed between direct and sensitivity calculations for U238 are significant (up to a few hundreds of pcm) and could explain most of the discrepancy systematically seen in every configuration. In Appendix 2, the orange bar (labelled "*TOTAL (U8 direct)*") shows the total library impact calculated by adding all the contributions but U238 to the direct U238 effect. In that case, the discrepancy is strongly reduced, especially for "plutonium" cores.

4. Discussion

The differences (up to 550 pcm for SNEAK7B) observed between a direct calculation and a cross-section-based sensitivity study were not expected since the successful completion of JEF-2.2 adjustment studies [9] and require more investigations. However, larger effect (1700 pcm for ZPPR-9 when using JENDL-2 or JENDL-3.1≈JEF-2.2 matrices) had already been reported [10].

• ***Leakage effect*** : Table 4 shows k_{eff} differences between JEFF-3.0 and JEF-2.2 U-238 obtained from an actual core calculation (Δk^{core}) and a reflected (pseudo-infinite) cell configuration (Δk^{∞}). The uranium 238 data substitution is done within the JEF-2.2 based ECCO library. These cell calculations are made with the 172 groups X-MAS structure (which corresponds to the first step of the ECCO reference calculation route [11]).

Table 4 - k_{eff} differences between ^{238}U JEFF-3.0 and JEF-2.2

name	Δk^{core} (pcm)	Δk^{∞} (pcm)
MAS1B	-65	-109
R290	-65	-102
SNEAK9C1	-71	-129
R260	-72	-102
SNEAK9A	-78	-122
R212	-85	-109
R190	-112	-131
R390	-121	-182
Z260	-127	-128
SNEAK9C2	-139	-159
Z390	-141	-230
MAS1AP	-143	-183
ZONA3	-154	-291
SNEAK9B	-169	-211
SNEAK7A	-171	-245
SNEAK7B	-395	-411

The fact that the Δk results are similar suggests that the observed effect is a pure nuclear data one and has no strong link with the core geometry nor any possible preferential neutron leakage effect.

The last row result of Table 4 has been confirmed by a Monte-Carlo (MCNP4C2) infinite cell calculation: Δk^{∞} (SNEAK7B) = (–449 ± 30) pcm. In that particular case, the uranium 238 data substitution was done within a JEF-2.2 based ACE library with no probability tables.

• ***Group structure*** : SNEAK7B configuration has been calculated with the VITAMIN-J (175 groups) structure instead of the more usual ECCO-33G. Figure 8 clearly shows that this finer structure could have been more appropriate to describe an effect in the energy range of inelastic scattering data. However, both calculation routes give very similar results for k-effective and sensitivity values.

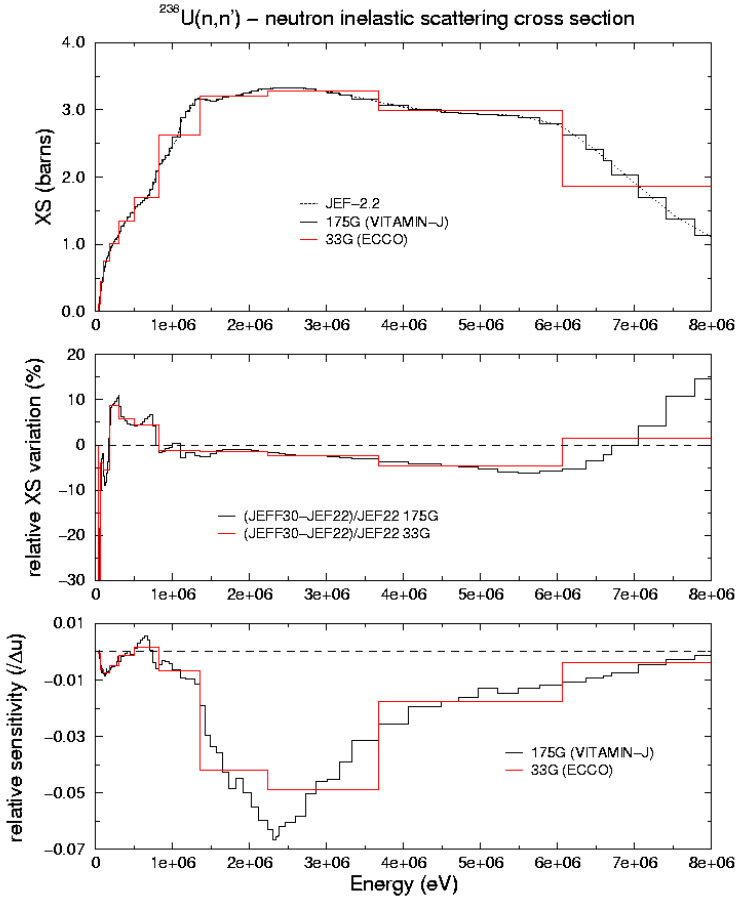

Figure 8 - SNEAK7B k_{eff} sensitivity to $^{238}U(n,n')$

• ***Transfer matrix*** : The double differential transfer cross section σ(E→E', Ω→Ω') depends on the cosine of the scattering angle $\mu = \vec{\Omega}.\vec{\Omega}' = \cos\theta$,

$$\sigma\left(E \to E', \vec{\Omega} \to \vec{\Omega}'\right) = \sum_{\ell=0}^{\infty} \frac{2\ell+1}{4\pi} \sigma_{\ell}\left(E \to E'\right) P_{\ell}(\mu)$$

Figure 9 displays the angular behaviour of the first two Legendre polynomials $P_{\ell=0} = 1$ and $P_{\ell=1} = \cos\theta$. The P_0 term is isotropic whereas the P_1 term tends to increase the cross section at forward angles ($P_1>0$) and to decrease it at backward angles ($P_1<0$).

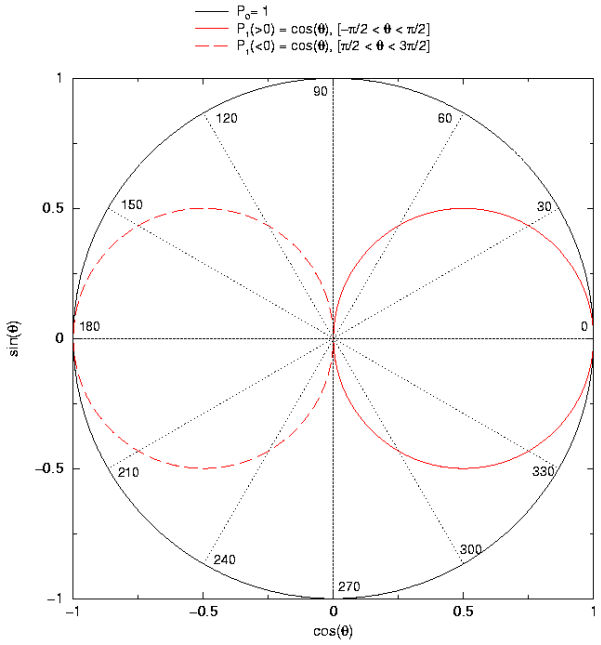

Figure 9 - Polar plot of $P_0=1$ and $P_1=\cos(\theta)$ Legendre polynomials

In the following pages, Figure 10 shows the energy transfer matrix in the ECCO-33 group structure for the first angular momentum σ_0 (the isotropic component) of the inelastic scattering reaction on ^{238}U. Actually, JEFF-3.0 and JEF-2.2 data only slightly differ up to 2-3 MeV and more significantly at higher incident energies.

The inelastic scattering σ_1 component (Figure 11) exhibits much larger differences but is negligible in absolute intensity (compared to σ_0). However, one should not forget that $\sigma_\ell P_\ell$ is weighted by the $(2\ell+1)$ factor,

$$\sigma\left(E \to E', \vec{\Omega} \to \vec{\Omega}'\right) = \frac{1}{4\pi}\left(\sigma_0\left(E \to E'\right) + 3\,\sigma_1\left(E \to E'\right)\cos\theta\right)$$

thus at forward angle the P_1 contribution might not be that negligible and could therefore contribute significantly to the difference between JEFF-3.0 and JEF-2.2 data. Actually, JEFF-3.0 inelastic data are generally less forward peaked than in the JEF-2.2 evaluation.

Unfortunately, k-effective sensitivity studies to the ^{238}U(n,n') energy transfer matrix are difficult to perform with present tools. Therefore, a quantitative study of the effect on k-effective of the observed differences in the transfer matrix could not be immediately performed to confirm the direct integral observations.

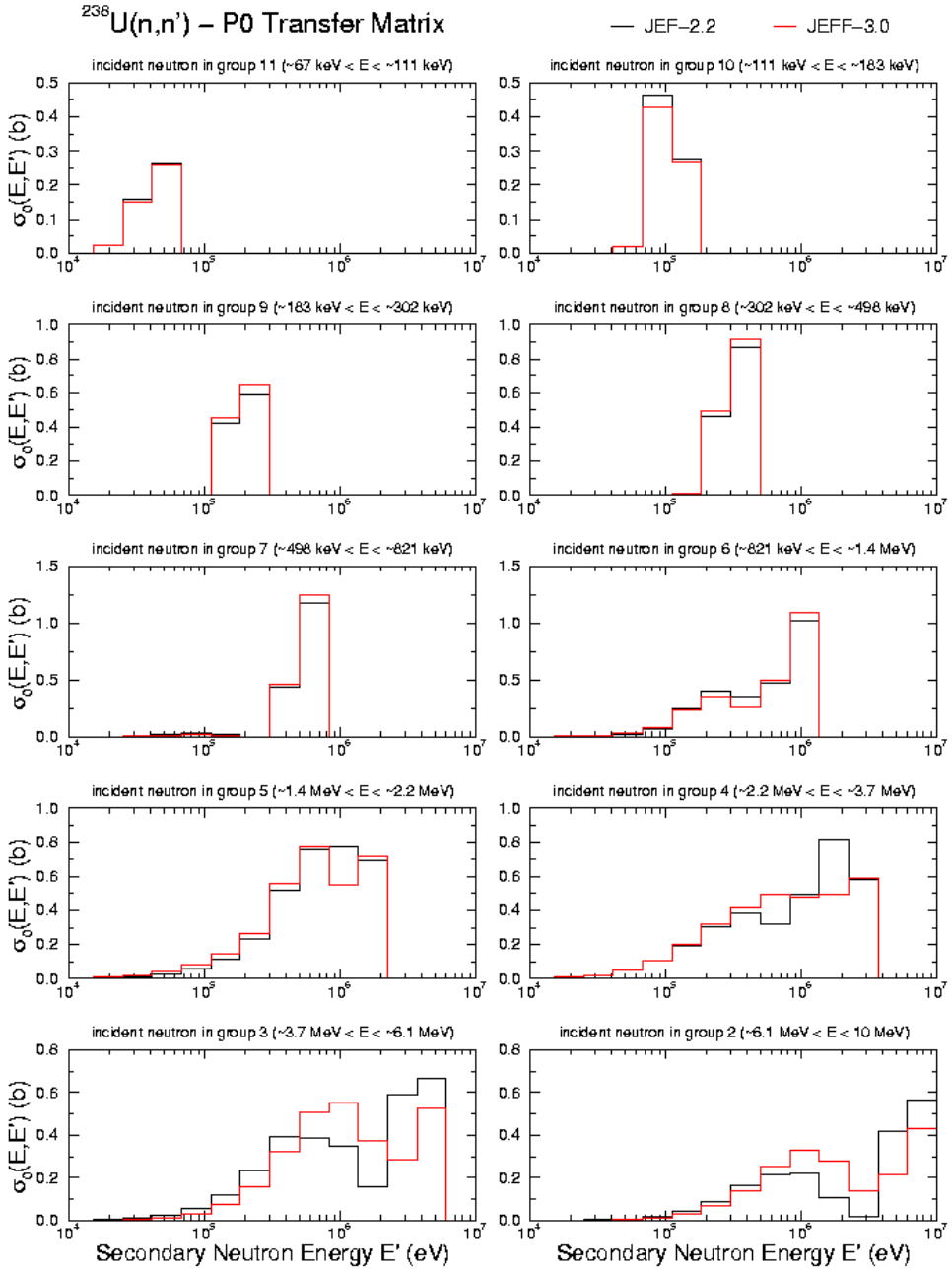

Figure 10 - P_0 transfer matrix for neutron inelastic scattering on ^{238}U

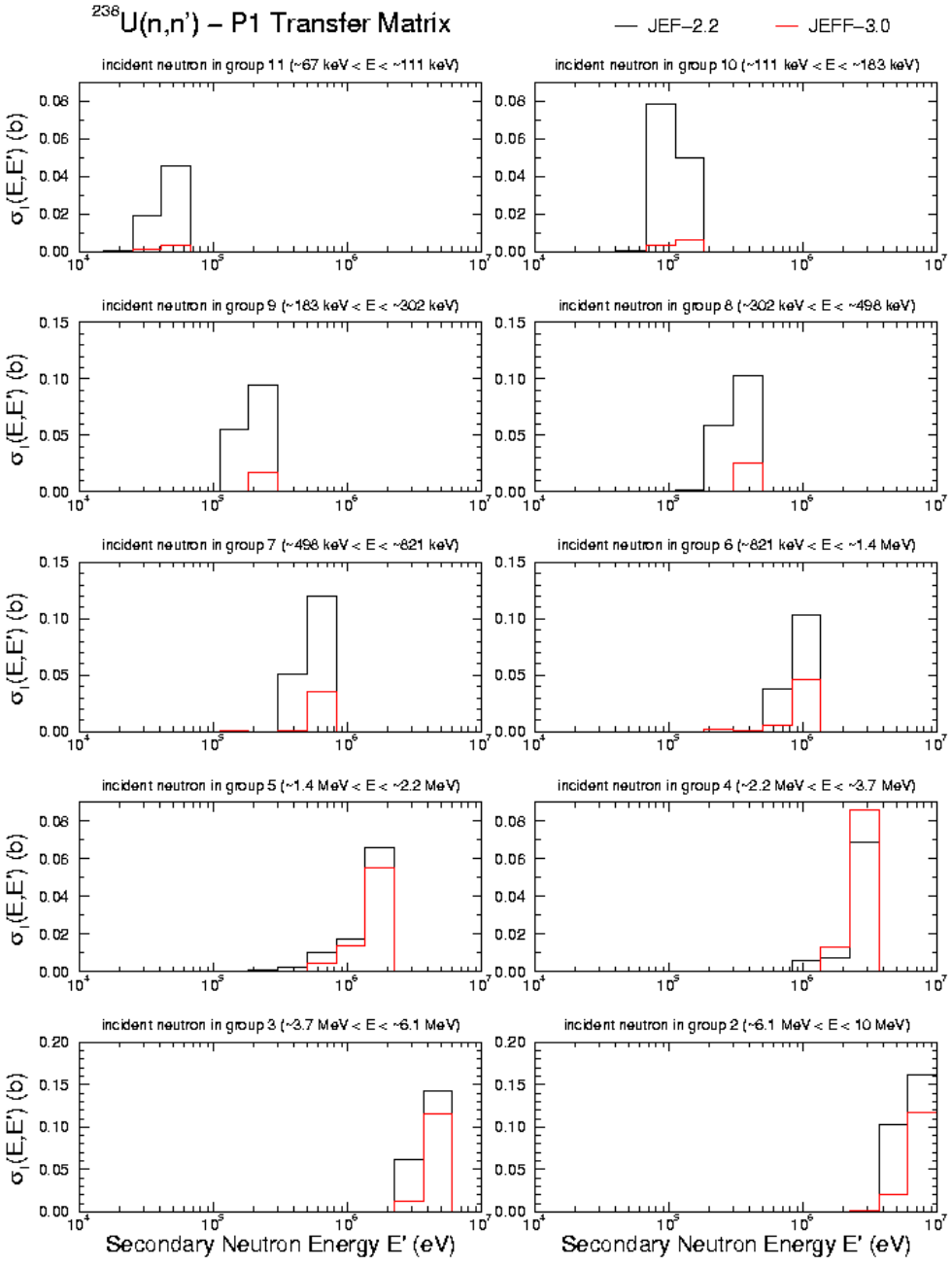

Figure 11 - P_1 transfer matrix for neutron inelastic scattering on ^{238}U

5. Conclusions

Generally, the results obtained with the new JEFF-3.0 library for the present set of fast spectrum experiments confirm the trends deduced from specific integral validation studies [1] [2] [8] and expected from the observed differences with the previous JEF(-2.2) evaluated data. The main integral trend is a decrease of the calculated k-effective (more pronounced for uranium cores) and buckling (uranium cores only), the changes detected in spectral indices being not as significant.

For "uranium" cores, the keys responsible of this integral trend are $^{235}U(n,\gamma)$ and ν_{tot} nuclear data modifications. These changes improve the calculated-over-experimental ratio for both k-effective and buckling integral values.

For "plutonium" cores, the situation is not as simple because the modifications made in ^{238}U, ^{239}Pu and ^{23}Na evaluations play a more significant role compared to the previous core types. These changes have almost no effect on buckling calculations, but do not improve the calculated-over-experimental ratio for k-effective value. Nevertheless, the present work clearly assesses every isotope contribution, and could guide future evaluation effort. Moreover, there is already room for improvement since ^{238}U capture and fission cross-sections, two key parameters to simulate fast spectrum experiments, have not been re-evaluated for JEFF-3.0.

Finally, some unexpected differences between direct and sensitivity calculations have not yet been fully explained in a quantitative way. Although, there are probably due to the changes made in the energy distribution of ^{238}U inelastic scattering reaction, which appears to be one of the most k_{eff}-sensitive difference between JEFF-3.0 and JEF-2.2 library for "plutonium" cores.

Acknowledgements

The author would like to thank Robert Jacqmin for his helpful comments and Olivier Litaize for having performed the MCNP calculations.

References

[1] "Further Integral Validation of the Pu-239 CEA Evaluation Adopted in JEFF-3.0", E. Dupont, P. Dos Santos Uzarralde, J.-C. Sublet, JEFF/DOC-918, April 2002.

[2] "JEFF-3.0 Uranium 235 and 238 Trends in Fast Spectrum Experiments", E. Dupont, J.-C. Sublet, A. Nouri, JEFF/DOC-915, April 2002.

[3] "JEFF-3.0 Trends Derived from the PROFIL Fast Spectrum Experiments", E. Dupont, J. Tommasi, A. Nouri, JEF/DOC-921, April 2002.

[4] "JEFF-3.0: NJOY99 and CALENDF-2002 processing – Viewpoint, prospect and solutions", J.-C. Sublet, P. Ribon, JEFF/DOC-934, December 2002.

[5] "The ERANOS Code and Data System for Fast Reactor Neutronic Analyses", G. Rimpault et al., International Conference *Physor 2002*, Seoul, Korea, October 7-10, 2002.

[6] "Isotopic Compositions of the Elements 1997", K. Rosman, P. Taylor, IUPAC Commission on Atomic Weights and Isotopic Abundances, 1997.

[7] "New Evaluation of ^{239}Pu data", P. Romain et al., JEF/DOC-919, April 2002.

[8] "Etude des multiplicités et des spectres de neutrons prompts de fission du ^{239}Pu dans l'expérience JEZEBEL", C. Le Luel and B. Morillon, private communication.

[9] "The JEF-2.2 Nuclear Data Library", OECD-NEA/DB JEFF Report 17, April 2000.

[10] Final report of the WPEC subgroup 4 on "^{238}U capture and inelastic cross-sections", NEA/NSC/WPEC/DOC(1999) volume 4.

[11] "Schéma de calcul de référence du formulaire ERANOS et orientations pour le schéma de calcul de projet", G. Rimpault et al., private communication.

Appendix 1

The nine following figures show the most important reactions for the core configurations under study. Uranium-238 fission and disappearance cross-sections are not plotted because they are identical in JEFF-3.0 and JEF-2.2 libraries.

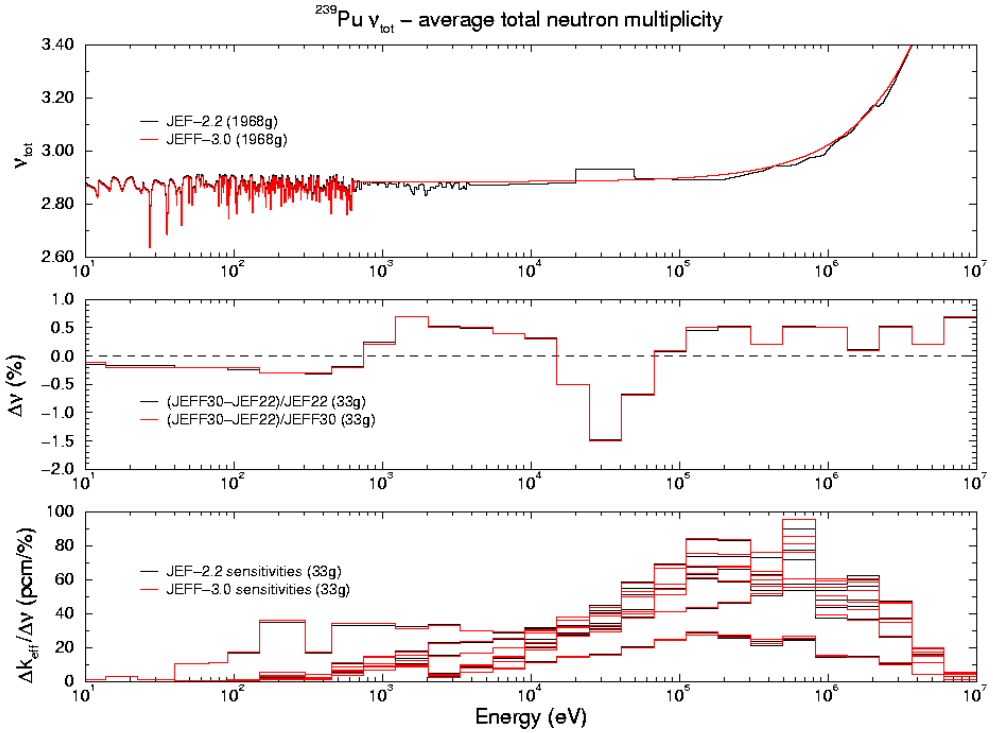

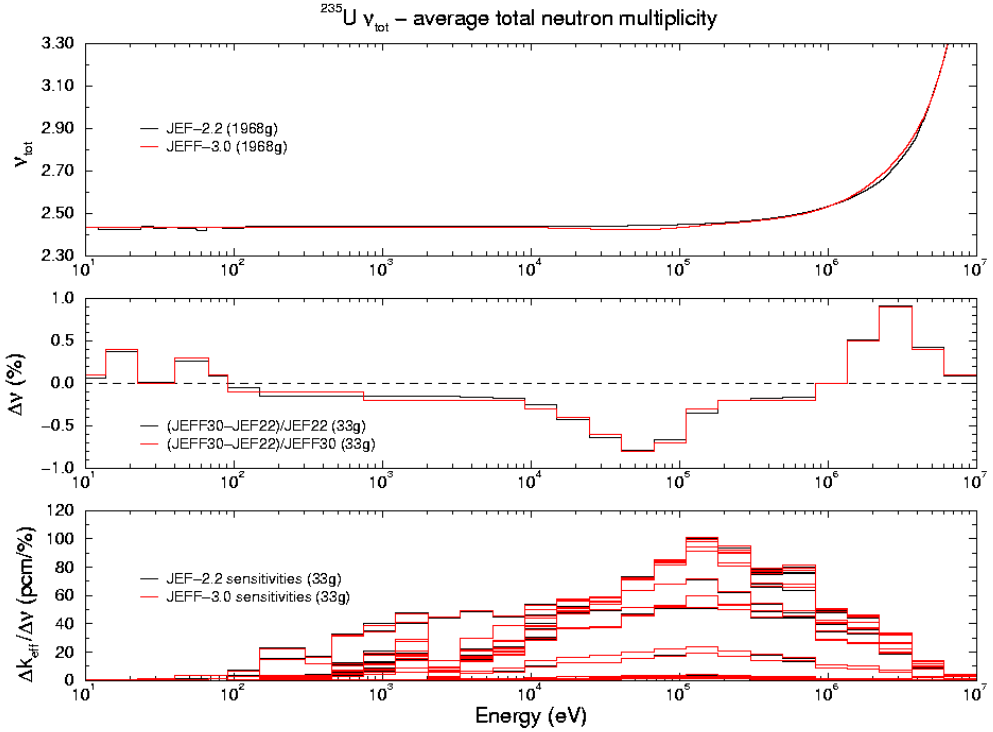

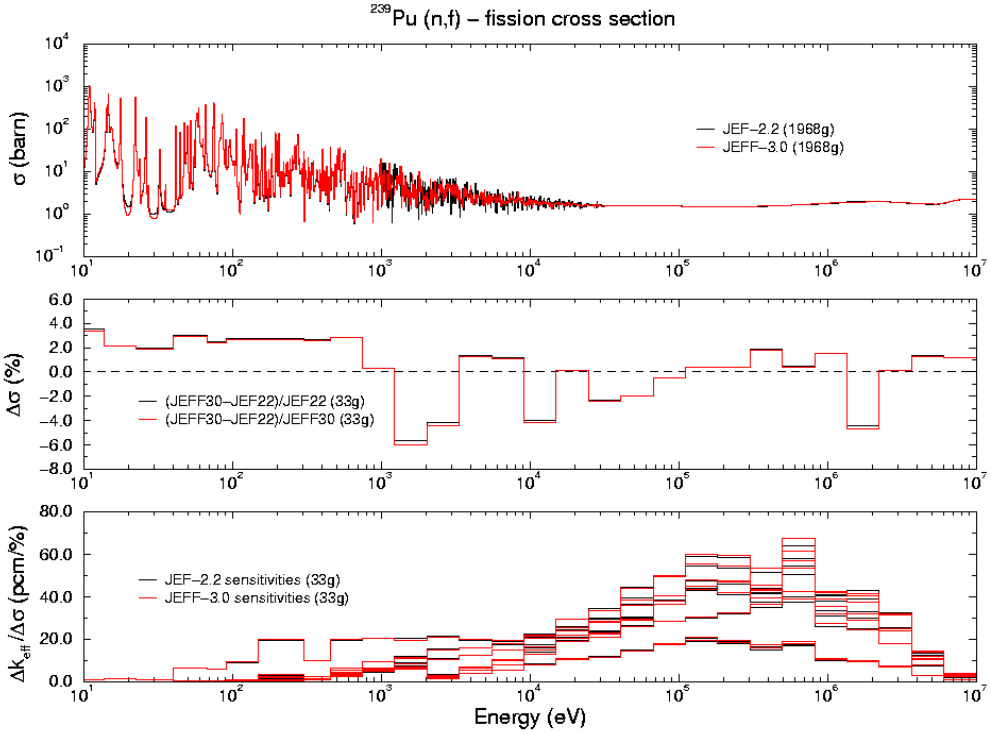
239Pu (n,f) – fission cross section
σ (barn)
JEF–2.2 (1968g)
JEFF–3.0 (1968g)
Δσ (%)
(JEFF30–JEF22)/JEF22 (33g)
(JEFF30–JEF22)/JEFF30 (33g)
ΔkEff /Δσ (pcm/%)
JEF–2.2 sensitivities (33g)
JEFF–3.0 sensitivities (33g)
Energy (eV)

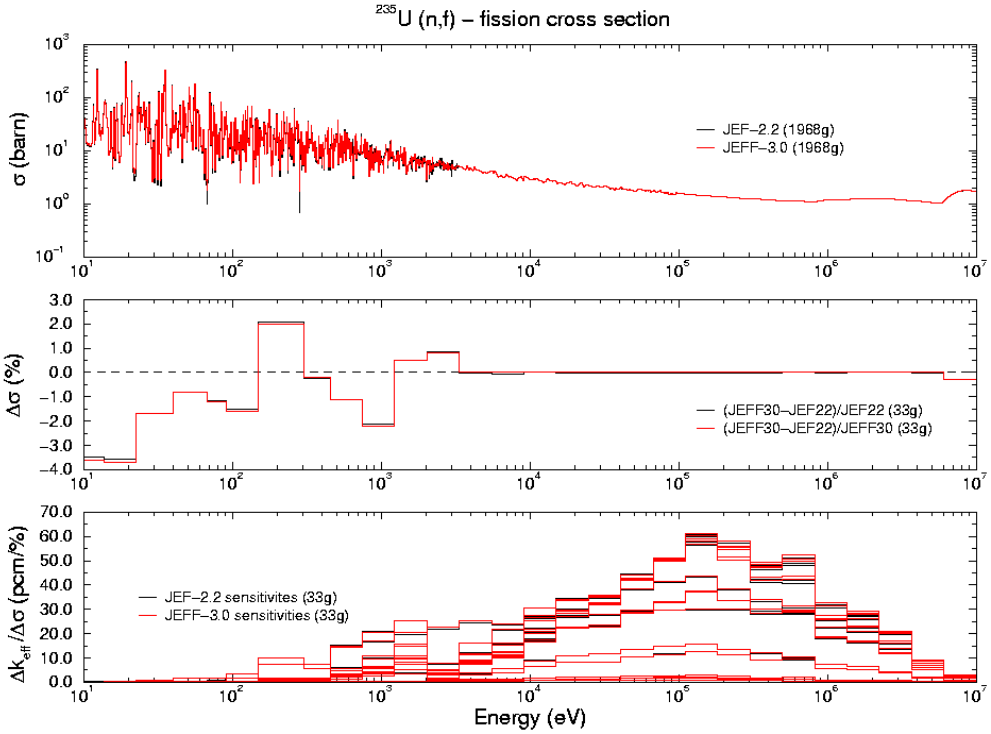
235U (n,f) – fission cross section
σ (barn)
JEF–2.2 (1968g)
JEFF–3.0 (1968g)
Δσ (%)
(JEFF30–JEF22)/JEF22 (33g)
(JEFF30–JEF22)/JEFF30 (33g)
ΔkEff /Δσ (pcm/%)
JEF–2.2 sensitivites (33g)
JEFF–3.0 sensitivities (33g)
Energy (eV)

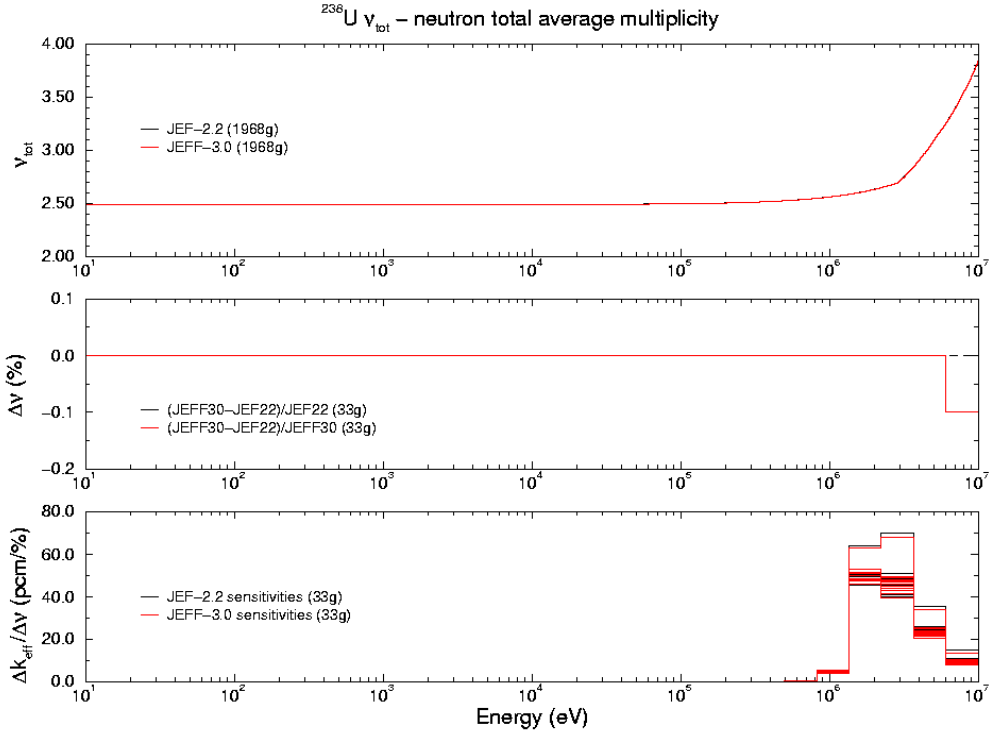
^{238}U ν_{tot} – neutron total average multiplicity
ν_{tot}
JEF–2.2 (1968g)
JEFF–3.0 (1968g)
Δν (%)
(JEFF30–JEF22)/JEF22 (33g)
(JEFF30–JEF22)/JEFF30 (33g)
$\Delta k_{eff}/\Delta\nu$ (pcm/%)
JEF–2.2 sensitivities (33g)
JEFF–3.0 sensitivities (33g)
Energy (eV)

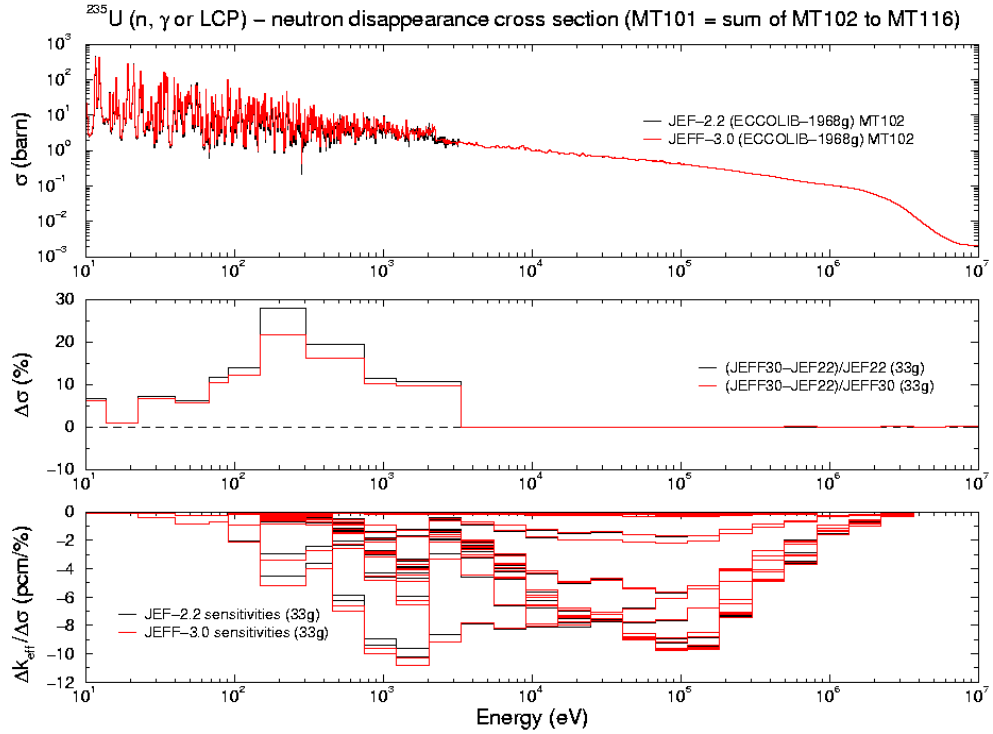
^{235}U (n, γ or LCP) – neutron disappearance cross section (MT101 = sum of MT102 to MT116)
σ (barn)
JEF–2.2 (ECCOLIB–1968g) MT102
JEFF–3.0 (ECCOLIB–1968g) MT102
Δσ (%)
(JEFF30–JEF22)/JEF22 (33g)
(JEFF30–JEF22)/JEFF30 (33g)
$\Delta k_{eff}/\Delta\sigma$ (pcm/%)
JEF–2.2 sensitivities (33g)
JEFF–3.0 sensitivities (33g)
Energy (eV)

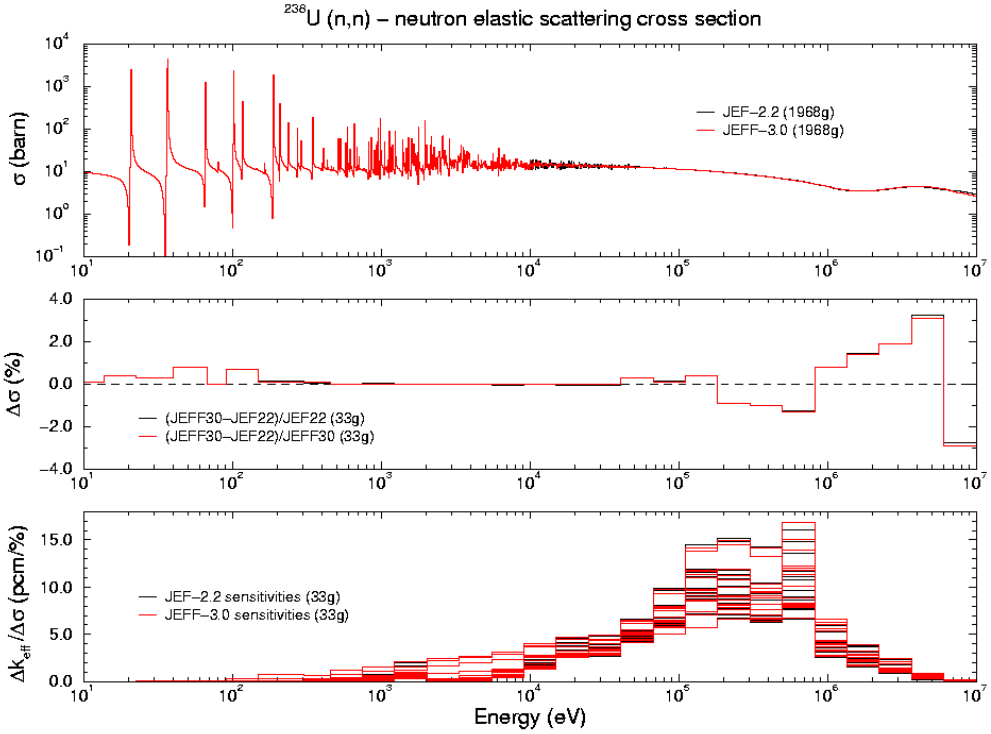
^{238}U (n,n) – neutron elastic scattering cross section
σ (barn)
JEF–2.2 (1968g)
JEFF–3.0 (1968g)
Δσ (%)
(JEFF30–JEF22)/JEF22 (33g)
(JEFF30–JEF22)/JEFF30 (33g)
Δk$_{eff}$/Δσ (pcm/%)
JEF–2.2 sensitivities (33g)
JEFF–3.0 sensitivities (33g)
Energy (eV)

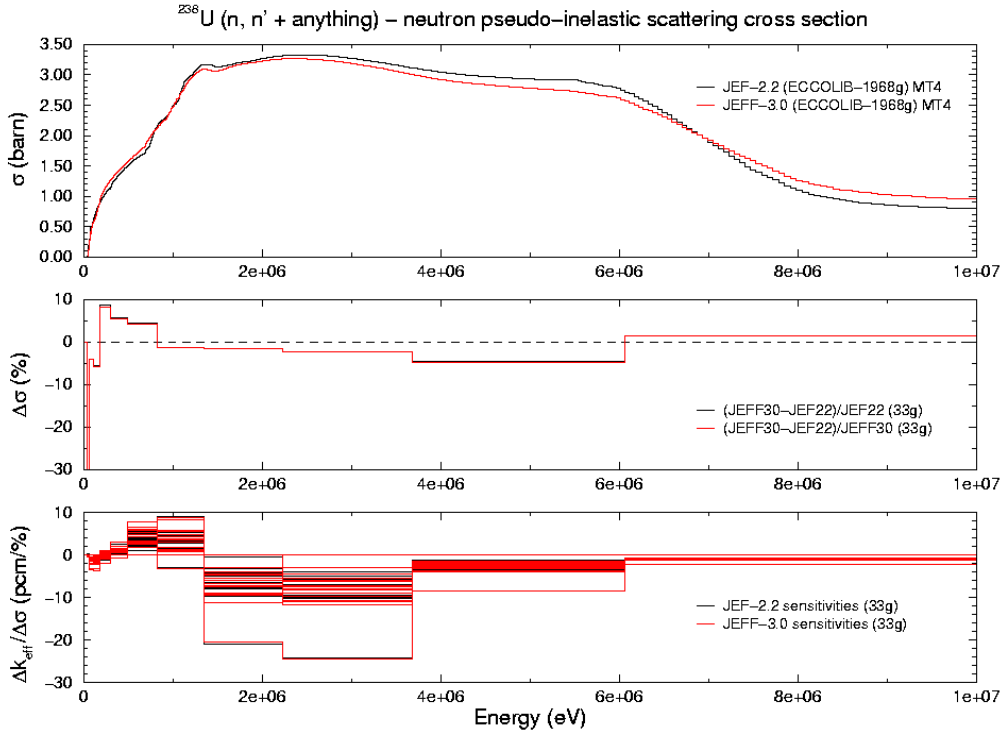
^{238}U (n, n' + anything) – neutron pseudo–inelastic scattering cross section
σ (barn)
JEF–2.2 (ECCOLIB–1968g) MT4
JEFF–3.0 (ECCOLIB–1968g) MT4
Δσ (%)
(JEFF30–JEF22)/JEF22 (33g)
(JEFF30–JEF22)/JEFF30 (33g)
Δk$_{eff}$/Δσ (pcm/%)
JEF–2.2 sensitivities (33g)
JEFF–3.0 sensitivities (33g)
Energy (eV)

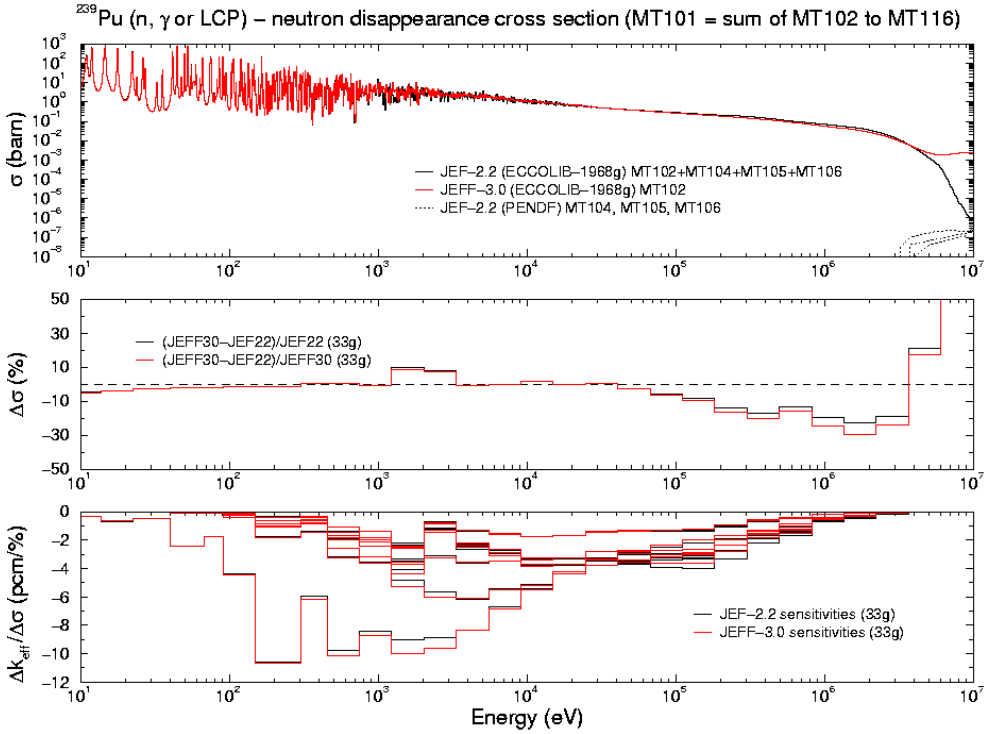
239Pu (n, γ or LCP) – neutron disappearance cross section (MT101 = sum of MT102 to MT116)
σ (barn)
JEF–2.2 (ECCOLIB–1968g) MT102+MT104+MT105+MT106
JEFF–3.0 (ECCOLIB–1968g) MT102
JEF–2.2 (PENDF) MT104, MT105, MT106
Δσ (%)
(JEFF30–JEF22)/JEF22 (33g)
(JEFF30–JEF22)/JEFF30 (33g)
Δk_eff/Δσ (pcm/%)
JEF–2.2 sensitivities (33g)
JEFF–3.0 sensitivities (33g)
Energy (eV)

In the following figures, one has plotted some less sensitive reactions. However, due to large differences between JEFF-3.0 and JEF-2.2 for these particular data, their impact on a k_{eff} calculation is not negligible.

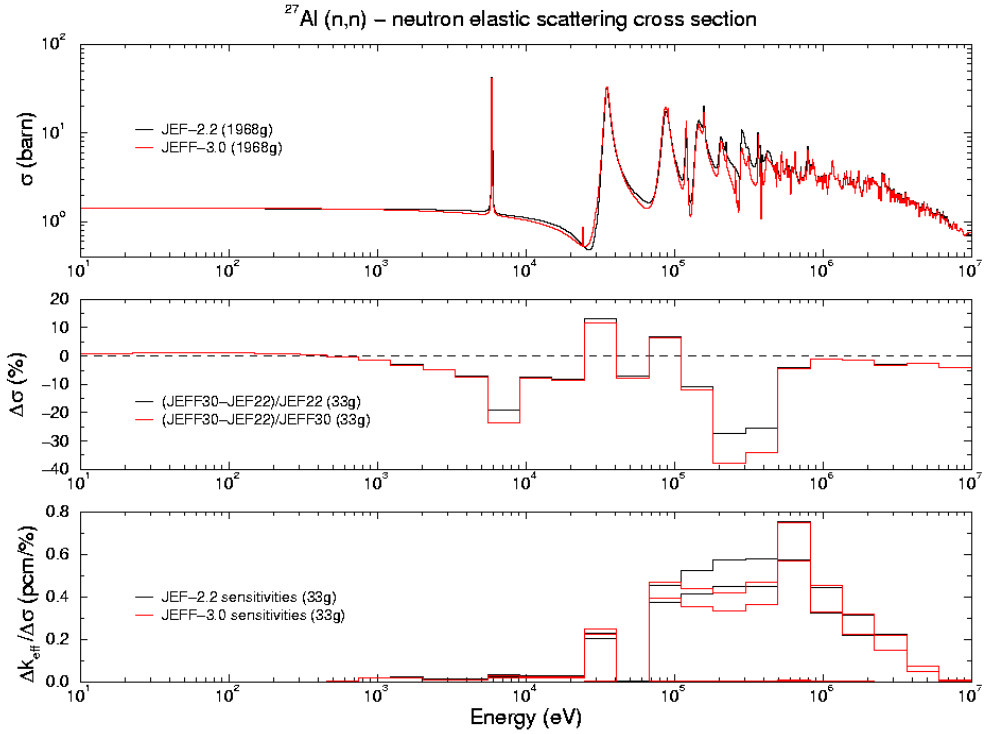

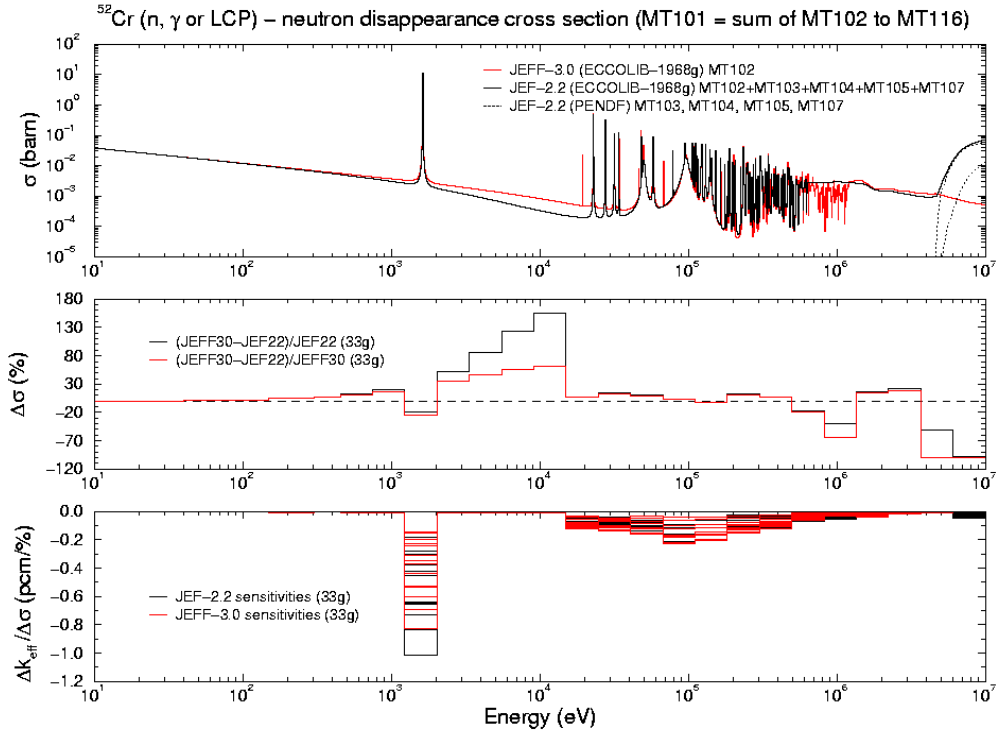

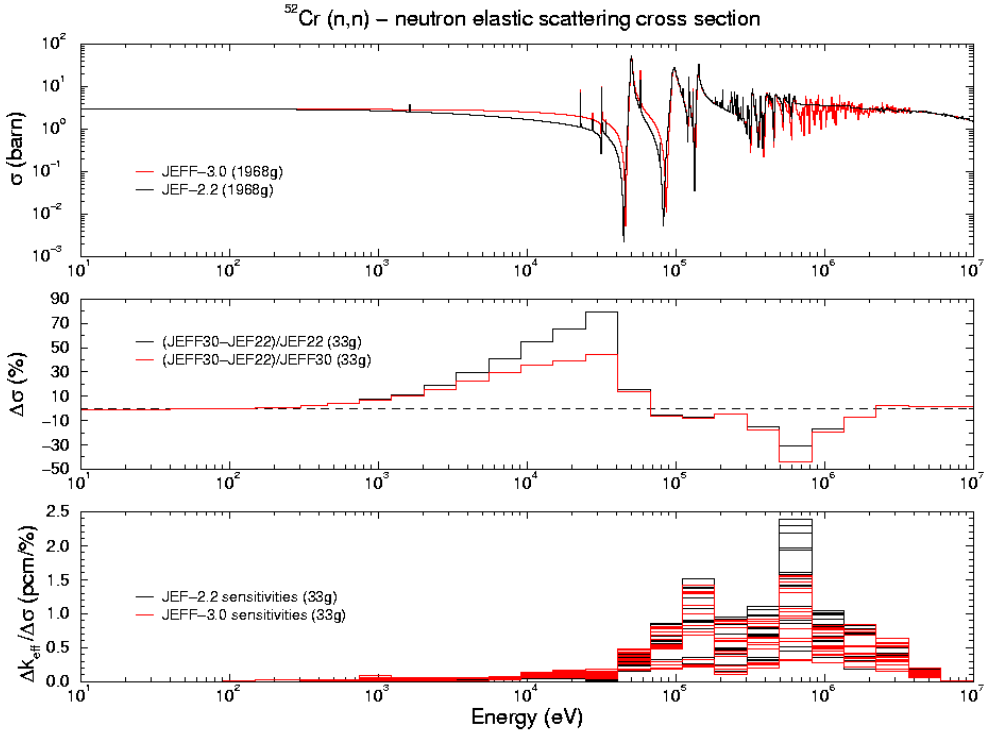
52Cr (n,n) – neutron elastic scattering cross section
σ (barn)
JEFF–3.0 (1968g)
JEF–2.2 (1968g)
Δσ (%)
(JEFF30–JEF22)/JEF22 (33g)
(JEFF30–JEF22)/JEFF30 (33g)
Δkeff/Δσ (pcm/%)
JEF–2.2 sensitivities (33g)
JEFF–3.0 sensitivities (33g)
Energy (eV)

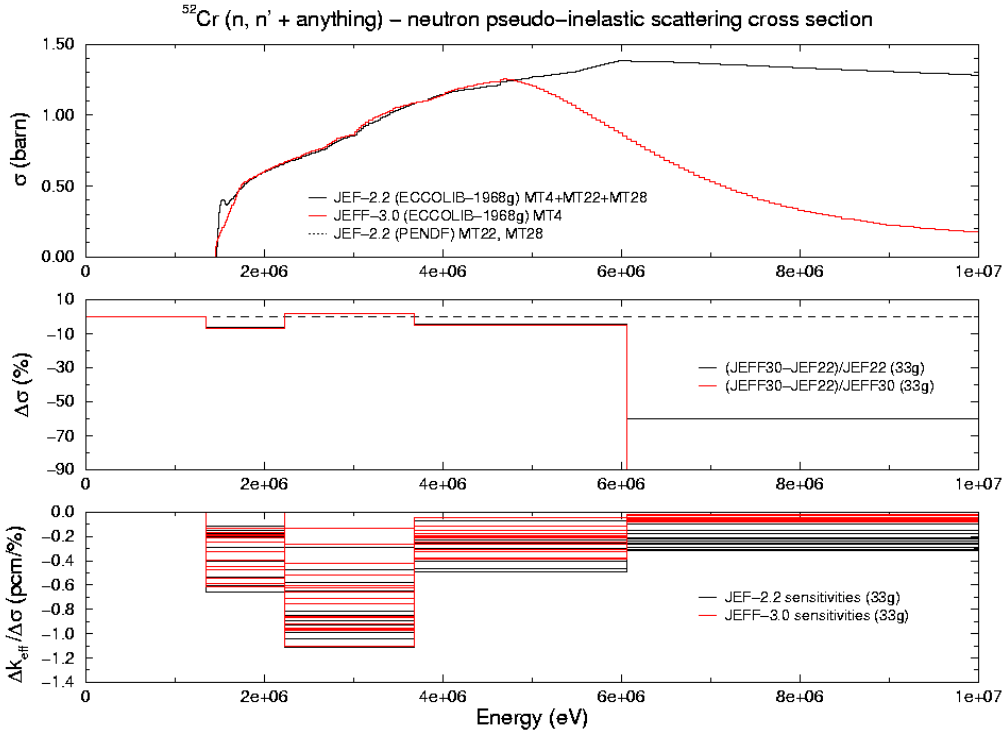
52Cr (n, n' + anything) – neutron pseudo–inelastic scattering cross section
σ (barn)
JEF–2.2 (ECCOLIB–1968g) MT4+MT22+MT28
JEFF–3.0 (ECCOLIB–1968g) MT4
JEF–2.2 (PENDF) MT22, MT28
Δσ (%)
(JEFF30–JEF22)/JEF22 (33g)
(JEFF30–JEF22)/JEFF30 (33g)
Δkeff/Δσ (pcm/%)
JEF–2.2 sensitivities (33g)
JEFF–3.0 sensitivities (33g)
Energy (eV)

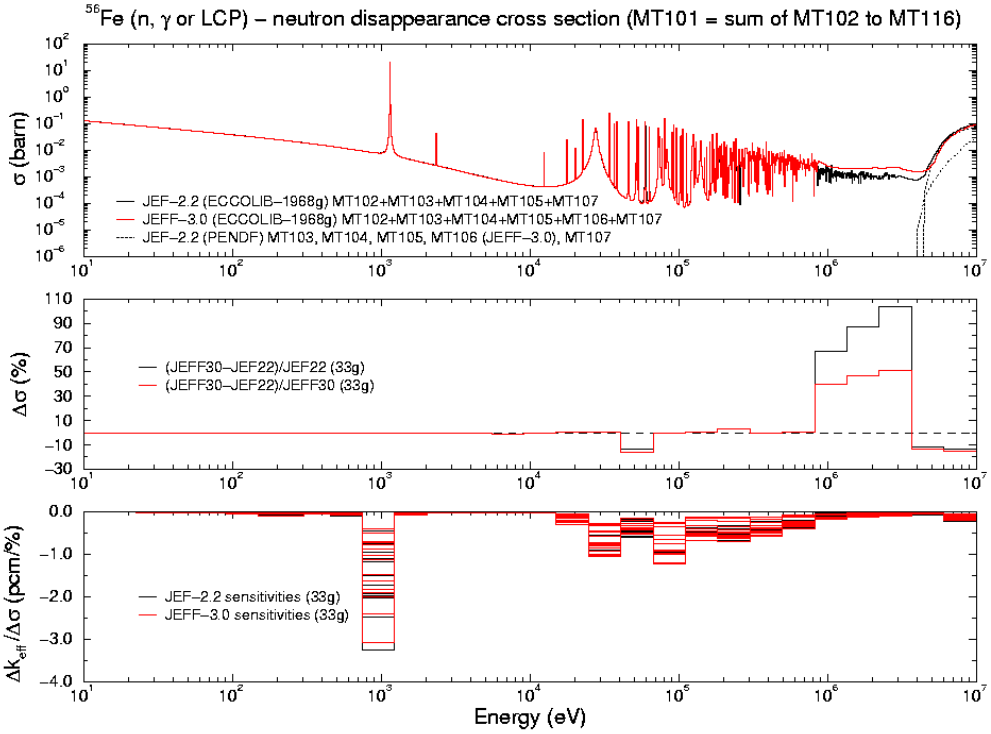
56Fe (n, γ or LCP) – neutron disappearance cross section (MT101 = sum of MT102 to MT116)
σ (barn)
JEF–2.2 (ECCOLIB–1968g) MT102+MT103+MT104+MT105+MT107
JEFF–3.0 (ECCOLIB–1968g) MT102+MT103+MT104+MT105+MT106+MT107
JEF–2.2 (PENDF) MT103, MT104, MT105, MT106 (JEFF–3.0), MT107
Δσ (%)
(JEFF30–JEF22)/JEF22 (33g)
(JEFF30–JEF22)/JEFF30 (33g)
ΔkeffΔσ (pcm/%)
JEF–2.2 sensitivities (33g)
JEFF–3.0 sensitivities (33g)
Energy (eV)

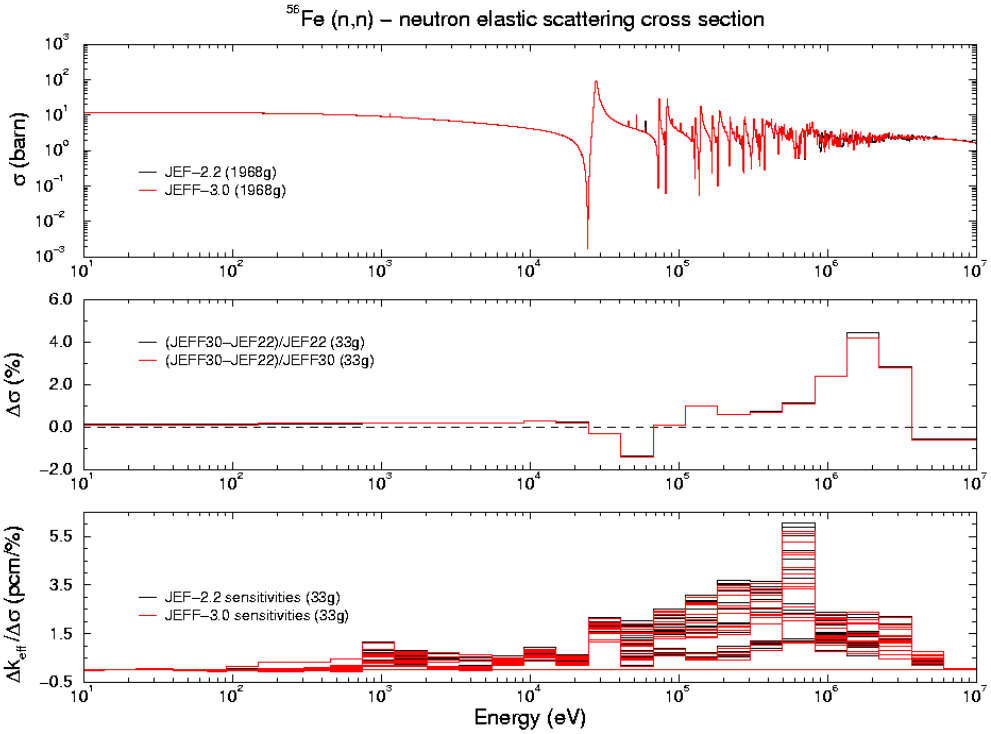
56Fe (n,n) – neutron elastic scattering cross section
σ (barn)
JEF–2.2 (1968g)
JEFF–3.0 (1968g)
Δσ (%)
(JEFF30–JEF22)/JEF22 (33g)
(JEFF30–JEF22)/JEFF30 (33g)
ΔkeffΔσ (pcm/%)
JEF–2.2 sensitivities (33g)
JEFF–3.0 sensitivities (33g)
Energy (eV)

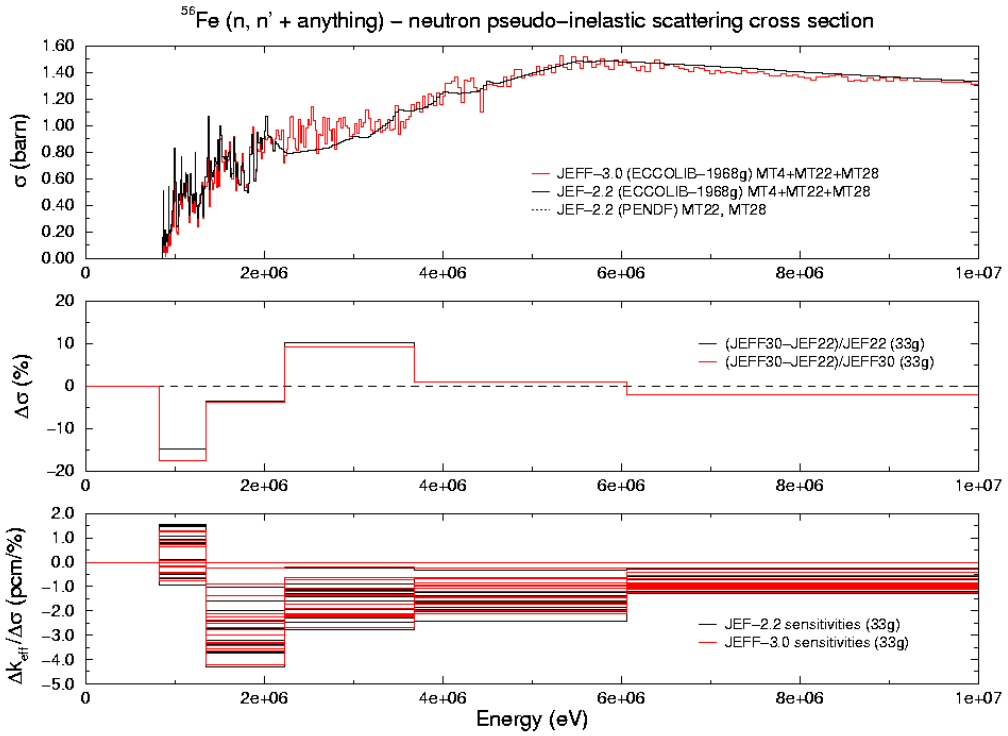
56Fe (n, n' + anything) – neutron pseudo–inelastic scattering cross section
σ (barn)
JEFF–3.0 (ECCOLIB–1968g) MT4+MT22+MT28
JEF–2.2 (ECCOLIB–1968g) MT4+MT22+MT28
JEF–2.2 (PENDF) MT22, MT28
Δσ (%)
(JEFF30–JEF22)/JEF22 (33g)
(JEFF30–JEF22)/JEFF30 (33g)
ΔkeffΔσ (pcm/%)
JEF–2.2 sensitivities (33g)
JEFF–3.0 sensitivities (33g)
Energy (eV)

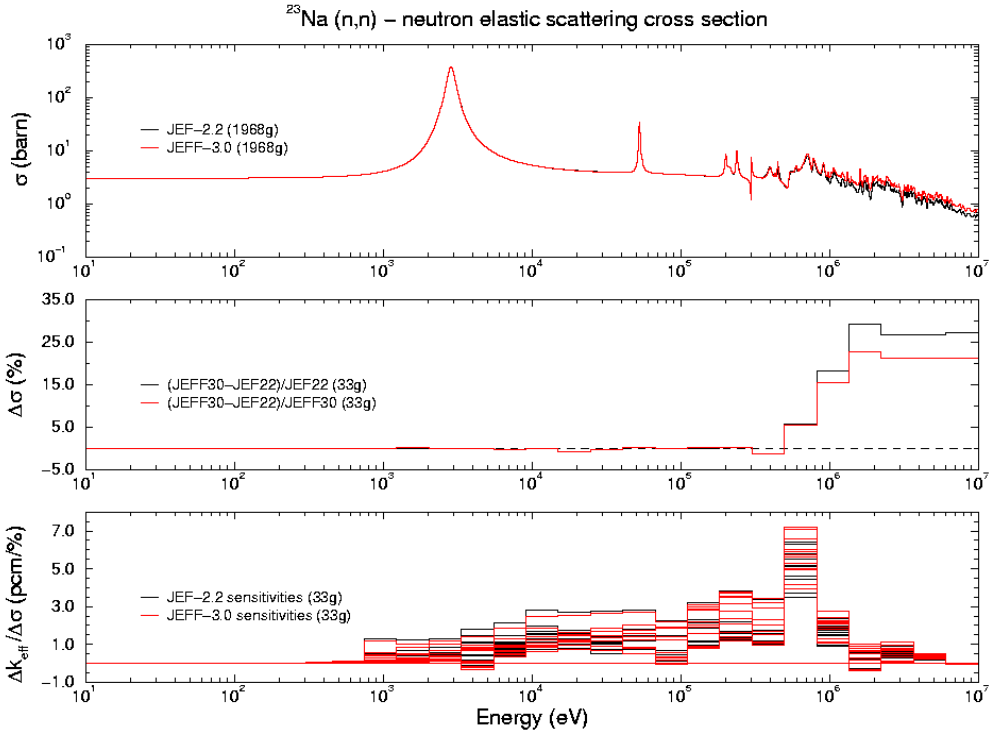
23Na (n,n) – neutron elastic scattering cross section
σ (barn)
JEF–2.2 (1968g)
JEFF–3.0 (1968g)
Δσ (%)
(JEFF30–JEF22)/JEF22 (33g)
(JEFF30–JEF22)/JEFF30 (33g)
ΔkeffΔσ (pcm/%)
JEF–2.2 sensitivities (33g)
JEFF–3.0 sensitivities (33g)
Energy (eV)

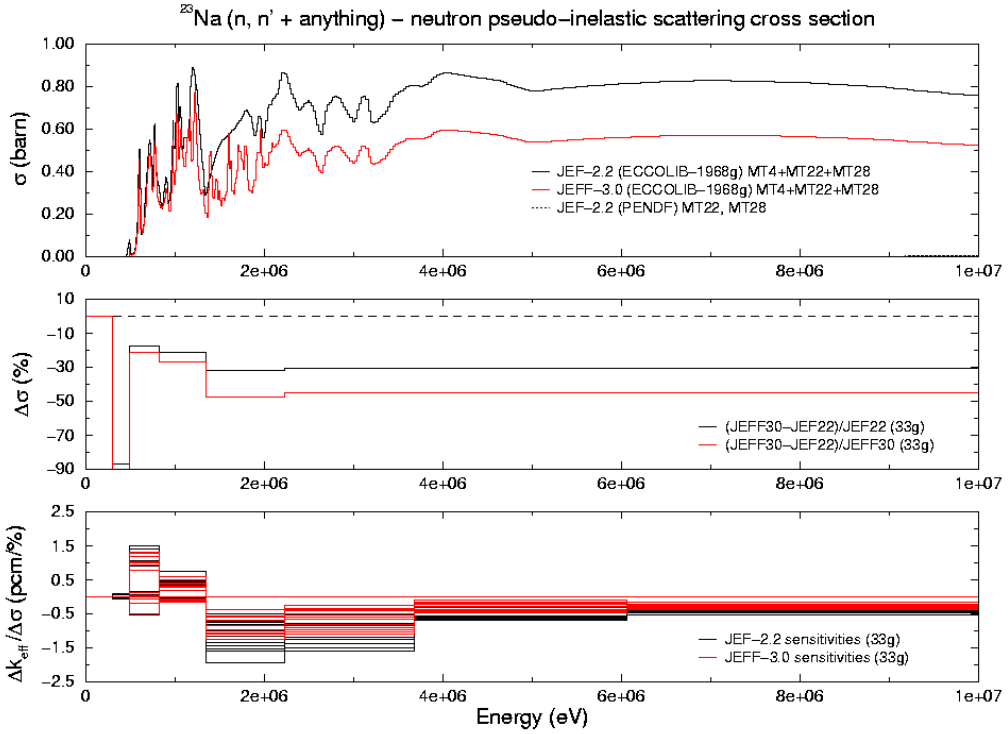
^{23}Na (n, n' + anything) – neutron pseudo–inelastic scattering cross section
σ (barn)
JEF–2.2 (ECCOLIB–1968g) MT4+MT22+MT28
JEFF–3.0 (ECCOLIB–1968g) MT4+MT22+MT28
JEF–2.2 (PENDF) MT22, MT28
Δσ (%)
(JEFF30–JEF22)/JEF22 (33g)
(JEFF30–JEF22)/JEFF30 (33g)
$\Delta k_{eff}/\Delta\sigma$ (pcm/%)
JEF–2.2 sensitivities (33g)
JEFF–3.0 sensitivities (33g)
Energy (eV)

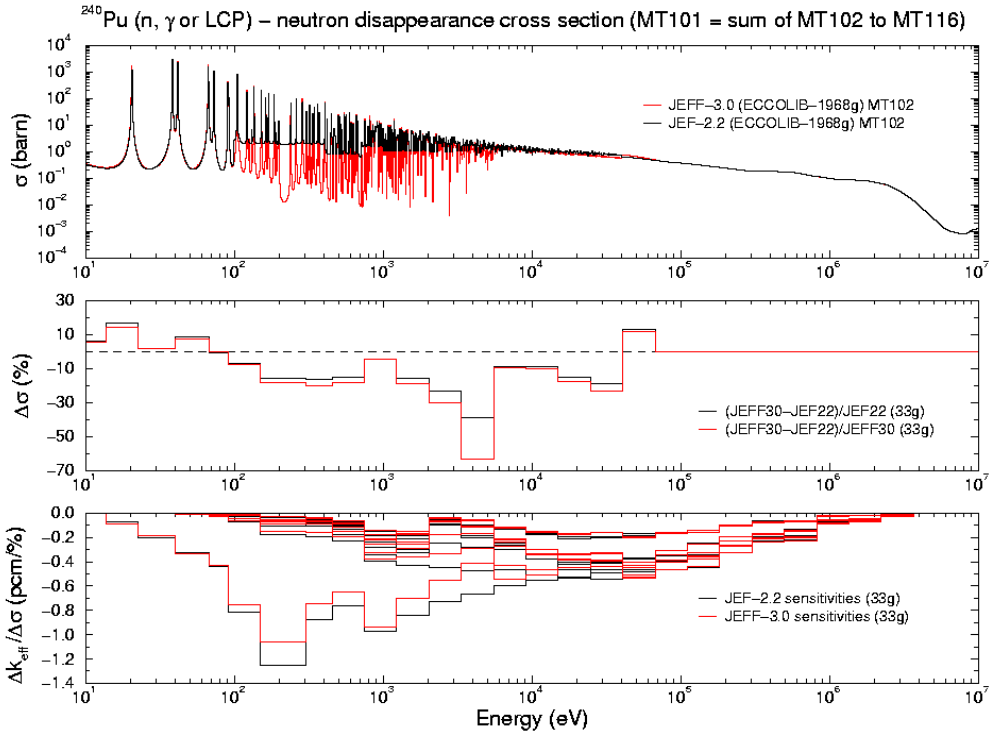
^{240}Pu (n, γ or LCP) – neutron disappearance cross section (MT101 = sum of MT102 to MT116)
σ (barn)
JEFF–3.0 (ECCOLIB–1968g) MT102
JEF–2.2 (ECCOLIB–1968g) MT102
Δσ (%)
(JEFF30–JEF22)/JEF22 (33g)
(JEFF30–JEF22)/JEFF30 (33g)
$\Delta k_{eff}/\Delta\sigma$ (pcm/%)
JEF–2.2 sensitivities (33g)
JEFF–3.0 sensitivities (33g)
Energy (eV)

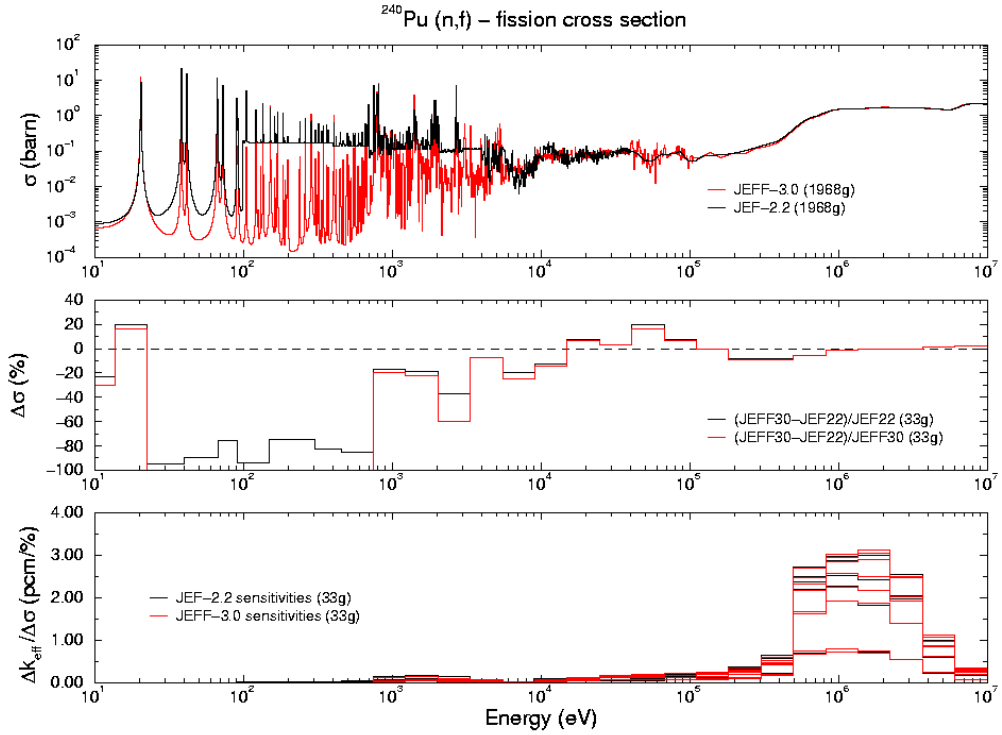
240Pu (n,f) – fission cross section
σ (barn)
JEFF–3.0 (1968g)
JEF–2.2 (1968g)
Δσ (%)
(JEFF30–JEF22)/JEF22 (33g)
(JEFF30–JEF22)/JEFF30 (33g)
Δk_eff /Δσ (pcm/%)
JEF–2.2 sensitivities (33g)
JEFF–3.0 sensitivities (33g)
Energy (eV)

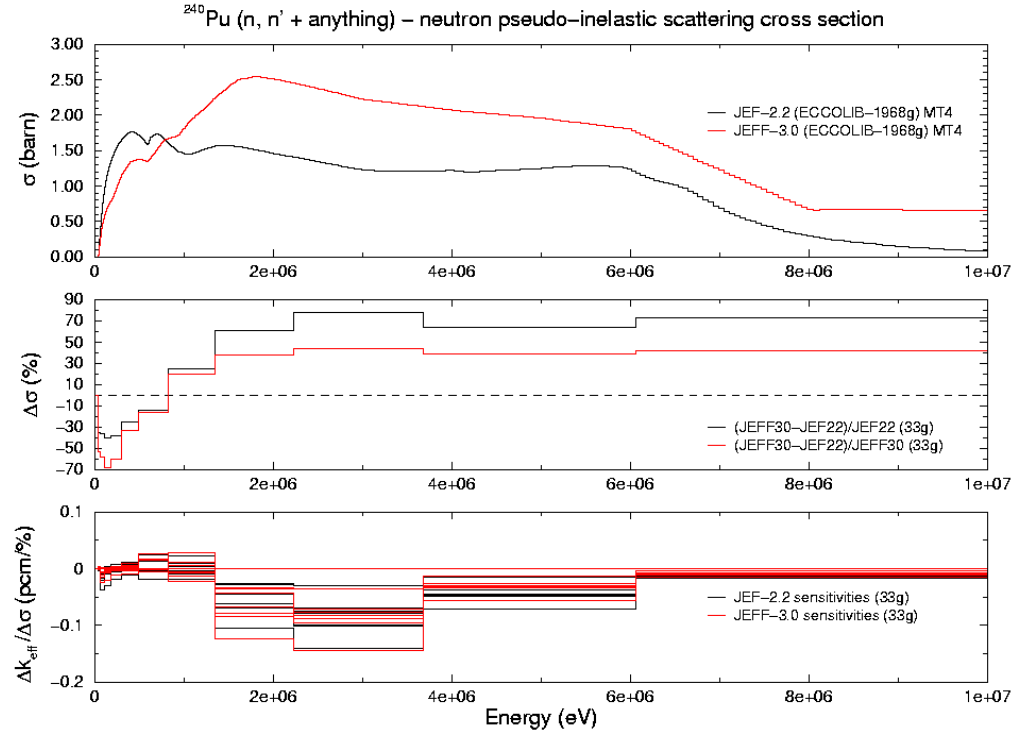
240Pu (n, n' + anything) – neutron pseudo–inelastic scattering cross section
σ (barn)
JEF–2.2 (ECCOLIB–1968g) MT4
JEFF–3.0 (ECCOLIB–1968g) MT4
Δσ (%)
(JEFF30–JEF22)/JEF22 (33g)
(JEFF30–JEF22)/JEFF30 (33g)
Δk_eff /Δσ (pcm/%)
JEF–2.2 sensitivities (33g)
JEFF–3.0 sensitivities (33g)
Energy (eV)

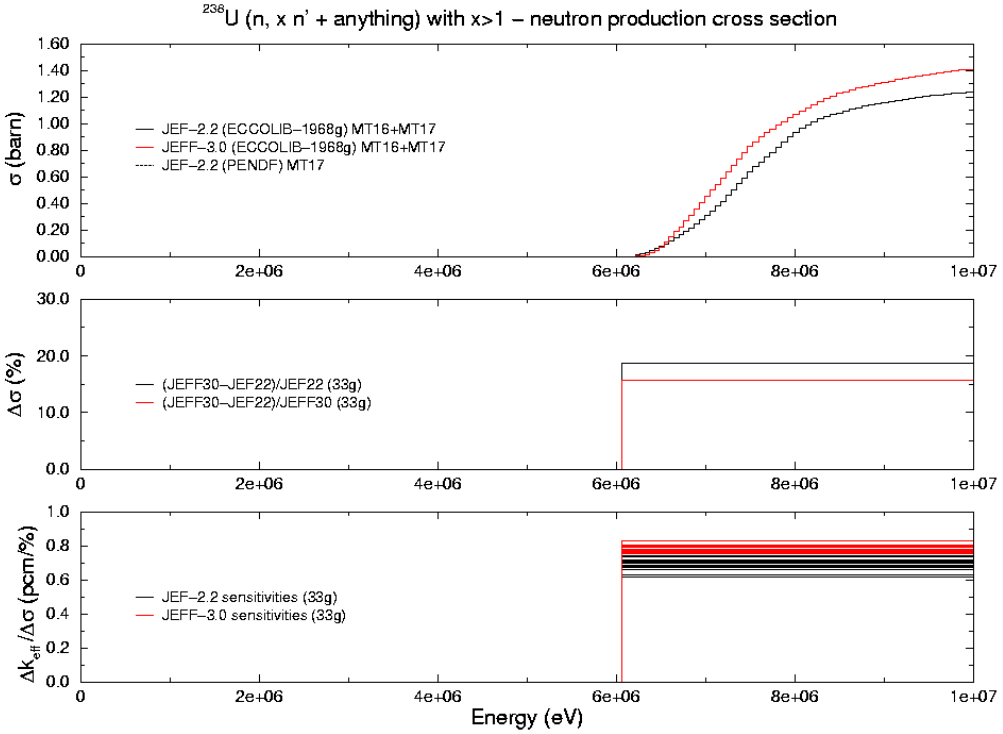
^{238}U (n, x n' + anything) with x>1 – neutron production cross section
σ (barn)
JEF–2.2 (ECCOLIB–1968g) MT16+MT17
JEFF–3.0 (ECCOLIB–1968g) MT16+MT17
JEF–2.2 (PENDF) MT17
Δσ (%)
(JEFF30–JEF22)/JEF22 (33g)
(JEFF30–JEF22)/JEFF30 (33g)
Δk$_{eff}$/Δσ (pcm/%)
JEF–2.2 sensitivities (33g)
JEFF–3.0 sensitivities (33g)
Energy (eV)

Appendix 2

The eight following histograms (MAS1AP to SNEAK7B) show for every "plutonium" core, the main differential contributions to the calculated k_{eff} difference when using JEFF-3.0 and JEF-2.2 libraries.

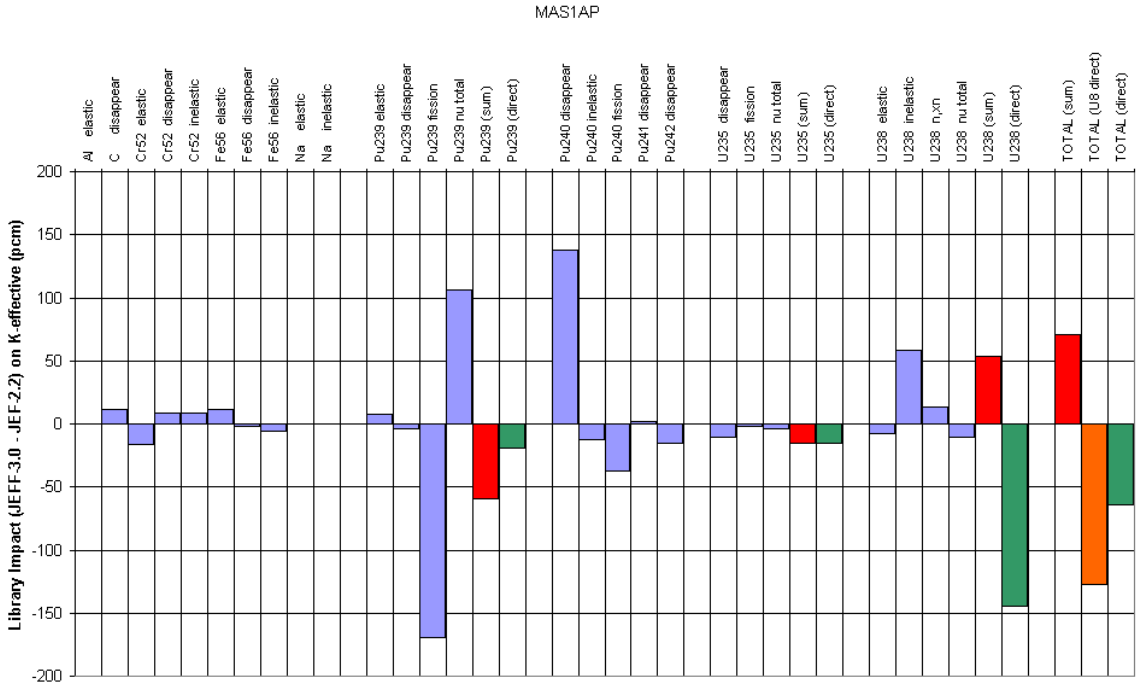

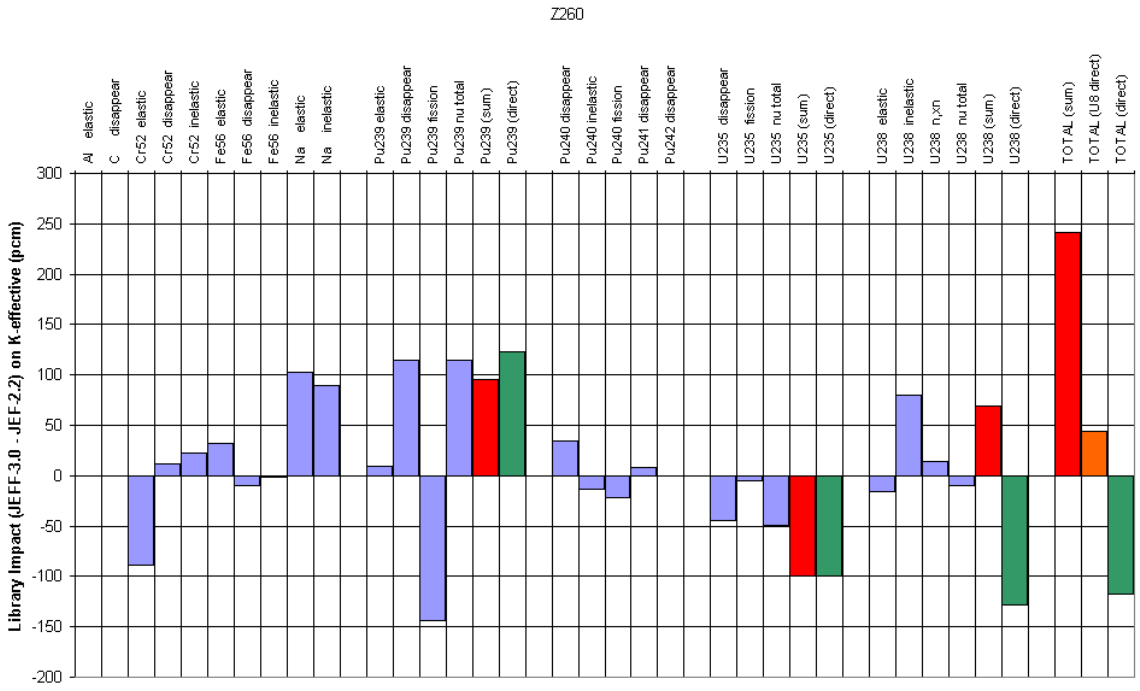

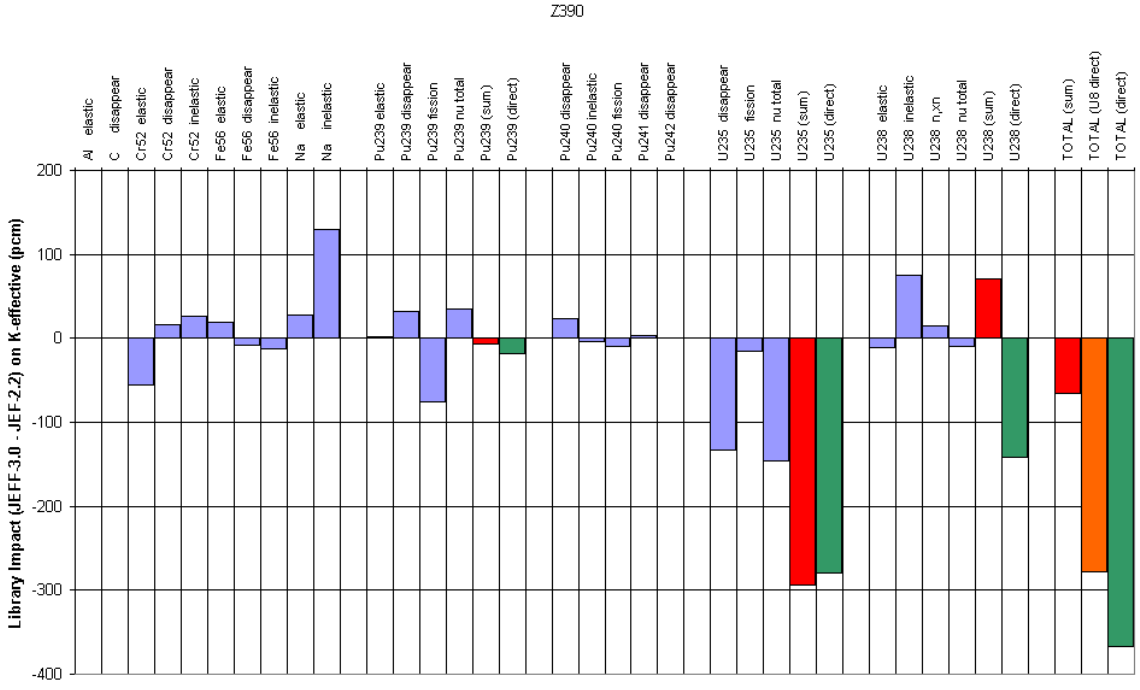
Z390
Library Impact (JEFF-3.0 - JEF-2.2) on K-effective (pcm)
200
100
0
-100
-200
-300
-400
Al elastic
C disappear
Cr52 elastic
Cr52 disappear
Cr52 inelastic
Fe56 elastic
Fe56 disappear
Fe56 inelastic
Na elastic
Na inelastic
Pu239 elastic
Pu239 disappear
Pu239 fission
Pu239 nu total
Pu239 (sum)
Pu239 (direct)
Pu240 disappear
Pu240 inelastic
Pu240 fission
Pu241 disappear
Pu242 disappear
U235 disappear
U235 fission
U235 nu total
U235 (sum)
U235 (direct)
U238 elastic
U238 inelastic
U238 n,xn
U238 nu total
U238 (sum)
U238 (direct)
TOTAL (sum)
TOTAL (U8 direct)
TOTAL (direct)

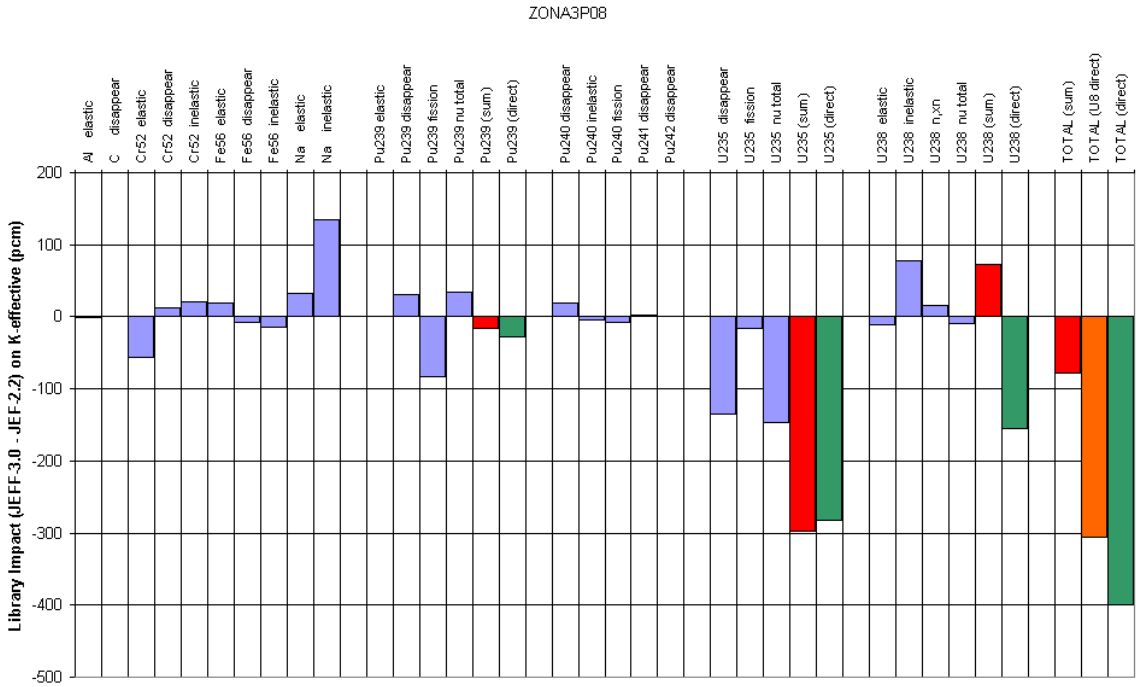
ZONA3P08
Library Impact (JEFF-3.0 - JEF-2.2) on K-effective (pcm)
200
100
0
-100
-200
-300
-400
-500
Al elastic
C disappear
Cr52 elastic
Cr52 disappear
Cr52 inelastic
Fe56 elastic
Fe56 disappear
Fe56 inelastic
Na elastic
Na inelastic
Pu239 elastic
Pu239 disappear
Pu239 fission
Pu239 nu total
Pu239 (sum)
Pu239 (direct)
Pu240 disappear
Pu240 inelastic
Pu240 fission
Pu241 disappear
Pu242 disappear
U235 disappear
U235 fission
U235 nu total
U235 (sum)
U235 (direct)
U238 elastic
U238 inelastic
U238 n,xn
U238 nu total
U238 (sum)
U238 (direct)
TOTAL (sum)
TOTAL (U8 direct)
TOTAL (direct)

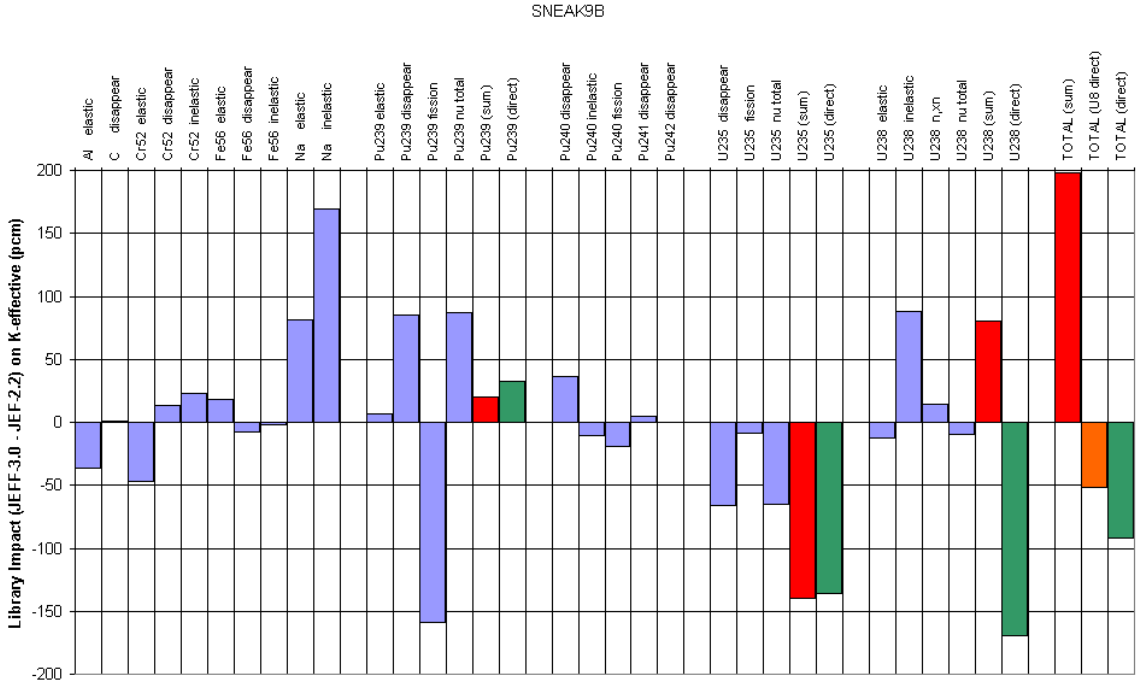
SNEAK9B
Library Impact (JEFF-3.0 - JEF-2.2) on K-effective (pcm)
200
150
100
50
0
-50
-100
-150
-200
Al elastic
C disappear
Cr52 elastic
Cr52 disappear
Cr52 inelastic
Fe56 elastic
Fe56 disappear
Fe56 inelastic
Na elastic
Na inelastic
Pu239 elastic
Pu239 disappear
Pu239 fission
Pu239 nu total
Pu239 (sum)
Pu239 (direct)
Pu240 disappear
Pu240 inelastic
Pu240 fission
Pu241 disappear
Pu242 disappear
U235 disappear
U235 fission
U235 nu total
U235 (sum)
U235 (direct)
U238 elastic
U238 inelastic
U238 n,xn
U238 nu total
U238 (sum)
U238 (direct)
TOTAL (sum)
TOTAL (U8 direct)
TOTAL (direct)

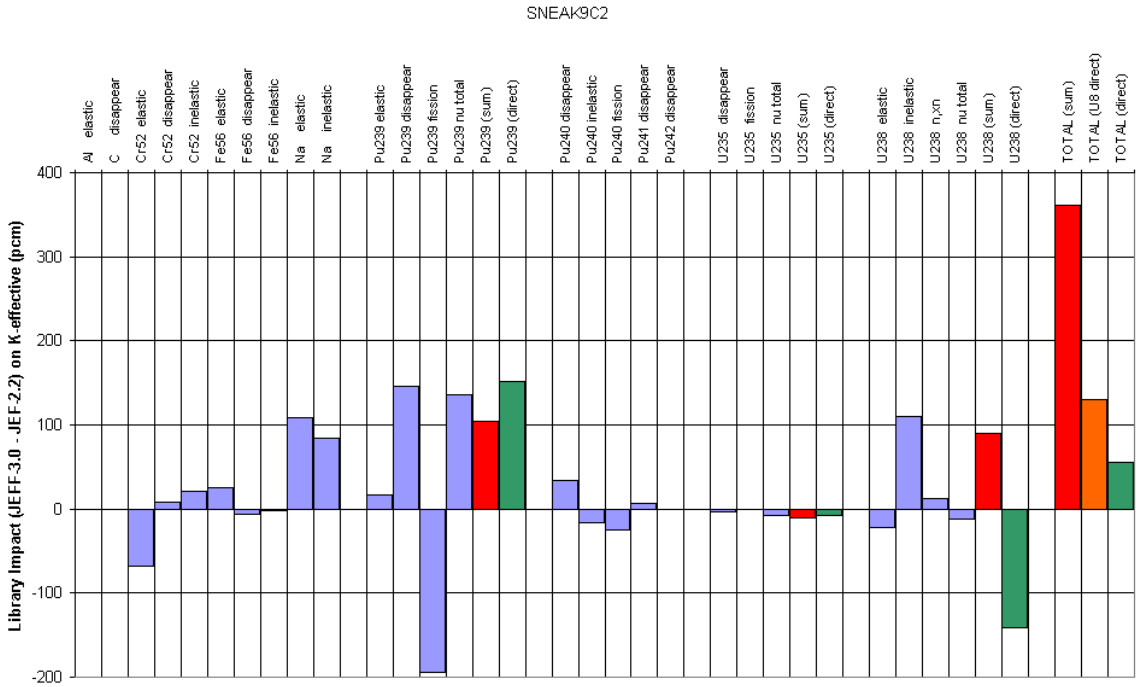
SNEAK9C2
Library Impact (JEFF-3.0 - JEF-2.2) on K-effective (pcm)
400
300
200
100
0
-100
-200
Al elastic
C disappear
Cr52 elastic
Cr52 disappear
Cr52 inelastic
Fe56 elastic
Fe56 disappear
Fe56 inelastic
Na elastic
Na inelastic
Pu239 elastic
Pu239 disappear
Pu239 fission
Pu239 nu total
Pu239 (sum)
Pu239 (direct)
Pu240 disappear
Pu240 inelastic
Pu240 fission
Pu241 disappear
Pu242 disappear
U235 disappear
U235 fission
U235 nu total
U235 (sum)
U235 (direct)
U238 elastic
U238 inelastic
U238 n,xn
U238 nu total
U238 (sum)
U238 (direct)
TOTAL (sum)
TOTAL (U8 direct)
TOTAL (direct)

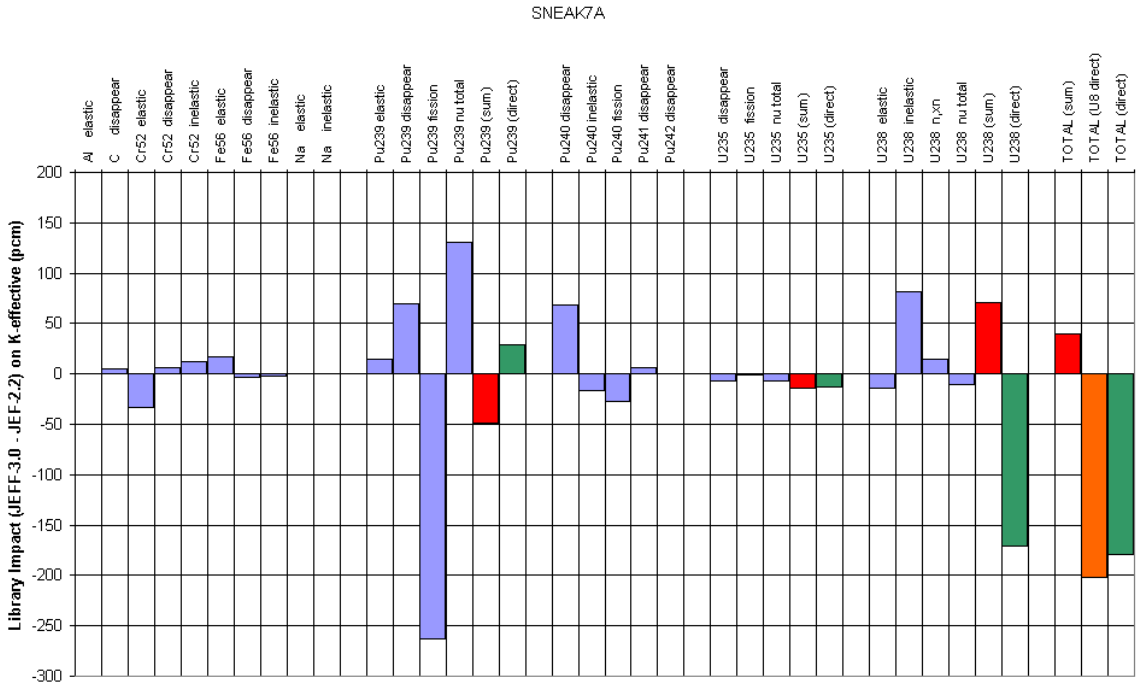
SNEAK7A
Library Impact (JEFF-3.0 - JEF-2.2) on K-effective (pcm)
200
150
100
50
0
-50
-100
-150
-200
-250
-300
Al elastic
C disappear
Cr52 elastic
Cr52 disappear
Cr52 inelastic
Fe56 elastic
Fe56 disappear
Fe56 inelastic
Na elastic
Na inelastic
Pu239 elastic
Pu239 disappear
Pu239 fission
Pu239 nu total
Pu239 (sum)
Pu239 (direct)
Pu240 disappear
Pu240 inelastic
Pu240 fission
Pu241 disappear
Pu242 disappear
U235 disappear
U235 fission
U235 nu total
U235 (sum)
U235 (direct)
U238 elastic
U238 inelastic
U238 n,xn
U238 nu total
U238 (sum)
U238 (direct)
TOTAL (sum)
TOTAL (U8 direct)
TOTAL (direct)

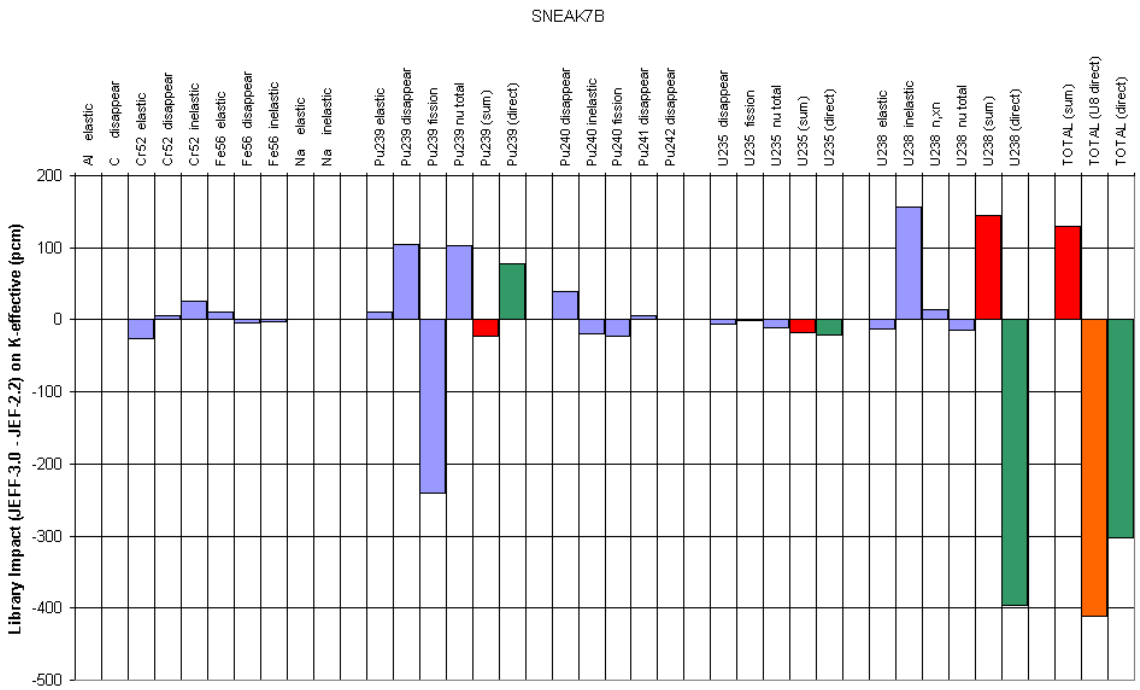
SNEAK7B
Library Impact (JEFF-3.0 - JEF-2.2) on K-effective (pcm)
200
100
0
-100
-200
-300
-400
-500
Al elastic
C disappear
Cr52 elastic
Cr52 disappear
Cr52 inelastic
Fe56 elastic
Fe56 disappear
Fe56 inelastic
Na elastic
Na inelastic
Pu239 elastic
Pu239 disappear
Pu239 fission
Pu239 nu total
Pu239 (sum)
Pu239 (direct)
Pu240 disappear
Pu240 inelastic
Pu240 fission
Pu241 disappear
Pu242 disappear
U235 disappear
U235 fission
U235 nu total
U235 (sum)
U235 (direct)
U238 elastic
U238 inelastic
U238 n,xn
U238 nu total
U238 (sum)
U238 (direct)
TOTAL (sum)
TOTAL (U8 direct)
TOTAL (direct)

These last eight histograms (R390 to SNEAK9C1) show for every "uranium" core, the main differential contributions to the calculated k_{eff} difference when using JEFF-3.0 and JEF-2.2 libraries.

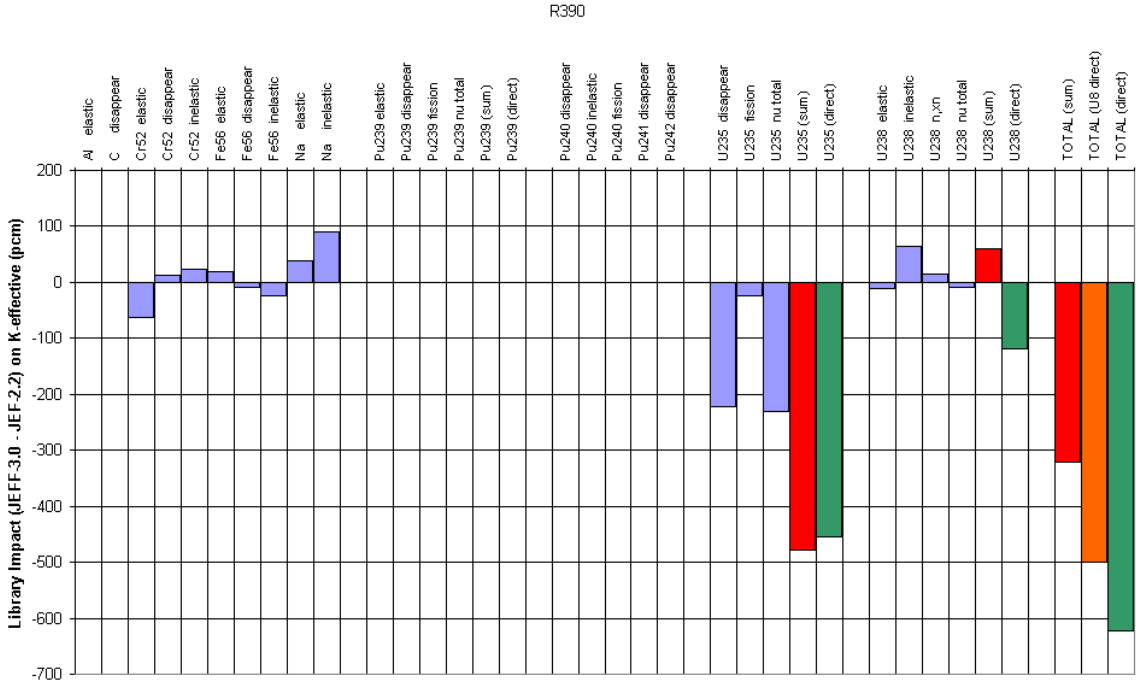

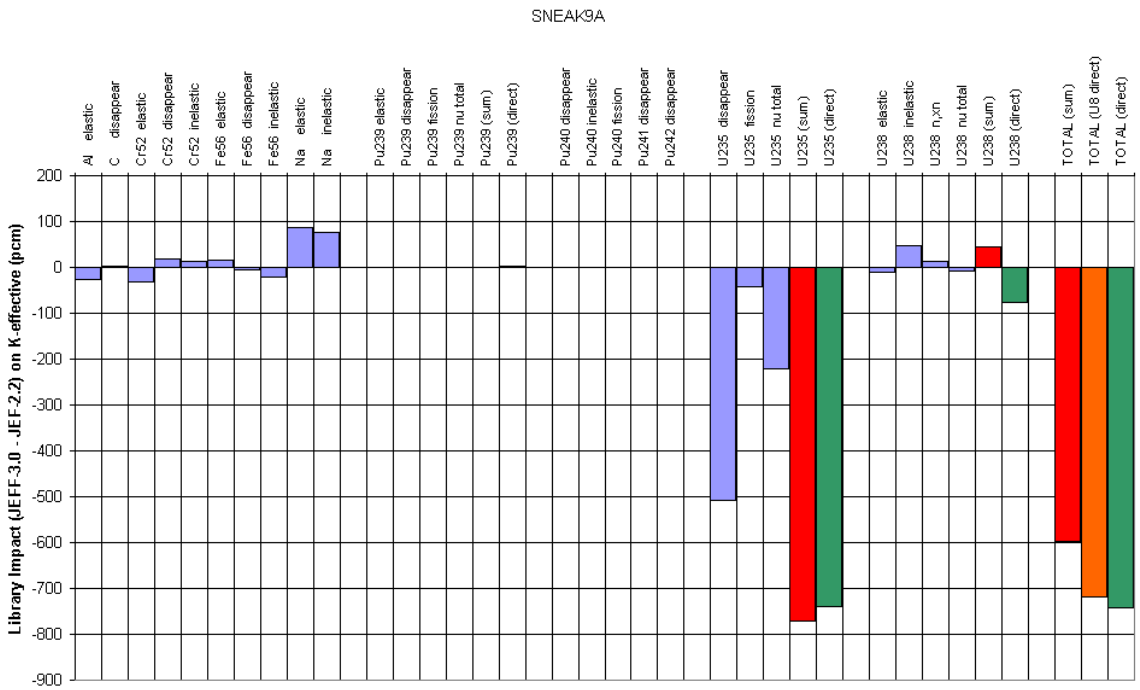

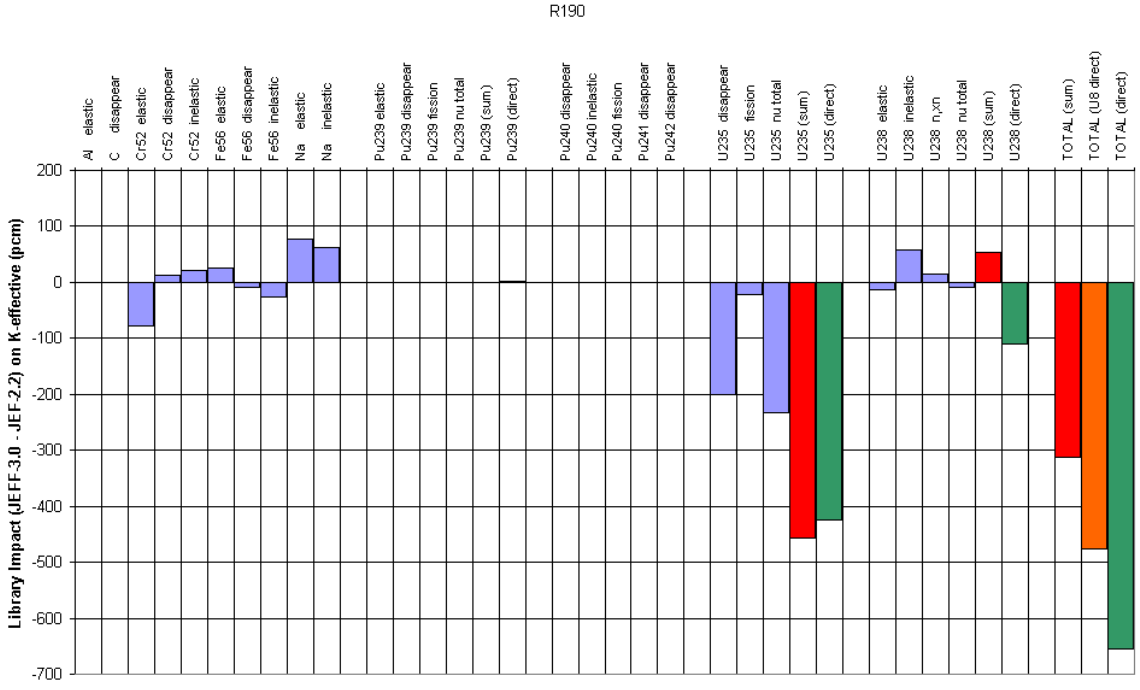
R190
Library Impact (JEFF-3.0 - JEF-2.2) on K-effective (pcm)
200
100
0
-100
-200
-300
-400
-500
-600
-700
Al elastic
C disappear
Cr52 elastic
Cr52 disappear
Cr52 inelastic
Fe56 elastic
Fe56 disappear
Fe56 inelastic
Na elastic
Na inelastic
Pu239 elastic
Pu239 disappear
Pu239 fission
Pu239 nu total
Pu239 (sum)
Pu239 (direct)
Pu240 disappear
Pu240 inelastic
Pu240 fission
Pu241 disappear
Pu242 disappear
U235 disappear
U235 fission
U235 nu total
U235 (sum)
U235 (direct)
U238 elastic
U238 inelastic
U238 n,xn
U238 nu total
U238 (sum)
U238 (direct)
TOTAL (sum)
TOTAL (U8 direct)
TOTAL (direct)

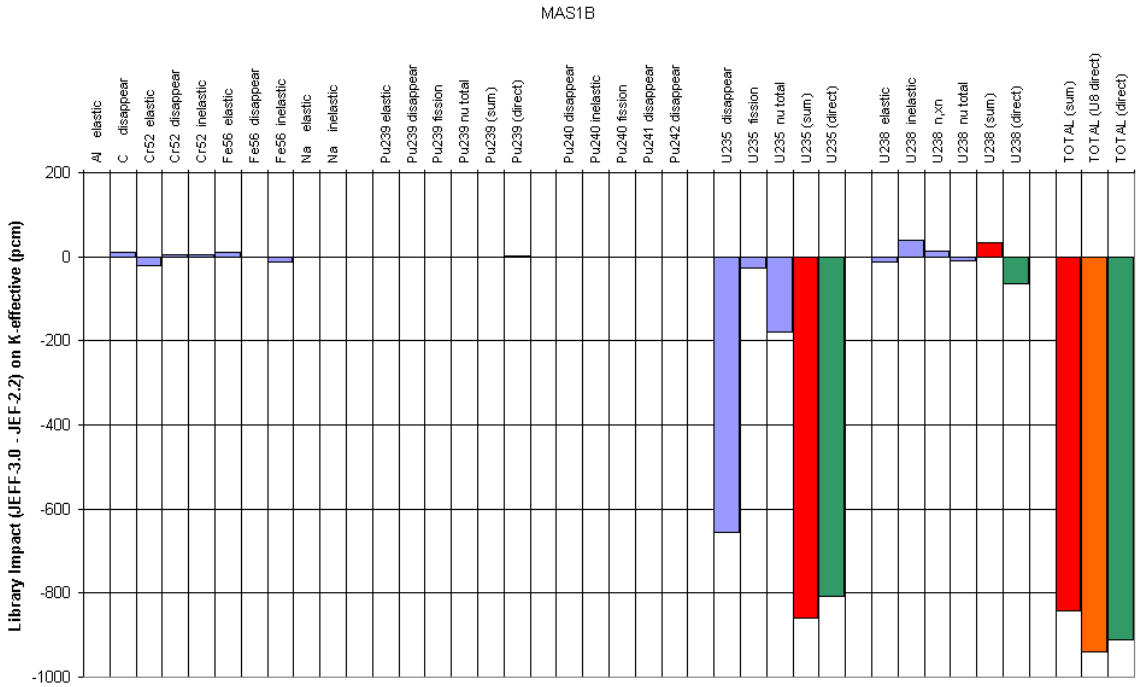
MAS1B
Library Impact (JEFF-3.0 - JEF-2.2) on K-effective (pcm)
200
0
-200
-400
-600
-800
-1000
Al elastic
C disappear
Cr52 elastic
Cr52 disappear
Cr52 inelastic
Fe56 elastic
Fe56 disappear
Fe56 inelastic
Na elastic
Na inelastic
Pu239 elastic
Pu239 disappear
Pu239 fission
Pu239 nu total
Pu239 (sum)
Pu239 (direct)
Pu240 disappear
Pu240 inelastic
Pu240 fission
Pu241 disappear
Pu242 disappear
U235 disappear
U235 fission
U235 nu total
U235 (sum)
U235 (direct)
U238 elastic
U238 inelastic
U238 n,xn
U238 nu total
U238 (sum)
U238 (direct)
TOTAL (sum)
TOTAL (U8 direct)
TOTAL (direct)

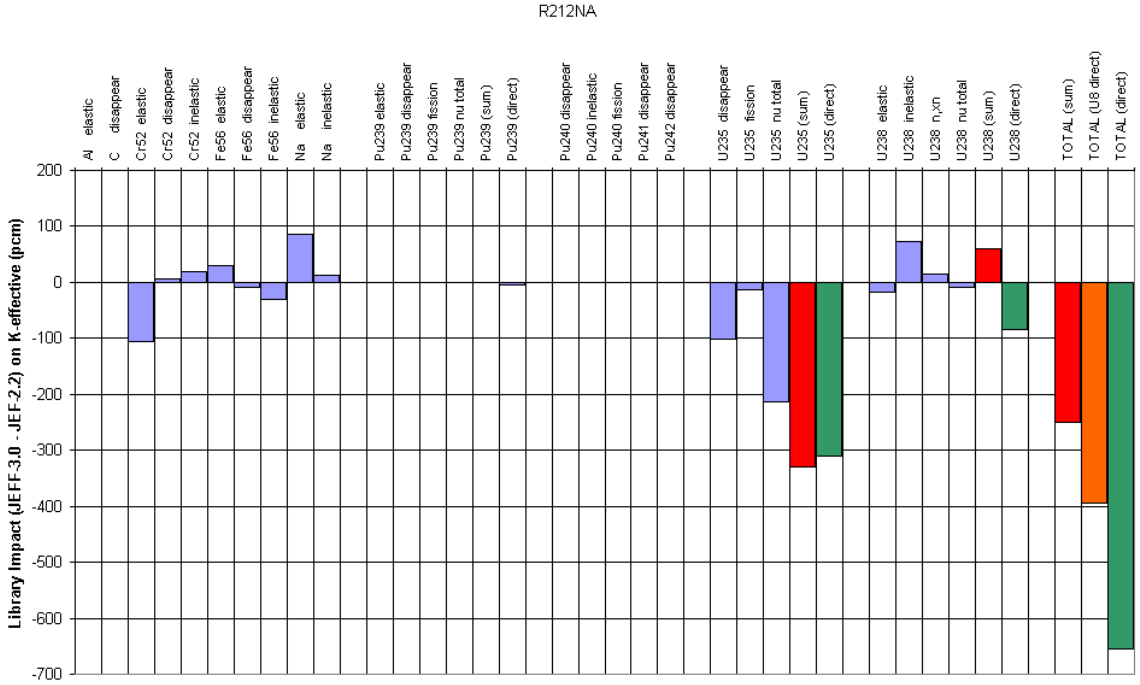
R212NA
Library Impact (JEFF-3.0 - JEF-2.2) on K-effective (pcm)
200
100
0
-100
-200
-300
-400
-500
-600
-700
Al elastic
C disappear
Cr52 elastic
Cr52 disappear
Cr52 inelastic
Fe56 elastic
Fe56 disappear
Fe56 inelastic
Na elastic
Na inelastic
Pu239 elastic
Pu239 disappear
Pu239 fission
Pu239 nu total
Pu239 (sum)
Pu239 (direct)
Pu240 disappear
Pu240 inelastic
Pu240 fission
Pu241 disappear
Pu242 disappear
U235 disappear
U235 fission
U235 nu total
U235 (sum)
U235 (direct)
U238 elastic
U238 inelastic
U238 n,xn
U238 nu total
U238 (sum)
U238 (direct)
TOTAL (sum)
TOTAL (U8 direct)
TOTAL (direct)

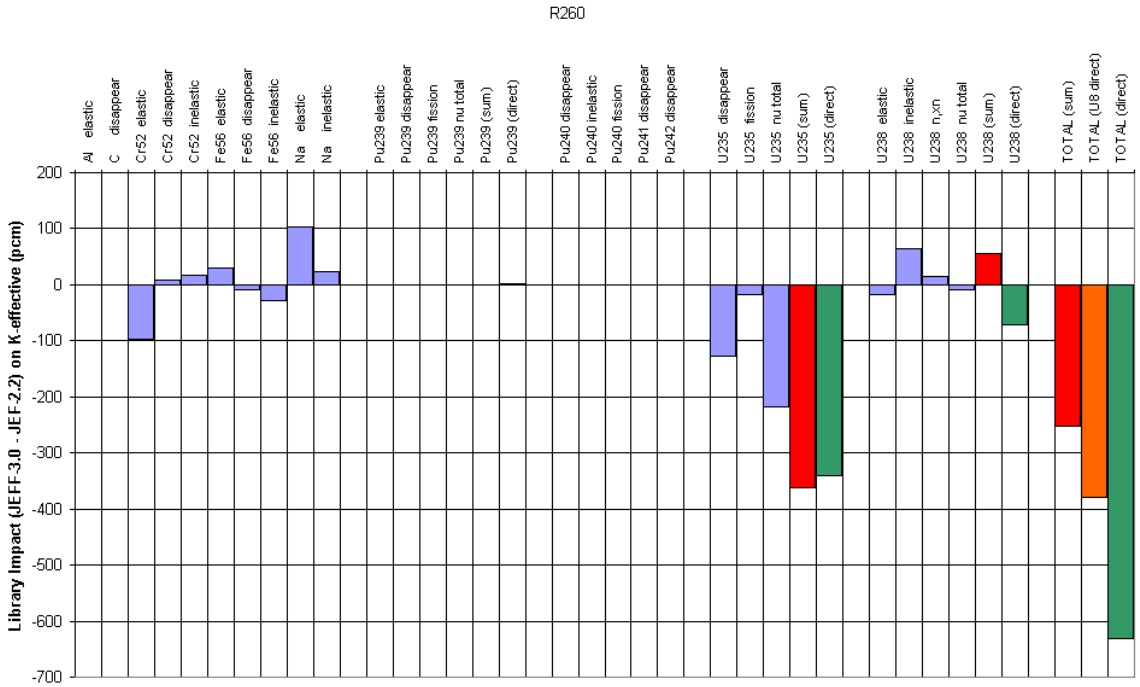
R260
Library Impact (JEFF-3.0 - JEF-2.2) on K-effective (pcm)
200
100
0
-100
-200
-300
-400
-500
-600
-700
Al elastic
C disappear
Cr52 elastic
Cr52 disappear
Cr52 inelastic
Fe56 elastic
Fe56 disappear
Fe56 inelastic
Na elastic
Na inelastic
Pu239 elastic
Pu239 disappear
Pu239 fission
Pu239 nu total
Pu239 (sum)
Pu239 (direct)
Pu240 disappear
Pu240 inelastic
Pu240 fission
Pu241 disappear
Pu242 disappear
U235 disappear
U235 fission
U235 nu total
U235 (sum)
U235 (direct)
U238 elastic
U238 inelastic
U238 n,xn
U238 nu total
U238 (sum)
U238 (direct)
TOTAL (sum)
TOTAL (U8 direct)
TOTAL (direct)

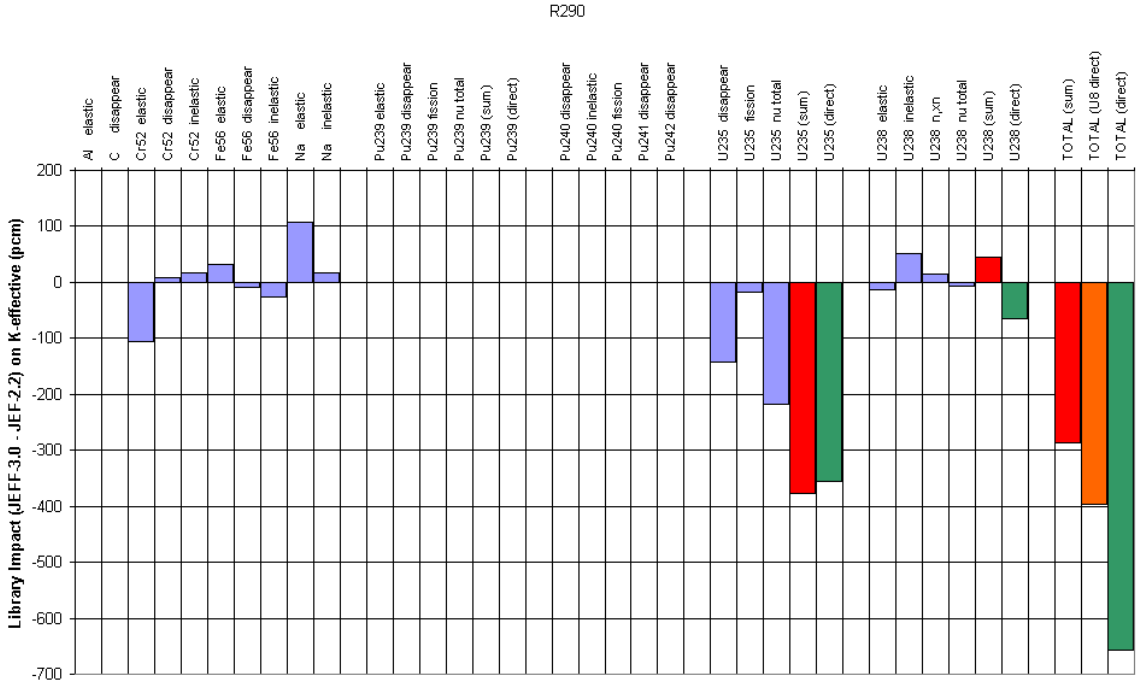
R290
Library Impact (JEFF-3.0 - JEF-2.2) on K-effective (pcm)
200
100
0
-100
-200
-300
-400
-500
-600
-700
Al elastic
C disappear
Cr52 elastic
Cr52 disappear
Cr52 inelastic
Fe56 elastic
Fe56 disappear
Fe56 inelastic
Na elastic
Na inelastic
Pu239 elastic
Pu239 disappear
Pu239 fission
Pu239 nu total
Pu239 (sum)
Pu239 (direct)
Pu240 disappear
Pu240 inelastic
Pu240 fission
Pu241 disappear
Pu242 disappear
U235 disappear
U235 fission
U235 nu total
U235 (sum)
U235 (direct)
U238 elastic
U238 inelastic
U238 n,xn
U238 nu total
U238 (sum)
U238 (direct)
TOTAL (sum)
TOTAL (U8 direct)
TOTAL (direct)

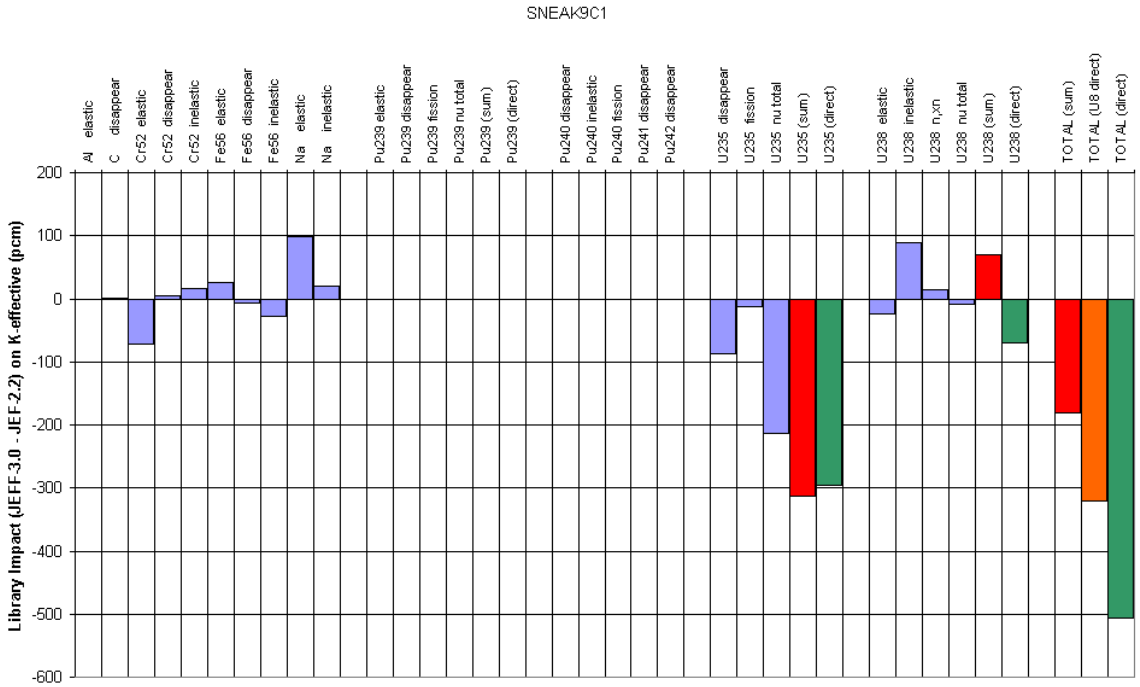
SNEAK9C1
Library Impact (JEFF-3.0 - JEF-2.2) on K-effective (pcm)
200
100
0
-100
-200
-300
-400
-500
-600
Al elastic
C disappear
Cr52 elastic
Cr52 disappear
Cr52 inelastic
Fe56 elastic
Fe56 disappear
Fe56 inelastic
Na elastic
Na inelastic
Pu239 elastic
Pu239 disappear
Pu239 fission
Pu239 nu total
Pu239 (sum)
Pu239 (direct)
Pu240 disappear
Pu240 inelastic
Pu240 fission
Pu241 disappear
Pu242 disappear
U235 disappear
U235 fission
U235 nu total
U235 (sum)
U235 (direct)
U238 elastic
U238 inelastic
U238 n,xn
U238 nu total
U238 (sum)
U238 (direct)
TOTAL (sum)
TOTAL (U8 direct)
TOTAL (direct)

2.2.2 Analyse des expériences PROFIL pour la validation des données

Certaines mesures en réacteurs sont moins "intégrales" que le k_{eff} et peuvent même permettre de valider (presque) directement des sections efficaces. On peut citer par exemple les expériences PROFIL et PROFIL2 réalisées dans le réacteur Phénix. Ces expériences d'irradiation de nombreux échantillons isotopiquement purs sont une source d'information sur les sections efficaces des actinides et des produits de fission [Dupont 02b] [Dupont 05c] [Tommasi 06].

Les résultats présentés dans le tableau suivant montrent la bonne qualité globale des sections efficaces des actinides de JEFF-3.0 et indiquent les données à améliorer. La colonne *"$\Delta\sigma/\sigma$ (%)"* indique la tendance déduite de l'écart calcul-expérience *"C/E (ratio)"* en tenant compte de la sensibilité de ce ratio à la section efficace.

Concernant le cycle Th/U, les sections efficaces de capture de Th-232 et U-233 sont encore nettement sous-estimées. Pour ce qui est du cycle U/Pu, l'amélioration doit porter principalement sur les sections de capture de Pu-241,242 (et dans une moindre mesure Pu-240 et Np-237), ainsi que sur les sections et sur le taux d'embranchement de la capture de Am-241.

Résultats des irradiations PROFIL pour les actinides des cycles Th/U et U/Pu

Échantillon	***Ratio étudié***	***C/E (ratio)***	***Expérience***	***Section-efficace (σ)***	***$\Delta\sigma/\sigma$ (%)***
^{232}Th	^{233}U/^{232}Th	0.836 ± 0.076	PROFIL2	^{232}Th(n,γ)	-19.0
^{233}U	^{234}U/^{233}U	0.915 ± 0.001	PROFIL2	^{233}U(n,γ)	-9.4
^{234}U	^{235}U/^{234}U	1.031 ± 0.002	PROFIL2	^{234}U(n,γ)	2.9
^{238}U	^{239}Pu/^{238}U	1.011 ± 0.003	PROFIL	^{238}U(n,γ)	1.1
^{237}Np	^{238}Pu/^{237}Np	0.94 ± 0.013	PROFIL2	^{237}Np(n,γ)	-5.6
^{238}Pu	^{239}Pu/^{238}Pu	1.019 ± 0.008	PROFIL	^{238}Pu(n,γ)	1.6
^{239}Pu	^{240}Pu/^{239}Pu	0.979 ± 0.002	PROFIL	^{239}Pu(n,γ)	-2.1
^{240}Pu	^{241}Pu/^{240}Pu	1.052 ± 0.005	PROFIL	^{240}Pu(n,γ)	4.8
^{241}Pu	^{242}Pu/^{241}Pu	1.093 ± 0.007	PROFIL	^{241}Pu(n,γ)	9.8
^{242}Pu	^{243}Am/^{242}Pu	1.209 ± 0.018	PROFIL	^{242}Pu(n,γ)	16.9
^{241}Am	^{242m}Am/^{241}Am	1.087 ± 0.019	PROFIL	^{241}Am(n,γ)^{242m}Am(1)	7.4
^{241}Am	^{238}Pu/^{241}Am	1.055 ± 0.016	PROFIL	^{241}Am(n,γ)^{242gs}Am(1)	4.8
^{241}Am	^{242}Pu/^{241}Am	1.063 ± 0.015	PROFIL	^{241}Am(n,γ)^{242gs}Am(1)	5.4
^{241}Am	^{242}Cm/^{241}Am	1.045 ± 0.012	PROFIL	^{241}Am(n,γ)^{242gs}Am(1)	4.0
^{244}Cm	^{245}Cm/^{244}Cm	0.974 ± 0.003	PROFIL2	^{244}Cm(n,γ)	-2.5

(1) Avec un rapport d'embranchement de 15% vers l'état métastable ($T_{1/2}$ ~141 ans) et de 85% vers l'état fondamental ($T_{1/2}$ ~16h)

Une analyse similaire des résultats PROFIL a caractérisé le degré de précision des sections efficaces de capture des produits de fission de JEFF-3.0 et mis en évidence les améliorations nécessaires. Parmi les 19 produits de fission étudiés et listés dans le tableau suivant, la moitié est relativement satisfaisante ($\Delta\sigma/\sigma$ < 10%) :

Mo-95,97, Ru-101, Pd-106, Cs-133,134, Nd-144, Sm-149,150, Eu-153,

tandis que l'autre moitié est responsable d'écarts calcul/expérience supérieurs à 10% :

Pd-105,107, Nd-143,145, Sm-147,148,151, Eu-151,154.

Résultats des irradiations PROFIL pour les produits de fission

Échantillon	***Ratio étudié***	***C/E (ratio)***	***Expérience***	***Section-efficace (σ)***	***$\Delta\sigma/\sigma$ (%)***
^{97}Mo	^{98}Mo/^{97}Mo	1.005 ± 0.038	PROFIL	^{97}Mo(n,γ)	0.5
^{149}Sm	^{150}Sm/^{149}Sm	0.993 ± 0.006	PROFIL	^{149}Sm(n,γ)	–0.6
^{153}Eu	^{154}Eu/^{153}Eu	0.983 ± 0.004	PROFIL2	^{153}Eu(n,γ)	–1.4
^{144}Nd	^{145}Nd/^{144}Nd	0.975 ± 0.009	PROFIL2	^{144}Nd(n,γ)	–2.3
^{133}Cs	^{134}Cs/^{133}Cs	0.944 ± 0.001	PROFIL	^{133}Cs(n,γ)	–5.8
^{143}Nd	^{145}Nd/^{144}Nd	0.938 ± 0.016	PROFIL2	^{144}Nd(n,γ)	–6.0
^{106}Pd	^{107}Pd/^{106}Pd	0.937 ± 0.005	PROFIL2	^{106}Pd(n,γ)	–6.6
^{149}Sm	^{151}Sm/^{150}Sm	0.933 ± 0.005	PROFIL	^{150}Sm(n,γ)	–7.2
^{101}Ru	^{102}Ru/^{101}Ru	1.084 ± 0.006	PROFIL	^{101}Ru(n,γ)	7.5
^{133}Cs	^{135}Cs/^{134}Cs	0.927 ± 0.002	PROFIL	^{134}Cs(n,γ)	–7.9
^{95}Mo	^{96}Mo/^{95}Mo	1.105 ± 0.027	PROFIL	^{95}Mo(n,γ)	9.3
^{147}Sm	^{149}Sm/^{148}Sm	1.134 ± 0.014	PROFIL2	^{148}Sm(n,γ)	10.8
^{144}Nd	^{146}Nd/^{145}Nd	1.131 ± 0.006	PROFIL2	^{145}Nd(n,γ)	11.1
^{143}Nd	^{144}Nd/^{143}Nd	1.139 ± 0.014	PROFIL2	^{143}Nd(n,γ)	11.6
^{105}Pd	^{106}Pd/^{105}Pd	0.888 ± 0.003	PROFIL	^{105}Pd(n,γ)	–12.0
^{106}Pd	^{108}Pd/^{107}Pd	1.173 ± 0.049	PROFIL2	^{107}Pd(n,γ)	14.5
^{147}Sm	^{148}Sm/^{147}Sm	1.194 ± 0.006	PROFIL2	^{147}Sm(n,γ)	14.5
^{145}Nd	^{146}Nd/^{145}Nd	1.202 ± 0.003	PROFIL	^{145}Nd(n,γ)	16.3
^{151}Sm	^{152}Sm/^{151}Sm	1.285 ± 0.004	PROFIL2	^{151}Sm(n,γ)	17.5
^{153}Eu	^{152}Eu/^{151}Eu	1.322 ± 0.020	PROFIL2	^{151}Eu(n,γ)	17.8
^{153}Eu	^{155}Eu/^{154}Eu	2.040 ± 0.019	PROFIL2	^{154}Eu(n,γ)	47.6

La publication complète de ce travail [Tommasi 06] suit dans les pages suivantes.

[Tommasi 06]

J. Tommasi, E. Dupont and P. Marimbeau, Analysis of sample irradiation experiments in Phenix for JEFF-3.0 nuclear data validation, Nuclear Science and Engineering 154, 119 (2006)

http://doi.org/10.13182/NSE154-119

NUCLEAR SCIENCE AND ENGINEERING: **154**, 119–133 (2006)

Analysis of Sample Irradiation Experiments in Phénix for JEFF-3.0 Nuclear Data Validation

J. Tommasi,* E. Dupont, and P. Marimbeau

Commissariat à l'Energie Atomique, Cadarache, DER/SPRC bldg 230
13108 Saint Paul lez Durance, France

Received May 31, 2005
Accepted November 3, 2005

Abstract—*The PROFIL and PROFIL-2 experiments performed in the Phénix demonstration fast reactor irradiated 130 small separate samples containing almost pure isotopes. These highly accurate experiments are a very specific and powerful source of information on the nuclear data of major and minor actinides and several fission products. Their analysis was carried out using the ERANOS-2.0 code system associated to JEFF-3.0 cross-section data, UKFY3.5 fission yield data, and JEF-2.2 decay data. The consistency of the results demonstrates the overall good quality of the actinide nuclear data and experimental techniques used and points out where specific improvement is necessary: fission yields of ^{235}U on neodymium isotopes; integral capture cross sections of ^{232}Th, ^{233}U, ^{241}Pu, ^{242}Pu, and ^{241}Am (and to a lesser extent, ^{240}Pu and ^{237}Np); and branching ratios for ^{241}Am capture. A similar analysis characterizes the degree of accuracy of the integral capture cross sections of 19 fission products. Future plans include the analysis of two new experiments of the same kind, included in the current Phénix experimental program, and the use of a consistent set (cross sections, fission yields, and decay data) of the latest JEFF-3.1 nuclear data files.*

I. INTRODUCTION

The irradiation of pure isotope samples in a well-characterized flux is a powerful technique to collect accurate information on integral capture rates and cross sections. This method may be used for all isotopes changed by neutron capture into a stable or long-lived nuclide and is based on the measurement of the composition change induced by irradiation.

Three such experiments have been carried out in French fast spectrum reactors: two in the Phénix demonstration reactor [250 MW(electric)] and one in the Super-Phénix prototype fast reactor [1200 MW(electric)]. Unfortunately, the experimental pin irradiated in the Super-Phénix reactor could not be dismantled and analyzed after reactor shutdown. The Phénix experiments have been analyzed in the past, using code systems and nuclear data available at the time.[1,2] The aim of this work is to analyze these experiments using more recent (and presumably more accurate) calculational tools and nuclear data sets. This contributes to the validation of these new tools and data sets. The two experiments analyzed, named PROFIL and PROFIL-2, are briefly described in Sec. II, with indications on experimental techniques and their accuracies.

Sections III and IV describe the calculational methods and the assumptions used to perform the analysis of the experiments. This analysis is based on the use of the ERANOS2.0 code system (see Sec. III.B for a brief description of ERANOS) fed with JEFF-3.0 cross-section, UKFY3.5 fission yield, and JEF-2.2 decay data libraries.

The main results of the analysis are gathered in Sec. V, dealing in turn with results relative to the monitoring samples (boron and lithium samples, neodymium buildup by fission in ^{235}U, and other samples), the actinide samples, and the fission product samples. Conclusions are given in Sec. VI.

*E-mail: jean.tommasi@cea.fr

Note that throughout the paper, the uncertainties related to the ratios of calculation to experiment (C/E) are the upper value between the dispersion of individual C/Es (when there are many available) and the experimental uncertainty on concentration ratio measurements (with a quadratic combination if many sample measurements are available). Experimental uncertainties on nuclear data (integral cross sections, fission yields, decay constants, and branching ratios) are never taken into account, but rather are quoted separately when necessary. All uncertainties correspond to 1σ.

II. THE EXPERIMENTS

II.A. Irradiation Conditions

The PROFIL experiment took place during the first three irradiation cycles of the Phénix reactor from January 1974 to January 1975 for a total of 179 equivalent full-power days (EFPDs). The loading of this Phénix startup core included 58 $(U,Pu)O_2$ subassemblies (inner part of the core) and 48 enriched UO_2 subassemblies (outer part of the core). The PROFIL-2 experiment lasted for four Phénix irradiation cycles from July 1979 to September 1980 for a total of 316 EFPDs with a full $(U,Pu)O_2$ core loading.

The PROFIL experimental pin containing 46 separate samples was loaded close to the center of a 217-pin standard hexagonal fuel subassembly placed at the geometric center of the Phénix core. PROFIL-2 involved two experimental pins containing 42 separate samples each. They were loaded close to the center of a single standard fuel subassembly contiguous to the central subassembly of the Phénix core. This means that in both cases, the experimental device was placed in a quasi-asymptotic flux region far from control rods or other perturbations in order to obtain clean and well-characterized irradiation conditions.

II.B. The Separate Nuclide Samples

Within the PROFIL experimental pin, each actinide sample is enclosed within a simple stainless steel container, and each fission product sample, inside a double stainless steel container (see Fig. 1), whereas all the PROFIL-2 samples are enclosed inside such a double container.

The double container allows one to minimize the amount of activated steel dissolved with the sample deposit and then to enhance the quality of postirradiation analyses: The thick external container, providing good mechanical strength, is removed in a hot cell and handled as waste, while only the thin inner container is dissolved with the sample.

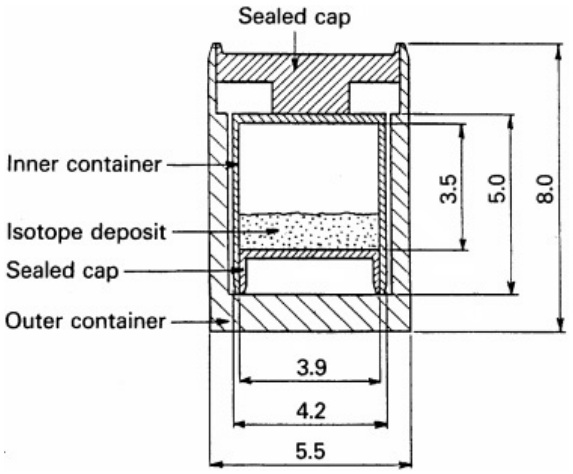

Fig. 1. Stainless steel double container for PROFIL irradiations.[1] Dimensions are given in millimetres.

At least two samples of each isotope loaded are manufactured for each experiment to provide best against the risks of sample damage during pin dismantling or errors in sample isotopic analysis. The number of different samples in each experimental pin is recorded in Table I. The numerous ^{235}U samples are evenly distributed over the experimental pin length to provide a fluence level and axial shape monitoring. A few natural boron and lithium samples are used also as standards for fluence monitoring. Figure 2 provides an example of the chemical forms of the various sample deposits and of their masses. The isotopic purity of the samples ranges from 90 to 100%, being higher than 95% for most samples.

II.C. Experimental Techniques and Accuracies

After irradiation, the samples are cut from the experimental pins and put into solution (in case of a double container, the external container is removed before dissolution). Mass spectrometry is used to measure isotopic compositions with simple or double isotopic dilution and well-characterized tracers. In some cases, alpha or gamma spectrometry is used instead. All the isotopic analysis results are presented as ratios of concentrations. The claimed experimental uncertainty is often much lower than 1%, but often the lack of consistency of the results obtained for a set of presumably identical samples leads to an increase of these values, but never exceeding ≈2.5% for the ratios involving isotopes present in significant amounts. For isotopes present in small amounts, the uncertainty may exceed 5%.

TABLE I

Experimental Sample Number by Type in the PROFIL Pin and in the Two PROFIL-2 Pins*

	PROFIL	PROFIL-2 A + B		PROFIL	PROFIL-2 A + B
^{232}Th	—	1 + 2	^{92}Zr	—	2 + 1
^{233}U	—	1 + 2	^{95}Mo	2	—
^{234}U	—	2 + 1	^{97}Mo	2	—
^{235}U	6	7 + 7	^{101}Ru	3	—
^{238}U	3	3 + 3	^{105}Pd	2	—
^{237}Np	—	2 + 1	^{106}Pd	—	2 + 2
^{238}Pu	2	2 + 1	^{133}Cs	2	—
^{239}Pu	3	2 + 2	^{143}Nd	—	1 + 2
^{240}Pu	3	2 + 2	^{144}Nd	—	1 + 2
^{241}Pu	3	—	^{145}Nd	2	—
^{242}Pu	3	2 + 2	^{147}Sm	—	1 + 2
^{241}Am	2	2 + 2	^{149}Sm	2	—
^{243}Am	—	2 + 1	^{151}Sm	—	1 + 2
^{244}Cm	—	2 + 2	^{153}Eu	—	2 + 1
Actinides	25	30 + 28	Fission products	15	10 + 12
			Natural boron	3	2 + 2
			Natural lithium	3	—

*PROFIL pin with 46 samples; PROFIL-2 pins labeled A and B with 42 samples each.

III. ANALYSIS METHODOLOGY

III.A. Burnup Equations Analysis

We use as a template the following linear differential system to describe an open linear sequence of reactions involving a mother nuclide and its successive descendants:

$$\begin{cases} \dfrac{dN_1}{dt} = \alpha_1 N_1 & \text{with } N_1(0) = 1 \\ \dots \\ \dfrac{dN_i}{dt} = \beta_{i-1} N_{i-1} + \alpha_i N_i & \text{with } N_i(0) = 0 \\ \dots \\ \dfrac{dN_n}{dt} = \beta_{n-1} N_{n-1} + \alpha_n N_n & \text{with } N_n(0) = 0 \ . \end{cases} \tag{1a}$$

This is a particular case of the well-known Bateman equations. The value α_k is the disappearance rate of nuclide k, i.e., the sum of the absorption rate and the natural decay rate: $\alpha_k = -(\sigma_{a,k}\Phi + \lambda_k)$. The value β_k is the production rate of nuclide $k + 1$ from nuclide k by capture or decay: $\beta_k = \sigma_{c,k}\Phi + \lambda_k f_{k\to k+1}$ (where Φ is the neutron flux and $f_{k\to k+1}$ is the branching ratio of the decay of nuclide k to nuclide $k + 1$; the possible remaining decay of nuclide k is supposed to branch outside of nuclides N_1 to N_n). The aforementioned system can be written in a more compact matrix form:

$$\frac{d\vec{N}}{dt} = \mathbf{M}\vec{N} \ , \quad \text{with } \vec{N}(0) = \begin{pmatrix} 1 \\ 0 \\ \vdots \\ \vdots \\ \vdots \\ 0 \end{pmatrix}$$

and

$$\mathbf{M} = \begin{pmatrix} \alpha_1 & 0 & \dots & \dots & \dots & 0 \\ \beta_1 & \alpha_2 & \ddots & & & \vdots \\ 0 & \beta_2 & \alpha_3 & \ddots & & \vdots \\ \vdots & \ddots & \ddots & \ddots & \ddots & \vdots \\ \vdots & & \ddots & \beta_{n-2} & \alpha_{n-1} & 0 \\ 0 & \dots & \dots & 0 & \beta_{n-1} & \alpha_n \end{pmatrix} . \tag{1b}$$

The solution of Eq. (1b) then takes the form of a matrix exponential:

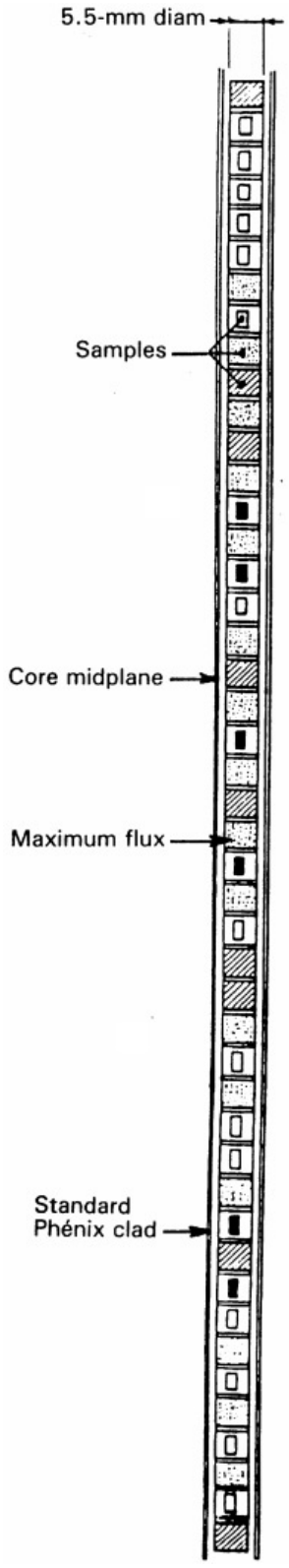

Position (mm)	Isotope	Chemical form	Mass (mg)
180	^{235}U	UO_2	22
170	^{145}Nd	Nd_2O_3	22
160	^{105}Pd	Palladium	21.7
150	^{133}Cs	CsF	23.4
140	^{101}Ru	Ruthenium	19.6
130	^{95}Mo	Molybdenum	21.5
120	^{238}Pu	PuO_2	14
110	^{97}Mo	Molybdenum	21.7
100	^{239}Pu	PuO_2	~10
90	^{235}U	UO_2	22.5
80	^{241}Am	AmO_2	10.0
70	^{238}U	UO_2	22.3
60	^{240}Pu	PuO_2	3.7
50	Natural lithium	LiF	3.8
40	^{242}Pu	PuO_2	29
30	Natural boron	Boron	1.1
20	^{149}Sm	Sm_2O_3	25.8
10	^{241}Pu	PuO_2	4.3
0	^{235}U	UO_2	24.1
−10	^{239}Pu	PuO_2	~10
−20	Natural boron	Boron	1.0
−30	^{240}Pu	PuO_2	6
−40	^{238}U	UO_2	23
−50	^{241}Pu	PuO_2	5
−60	Natural lithium	LiF	3.7
−70	^{239}Pu	PuO_2	~10
−80	^{101}Ru	Ruthenium	20
−90	^{235}U	UO_2	23.9
−100	^{238}U	UO_2	23.7
−110	^{240}Pu	PuO_2	6.3
−120	^{133}Cs	CsF	22.4
−130	^{242}Pu	PuO_2	27
−140	^{95}Mo	Molybdenum	21.9
−150	^{105}Pd	Palladium	20
−160	^{241}Pu	PuO_2	12.5
−170	Natural boron	Boron	1.3
−180	^{235}U	UO_2	24.5
−190	Natural lithium	LiF	4.2
−200	^{101}Ru	Ruthenium	19
−210	^{242}Pu	PuO_2	25
−220	^{145}Nd	Nd_2O_3	20.2
−230	^{238}Pu	PuO_2	12.6
−240	^{97}Mo	Molybdenum	19.7
−250	^{241}Am	AmO_2	13.7
−260	^{149}Sm	Sm_2O_3	22.9
−270	^{235}U	UO_2	25

Fig. 2. Axial layout of the PROFIL pin in Phénix.[1]

$$\vec{N}(t) = \exp(\mathbf{M}t)\vec{N}(0) = \left(\mathbf{I} + t\mathbf{M} + \frac{t^2}{2!}\mathbf{M}^2 + \cdots + \frac{t^k}{k!}\mathbf{M}^{\mathbf{k}} + \cdots\right)\vec{N}(0) \ . \tag{2}$$

This power series expansion of the matrix exponential can be used (see Appendix) to establish the following limited expansion:

$$N_k(t) = \left(\prod_{i=1}^{k-1}\beta_i\right)\cdot\frac{t^{k-1}}{(k-1)!}\cdot\left[1 + \frac{t}{k}\sum_{i=1}^{k}\alpha_i + o(t)\right] \ , \tag{3}$$

where the usual notation $o(t^m)$ stands for terms of order higher than m in t. This shows that the ratio $R_k = N_{k+1}/N_k$ is approximately proportional to the time variable (t):

$$R_k(t) = \frac{N_{k+1}(t)}{N_k(t)} = \frac{\beta_k t}{k}\left[1 + \frac{\alpha_{k+1} - \frac{1}{k}\sum_{i=1}^{k}\alpha_i}{k+1}\,t + o(t)\right] \ . \tag{4}$$

The relationship between R_k and β_k and t being close to proportionality for small enough time or fluence values, the sensitivities of R_k to β_k and t will be close to unity under the same assumption, as given in Eqs. (5a) and (5b), while the form of Eq. (4) shows that the sensitivities to other nuclear data will all be of order 1 in t, i.e., much smaller than the sensitivities to β_k and t. In the case of long-lived or stable nuclides, $S(R_k, \beta_k)$ is the sensitivity to the integral transition cross section (most often capture), and $S(R_k, t)$ is the sensitivity to time or fluence:

$$S(R_k, \beta_k) = \frac{\partial R_k}{R_k}\Big/\frac{\partial \beta_k}{\beta_k} = 1 + \frac{\beta_k t}{k(k+1)} + o(t) \tag{5a}$$

and

$$S(R_k, t) = \frac{\partial R_k}{R_k}\Big/\frac{\partial t}{t} = 1 + \frac{\alpha_{k+1} - \frac{1}{k}\sum_{i=1}^{k}\alpha_i}{k+1}\,t + o(t) \ . \tag{5b}$$

This is the main incentive to achieve a very good isotopic purity in the samples: The ratios R_k are then almost proportional to the transition cross section from nuclide k to nuclide $k+1$, with a very limited dependence on other nuclear data, provided that the irradiation time or the fluence is small enough, i.e., that all the reaction rates $\alpha_i t$ are much lower than 1 [as the nonzero terms in the matrix $(\mathbf{M}t)^k$ are of global degree k in the $\alpha_i t$ and $\beta_i t$ and as $|\beta_i t| < |\alpha_i t|$, the neglected terms in Eq. (4) are at least of second order in the $\alpha_i t$]. Under these conditions, the analysis of these ratios provides direct valuable information on the integral transition cross sections.

However, if we depart from the ideal conditions of the aforementioned analysis, i.e., for large fluences and/or initial concentrations $(Q_1, Q_2, \ldots, Q_k, \ldots, Q_n) \neq (1,0,\ldots,0,\ldots,0)$, the explicit calculation of sensitivities to nuclear data or initial conditions becomes inextricably difficult. This is why we use a perturbation theory formalism[3–6] to derive convenient numerical expressions for the sensitivities of final concentrations to initial concentrations and to integral cross sections or decay constants. Starting from the usual forward burnup equations,

$$\begin{cases} \dfrac{d\vec{N}}{dt} = \mathbf{M_i}\vec{N} \quad \text{over } [t_i, t_{i+1}] \text{ for } i = 0,\ldots,n-1 \\ \vec{N}(t_0) = \vec{Q} \ , \end{cases} \tag{6a}$$

we derive the adjoint equations:

$$\begin{cases} \vec{N}^* \text{ continuous over } [t_0, t_n] \\ \vec{N}^*(t_n) = \vec{u}_k \\ \dfrac{d\vec{N}^*}{dt} + \mathbf{M_i^*}\vec{N}^* = 0 \quad \text{over } [t_i, t_{i+1}], \text{ for } i = 0,\ldots,n-1 \ , \end{cases} \tag{6b}$$

where the adjoint burnup matrix $\mathbf{M_i^*}$ is the transpose of the forward burnup matrix $\mathbf{M_i}$, and $\vec{u}_k$ is the n vector with all components equal to zero except the k'th one, equal to 1.

After some classical algebra, this leads to a formula relating the variation of the concentration of nuclide k at the end of irradiation $N_k(t_n)$ to the variations $\delta\vec{Q}$ of the initial concentrations and $\delta\mathbf{M_i}$ of the burnup matrices (the standard scalar product of two n vectors $\vec{u}$ and $\vec{v}$ is noted $\langle\vec{u},\vec{v}\rangle$):

$$\delta[N_k(t_n)] = \langle\vec{N}^*(t_0), \delta\vec{Q}\rangle + \sum_{i=0}^{n-1}\int_{t_i}^{t_{i+1}}\langle\vec{N}^*, \delta\mathbf{M_i}\vec{N}\rangle\,dt \ . \tag{7}$$

This allows us to compute the sensitivity of the final concentration of nuclide i to the initial concentration of nuclide j (the sensitivity of a variable quantity V to a parameter p being defined as the ratio $(dV/V)/(dp/p)$):

$$S[N_i(t_n), Q_j] = \frac{N_j^*(t_0)\delta Q_j}{N_i(t_n)}\Big/\frac{\delta Q_j}{Q_j} = \frac{N_j^*(t_0)Q_j}{N_i(t_n)} \ . \tag{8a}$$

Furthermore, as the burnup matrices **M** are linear with respect to cross sections, fluxes, decay constants, and branching ratios, the nonzero terms in the variation $\delta\mathbf{M}$ of the burnup matrix due to a variation δp of any one of these scalar parameters are the coefficients other than p of the products involving p, multiplied by δp:

$$S[N_i(t_n), p] = \left. \frac{\sum_{i=0}^{n-1} \int_{t_i}^{t_{i+1}} \langle \vec{N}^*, \delta\mathbf{M}\vec{N} \rangle \, dt}{N_i(t_n)} \right/ \frac{\delta p}{p}$$

$$= \frac{\sum_{i=0}^{n-1} \int_{t_i}^{t_{i+1}} \langle \vec{N}^*, \mathbf{M_p}\vec{N} \rangle \, dt}{N_i(t_n)} \quad , \qquad (8b)$$

where $\mathbf{M_p}$ is the restriction of **M** to the products containing p, all other terms being equal to zero.

It has been implicitly assumed here that the neutron flux Φ (level and spectrum) does not depend on the nuclear data variations. This is true for nuclides not present in the Phénix core (e.g., ^{232}Th) and is a good approximation for nuclides with a small impact on the neutron balance of the core (e.g., ^{235}U for PROFIL-2, most fission products, and most capture reactions), but it is questionable for nuclides or reactions important for the neutron balance of the core (mainly, ^{238}U and ^{239}Pu, and ^{235}U for PROFIL). However, for small capture and fission nuclear data variations, the main effect is expected from a flux level change through the core power normalization, rather than from a spectrum shift. As the sensitivity of the core power and then of the flux level to capture cross sections is low, the global effect is expected to be small on the computed sensitivities of the N_{i+1}/N_i ratios to capture cross sections. For sensitivities to fission cross sections, a part of the sensitivity to fluence proportional to the fractional contribution to the core fission rate should be subtracted from the value computed by the aforementioned method. In Phénix, this effect would be important only for ^{239}Pu and ^{238}U (and ^{235}U for PROFIL).[a] Nevertheless, it is worth noting that the fluence normalization performed (see Sec. IV) would almost cancel this impact, because the sensitivities to fluence are similar and close to 1 for all the ratios investigated.

III.B. Neutronic Calculations

The deterministic code system ERANOS2.0 (Ref. 7) is used throughout this study, fed by cross-section libraries based on JEFF-3.0–evaluated data files.[8] Fission yields for neodymium isotopes are taken from the UKFY3.5 evaluation[9] developed from the UKFY3 evaluation.[10] Decay data are taken from JEF-2.2 recommendations because the JEFF3 decay data files were not yet available at the time this work was performed.

Cell and lattice calculations are performed with the ECCO module[11] (collision probability method in many groups, using the subgroup method for self-shielding) in the ERANOS2.0 code system. Fuel cells are described as a two-dimensional (2-D) hexagonal lattice of 217 pins inside a structure tube, and all other regions (fertile blankets, reflectors, and shields) are described as homogeneous cells. A calculational step with a fine energy grid (1968 energy groups) using the most detailed geometric description available is performed and is followed by a condensation (to 33 energy groups) and a homogenization in order to feed a full-core calculation, carried out using a 3-D finite difference diffusion solver. The core flux solvers available in ERANOS are finite difference diffusion (1-, 2-, and 3-D geometries), finite difference S_n transport (1- and 2-D geometries), and variational nodal transport (2- and 3-D geometries). Here, the use of 3-D diffusion has been assumed accurate enough, as the experimental samples are placed in a quasi-asymptotic flux region. A single average control rod position has been assumed for each Phénix cycle.

The 33-group cross sections for the experimental samples have been processed by an ECCO calculation representing a 2-D subassembly with its central fuel pin replaced by a steel pin with steel density representative of the homogenization of the clad and the sample containers. This allows one to account for specific self-shielding effects. As the masses of sample deposits are small (generally much less than 30 mg each), traces of all the nuclides involved in the sample burnup have been put in the homogenized steel central region.

The detailed burnup calculations of the samples, taking into account a rather detailed burnup and decay history, are carried out using the MECCYCO subset[12] of the ERANOS2.0 package. Adjoint burnup and sensitivity calculation modules are implemented in this subset and enable calculations of sensitivities of final concentrations to nuclear data changes.

III.C. Axial Flux Shape Scaling

Several scaling operations must be performed on the raw calculational results. First, a shift in height of the experimental sample column is made to minimize the axial dispersion of the C/E ratios for the ^{235}U samples evenly distributed over the experimental pin height. The possible reasons for this axial shift from the expected position are the approximate treatment of control rods (only one average position per cycle) and/or a bad positioning of the experimental sample column at the pin-filling stage. As a result, shifting the experimental samples columns down by 3 to 4 cm, achieves a very low dispersion on the C/E ratios associated with the prediction of

[a]The fractional contributions to the fission rate are 40% ^{235}U + 11% ^{238}U + 45% ^{239}Pu for PROFIL, and 13% ^{238}U + 73% ^{239}Pu for PROFIL-2.

the $^{236}U/^{235}U$ ratio in the ^{235}U samples (the standard deviation is then only ≈0.2% of the average value).

III.D. Fluence Gap Between the Two PROFIL-2 Pins

The two pins A and B of the PROFIL-2 experiment are irradiated up to slightly different fluences, as they are placed in two different positions of the same fuel subassembly. However, the angular position of this subassembly cannot be monitored in Phénix, and so its actual angular orientation is unknown. Nevertheless, the collection of consistent data on all samples of the same isotope located at the same height in pins A and B allows one to infer that pin B is the closest one to the core center and with a fluence 1.4 (±0.8)% higher than pin A. This is accounted for in Sec. IV (as the raw calculational results refer to the exact center of the PROFIL-2 subassembly).

IV. THE FLUENCE NORMALIZATION ISSUE

The final scaling operation is performed at the global fluence level. It is necessary in order to relate unequivocally discrepancies between calculation and experiment to the inadequate knowledge of some nuclear data. Indeed, uncertainties on the reactor power level measurements, energy deposition data used in calculations, core compositions, and loading may have a significant impact on the overall fluence prediction. This scaling is usually made by referring to specific measurements related to a fission rate indicator (e.g., the ratio $^{148}Nd/^{235}U$, assuming the cumulated fission yield of ^{235}U on ^{148}Nd is accurately known) or an absorption rate indicator on nuclides with well-known, standard cross sections (such as ^{10}B and ^{6}Li, having $1/v$ absorption cross sections with no resonant structure). However, for reasons detailed hereafter, these indicators could not be used here, and we used instead ^{235}U absorption indicators such as the ratios $^{234}U/^{235}U$, $^{238}U/^{235}U$ (mainly sensitive to fission), and $^{236}U/^{235}U$ (mainly sensitive to capture).

IV.A. Neodymium Produced by Fission

As mentioned previously, the usual way to normalize the fluence is to check specific well-known fission or absorption indicators. Table II shows the C/E ratios for the prediction of neodymium fission yields, using experimental cumulated fission yields from the UKFY3.5 file. The results are clearly inconsistent as there is a drift on C/Es with respect to atomic mass number A from $A = 143$ to $A = 150$, far exceeding the claimed experimental uncertainties on fission yields.

If we restrict to ^{148}Nd only, Table III shows large discrepancies on C/E ratios over the four nuclides checked, exceeding again the claimed experimental uncertainties on cumulated fission yields. These four nuclides have been selected because in the ^{235}U, ^{239}Pu, and ^{241}Pu samples, almost all the fissions are due to the initial isotope, and in the ^{238}U samples, approximately two-thirds of the fissions are due to ^{238}U and one-third to ^{239}Pu.

TABLE II

The ^{235}U Samples: C/E Ratios for the Prediction of the Neodymium/^{235}U Ratios Before Fluence Adjustment

	PROFIL	PROFIL-2	$\delta Y/Y$ [a] (%)
$^{143}Nd/^{235}U$	1.001 ± 0.006	1.018 ± 0.008	1.1
$^{144}Nd/^{235}U$	1.048 ± 0.017	1.032 ± 0.005	1.5
$^{145}Nd/^{235}U$	1.045 ± 0.006	1.060 ± 0.013	1.9
$^{146}Nd/^{235}U$	1.058 ± 0.011	1.071 ± 0.006	1.9
$^{148}Nd/^{235}U$	1.073 ± 0.005	1.072 ± 0.012	1.2
$^{150}Nd/^{235}U$	1.113 ± 0.006	1.086 ± 0.014	2.4
$S(\Phi t)$ [b]	≈1.12	≈1.24	

[a] $\delta Y/Y$ is the relative uncertainty of the experimental cumulated fission yield in the UKFY3.5 file.

[b] $S(\Phi t)$ is the sensitivity of any of these C/E ratios to fluence.

TABLE III

The C/E Ratios for the Prediction of the (^{148}Nd/Actinide) Ratios Before Fluence Adjustment

	PROFIL	PROFIL-2	$\delta Y/Y$ [a] (%)
^{235}U	1.073 ± 0.005 $S(\Phi t)$ [b] ≈ 1.11	1.072 ± 0.012 $S(\Phi t) \approx 1.24$	1.2
^{238}U	1.022 ± 0.009 $S(\Phi t) \approx 1.25$	—	1.6
^{239}Pu	—	1.046 ± 0.014 $S(\Phi t) \approx 1.24$	1.7
^{241}Pu	1.003 ± 0.007 $S(\Phi t) \approx 1.16$	—	2.5

[a] $\delta Y/Y$ is the relative uncertainty of the experimental cumulated fission yield in the UKFY3.5 file.

[b] $S(\Phi t)$ is the sensitivity of any of these C/E ratios to fluence.

IV.B. Boron and Lithium Samples

Table IV gives the C/E ratios relative to the boron and lithium samples. Boron and lithium samples yield

TABLE IV

The C/E Ratios for the Prediction of the ^{10}B or ^{6}Li Depletion Before Fluence Adjustment

	PROFIL	PROFIL-2
$^{10}B/^{11}B$	0.969 ± 0.010 $S(\Phi t)^a \approx 0.87$	1.043 ± 0.013 $S(\Phi t) \approx 0.78$
$^{7}Li/^{6}Li$	1.025 ± 0.014 $S(\Phi t) \approx 1.05$	—

[a] $S(\Phi t)$ is the sensitivity of any of these C/E ratios to fluence.

discrepant C/E values for the PROFIL experiment. It is thought that despite special precautions taken to minimize the possible contamination of the boron solution, such as using pure quartz glassware, the measurement does not reflect the true $^{10}B/^{11}B$ ratio in the irradiated boron sample. Unfortunately, the results obtained on boron samples for the PROFIL-2 experiment cannot be checked against results on lithium samples.

IV.C. The ^{235}U Absorption

Finally, because the aforementioned standard fission or absorption indicators yield so widespread and inconsistent results (as a whole), we decided to rely on the following method, based on a detailed analysis of the $^{234}U/^{235}U$, $^{236}U/^{235}U$, and $^{235}U/^{238}U$ ratios in the ^{235}U samples. Table V shows that these ratios are highly sensitive to the ^{235}U integral absorption cross section: $^{234}U/^{235}U$ and $^{235}U/^{238}U$ are much more sensitive to fission than to capture, while the contrary is true for $^{236}U/^{235}U$. Other nuclides than ^{235}U have a limited impact on the prediction of $^{236}U/^{235}U$ and $^{235}U/^{238}U$, while inaccurate

TABLE V

The ^{235}U Samples: Sensitivity of the $^{234}U/^{235}U$, $^{236}U/^{235}U$, and $^{235}U/^{238}U$ Ratios to Integral Cross Sections and to Fluence

$^{234}U/^{235}U$		$^{236}U/^{235}U$		$^{235}U/^{238}U$	
^{234}U capture	−0.43	^{235}U capture	1.05	^{235}U capture	0.22
^{234}U fission	−0.25	^{235}U fission	0.17	^{235}U fission	0.75
^{235}U capture	0.39	^{236}U capture	−0.04	^{238}U capture	−0.11
^{235}U fission	1.35	^{236}U fission	−0.01	^{238}U fission	−0.02
$^{235}U(n,2n)$	0.07				
		Fluence	1.17	Fluence	0.83
Fluence	1.14				

TABLE VI

The ^{235}U Samples: C/E for the $^{234}U/^{235}U$, $^{236}U/^{235}U$, and $^{235}U/^{238}U$, After Fluence Normalization

Ratios	Samples	PROFIL	PROFIL-2
$^{234}U/^{235}U$	^{235}U	0.979 ± 0.016	1.000 ± 0.004
$^{235}U/^{238}U$	^{235}U	1.011 ± 0.048	1.000 ± 0.004
$^{236}U/^{235}U$	^{234}U	—	1.005 ± 0.004
	^{235}U	1.004 ± 0.002	1.004 ± 0.001

^{234}U cross sections may have a significant impact on the prediction of $^{234}U/^{235}U$.

A reduction by 2.0% of the computed fluence allows a quasi-perfect match of all three ratios for the PROFIL-2 experiment with a very limited experimental dispersion for each ratio (Table VI). For the PROFIL experiment, the larger dispersions on the C/E ratios for the prediction of the $^{234}U/^{235}U$ and $^{235}U/^{238}U$ ratios (Table VI) prompt the normalization of the fluence to obtain the same C/E for the prediction of the $^{236}U/^{235}U$ ratio as for PROFIL-2. That means a reduction of the computed fluence by 0.55%. These fluence reductions lie within the experimental uncertainty on Phénix power measurement.

V. MAIN RESULTS

Using the computed sensitivity to the fluence level, all the C/E results quoted in Tables VII through XIII have been corrected by the fluence adjustments given in Sec. IV.C. The concentration ratios Y/X generally have sensitivities close to 1 to the integral transition cross section $\sigma_{X\rightarrow Y}$ [generally capture or, in two cases, $(n,2n)$] and to the fluence level. These two sensitivities are also given in Tables IX through XIII, the sensitivity to fluence being given between brackets. The difference between these two values is due to the sensitivities to reaction cross sections other than $\sigma_{X\rightarrow Y}$ and is generally higher for the samples of the PROFIL-2 experiment (higher fluence). When relevant, sensitivities to decay constants are given in the core of the text.

V.A. Fluence Indicators and Overall Consistency of the Fluence Adjustment

The results obtained for ^{148}Nd buildup by fission after the fluence adjustment are listed in Table VII. There are great overestimations of the ^{148}Nd buildup in the ^{238}Pu and ^{241}Am samples. In the ^{238}Pu samples, ~85% of the fissions are due to ^{238}Pu itself, and the uncertainty given for the cumulative fission yield of ^{148}Nd in the UKFY3.5 file is high. Its value, 34%, is consistent with the C/E ratio observed. Fissions in the ^{241}Am samples occur on ^{241}Am, ^{242m}Am, and ^{238}Pu, with uncertainties

TABLE VII

The C/E Ratios for ^{148}Nd Buildup by Fission and Boron or Lithium Depletion After Fluence Normalization

Ratio	Samples	PROFIL	PROFIL-2
^{148}Nd/^{235}U	^{235}U	1.066 ± 0.005	1.045 ± 0.012
^{148}Nd/^{238}U	^{238}U	1.015 ± 0.009	—
^{148}Nd/^{238}Pu	^{238}Pu	1.31 ± 0.02	—
^{148}Nd/^{239}Pu	^{239}Pu	—	1.020 ± 0.013
^{148}Nd/^{240}Pu	^{240}Pu	—	1.078 ± 0.022
^{148}Nd/^{241}Pu	^{241}Pu	0.997 ± 0.007	—
^{148}Nd/^{242}Pu	^{242}Pu	0.971 ± 0.033	0.976 ± 0.019
^{148}Nd/^{241}Am	^{241}Am	1.59 ± 0.07	—
^{10}B/^{11}B	Natural boron	0.964 ± 0.010	1.032 ± 0.013
^{7}Li/^{6}Li	Natural lithium	1.019 ± 0.014	—

on ^{148}Nd fission yields ranging from 31 to 37%. Nevertheless, these high uncertainties hardly explain the very high discrepancy between calculation and experiment for the ^{148}Nd/^{241}Am ratio.

The ^{148}Nd buildup in the ^{240}Pu samples is overestimated, with a discrepancy between calculation and experiment exceeding the uncertainties on ^{148}Nd buildup by fission associated with ^{240}Pu and ^{241}Pu (5 and 2.5%, respectively).

The ^{148}Nd buildup by fission is predicted with small discrepancies (<3%) in the ^{238}U, ^{239}Pu, ^{241}Pu, and even ^{242}Pu samples. However, for the ^{235}U samples, the discrepancy between calculation and experiment amounts to an average 5.5%.

To test the consistency of UKFY3.5 data, we checked the difference between UKFY3.5 and ENDF/B-VI.5 (Ref. 13) cumulated fission yield data for neodymium buildup by fission in the ^{235}U, ^{239}Pu, and ^{241}Pu samples. These samples have been selected because the fissions within occur almost entirely on the main nuclide of the sample. Because the neodymium isotope buildup by fission is almost exactly proportional to the cumulative fission yields (because the absorption cross sections of the neodymium isotopes are low in a fast spectrum, with a maximum of ≈0.5 b for ^{145}Nd), a simple scaling based on the ratio between the ENDF/B-VI.5 and the UKFY3.5 yields can be performed.

The results are shown in Table VIII. They show that the use of ENDF/B-VI.5 data does not reduce the global inconsistency observed for the neodymium buildup in the ^{235}U samples, but the dispersion between the C/E associated with the six neodymium isotopes measured is reduced, especially for the PROFIL-2 samples. Furthermore, the already good agreement between calculation and experiment is noticeably improved on the whole for the ^{239}Pu and ^{241}Pu samples.

We conclude that the proposed fluence adjustment is sound, being based on a good agreement between calculation and experiment for several measured parameters: ^{238}U, ^{239}Pu, and ^{241}Pu fissions related to neodymium buildup, ^{6}Li depletion, and finally ^{235}U absorption. However, a discrepant behavior remains for neodymium isotope buildup prediction in the ^{235}U samples. Either the experimental cumulative yields for ^{235}U fast fission on neodymium isotopes or the specific measurement methods for Nd/^{235}U measurement may be questioned, and specific future feedback from the PROFIL-R and PROFIL-M experiments will be extremely valuable (see Sec. VI).

V.B. Actinides of the Th/U Cycle

The results for actinides of the Th/U cycle are given in Table IX. The ^{233}U/^{232}Th ratio is underestimated by 16 ± 8%. This high uncertainty results from

TABLE VIII

The C/E Ratios for Neodymium Buildup by Fission for ^{235}U, ^{239}Pu, and ^{241}Pu Samples After Fluence Normalization*

Actinide	^{143}Nd	^{144}Nd	^{145}Nd	^{146}Nd	^{148}Nd	^{150}Nd
^{235}U (PROFIL)	0.995 ± 0.006	1.041 ± 0.017	1.039 ± 0.006	1.051 ± 0.011	1.066 ± 0.005	1.106 ± 0.006
	1.031 ± 0.006	1.078 ± 0.017	1.034 ± 0.006	1.047 ± 0.011	1.053 ± 0.005	1.081 ± 0.006
^{235}U (PROFIL-2)	0.993 ± 0.008	1.006 ± 0.005	1.034 ± 0.013	1.045 ± 0.006	1.045 ± 0.012	1.059 ± 0.014
	1.028 ± 0.008	1.042 ± 0.005	1.029 ± 0.013	1.041 ± 0.006	1.033 ± 0.012	1.035 ± 0.014
^{239}Pu (PROFIL-2)	0.971 ± 0.014	0.951 ± 0.014	0.999 ± 0.014	1.022 ± 0.014	1.020 ± 0.014	1.014 ± 0.014
	1.009 ± 0.014	0.994 ± 0.014	0.986 ± 0.014	0.993 ± 0.014	0.996 ± 0.014	0.999 ± 0.014
^{241}Pu (PROFIL)	0.980 ± 0.007	0.972 ± 0.007	0.981 ± 0.007	0.994 ± 0.007	0.997 ± 0.007	0.975 ± 0.007
	0.997 ± 0.007	0.970 ± 0.007	0.999 ± 0.007	1.019 ± 0.007	1.007 ± 0.007	0.999 ± 0.007

*For each actinide, the first line is obtained using UKFY3.5 fission yield data for neodymium isotopes, and the second one, using ENDF/B-VI.5 fission yield data.

TABLE IX

The C/E and Sensitivities for the Actinides of the Th/U Cycle After Fluence Normalization—Main Results

Ratios	Samples	PROFIL-2	
		C/E	Sensitivities
$^{233}U/^{232}Th$	^{232}Th	0.836 ± 0.076	1.03 (0.83)
$^{234}U/^{233}U$	^{233}U	0.915 ± 0.001	0.99 (1.19)
$^{235}U/^{234}U$	^{233}U	1.028 ± 0.019	1.18 (1.01)
	^{234}U	1.031 ± 0.002	1.05 (0.88)

an inconsistency between the two sample measurements available. This inconsistency and the poor number of sample measurements available do not allow one to draw unambiguous conclusions. If confirmed by future PROFIL-type experiments foreseen in Phénix (see Sec. VI), this underestimation would mean that the breeding capability of a Th/U fast reactor is probably underestimated by calculations based on the capture cross-section data used here. The $^{234}U/^{233}U$ ratio is also underestimated, by ≈9%, while the $^{235}U/^{234}U$ ratio is overestimated by ≈3%. The sensitivities of the ratios $^{233}U/^{232}Th$ and $^{234}U/^{233}U$ to the integral fission cross section of ^{233}U are important (−0.17 and +0.31, respectively) as is the sensitivity of the ratio $^{235}U/^{234}U$ to the integral fission cross section of ^{235}U (−0.15).

V.C. Major Actinides of the U/Pu Cycle

The results for major actinides of the U/Pu cycle are provided in Table X. The ratios $^{237}Np/^{238}U$ and $^{238}Pu/^{239}Pu$ provide information on the $(n,2n)$ integral reactions of ^{238}U and ^{239}Pu and are underestimated by ≈7 and ≈20%, respectively. This may be due not only to poor knowledge of these $(n,2n)$ data but also, as the $(n,2n)$ is a threshold reaction, to a slightly poor prediction of the neutron flux at high energy (several mega-electron-volts), due to other nuclear data.

The $^{239}Pu/^{238}U$ and $^{240}Pu/^{239}Pu$ ratios are well predicted, with C/Es differing from unity by <2% and consistent with the ratios associated with ^{235}U absorption rates that are given in Table VI. The $^{239}Pu/^{238}Pu$ ratio is overestimated by ≈3% but has relatively high sensitivities to ^{238}Pu integral fission cross section (0.2 to 0.3) and to ^{239}Pu integral fission cross section (−0.3 to −0.4). The $^{241}Pu/^{240}Pu$ ratio is overestimated by ≈4%, with sensitivities to the ^{241}Pu integral fission cross section ranging from −0.08 to −0.20 and sensitivities to the ^{241}Pu β-decay constant ranging from −0.06 to −0.16. The $^{242}Pu/^{241}Pu$ ratio is overestimated by 10 to 15%, and the $^{243}Am/^{242}Pu$ ratio, by 15 to 20%.

V.D. Minor Actinides of the U/Pu Cycle

Results for minor actinides of the U/Pu cycle are given in Table XI. The main point is the adjustment of the branching ratio in the capture path of ^{241}Am, as shown in Fig. 3. Branching values of 85% on the short-lived ground state of ^{242}Am and 15% on the long-lived

TABLE X

The C/E and Sensitivities for the Major Actinides of the U/Pu Cycle After Fluence Normalization—Main Results

Ratios	Samples	PROFIL		PROFIL-2	
		C/E	Sensitivities	C/E	Sensitivities
$^{239}Pu/^{238}U$	^{235}U	1.008 ± 0.008	1.01 (0.92)	—	—
	^{238}U	1.011 ± 0.003	1.01 (0.90)	1.023 ± 0.002	1.02 (0.84)
$^{237}Np/^{238}U$	^{238}U	—	—	0.933 ± 0.029	0.99 (0.83)
$^{239}Pu/^{238}Pu$	^{238}Pu	1.019 ± 0.008	1.17 (0.93)	1.035 ± 0.001	1.10 (0.94)
$^{240}Pu/^{239}Pu$	^{238}U	1.001 ± 0.001	0.91 (1.02)	0.978 ± 0.006	0.94 (1.02)
	^{239}Pu	0.979 ± 0.002	1.02 (1.07)	0.977 ± 0.001	1.03 (1.13)
$^{238}Pu/^{239}Pu$	^{239}Pu	0.809 ± 0.041	0.99 (1.04)	0.733 ± 0.126	0.89 (1.19)
$^{241}Pu/^{240}Pu$	^{239}Pu	1.044 ± 0.011	1.01 (0.93)	1.036 ± 0.004	1.01 (0.82)
	^{240}Pu	1.052 ± 0.005	1.02 (0.90)	1.039 ± 0.006	1.04 (0.83)
$^{242}Pu/^{241}Pu$	^{240}Pu	1.166 ± 0.027	1.00 (1.03)	1.115 ± 0.029	0.93 (0.99)
	^{241}Pu	1.093 ± 0.007	0.87 (1.09)	—	—
$^{243}Am/^{242}Pu$	^{242}Pu	1.209 ± 0.018	1.02 (0.95)	1.147 ± 0.028	1.04 (0.90)

TABLE XI

The C/E and Sensitivities for the Minor Actinides of the U/Pu Cycle After Fluence Normalization—Main Results

Ratios	Samples	PROFIL		PROFIL-2	
		C/E	Sensitivities	C/E	Sensitivities
$^{238}Pu/^{237}Np$	^{237}Np	—	—	0.940 ± 0.013	1.13 (1.00)
$^{242m}Am/^{241}Am$	^{241}Am	1.087 ± 0.019	1.08 (0.94)	1.076 ± 0.002	1.15 (0.88)
$^{238}Pu/^{241}Am$		1.055 ± 0.016	1.09 (1.04)	1.107 ± 0.019	1.18 (1.07)
$^{242}Pu/^{241}Am$	^{241}Am	1.063 ± 0.015	1.09 (1.07)	1.097 ± 0.026	1.18 (1.13)
$^{242}Cm/^{241}Am$		1.045 ± 0.012	1.07 (1.03)	—	—
$^{244}Cm/^{243}Am$	^{242}Pu	1.000 ± 0.067	1.03 (1.01)	—	—
	^{243}Am	—	—	—	—
$^{245}Cm/^{244}Cm$	^{244}Cm	—	—	0.974 ± 0.003	1.07 (0.79)

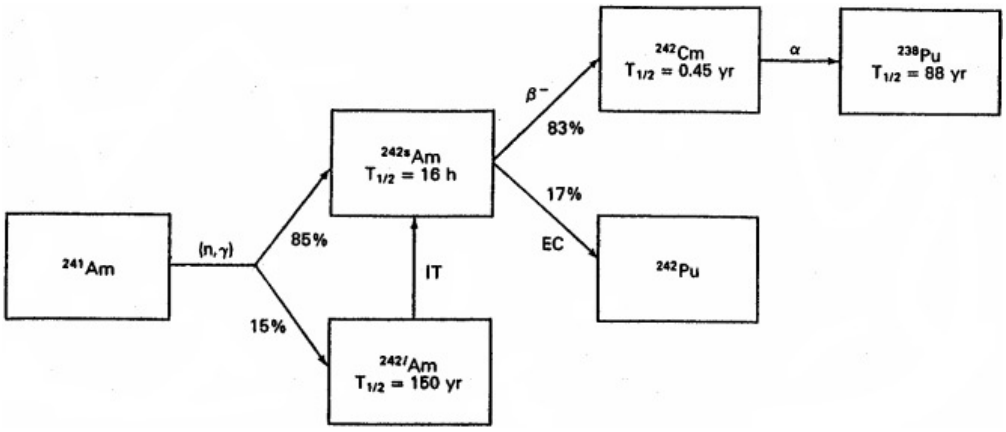

Fig. 3. Decay scheme related to ^{241}Am capture, with modified branching values.[1]

metastable state of ^{242}Am have been obtained. They provide the best consistency between the C/E values of the ratio $^{242m}Am/^{241}Am$ for one branch and the ratios $^{238}Pu/^{241}Am$, $^{242}Pu/^{241}Am$, and $^{242}Cm/^{241}Am$ for the other branch, with an overall overestimation of these ratios by 5 to 10%. These branching values reproduce those obtained independently in a previous work.[1] The branching ratio in ^{241}Am capture depends on the energy of the incident neutron, globally decreasing from lower to higher energies. This means the aforementioned branching ratio is an average value over the ^{241}Am capture rate distribution in energy. Here, the average capture energy by ^{241}Am is 110 keV, with two-thirds of the captures occurring between 50 and 300 keV, and 90% between 1 and 800 keV. The value obtained for the branching ratio is then representative of a sodium-cooled fast reactor core spectrum. The $^{238}Pu/^{237}Np$ ratio is underestimated by ≈6%. Although ^{243}Am samples were irradiated in the PROFIL-2 experiment, the ratio $^{244}Cm/^{243}Am$ could not be measured, and the only piece of information available on this ratio was drawn from the analysis of the ^{242}Pu samples in the PROFIL experiment, with rather high experimental uncertainties. The $^{245}Cm/^{244}Cm$ ratio is underestimated by ≈3%, with a rather high sensitivity to the integral fission cross section of ^{245}Cm (−0.30). The sensitivities to decay constants remain low (i.e., <0.1 in magnitude), except for the $^{242}Cm/^{241}Am$ ratio. In this case, the sensitivity to the decay constant of ^{242}Cm is extremely high (−4.6); the reason is that the isotopic analysis was carried out after several ^{242}Cm half-lives.

V.E. Fission Products

The results are provided in Table XII for the PROFIL experiment and in Table XIII for the PROFIL-2 experiment. They can be grouped according to the

TABLE XII

The C/E for the Fission Product Samples of the PROFIL Experiment After Fluence Normalization

Ratio	Sample	PROFIL	
		C/E	Sensitivities
$^{96}Mo/^{95}Mo$	^{95}Mo	1.105 ± 0.027	1.02 (1.01)
$^{98}Mo/^{97}Mo$	^{97}Mo	1.005 ± 0.038	1.03 (1.01)
$^{102}Ru/^{101}Ru$	^{101}Ru	1.084 ± 0.006	1.03 (1.02)
$^{106}Pd/^{105}Pd$	^{105}Pd	0.888 ± 0.003	1.05 (1.03)
$^{134}Cs/^{133}Cs$	^{133}Cs	0.944 ± 0.001	1.02 (1.00)
$^{135}Cs/^{134}Cs$	^{133}Cs	0.927 ± 0.002	1.00 (1.00)
$^{146}Nd/^{145}Nd$	^{145}Nd	1.202 ± 0.003	1.03 (1.02)
$^{150}Sm/^{149}Sm$	^{149}Sm	0.993 ± 0.006	1.09 (1.07)
$^{151}Sm/^{150}Sm$	^{149}Sm	0.933 ± 0.005	1.00 (0.90)

TABLE XIII

The C/E for the Fission Product Samples of the PROFIL-2 Experiment After Fluence Normalization

Ratio	Sample	PROFIL-2	
		C/E	Sensitivities
$^{107}Pd/^{106}Pd$	^{106}Pd	0.937 ± 0.005	1.02 (0.93)
$^{108}Pd/^{107}Pd$	^{106}Pd	1.173 ± 0.049	1.02 (1.01)
$^{144}Nd/^{143}Nd$	^{143}Nd	1.139 ± 0.014	1.05 (1.02)
$^{145}Nd/^{144}Nd$	^{143}Nd	0.938 ± 0.016	1.11 (0.87)
	^{144}Nd	0.975 ± 0.009	1.13 (0.96)
$^{146}Nd/^{145}Nd$	^{144}Nd	1.131 ± 0.006	1.04 (0.86)
$^{148}Sm/^{147}Sm$	^{147}Sm	1.194 ± 0.006	1.12 (1.08)
$^{149}Sm/^{148}Sm$	^{147}Sm	1.134 ± 0.014	1.09 (0.75)
$^{152}Sm/^{151}Sm$	^{151}Sm	1.285 ± 0.004	1.27 (1.23)
$^{152}Eu/^{151}Eu$	^{153}Eu	1.322 ± 0.020	1.37 (1.04)
$^{154}Eu/^{153}Eu$	^{153}Eu	0.983 ± 0.004	1.20 (0.97)
$^{155}Eu/^{154}Eu$	^{153}Eu	2.040 ± 0.019	1.07 (1.04)

deviation of the C/E from unity (underestimations are underlined):

1. <5% ^{97}Mo, ^{144}Nd, ^{149}Sm, ^{153}Eu
2. from 5 to 10% ^{101}Ru, ^{106}Pd, ^{133}Cs, ^{134}Cs, ^{150}Sm
3. from 10 to 15% ^{95}Mo, ^{105}Pd, ^{143}Nd, ^{145}Nd, ^{148}Sm
4. from 15 to 20% ^{107}Pd, ^{147}Sm
5. from 20 to 35% ^{151}Sm, ^{151}Eu
6. a factor 2 ^{154}Eu.

The only significant sensitivities to decay constants are the sensitivities to the decay constant of ^{134}Cs (−0.79 for the ratio $^{134}Cs/^{133}Cs$ and +0.70 for the ratio $^{135}Cs/^{134}Cs$), ^{154}Eu (−0.45 for the ratio $^{154}Eu/^{153}Eu$ and +0.48 for the ratio $^{155}Eu/^{154}Eu$), and ^{155}Eu (−0.83 for the ratio $^{155}Eu/^{154}Eu$).

V.F. Comparison Between JEF-2.2 and JEFF-3.0 Data

It is relevant to check whether predictions have been improved by using JEFF-3.0 cross-section data instead of older JEF-2.2 data. The whole analysis has not been repeated with JEF-2.2 data; rather, a full cell calculation has been performed as described in Sec. III.B but using JEF-2.2 data, and the resulting integral capture cross sections of many nuclides (collapsed over the neutron spectrum computed) have been compared to the values already obtained from the same computational scheme with JEFF-3.0 data. The resulting variations of integral capture cross sections are given in Table XIV for actinides and Table XV for fission products. According to their computational procedure, these changes do not reflect only the cross-section changes in the evaluated files themselves but also the slight change in neutron spectrum induced by the cross-section variations of the most important nuclides in the neutron balance of the cell.

Among the significant integral capture cross-section variations from JEF-2.2 to JEFF-3.0, Table XIV shows that the lower integral capture cross sections for ^{232}Th and ^{233}U result in worsening the C/E obtained for the ^{232}Th and ^{233}U samples (see also Table IX), while the significant cross-section variations associated with ^{235}U, ^{240}Pu, ^{241}Pu, and ^{244}Cm result in an improvement of the prediction of the ^{236}U, ^{241}Pu, ^{242}Pu, and ^{245}Cm build-ups, respectively (see also Tables VI, X, and XI). On the other hand, the small changes in ^{242}Pu and ^{241}Am are not

TABLE XIV

Integral Capture Cross-Section Variations from JEF-2.2 to JEFF-3.0 for Actinides

Actinide	Variation (%)
^{232}Th	−7.2
^{233}U	−5.1
^{234}U	−0.6
^{235}U	+4.0
^{238}U	−0.9
^{237}Np	−0.9
^{238}Pu	−1.4
^{239}Pu	−1.3
^{240}Pu	−10.5
^{241}Pu	−10.6
^{242}Pu	−1.4
^{241}Am	−0.8
^{243}Am	−1.0
^{244}Cm	−8.3

TABLE XV

Integral Capture Cross-Section Variations from JEF-2.2 to JEFF-3.0 for Fission Products

Fission Product	Variation (%)
^{95}Mo	+2.3
^{97}Mo	−1.2
^{101}Ru	−1.1
^{105}Pd	−1.2
^{106}Pd	−1.3
^{107}Pd	−1.3
^{133}Cs	−0.7
^{134}Cs	−1.1
^{143}Nd	−0.6
^{144}Nd	−1.4
^{145}Nd	−0.6
^{147}Sm	−0.2
^{148}Sm	−0.1
^{149}Sm	−10.7
^{150}Sm	0.0
^{151}Sm	−0.8
^{151}Eu	+0.2
^{153}Eu	−5.4
^{154}Eu	−1.7

enough to correct the discrepancies observed between calculation and experiment (see Tables X and XI).

The variations in fission product integral capture cross sections are generally small (see Table XV) and probably due to a great extent to the neutron spectrum change. However, a few nuclides exhibit more significant changes: the 2.3% increase in ^{95}Mo capture cross section increases the discrepancy between calculation and experiment (see also Table XII), while the 10.7% reduction in ^{149}Sm capture and the 5.4% reduction in ^{153}Eu capture both improve the agreement between calculation and experiment (see Tables XII and XIII). Despite the very bad prediction of the ^{151}Sm, ^{151}Eu, and ^{154}Eu capture rates, no significant change of their integral capture cross sections has occurred between JEF-2.2 and JEFF-3.0 data.

VI. CONCLUSIONS

The analysis of the PROFIL and PROFIL-2 separate sample irradiation experiments in Phénix has been carried out using the ERANOS-2.0 code system associated with JEFF-3.0 cross-section data, UKFY3.5 fission yield data, and JEF-2.2 decay data as part of their validation process. These highly accurate experiments, involving separate samples of almost pure isotopes, correlate strongly the C/E to individual integral (mainly capture) cross sections and branching ratios, and as such they are a very specific and powerful source of information on the nuclear data of major and minor actinides and several fission products.

The degree of accuracy of the integral cross sections processed from the JEFF-3.0–evaluated files can be inferred from the C/E and sensitivity values quoted in Tables IX through XIII. The main advantage of this kind of experiment is that most of these sensitivities are close to 1: then the C/E ratios provide quite a direct clue to the accuracy of the capture integral cross section of the main nuclide of each sample. The analysis shows the overall good quality of the actinide nuclear data used and points out where specific nuclear data improvement is necessary: fission yields of ^{235}U on neodymium isotopes (unless there was a systematic bias in the PROFIL and PROFIL-2 isotopic analyses relative to neodymium buildup in the ^{235}U samples), integral capture cross sections of ^{232}Th, ^{233}U, ^{241}Pu, ^{242}Pu, and ^{241}Am (and to a lesser extent ^{240}Pu and ^{237}Np), and branching ratios for ^{241}Am capture. A similar analysis characterized the degree of accuracy of the integral capture cross sections of 19 fission products.

When there are significant differences between JEF-2.2 and JEFF-3.0 integral capture cross-section data, the use of the JEFF-3.0 data generally improves the C/E ratios. This is the case for ^{235}U, ^{240}Pu, ^{241}Pu, and ^{244}Cm among actinides and ^{149}Sm and ^{153}Eu among fission products. However, the change in ^{232}Th and ^{233}U integral capture cross sections degrades the comparison to experiment. Furthermore, several integral capture cross sections are not significantly changed, whereas a great discrepancy between calculation and experiment is observed, e.g., ^{242}Pu, ^{145}Nd, ^{107}Pd, ^{147}Sm, ^{151}Sm, ^{151}Eu, and ^{154}Eu.

Two other experiments of the same kind, namely PROFIL-R (fast spectrum) and PROFIL-M (spectrum softened by a thick $^{11}B_4C$ sheath around the experimental pins) are included in the current Phénix experimental program.[14] Additional useful data on actinides and especially fission products are expected from these experiments.[b] When they are completed, their analyses will provide additional useful data in a standard and a slightly moderated neutron spectra, respectively. In addition, more detailed and systematic indications about data improvement needs with respect to the incident neutron energy can be drawn by using a statistical adjustment procedure based on sensitivity analysis and a priori covariance data. Finally, all these results will prove very useful for the accurate design of future fast reactor concepts loaded with a high-burnup fuel containing low-grade plutonium and nonnegligible amounts of minor actinides.

The latest JEFF-3.1 cross-section data should give results that are similar to those from JEFF-3.0 for the

[b]The PROFIL-R irradiation ended by August 2005. The PROFIL-M started in August 2006 and will end by March 2008. Dissolutions and isotopic analyses are scheduled to last until 2010.

major actinides of the U/Pu cycle, thanks to rather comparable integral data in the fast energy range. Moreover, the small change in the ^{240}Pu capture cross section should slightly improve the comparison to experiment. The Th/U cycle actinide data have been revised in JEFF-3.1. The new ^{232}Th capture cross section should reduce the discrepancy observed. However, the new ^{234}U capture cross section should degrade the comparison to experiment, and the discrepancy observed for the ^{233}U integral capture cross section should remain. The changes in minor actinide data from JEFF-3.0 to JEFF-3.1 should improve the comparison to experiment in the case of ^{241}Am but degrade it for ^{243}Am. Other actinide C/E would remain almost unaltered. Among the fission products studied here, only ^{95}Mo data have been revised in JEFF-3.1, and its new capture cross section should improve the comparison to experiment.

APPENDIX

The principle of the derivations leading to Eqs. (3) and (4) is briefly given here. The generic element M_{ij}^k of the matrix $\mathbf{M^k}$ is $M_{ij}^k = (\prod_{m=j}^{i-1} \beta_m) \cdot s_{ij}^k$, with the following definitions and conventions (in M_{ij}^k and s_{ij}^k, k is an index, not an exponent):

1. for $j > i$, $\prod_{m=j}^{i-1} \beta_m = 1$ and $s_{ij}^k = 0$ (the matrix $\mathbf{M^k}$ is lower triangular, as is $\mathbf{M}$)
2. for $j \le i$ then, according to the value of the power k:
   a. if $k < i - j$: $s_{ij}^k = 0$
   b. if $k = i - j$: $s_{ij}^k = 1$
   c. if $k > i - j$: s_{ij}^k = sum of the monomials of degree $k - i + j$ in $\alpha_j, \alpha_{j+1}, \ldots, \alpha_i$ (example: $s_{31}^5 = \alpha_1^3 + \alpha_2^3 + \alpha_3^3 + \alpha_1^2\alpha_2 + \alpha_1^2\alpha_3 + \alpha_2^2\alpha_1 + \alpha_2^2\alpha_3 + \alpha_3^2\alpha_1 + \alpha_3^2\alpha_2 + \alpha_1\alpha_2\alpha_3$).

The aforementioned generic assumption on the value of M_{ij}^k is true for the peculiar case $k = 1$. If we assume it true for a given value of the power k, then, provided that the only nonzero terms of the matrix $\mathbf{M}$ are of the forms $M_{jj} = \alpha_j$ and $M_{j+1j} = \beta_j$:

$$M_{ij}^{k+1} = \alpha_j M_{ij}^k + \beta_j M_{ij+1}^k$$

$$= \alpha_j \left(\prod_{m=j}^{i-1} \beta_m \right) s_{ij}^k + \beta_j \left(\prod_{m=j+1}^{i-1} \beta_m \right) s_{ij+1}^k$$

$$= \left(\prod_{m=j}^{i-1} \beta_m \right) (\alpha_j s_{ij}^k + s_{ij+1}^k) \quad .$$

The first line shows that for $j > i$, $M_{ij}^{k+1} = 0$ as this is already true for $\mathbf{M^k}$. For $j \le i$, we can check easily that $s_{ij}^{k+1} = \alpha_j s_{ij}^k + s_{ij+1}^k$:

1. true for $k < i - j - 1$ (all s terms equal 0)
2. true for $k = i - j - 1$ ($s_{ij}^k = 0$ and $s_{ij}^{k+1} = s_{ij+1}^k = 1$)
3. true for $k = i - j$ (if $i = j$ then $s_{ii}^{k+1} = \alpha_i^{k+1}$, $s_{ii}^k = \alpha_i^k$, and $s_{ii+1}^k = 0$; if $i > j$ then $s_{ij}^{k+1} = \alpha_j + \alpha_{j+1} + \cdots + \alpha_i$, $s_{ij}^k = 1$, and $s_{ij+1}^k = \alpha_{j+1} + \cdots + \alpha_i$)
4. true for $k > i - j$ (s_{ij}^{k+1} is the sum of all the products of $\alpha_j, \alpha_{j+1}, \ldots, \alpha_i$ with a global degree $k - i + j + 1$; we can split this sum into two terms: the first involves all the products involving at least one α_j factor and writes $\alpha_i s_{ij}^k$; the second involves all the products with no α_j factor and writes s_{ij+1}^k).

By construction, all the components of the vector $\vec{N}(0)$ equal zero, except the first one. Hence, only the first column of the successive powers of the matrix $\mathbf{M}$ is used to compute $\vec{N}(t)$. In particular,

$$N_k(t) = (\exp \mathbf{M})_{k1} = \sum_{\ell=0}^{\infty} M_{k1}^{\ell} \frac{t^{\ell}}{\ell!} \quad .$$

But for $\ell < k - 1$, $M_{k1}^{\ell} = 0$; for $\ell = k - 1$, $M_{k1}^{\ell} = \prod_{m=1}^{k-1} \beta_m$; and for $\ell = k$, $M_{k1}^k = \prod_{m=1}^{k-1} \beta_m \cdot \sum_{m=1}^{k} \alpha_m$. This allows us to write the following limited expansion:

$$N_k(t) = M_{k1}^{k-1} \cdot \frac{t^{k-1}}{(k-1)!} + M_{k1}^k \cdot \frac{t^k}{k!} + o(t^k)$$

$$= \left(\prod_{i=1}^{k-1} \beta_i \right) \cdot \frac{t^{k-1}}{(k-1)!} \cdot \left[1 + \frac{t}{k} \sum_{i=1}^{k} \alpha_i + o(t) \right] \quad .$$

This is Eq. (3). Finally, the first-order expansion of the ratio N_{k+1}/N_k yields Eq. (4):

$$R_k(t) = \frac{N_{k+1}(t)}{N_k(t)} = \frac{\beta_k t}{k} \left[1 + \frac{t}{k+1} \sum_{i=1}^{k+1} \alpha_i - \frac{t}{k} \sum_{i=1}^{k} \alpha_i + o(t) \right]$$

$$= \frac{\beta_k t}{k} \left[1 + \frac{\alpha_{k+1} - \frac{1}{k} \sum_{i=1}^{k} \alpha_i}{k+1} t + o(t) \right] \quad .$$

We can now derive the sensitivities of $R_k(t)$ to β_k and t. As $\alpha_k = -(\sigma_{a,k}\Phi + \lambda_k)$ and $\beta_k = \sigma_{c,k}\Phi + \lambda_k f_{k \to k+1}$ (see Sec. III.A), α_k may be written as $\alpha_k = \gamma_k - \beta_k$, where γ_k does not depend on β_k. If we consider $R_k(t)$ as a function of β_k alone, we can write

$$\frac{dR_k}{d\beta_k} = \frac{R_k}{\beta_k} + \frac{R_k}{1 + O(t)} \left[\frac{t}{k(k+1)} + o(t) \right]$$

or

$$\frac{dR_k}{d\beta_k} \Big/ \frac{R_k}{\beta_k} = 1 + \frac{\beta_k t}{k(k+1)} + o(t) \quad .$$

This is Eq. (5a). If we consider $R_k(t)$ as a function of t alone, we can write in turn

$$\frac{dR_k}{dt} = \frac{R_k}{t} + \frac{R_k}{1+O(t)}\left[\frac{\alpha_{k+1} - \frac{1}{k}\sum_{i=1}^{k}\alpha_i}{k+1} + O(t)\right]$$

or

$$\frac{dR_k}{dt}\Big/\frac{R_k}{t} = 1 + \frac{\alpha_{k+1} - \frac{1}{k}\sum_{i=1}^{k}\alpha_i}{k+1}\,t + o(t) \quad .$$

This is Eq. (5b).

REFERENCES

1. A. D'ANGELO, F. CLERI, P. MARIMBEAU, M. SALVATORES, and J. P. GROUILLER, "Analysis of Sample and Fuel Pin Irradiation in PHÉNIX for Basic Nuclear Data Validation," *Nucl. Sci. Eng.*, **105**, 244 (1990).

2. R. SOULE and E. FORT, "Contribution to the Validation of JEF2 Actinide Nuclear Data: Analysis of Fuel and Sample Irradiation Experiments in PHÉNIX," *Proc. Global '97 Int. Conf. Future Nuclear Systems*, Yokohama, Japan, September 1997.

3. A. GANDINI, M. SALVATORES, and L. TONDINELLI, "New Developments in Generalized Perturbation Methods in the Nuclide Field," *Nucl. Sci. Eng.*, **62**, 339 (1977).

4. J. M. KALLFELZ, G. B. BRUNA, G. PALMIOTTI, and M. SALVATORES, "Burnup Calculations with Time-Dependent Generalized Perturbation Theory," *Nucl. Sci. Eng.*, **62**, 304 (1977).

5. D. G. CACUCI, *Sensitivity and Uncertainty Analysis Theory*, Vol. 1, Chapman & Hall/CRC, Boca Raton, Florida (2003).

6. A. GANDINI, "Uncertainty Analysis and Experimental Data Transposition Methods Based on Perturbation Theory," *Uncertainty Analysis*, Y. RONEN, Ed., CRC Press, Boca Raton, Florida (1988).

7. G. RIMPAULT, D. PLISSON, J. TOMMASI, R. JACQMIN, J. M. RIEUNIER, D. VERRIER, and D. BIRON, "The ERANOS Code and Data System for Fast Reactor Neutronic Analyses," *Proc. Int. Conf. PHYSOR 2002: The New Frontiers of Nuclear Technology—Reactor Physics, Safety and High-Performance Computing*, Seoul, Korea, October 7–10, 2002.

8. Organisation for Economic Co-operation and Development, available on the Internet at http://www.nea.fr/html/dbdata/projects/nds_jef.htm; see also R. JACQMIN et al., "The JEFF-3.0 Nuclear Data Library," *Proc. Int. Conf. PHYSOR 2002: The New Frontiers of Nuclear Technology—Reactor Physics, Safety and High-Performance Computing*, Seoul, Korea, October 7–10, 2002.

9. Organisation for Economic Co-operation and Development, available on the Internet at http://www.nea.fr/html/dbdata/projects/decay

10. R. W. MILLS, "Fission Product Yield Evaluation," PhD Thesis, University of Birmingham, United Kingdom (1995).

11. G. RIMPAULT, "Algorithmic Features of the ECCO Cell Code for Treating Heterogeneous Fast Reactor Subassemblies," *Proc. Int. Conf. Mathematics and Computation, Reactor Physics, and Environmental Analyses*, Portland, Oregon, April 30–May 4, 1995.

12. J. P. GROUILLER, G. FLAMENBAUM, and G. GILLET, "Cycle du combustible des réacteurs à neutrons rapides. Système de codes MECCYCO," *Proc. Int. Conf. PHYSOR'90: Physics of Reactors—Operation, Design and Computation*, Marseille, France, April 22–26, 1990, Vol. 2, p. XI-24.

13. T. R. ENGLAND and B. F. RIDER, "Evaluation and Compilation of Fission Product Yields 1993," LA-UR-94-3106, Los Alamos National Laboratory (1993); see also http://ie.lbl.gov/fission.html

14. G. GAILLARD-GROLEAS, F. SUDREAU, and D. WARIN, "Phénix Irradiation Program on Fuels and Targets for Transmutation," *Proc. Int. Conf. GLOBAL 2003: Atoms for Prosperity—Updating Eisenhower's Global Vision for Nuclear Energy*, New Orleans, Louisiana, November 16–20, 2003.

3 La mesure et la modélisation des données

Malgré des avancées notables dans le développement de modèles *ab initio* en physique nucléaire, la mesure est toujours d'une façon ou d'une autre à la base de toutes les données évaluées indispensables à la majorité des applications.

Néanmoins, les modèles de réaction nucléaires constituent depuis longtemps l'ossature des évaluations, d'une part en garantissant le respect des lois de la physique et d'autre part en permettant de compléter les mesures manquantes.

3.1 La mesure

Dans le cadre du projet Mini-INCA, des mesures semi-intégrales ont été réalisées auprès du réacteur à haut flux de l'ILL à Grenoble. Ces mesures avaient pour objectif de mieux connaître les sections efficaces de capture et de fission des actinides mineurs dans le domaine thermique (de quelques dizaines à quelques centaines de milli-eV) [Bringer 07]. Deux techniques expérimentales ont été utilisées.

La première consistait en l'irradiation d'échantillons suivie de mesures des produits de réaction qui étaient identifiés soit via leur décroissance radioactive β ou α, soit par spectrométrie de masse [Gourgiotis 11,13].

La seconde technique était basée sur le développement et l'utilisation de chambres à fission miniatures permettant de mesurer en ligne l'évolution de la transmutation (par capture) et de l'incinération (par fission) des échantillons d'actinide [Letourneau 11].

Dans ces deux techniques la simulation numérique des expériences, et en particulier de la compétition entre les principales réactions nucléaires et décroissances radioactives affectant l'évolution de la composition des échantillons, a permis de remonter aux valeurs des sections efficaces recherchées. Ce type d'expériences nécessite une bonne connaissance du spectre en énergie des neutrons dans les canaux de mesure et plusieurs études ont été menées à ce sujet, notamment dans le cadre du stage de W. Monange [Monange 06].

Par ailleurs, des études de sensibilité aux données nucléaires de paramètres clés pour l'incinération des actinides mineurs en réacteurs ont également été réalisées dans le cadre de la thèse de O. Bringer. Ce travail a permis de mettre en évidence les données à améliorer pour permettre l'incinération du neptunium-237 et de l'américium-241 en réacteur dans de bonnes conditions [Bringer 08].

3.2 La modélisation

Concernant la modélisation des réactions nucléaires, le périmètre des travaux s'est élargi aux réactions induites par photons, notamment dans le cadre de la détection et de l'identification de matières nucléaires, dans des containers par exemple [Agelou 09]. Les recherches ont porté sur l'amélioration des données des actinides en utilisant les modèles de réactions nucléaires les plus performants [Raskinyte 06] [Dupont 07]. Une étude spécifique de l'absorption dans la résonance dipolaire géante des noyaux a fait l'objet du stage de E. Benguigui [Benguigui 09].

3.2.1 Modélisation des réactions photonucléaires

Les données nucléaires des réactions induites par photons sont importantes pour diverses applications, y compris la simulation de sources de neutrons intenses basées sur la production de photo-neutrons qui nécessite des données jusqu'à 130 MeV.

Aux basses énergies, inférieures à environ 30 MeV, la résonance dipolaire géante (GDR) est le mécanisme d'excitation dominant. À des énergies plus élevées, jusqu'au seuil des pions (environ 140 MeV), le modèle de la photoabsorption sur une paire neutron-proton (quasideuteron) devient dominant. La section efficace de photoabsorption est la somme de ces deux composantes.

L'étape de prééquilibre lors de l'émission de particules est traitée avec le modèle classique des excitons. À l'équilibre, les voies de désexcitation du noyau composé sont traitées dans le formalisme statistique de Hauser-Feshbach. Les coefficients de transmission des neutrons dans la voie de sortie sont calculés avec un potentiel optique déformé développé pour l'interaction neutron-actinide. Les coefficients de transmission à travers les barrières de fission sont calculés dans le cadre de la théorie des voies de fission de Bohr.

Ces calculs sont effectués à l'aide d'un code unique, TALYS, afin de modéliser de manière cohérente les sections efficaces de réaction, les spectres d'énergie des particules et les sections efficaces de production des résiduels pour toutes les voies ouvertes jusqu'à 130 MeV. Les paramètres des modèles ont été soigneusement choisis et ajustés si nécessaire afin de reproduire au mieux les données expérimentales pour les systèmes γ + Th-232, U-235,238 et Pu-239.

A titre d'illustration la figure ci-dessous présente les sections efficaces totale (γ,f) et partielles (γ,n_i f) pour la photofission du Th-232. L'ensemble de ce travail de modélisation est présenté dans la publication [Dupont 07] qui suit.

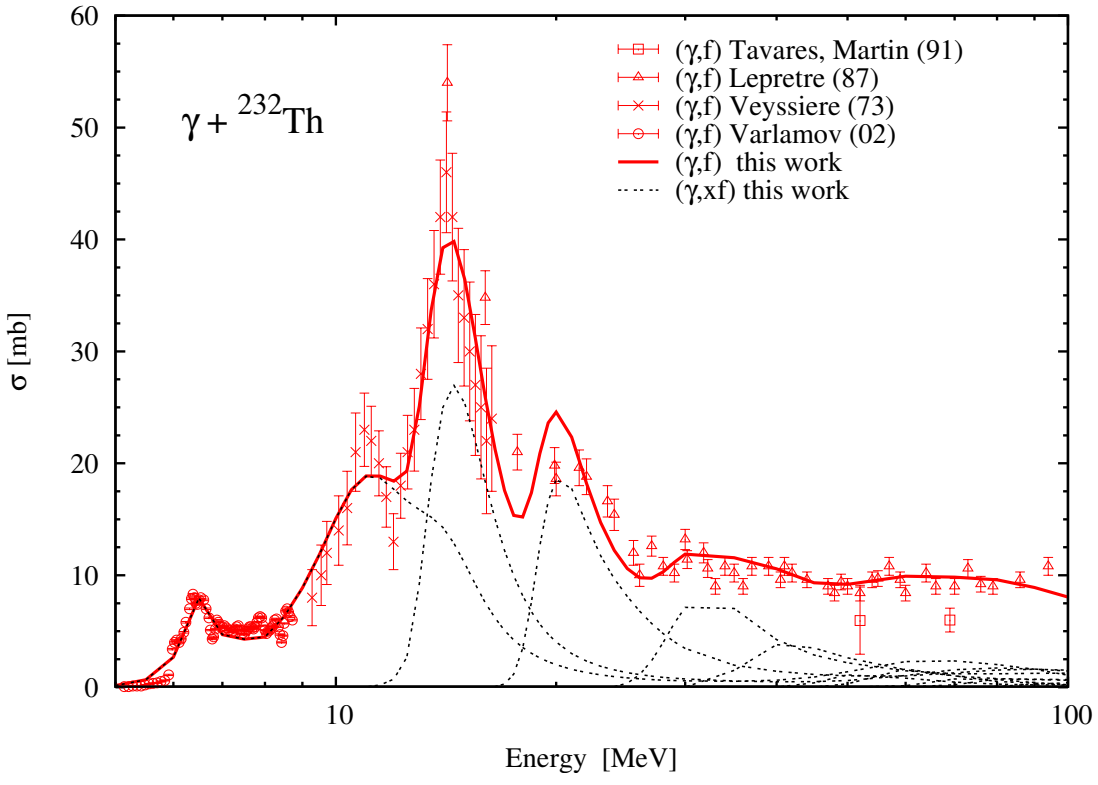

Modélisation des sections efficaces de photofission totale (γ, f) et partielles (γ, n_i f) du Th-232

[Dupont 07]

E. Dupont, et al., Photonuclear data evaluations of actinides up to 130 MeV, Int. Conf. on Nuclear Data for Science and Technology, Nice, France, p.685 (2007)

http://doi.org/10.1051/ndata:07497

International Conference on Nuclear Data for Science and Technology 2007
DOI: 10.1051/ndata:07497

Photonuclear data evaluations of actinides up to 130 MeV

E. Dupont[1,a], I. Raškinytė[1], A.J. Koning[2], and D. Ridikas[1]

[1] CEA Saclay, DSM/DAPNIA/SPhN, 91191 Gif-sur-Yvette, France
[2] NRG Petten, P.O. Box 25, 1755 ZG Petten, The Netherlands

Abstract. There is a renewed interest in photonuclear reactions for various applications such as active nuclear material detection techniques and radioactive ion beam or neutron production targets. However, contrary to the neutron induced reactions, evaluated nuclear data libraries contain little information for photons. In particular, there are very few photonuclear data evaluations of actinides above 20 MeV. This paper gives an overview of our on-going activities on photonuclear data evaluation of actinides up to 130 MeV.

1 Introduction

Nuclear data of photo-induced reactions are important for a variety of existing or emerging applications. Among them are radiation transport simulation and radiation shielding design of accelerators or innovative reactors, activation analysis, safeguards and inspection technologies. In terms of incident energies, the giant dipole resonance (GDR) region below 30 MeV is essential for most applications. However, photonuclear data up to 130 MeV are also necessary for the simulation of intense neutron sources and to complement the neutron and proton high-energy libraries.

Actinide cross section evaluations were reviewed in the framework of a specific IAEA coordinated research project [1]. Recently, major actinide cross sections and spectra were evaluated in the framework of a collaboration between LANL and CEA [2]. These evaluations were done for incident photon energies below 20 MeV. To our knowledge, ^{235}U, ^{238}U, and ^{237}Np from the JENDL Photonuclear Data File [3] are the only actinide evaluations available above 20 MeV.

The present work aims at the extension of actinide evaluations up to 130 MeV. This paper presents on-going evaluation activity for ^{232}Th [4], ^{235}U [4,5], ^{238}U, and ^{239}Pu [6]. Recent measurements of delayed neutron yields performed at CEA [7,8] will complement this evaluation effort and the outcome will be proposed for insertion into the Joint Evaluated Fission and Fusion (JEFF) library to respond to application needs.

2 Photonuclear reactions

In a photoreaction, the target nucleus is directly excited by the incident photon. Below a few tens of MeV, the main decay channels are neutron emission and fission only, because of the high Coulomb barrier of heavy nuclei. However, light charged particle emission may become significant at higher energies.

In this work, the photoabsorption process is described by the GDR and quasideuteron mechanisms. The preequilibrium step of particle emission is treated with the classical exciton model. At equilibrium, the compound nucleus decay channels are handled within the Hauser-Feshbach statistical formalism. Neutron transmission coefficients in the exit channel are calculated with a global deformed optical model potential (OMP) developed for neutron-actinide interaction. Finally, the transmission coefficients through fission barriers, described by inverted parabola, are calculated within the fission channels theory of Bohr.

These calculations are performed using one single code, TALYS [9], to model in a consistent way the reaction cross sections, particle energy spectra, and residual production cross sections of all open channels up to 130 MeV.

2.1 Photoabsorption

At low energies, below about 30 MeV, the GDR is the dominant excitation mechanism. At higher energies, up to the pion threshold (about 140 MeV), the phenomenological model of photoabsorption on a neutron-proton pair (quasideuteron, QD) becomes dominant. The photoabsorption cross section is the sum of these two components.

The GDR component of deformed nuclei, such as actinides, is given as a sum of two Lorentzians

$$\sigma_{GDR}(E_\gamma) = \sum_{i=1,2} \sigma_{E1,i} \frac{E_\gamma^2 \Gamma_{E1,i}^2}{(E_\gamma^2 - E_{E1,i}^2)^2 + E_\gamma^2 \Gamma_{E1,i}^2}, \qquad (1)$$

where $\sigma_{E1,i}$, $E_{E1,i}$, $\Gamma_{E1,i}$ are the GDR peak cross section, energy position and width respectively.

The QD component relates the photoabsorption cross section to the experimental deuteron photodisintegration cross section $\sigma_d(E_\gamma)$

$$\sigma_{QD}(E_\gamma) = \frac{L}{A} NZ \sigma_d(E_\gamma) f(E_\gamma), \qquad (2)$$

where L is the Levinger parameter [10] and $f(E_\gamma)$ is the Pauli-blocking function [11].

2.2 Nucleus decay

In the statistical approach, the competition between all decay channels involves major ingredients such as nuclear level

[a] Presenting author, e-mail: emmeric.dupont@cea.fr

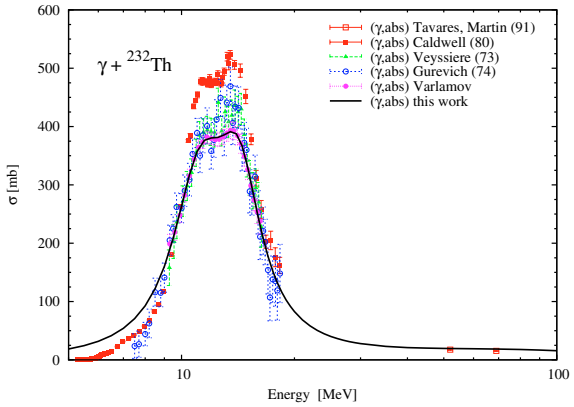

Fig. 1. Modelling of ^{232}Th photoabsorption cross section.

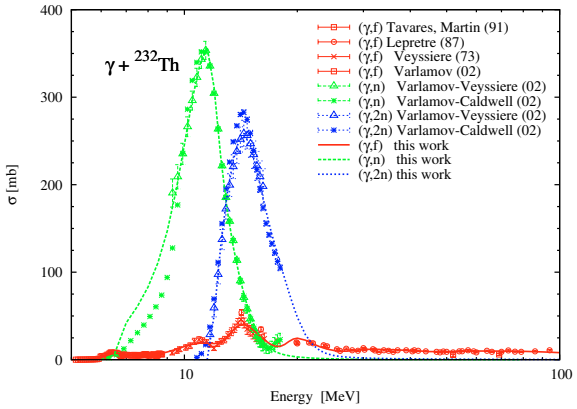

Fig. 2. Modelling of ^{232}Th (γ,n), (γ,2n) and (γ,f) cross sections.

density and transmission coefficients through optical potential or fission barrier. The nuclear level density is modelled using the Gilbert-Cameron composite formula [12] with an energy-dependent level density parameter [13]. The following paragraphs shortly describe the main models used to calculate neutron and fission transmission coefficients.

2.2.1 Neutron emission

Assuming time-reversal invariance of nuclear reactions, the exit channel in the (γ,n) reaction shares the same nuclear parameters as the entrance channel of the (n,γ) reaction. Therefore, neutron transmission coefficients for the exit channel are calculated with a global coupled-channels optical potential developed for neutron-actinide interaction up to 200 MeV by Soukhovitskii [14]. In the latter work, the optical potential parameters were adjusted to reproduce available neutron- and proton-induced cross sections on ^{238}U and ^{232}Th targets. This global potential together with local deformation parameters was used to calculate neutron transmission coefficients.

2.2.2 Fission channel

In this work, fission barriers are described by a double humped barrier model for all nuclei. One assumes that tunnelling through two barriers A and B can be separated into two steps, and the effective fission transmission coefficient is given by

$$T_{eff} = T_A \frac{T_B}{T_A + T_B}. \quad (3)$$

According to the fission channels theory of Bohr, the total fission transmission coefficient is the sum of the individual transmission coefficients for each transition state through which the nucleus may tunnel. The individual transmission coefficients are calculated using the Hill-Wheeler expression

$$T_{HW}(E) = \left[1 + exp\left(-2\pi \frac{E - B_f}{\hbar\omega}\right)\right]^{-1}, \quad (4)$$

where B_f is the barrier height relative to the nucleus ground state and $\hbar\omega$ is the barrier curvature. Those barrier parameters are adjusted to reproduce the experimental cross sections.

3 Calculations and results

The TALYS code contains models for comprehensive nuclear reaction calculations. The version TALYS-0.72 [15] of this code is used to reproduce the data available in the EXFOR database [16] and to fill any experimental gap with model predictions up to 130 MeV.

3.1 Thorium-232

Photoabsorption. A recent review of photoneutron emission measurements made by Varlamov [17] shows systematic discrepancies between Livermore [18] and Saclay [19] experimental data. In the present work, the ^{232}Th GDR parameters were adjusted to reproduce the corrected photoabsorption cross section proposed by Varlamov (fig. 1). The same GDR parameters were assumed for the ^{231}Th and ^{230}Th isotopes since no experimental data could be found.

Neutron emission. In the present calculations we have only used the first three states of the ground state rotational band together with unaltered optical potential parameters from Soukhovitskii [14]. In addition ^{231}Th + neutron transmission coefficients have also been used for ^{230}Th + neutron exit channel. The influence of these approximations on (γ,n), (γ,2n) and (γ,f) cross sections is negligible. The quadrupolar and hexadecapolar deformation parameters published by Soukhovitskii for ^{232}Th have been used for ^{231}Th and ^{230}Th also. In addition, the default normalization of the matrix element in TALYS exciton model was fine-tuned to better reproduce the experimental data (fig. 2).

Photofission. There are experimental evidences that the fission barrier of thorium isotopes is more complex than for uranium or plutonium isotopes. However, we have approximated the fission barriers with a double-humped barrier and ignore the splitting of the outer barrier. Nevertheless, the experimental ^{232}Th photofission cross section was rather well reproduced as shown in figure 3 which compares the calculated fission cross sections with measurements. The presence of a peak in the fission cross section between 6 and 7 MeV is due to 0^- and 1^- transition states located about half-a-MeV above the second fission barrier of ^{232}Th.

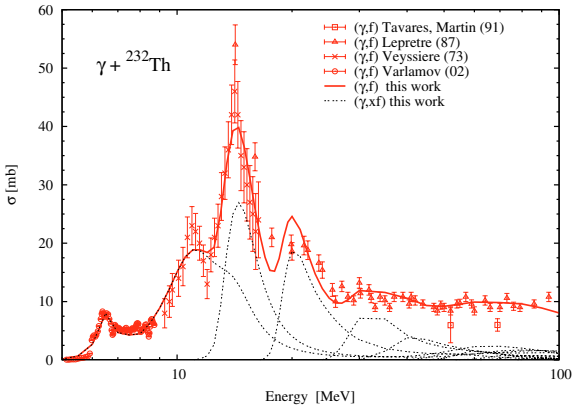

Fig. 3. Details of the ^{232}Th photofission cross section.

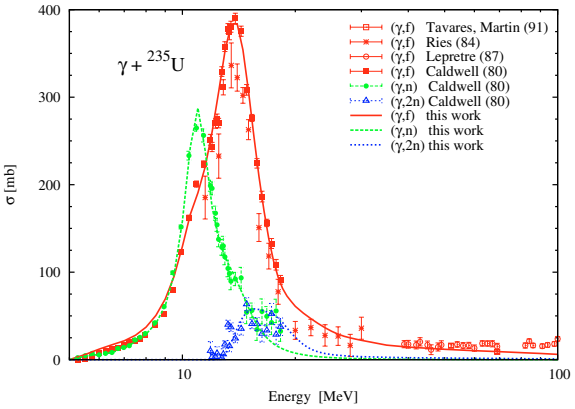

Fig. 5. Modelling of ^{235}U (γ,n), (γ,2n) and (γ,f) cross sections.

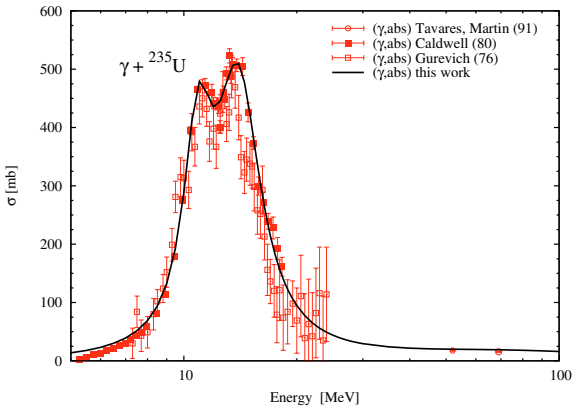

Fig. 4. Modelling of ^{235}U photoabsorption cross section.

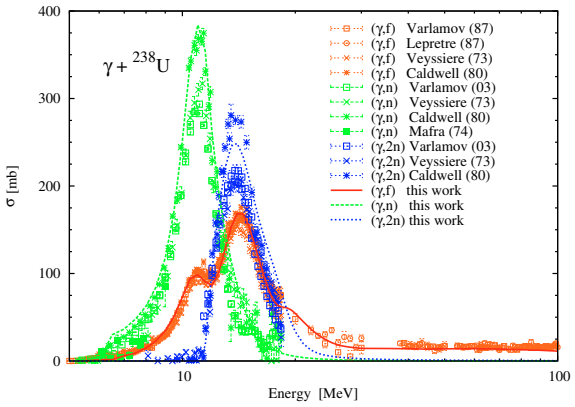

Fig. 6. Modelling of ^{238}U (γ,n), (γ,2n) and (γ,f) cross sections.

3.2 Uranium-235

Photoabsorption. The GDR parameters used in TALYS for uranium isotopes are from RIPL-2 [20]. The latter were adjusted onto experimental data by Caldwell [18]. Figure 4 shows a comparison between TALYS photoabsorption cross section and experimental data. Caldwell points are given as the sum of (γ,n), (γ,2n) and (γ,f) partial cross sections, while Gurevich [21] directly measured the total photoabsorption cross section.

Neutron emission. The neutron transmission coefficients for the ^{234}U + n exit channel were calculated with the global deformed OMP by Soukhovitskii [14] using the same approximation than in the ^{232}Th case. For the ^{234}U deformation parameters, we have used interpolated values between ^{233}U and ^{235}U parameters given in the reference [14]. The emission of photoneutrons above 12 MeV was further improved by adjusting the preequilibrium normalization constant (fig. 5).

Photofission. A number of calculations were done in order to find a set of fission barrier parameters which reproduce Caldwell [18] experimental data (fig. 5).

3.3 Uranium-238

Photoabsorption. This cross section is calculated using GDR parameters from RIPL-2 [20]. As for ^{235}U, the latter were adjusted to reproduce Caldwell measurements [18].

Neutron emission. All neutron transmission coefficients are calculated with Soukhovitskii global OMP using deformation parameters published in the reference [14]. Figure 6 shows that (γ,n) cross section is in good agreement with Caldwell measurement, which is a consequence of the GDR parameters choice. However, present results overestimate both Veyssiere [19] and Varlamov [17] data. New calculations using GDR parameters based on recommended data proposed by Varlamov are being performed.

Photofission. Starting from RIPL-2 fission barrier parameters, several iterations were necessary in order to reach an optimal reproduction of the experimental photofission cross sections (fig. 6).

3.4 Plutonium-239

Photoabsorption. Gurevich [21] and de Moraes [22] directly measured the photoabsorption cross section, whereas Berman [23] measured the main partial cross sections. Their sum also gives the total photoabsorption cross section. To be consistent with partial cross sections modelling, present GDR parameters are fitted on Berman data (fig. 7).

Neutron emission. To model the inverse ^{238}Pu + neutron channel we used the Soukhovitskii global OMP together with deformation parameters given in the reference [14] for the

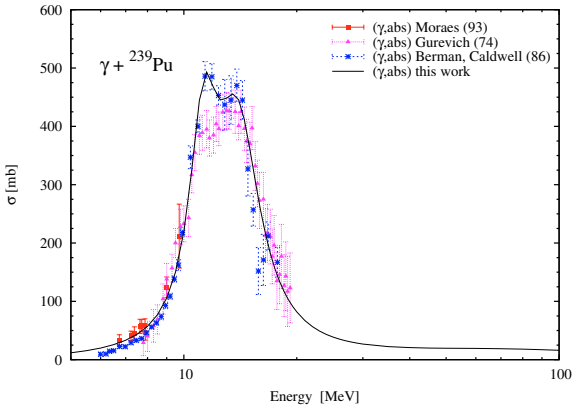

Fig. 7. Modelling of ^{239}Pu photoabsorption cross section.

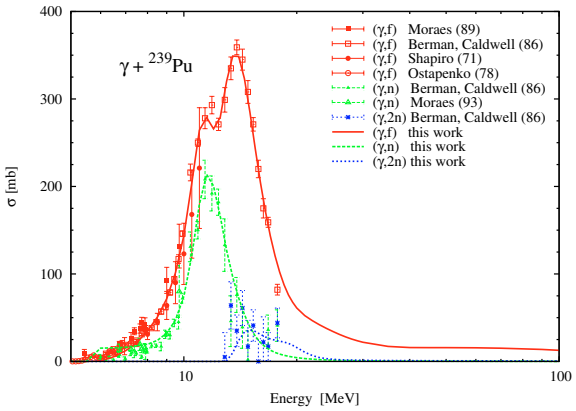

Fig. 8. Modelling of ^{239}Pu (γ,n), (γ,2n) and (γ,f) cross sections.

^{239}Pu nucleus. The same neutron transmission coefficients are used for the ^{237}Pu + neutron $(\gamma, 2n)$ exit channel. Results are displayed on figure 8.

Photofission. Figure 8 also shows a comparison of present calculations with experimental photofission data. Slight adjustments in fission barrier parameters were necessary to improve the agreement between calculation and measurements.

4 From calculation to evaluations

The present results are being converted into the ENDF-6 format thanks to TALYS/TEFAL formatting capabilities [24] and processed with the standard utility codes to check conformity with ENDF rules and procedures. As a final test, these evaluations will be processed through NJOY to build new MCNP(X) files and allow further validation of the quality of the data.

5 Conclusion and outlook

Photonuclear cross sections up to 130 MeV were calculated with the latest version of the TALYS code using a deformed optical potential by Soukhovitskii to model the neutron emission. The fission transmission coefficients were calculated using a double humped barrier model. Fission barriers heights and widths were adjusted in order to reproduce experimental data. Complete evaluated files will be available shortly for ^{232}Th, ^{235}U, ^{238}U and ^{239}Pu. These files will be proposed for insertion into the Joint Evaluated Fission and Fusion (JEFF) library to respond to application needs up to 130 MeV.

References

1. *Handbook on photonuclear data for applications – Cross sections and spectra*, IAEA Report, TECDOC-1178, 2000.
2. M.-L. Giacri-Mauborgne et al., Nucl. Sci. Eng. **153**, 33 (2006).
3. N. Kishida et al., *Proc. of the Int. Conf. on Nuclear Data for Science and Technology, Santa Fe, USA, 2004*.
4. I. Raškinytė et al., *Proc. of the Int. Conf. on Nuclear Reaction Mechanisms, Varenna, Italy, 2006.*
5. I. Raškinytė, E. Dupont, D. Ridikas, *Photonuclear Data Evaluation of* ^{235}U, JEFF Meeting, November 2005, JEF/DOC-1117, and CEA Saclay Report DAPNIA-06-101.
6. I. Raškinytė, E. Dupont, D. Ridikas, *Photonuclear Data Evaluation of* ^{239}Pu, CEA Saclay Report, DAPNIA-06-318, 2006.
7. A. Van Lauwe et al., *Proc. of the Int. Conf. on Nuclear Reaction Mechanisms, Varenna, Italy, 2006.*
8. D. Doré et al., *Delayed neutron yields and time spectra from photofission of actinides* (these proceedings).
9. A. Koning, S. Hilaire, M.C. Duijvestijn, *TALYS-1.0* (these proceedings).
10. J.S. Levinger, Phys. Rev. **84**, 43 (1951).
11. M.B. Chadwick et al., Phys. Rev. C **44**, 814 (1991).
12. A. Gilbert, A.G.W. Cameron, Can. J. Phys. **43**, 1446 (1965).
13. A.V. Ignatyuk, G.N. Smirenkin, A.S. Tishin, Sov. J. Nucl. Phys. **21**, 255 (1975).
14. E.Sh. Soukhovitskii et al., J. Phys. G Nucl. Part. Phys. **30**, 905 (2004).
15. A. Koning, S. Hilaire, M. Duijvestijn, *TALYS-0.72 – User manual*, NRG Report, December 2006.
16. Nuclear Reaction Data Centres Network (NRDC, IAEA), cf. http://www-nds.iaea.org/
17. V.V. Varlamov et al., *Consistent evaluation of photoneutron reaction cross sections using data obtained [...] at Livermore and Saclay*, IAEA Report, INDC(CCP)-440, 2004, p. 37.
18. J.T. Caldwell et al., Phys. Rev. C **21**, 1215 (1980).
19. A. Veyssiere et al., Nucl. Phys. A **199**, 45 (1973).
20. *Handbook for calculations of nuclear reaction data, RIPL-2*, IAEA report, TECDOC-1506, 2006.
21. G.M. Gurevich et al., Nucl. Phys. A **273**, 326 (1976).
22. M.A. de Moraes, M.F. Cesar, Physica Scripta **47**, 519 (1993).
23. B.L. Berman et al., Phys. Rev. C **34**, 2201 (1986).
24. A. Koning, *Creating ENDF-6 files with TALYS*, NRG Report, January 2007 (unpublished).

4 La nécessaire coordination internationale

Les bases de données nucléaires actuelles capitalisent des décennies de recherche, notamment grâce à la collaboration internationale qui s'est mise en place dès les années 60 dans le cadre de l'AIEA et de l'AEN. Les besoins d'amélioration existent toujours mais sont désormais très spécifiques et doivent être priorisés dans un contexte d'optimisation des ressources. Ce travail doit être fait dans une approche pluridisciplinaire en associant étroitement producteurs et utilisateurs de données.

A l'occasion d'un détachement à l'AEN (2009-2014) j'ai eu le privilège de pouvoir contribuer à de nombreuses activités transverses touchant toutes les facettes des données nucléaires : besoin, mesure, modélisation, évaluation et validation [Dupont 11a,14].

Parmi les principales réalisations on peut citer la compilation des données de réactions nucléaires dans la base EXFOR [Dupont 11b,11c] [Zeydina 14] [Otuka 11,14], le développement du logiciel de visualisation des données JANIS [Soppera 11,12,14], la participation au projet de bibliothèque JEFF [Koning 11] [Fischer 11,14] et aux groupes de travail du WPEC [Dupont 14]. Ces derniers sont des Groupes d'experts internationaux mandatés par l'AEN pour travailler ensemble à la résolution de problèmes communs aux principaux projets de bibliothèques de données (JEFF, ENDF, JENDL, etc.). Parmi les groupes auxquels j'ai participé et que j'ai contribué à coordonner, les deux plus importants et représentatifs de mes activités de recherche sont les sous-groupes SG33 et SG40-CIELO.

Le sous-groupe SG40-CIELO [Chadwick 14] visait à mettre en place un nouveau modèle collaboratif (Collaborative International Evaluated Library Organization) pour faciliter l'évaluation et la validation des données de réactions nucléaires à l'échelle mondiale en associant les projets nationaux/régionaux (JEFF, ENDF, JENDL) et les organisations internationales (AEN, AIEA). L'accent était mis sur l'évaluation de quelques isotopes prioritaires (H-1, O-16, Fe-56, U-235,238 et Pu-239) pour lesquels toutes les données mesurées et évaluées ont été examinées. Des anomalies ont été identifiées et certaines tendances intégrales prises en compte afin de garantir l'amélioration et la validation des évaluations CIELO. Ce projet pilote s'est conclu avec succès en 2017 [Chadwick 18] et les évaluations produites ont été adoptées dans les bibliothèques de données JEFF-3.3 et ENDF/B-VIII.0.

Le sous-groupe SG33 [Salvatores 14] consistait en l'organisation et l'analyse d'un benchmark international sur les méthodes d'assimilation d'expériences intégrales dans le but d'améliorer les valeurs et incertitudes des données nucléaires. Ce benchmark est basé sur des analyses de sensibilités des paramètres intégraux suivies d'ajustements statistiques des données similaires aux travaux décrits au début de la section 2.2 [Dupont 02a] [Dupont 03]. Le travail du sous-groupe SG33 est présenté dans la section et l'article suivants.

En outre, j'assure depuis 2016 la coordination du Groupe d'experts SG-C du WPEC en charge des demandes d'amélioration des données et de leur incertitude pour les applications du nucléaire via la « High Priority Request List » (HPRL) de l'AEN [Dupont 20]. Au-delà des demandes directes envoyées au SG-C par les utilisateurs de données, les experts du sous-groupe SG46 s'attellent à résoudre le problème inverse consistant à définir les incertitudes sur les données permettant d'atteindre des incertitudes cibles sur les paramètres intégraux d'un réacteur nucléaire. Ce type d'étude avait déjà été réalisé en 2005-2008 dans un cadre similaire (SG26) et les progrès réalisés depuis dans l'assimilation des expériences intégrales (SG33, SG39) et surtout dans l'estimation des incertitudes des données nucléaires appellent à une mise à jour de ce travail. Les premiers résultats, attendus en 2021, devraient être riche d'enseignements sur les données à améliorer en priorité.

4.1 Méthodes d'ajustement pour l'amélioration des données nucléaires

Dans le benchmark du sous-groupe SG33 les principales données nucléaires de quelques isotopes majeurs (essentiellement Na-23, Fe-56, U-235,238, et Pu-239) étaient ajustées pour minimiser l'écart entre les valeurs expérimentales et calculées pour un ensemble de 20 paramètres intégraux mesurés avec précision dans des maquettes de réacteur à spectre rapide. L'ajustement est réalisé sur la base d'un modèle simplifié dans lequel la variation des paramètres intégraux est calculée à partir de leurs coefficients de sensibilité aux données nucléaires. De manière générale la méthode d'assimilation/ajustement revient à minimiser le χ^2 suivant avec une contrainte de linéarité sur les corrections calculées :

$$\min_x\{\chi^2 = (x-\xi)^t C_x^{-1}(x-\xi) + (y-\eta)^t C_y^{-1}(y-\eta)\}$$

avec la contrainte de linéarité : $\eta = f(\xi) = y + S(\xi - x)$.

S est la matrice de sensibilité, x (la variable d'ajustement) et ξ sont les vecteurs des données nucléaires, y et η sont les vecteurs des paramètres intégraux, C_x et C_y sont les matrices de covariance des données nucléaires et des paramètres intégraux, respectivement.

La figure suivante présente un résultat typique d'ajustement d'une des sections efficaces considérées dans cet exercice.

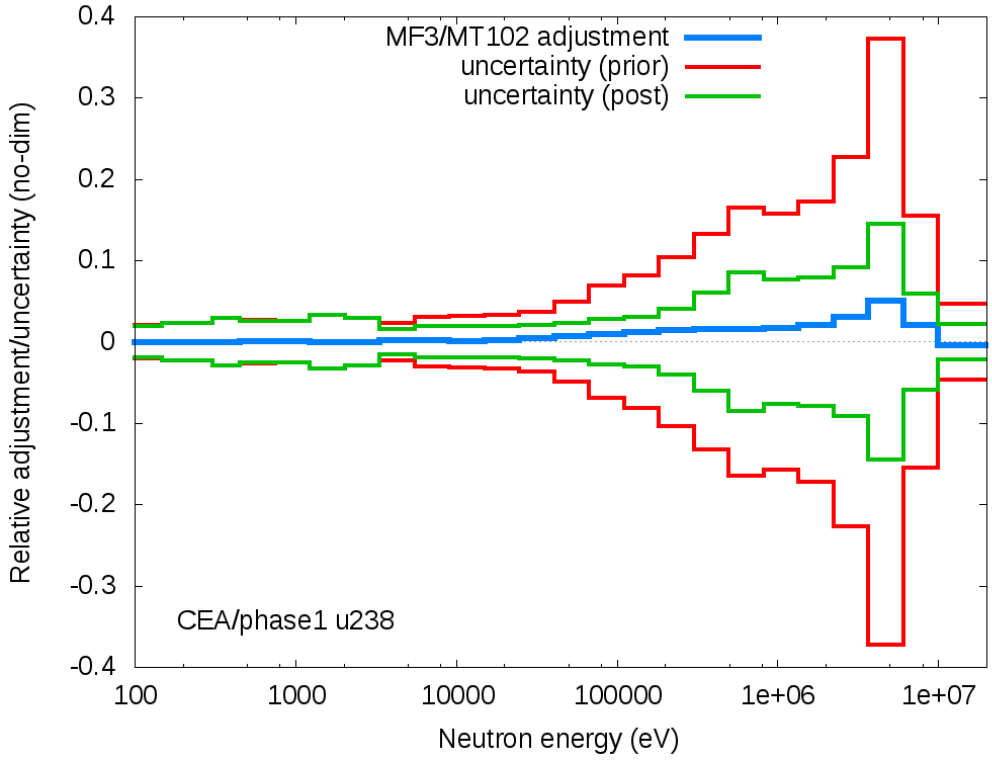

Exemple d'ajustement en fonction de l'énergie de la section efficace de capture de U-238

Les principaux enseignements du sous-groupe SG33 sont résumés ci-dessous ; les figures mentionnées sont celles de la référence [Salvatores 14] dont le papier est reproduit dans les pages suivantes.

- Les résultats des ajustements indiquent des tendances communes sur les données nucléaires importantes, y compris en partant de données différentes et de matrices de covariance différentes. À cet égard, ces méthodologies constituent un outil puissant d'amélioration des données nucléaires (et des incertitudes associées) quand elles sont utilisées de manière appropriée.

- L'ajustement doit porter sur toutes les données nucléaires sensibles afin de fournir des indications pertinentes (cf. les compensations entre l'ajustement de la section de diffusion inélastique et le spectre des neutrons prompts de fission du Pu-239 par exemple, Fig. 20). Il est aussi indispensable de couvrir un large éventail d'expériences intégrales (k_{eff}, coefficients de réactivité, indices de spectre, irradiations, transmissions) avec différents profils de sensibilité pour éviter ou limiter les effets de compensation dans l'ajustement.
- Des incertitudes très différentes sur les données donnent lieu à des ajustements différents (cf. Fig. 24 pour $^{235}U(n,\gamma)$ par exemple). Ce point renforce la nécessité de produire des données de covariance fiables et de bien comprendre l'effet de la sous/surestimation des incertitudes et/ou des corrélations (en énergie, entre réactions, etc.) sur les résultats.
- Dans certains cas l'ajustement est essentiellement guidé par les C/E initiaux de quelques paramètres intégraux seulement. Il est donc essentiel de bien quantifier les incertitudes et corrélations expérimentales, car elles déterminent le poids des paramètres intégraux dans le processus d'ajustement. En d'autres termes, une incertitude expérimentale sous-estimée peut conduire à des tendances biaisées sur l'ajustement des sections efficaces et à une surestimation de la réduction de l'incertitude des paramètres intégraux après ajustement.
- Les incertitudes finales calculées sur les paramètres intégraux dépendent peu des covariances des section efficaces choisies a priori; La réduction de l'incertitude finale est dictée par les incertitudes des expériences intégrales utilisées et ce sont les corrélations a posteriori qui sont principalement responsables de la réduction de l'incertitude des paramètres intégraux des systèmes de référence.

Ces résultats montrent que les différentes méthodes d'ajustement statistique utilisées pour l'analyse et la conception de réacteurs sont bien comprises et qu'elles sont essentiellement équivalentes. Ce travail a également permis de clarifier le rôle de l'ajustement des sections efficaces pour fournir un retour utile aux évaluateurs et aux expérimentateurs afin d'améliorer les données nucléaires et leurs incertitudes.

Des études ultérieures réalisées avec une base de données intégrales plus importante ont permis d'une part d'alerter les évaluateurs sur le manque de fiabilité des covariances évaluées et d'autre part de leur fournir des indications sur les données à corriger pour améliorer les simulations intégrales [Chadwick 18].

La publication [Salvatores 14] reproduite dans les pages suivantes présente tous ces résultats en détail.

[Salvatores 14]

M. Salvatores, et al. (E. Dupont), Methods and issues for the combined use of integral experiments and covariance data: results of a NEA international collaborative study, Nuclear Data Sheets 118, 38 (2014)

http://doi.org/10.1016/j.nds.2014.04.005

Available online at www.sciencedirect.com

ScienceDirect

Nuclear Data Sheets 118 (2014) 38–71

Nuclear Data Sheets

www.elsevier.com/locate/nds

Methods and Issues for the Combined Use of Integral Experiments and Covariance Data: Results of a NEA International Collaborative Study

M. Salvatores,[1,2,*] G. Palmiotti,[2] G. Aliberti,[3] P. Archier,[1] C. De Saint Jean,[1] E. Dupont,[4] M. Herman,[5] M. Ishikawa,[6] T. Ivanova,[7] E. Ivanov,[7] S.-J. Kim,[8] I. Kodeli,[9] G. Manturov,[10] R. McKnight,[3] S. Pelloni,[11] C. Perfetti,[12] A.J.M. Plompen,[13] B.T. Rearden,[12] D. Rochman,[14] K. Sugino,[6] A. Trkov,[9] W. Wang,[15] H. Wu,[15] and W.-S. Yang[3,16]

[1] *CEA, Nuclear Energy Division, Cadarache, Saint-Paul-lez-Durance, France*
[2] *Idaho National Laboratory (INL), Idaho Falls, ID, 83415, USA*
[3] *Argonne National Laboratory (ANL), Argonne, IL, 60439, USA*
[4] *OECD, Nuclear Energy Agency (NEA), Issy-les-Moulineaux, France*
[5] *National Nuclear Data Center, Brookhaven National Laboratory (BNL), Upton, NY, 11973, USA*
[6] *Japan Atomic Energy Agency (JAEA), Tokai-mura, Ibaraki, Japan*
[7] *Institut de Radioprotection et de Surete Nucleaire (IRSN), Fontenay-aux-Roses, France*
[8] *Korea Atomic Energy Research Institute (KAERI), Daejeon, South Korea*
[9] *Jozef Stefan Institute (JSI), Ljubljana, Slovenia*
[10] *Institute of Physics and Power Engineering (IPPE), Obninsk, Russia*
[11] *Paul Scherrer Institut (PSI), Villigen, Switzerland*
[12] *Oak Ridge National Laboratory (ORNL), Oak Ridge, TN, 37831, USA*
[13] *Institute for Reference Materials and Measurements (IRMM), Geel, Belgium*
[14] *Nuclear Research and Consultancy Group (NRG), Petten, The Netherlands*
[15] *China Institute of Atomic Energy (CIAE), China Nuclear Data Center, Beijing, China*
[16] *Purdue University, West Lafayette, IN, 47907, USA*

The Working Party on International Nuclear Data Evaluation Cooperation (WPEC) of the Nuclear Science Committee under the Nuclear Energy Agency (NEA/OECD) established a Subgroup (called "Subgroup 33") in 2009 on "Methods and issues for the combined use of integral experiments and covariance data." The first stage was devoted to producing the description of different adjustment methodologies and assessing their merits. A detailed document related to this first stage has been issued. Nine leading organizations (often with a long and recognized expertise in the field) have contributed: ANL, CEA, INL, IPPE, JAEA, JSI, NRG, IRSN and ORNL. In the second stage a practical benchmark exercise was defined in order to test the reliability of the nuclear data adjustment methodology. A comparison of the results obtained by the participants and major lessons learned in the exercise are discussed in the present paper that summarizes individual contributions which often include several original developments not reported separately.

The paper provides the analysis of the most important results of the adjustment of the main nuclear data of 11 major isotopes in a 33-group energy structure. This benchmark exercise was based on a set of 20 well defined integral parameters from 7 fast assembly experiments. The exercise showed that using a common shared set of integral experiments but different starting evaluated libraries and/or different covariance matrices, there is a good convergence of trends for adjustments. Moreover, a significant reduction of the original uncertainties is often observed. Using the a–posteriori covariance data, there is a strong reduction of the uncertainties of integral parameters for reference reactor designs, mainly due to the new correlations in the a–posteriori covariance matrix. Furthermore, criteria have been proposed and applied to verify the consistency of differential and integral data used in the adjustment. Finally, recommendations are given for an appropriate use of sensitivity analysis methods and indications for future work are provided.

* Corresponding author: massimo.salvatores@cea.fr

http://dx.doi.org/10.1016/j.nds.2014.04.005
0090-3752/2014 Published by Elsevier B.V.

CONTENTS

I. FRAMEWORK AND BACKGROUND

A. Scope and Objectives

Nuclear data uncertainty impact studies [1–3] have pointed out that the present uncertainties on nuclear data should be significantly reduced, in order to get the full benefit from advanced modeling and simulation initiatives that have been launched worldwide in recent years. Only a parallel effort in advanced simulation and in nuclear data improvement will be able to provide designers with more general and well validated calculation tools that would be able to meet design target accuracies.

Tight design target accuracies, required in order to comply with safety and optimization requirements and objectives, can only be met if very accurate nuclear data are used for a large number of isotopes, reaction types and energy ranges.

The required accuracies on the nuclear data are difficult to meet using only differential experiments, even if innovative experimental techniques are used.

The use of integral experiments has been essential in the past to ensure enhanced predictions for power fast reactor cores. In some cases, these integral experiments have been documented in an effective manner and associated uncertainties are well understood.

A combined use of scientifically based covariance data and of integral experiments can be made using advanced statistical adjustment techniques (see, *e.g.* [4–6]). These techniques can provide in a first step adjusted nuclear data for a wide range of applications, together with new, improved covariance data and bias factors (with reduced uncertainties) for the required design parameters, in order to meet design target accuracies.

Moreover, the role for cross section adjustment is more and more perceived as that of providing useful feedback to evaluators and differential measurement experimentalists in order to improve the knowledge of neutron cross sections to be used in a wider range of applications.

Despite its recognized potential, the adjustment process has raised legitimate questions related both to phys-

ical meaning of the individual (*i.e.*, by isotope, reaction type and energy range) "adjustments", and to possible compensation effects since integral experiments depend on a large number of parameters. Moreover, the first adjustments relied on uncertainty data essentially based on physicists' judgment and not on any formal approach.

It has also been pointed out that there exists no clear definition of the application domain of the adjusted multigroup data sets. When a new reactor concept is investigated, it is difficult to define what is the mathematical or physical extrapolation method (if any) to be used together with the previously adjusted data library. In any case, since the adjustments are performed at the multigroup level, they will also be related to the weighting function used to produce the original multigroup library and no unique procedures can be used to transfer the adjustments from the broad group level (where the adjustments are usually performed) to a fine group level or, even preferable, to the continuous energy level. Similarly, self-shielding effects are not necessarily accounted for explicitly.

Finally, the use of the a–posteriori covariance matrix (both variances and correlations) is not a self-evident exercise and in fact in many cases use is made only of a–posteriori variances.

The Working Party on International Nuclear Data Evaluation Cooperation (WPEC) of the OECD/NEA Nuclear Science Committee recognized the importance of these issues and established a Subgroup (called "Subgroup 33") on "Methods and issues for the combined use of integral experiments and covariance data". In its mandate "it is proposed for this WPEC Subgroup to study methods and issues of the combined use of integral experiments and covariance data, with the objective of recommending a set of best and consistent practices in order to improve evaluated nuclear data files. Indication should be provided on how to best exploit existing integral experiments, define new ones if needed, provide trends and feedback to nuclear data evaluators and measurers".

The Subgroup activity has been completed and a final report is being assembled. The present paper summarizes and discusses the main results and recommendations.

B. Activities of the Subgroup

In summary, the general understanding of the adjustment methods, their theory and application, suggests a number of potential difficulties that have to be examined carefully, in order to agree on the best approach which would allow taking full benefit from the potential of the method. This has been the general objective of the activity of the Subgroup.

The first step of the Subgroup activity was the compilation of a detailed report [7] with the assessment and comparison of the methodologies that the different participants to this Subgroup employ for adjustment of neutron cross section data using the observed discrepancies between calculated and measured values of integral experiments. To this purpose a documentation of the used adjustment methodologies, developed during more than three decades from the early sixties to the late nineties, has been provided by ANL, CEA, INL, IPPE, IRSN, JAEA, JSI, NRG, and ORNL. The report also includes the identification of merits and drawbacks of the existing adjustment methodologies, a comparison of mathematical formulation and specific features, and the criteria used for assessing the different methodologies.

In order to better understand the performance of these methodologies, the robustness of the results, their extrapolability and the impact of the uncertainties (not only on nuclear data but also on experiments and on methods) it has been decided to have the different organizations to participate to a common benchmark adjustment exercise to study these specific issues. In particular, it was agreed that the main objective of the benchmark would be to test different methods of nuclear data adjustment/assimilation and different sets of covariance data, for the purpose of reducing, *e.g.*, the design uncertainties of a particular type of sodium-cooled fast reactor. The benchmark made use of a single, limited set of selected integral experiments with fast neutron energy spectra and each organization used their own calculation methods and data.

C. The Adjustment Methodologies

As indicated above, the data statistical adjustment methods principles and mathematical formulations have been compared in a report [7]. Most of the methods, as reminded below, use practically the same mathematical formulation and that formulation is briefly summarized hereafter.

Let $\vec{E} = \vec{E}_i$ $(i = 1, \ldots, N_E)$ denote some experimental integral variables, and let $\vec{\sigma} = \vec{\sigma}_j$ $(j = 1, \ldots, N_\sigma)$ denote the multi-group parameters defining the model used to simulate these integral experiments, and $\vec{C}(\sigma)$ the associated calculated values to be compared with $\vec{E}$. Let $\vec{\sigma}_m$ and M_σ define the a priori expectation and covariance matrix of the multi-group parameters, and M_E define the experimental covariance matrix, including modeling covariance information when appropriate (*i.e.*, $M_E = V_e + V_m$). The evaluation of a–posterior expectation and covariances is done by finding the minimum of the following cost function (a generalised least-squares method)

$$\begin{aligned}\chi^2_{GLS} &= (\vec{\sigma} - \vec{\sigma}_m)^t M_\sigma^{-1} (\vec{\sigma} - \vec{\sigma}_m) \\ &+ (\vec{E} - \vec{C}(\sigma))^t M_E^{-1} (\vec{E} - \vec{C}(\sigma)). \end{aligned} \quad (1)$$

Information related to integral simulations is included in the $\vec{C}$ values as well as in their derivatives with respect to the multi-group parameters. Using a first order approximation, one can write

$$\vec{C}(\sigma) = \vec{C}(\sigma_m) + S \cdot (\vec{\sigma} - \vec{\sigma}_m)\,, \quad (2)$$

where S is a matrix ($N_E \times N_\sigma$) of calculated derivatives supposed to be constant (when the cross sections slightly change). Most of the time, S is given as relative sensitivity coefficients

$$S_{ij} = \frac{\delta C_i / C_i}{\delta \sigma_j / \sigma_j}. \quad (3)$$

From a mathematical point of view, the method is quite general and has been extensively used for many kinds of inverse problems. In the field of reactor physics, this approach has been already applied to validate and/or further improve the nuclear data used in the simulation of thermal and fast reactors.

As indicated above, the formulations used by the different participants have been compared in Ref. [7].

The following observations can be made:

- Seven organizations (ANL, CEA, INL, IPPE, JAEA, JSI and IRSN) apply equivalent equations for the adjustment, though the names of the theory differ.
- ORNL uses similar equations as the above organizations. However, a correction factor ($F_{m/k}$) is applied to the covariance matrix of integral experiments to account for the C/E discrepancy.
- The NRG approach is completely different. It is based on the Total Monte Carlo method to produce thousands of TALYS-based evaluated files using MC sampling of nuclear parameters. The method used by NRG solves the inverse problem of nuclear data adjustment by selecting the optimal combination of random files that best reproduce all integral experiments.

D. The Benchmark Exercise

Every participant to the benchmark exercise used the same integral experiment values (E) and uncertainties, but their own calculated values (C), sensitivity coefficients, and adjustment/assimilation methods. The benchmark consisted of a three-phase exercise:

- Phase I. All participants used their own initial cross sections, own nuclear data covariance matrices, with integral experiment and method correlation.
- Phase II. Some participants used their own initial cross sections, but different nuclear data covariance matrices. This step allows a better understanding of the impact of the nuclear data covariance on the adjustment.
- Phase III. Verification of the impact of the adjustments on a few "Target Systems."

Finally, the addition of a set of integral experiments allowed a test of the robustness of the previous adjustments (stress tests).

1. Benchmark Input

In order to limit the calculation effort and to point out major trends in a more clear way, the number of isotopes to be adjusted was limited to ten: ^{16}O, ^{23}Na, ^{56}Fe, ^{52}Cr, ^{58}Ni, ^{235}U, ^{238}U, ^{239}Pu, ^{240}Pu, ^{241}Pu plus ^{10}B for testing. On the contrary, all major reactions have been considered. Finally, several covariance data sets have been used.

A unique energy group structure (given in Table I) was also adopted.

TABLE I. 33 energy group structure (eV).

Group	Upper Energy	**Group**	Upper Energy	**Group**	Upper Energy
1	1.96×10^7	**12**	6.74×10^4	**23**	3.04×10^2
2	1.00×10^7	**13**	4.09×10^4	**24**	1.49×10^2
3	6.07×10^6	**14**	2.48×10^4	**25**	9.17×10^1
4	3.68×10^6	**15**	1.50×10^4	**26**	6.79×10^1
5	2.23×10^6	**16**	9.12×10^3	**27**	4.02×10^1
6	1.35×10^6	**17**	5.53×10^3	**28**	2.26×10^1
7	8.21×10^5	**18**	3.35×10^3	**29**	1.37×10^1
8	4.98×10^5	**19**	2.03×10^3	**30**	8.32×10^0
9	3.02×10^5	**20**	1.23×10^3	**31**	4.00×10^0
10	1.83×10^5	**21**	7.49×10^2	**32**	5.40×10^{-1}
11	1.11×10^5	**22**	4.54×10^2	**33**	1.00×10^{-1}

2. Nuclear Data

The following nuclear data were explicitly considered:

- Elastic scattering infinite-dilution cross section.
- Total inelastic scattering infinite-dilution cross section.
- Capture infinite-dilution cross section (this includes the ^{10}B(n,α) reaction).
- Fission infinite-dilution cross section.
- Average prompt fission neutron multiplicity ($\bar{\nu}$).
- Normalized prompt fission neutron spectrum.
- Average cosine of elastically scattered neutrons ($\bar{\mu}$).
- Average delayed fission neutron multiplicity ($\bar{\nu}_d$), as an optional adjustable parameter (on a voluntary basis). This proposal was driven by consideration of the impact of $\bar{\nu}_d$ on the integral C/E ratio value and uncertainty for Na void reactivity (measured in dollars). When not adjusting $\bar{\nu}_d$, the participants should have added the corresponding uncertainty to the C/E value of Na void reactivity in order to reduce their statistical weight.

The spectra of inelastically scattered neutrons have not been part of the benchmark exercise.

3. Nuclear Covariance Data

All participants used their own covariance data (Phase I, see above). However, in Phase II of the exercise, for comparison purposes and to disentangle effects from different a priori cross sections or covariance data, one common set of covariance data would be used by some of the participants, in addition to their own specific sets. The 33-group COMMARA-2.0 covariance data, developed by a BNL-LANL collaboration (see section III), was made available for that purpose.

E. Selection of Integral Experiments

The selection of fast neutron spectrum integral experiments has been based on the availability of well documented specifications and experimental uncertainties and possibly of some indication of uncertainty correlations. The selected experiments cover a wide range of fast neutron energy spectra, and include critical masses, spectral indices and, when available, selected Na void reactivity coefficients. In the notation used for spectral indices, Fij (or Cij) is the fission (or capture) rate of the isotope 23j of the element 9i (*i.e.*, U, Np, Pu for i=2,3,4, respectively), *e.g.*, F37 is the ^{237}Np fission rate. Detailed specifications on these integral experiments were taken from [8–10]:

- JEZEBEL ^{239}Pu configuration: 1 critical mass, 3 spectral indices: F28/F25, F49/F25, F37/F25,
- JEZEBEL ^{240}Pu configuration: 1 critical mass,
- FLATTOP Pu configuration: 1 critical mass, 2 spectral indices: F28/F25, F37/F25,
- ZPR6-7 standard configuration: 1 critical mass, 3 spectral indices: F28/F25, F49/F25, C28/F25,
- ZPR6-7 High ^{240}Pu content: 1 critical mass,
- ZPPR-9: 1 critical mass, 3 spectral indices: F28/F25, F49/F25, C28/F25, 2 Na void configurations: central void and leakage-dominated configurations,
- JOYO: 1 critical mass.

A specific activity has been devoted to the assessment of integral experiment covariance data that will be described in section IV.

F. Corrective Factors

The strategy proposed in order to avoid a full reanalysis of all experiments by the participants to the adjustment exercise has been to provide corrective factors obtained as a ratio between a very detailed (reference) calculation and a simplified one. Hence the C/E (Calculated/Experimental value) is obtained as

$$\frac{C}{E} = \frac{C^s C^f}{E}, \tag{4}$$

where E is the experimental value, C^s is the result coming from the simplified model calculation, and C^f is the corresponding corrective factor.

II. SENSITIVITY ANALYSIS

A major ingredient of any adjustment process is the sensitivity analysis. A number of theoretical developments and applications have been performed since the pioneering work of Usachev [11] that generalized the standard Wigner approach for critical nuclear reactors. In general these methods and approximations used in practical applications (*e.g.*, the use of first order sensitivity analysis) are well understood. However, the present activity offered a unique opportunity to perform a detailed international comparison on a set of well defined configurations. A number of issues were tackled and recommendations were formulated.

JAEA, INL, ANL, CEA and PSI have provided full sets of sensitivity coefficients for all integral parameters considered in the benchmark. Sensitivity coefficients for the effective multiplication factor $k_{\rm eff}$ have also been generated in a consistent manner by JSI and IRSN. ORNL has provided data but on a different energy group structure.

A. Methodologies

Sensitivity methods are well established, however in practical applications one has to specify if deterministic or Monte Carlo methods have been used and a number of ambiguities/approximations have to be eliminated or well understood in order to compare effectively the sensitivity coefficient produced by different groups. The main features of the different methods used within the Subgroup can be summarized as follows:

(1) For $k_{\rm eff}$, deterministic values of the sensitivity coefficients have been obtained by Standard Perturbation-Theory (SPT) techniques using transport-theory except for JAEA that made use of diffusion theory. More precisely, the various analyses were carried out on the basis of:

- SAGEP code [12], in conjunction with JENDL-4.0 data at JAEA,
- ERANOS code [13] in conjunction with ENDF/B-VII.0 data at INL and ANL, and
- ERANOS in conjunction with JEFF-3.1.1 and JEFF-3.1 data at CEA and PSI, respectively.

In addition, in conjunction with ENDF/B-VII.0 data, the code SUSD3D [14] was used together with DANTSYS [15] at JSI.

At IRSN, stochastic values of the sensitivity coefficients based on a multi-group approach have been obtained by TSUNAMI-3D which uses an adjoint based technique and is part of SCALE [16] in conjunction with ENDF/B-VII.0 data. The sensitivity coefficients take into account that a change of a given cross section may also influence other cross sections through modifications of their shielding factors. Thus, the TSUNAMI sensitivity coefficients are computed with the total instead of the partial derivatives as

$$S_{\sigma_x^i(g)} = \frac{dk}{k} \Big/ \frac{d\sigma_x^i(g)}{\sigma_x^i(g)} = \frac{\partial k}{k} \Big/ \frac{\partial \sigma_x^i(g)}{\sigma_x^i(g)} + \sum_j \sum_y \sum_h \left\{ \left(\frac{\partial k}{k} \Big/ \frac{\partial \sigma_y^i(h)}{\sigma_y^i(h)} \right) \left(\frac{\partial \sigma_y^j(h)}{\sigma_y^j(h)} \Big/ \frac{\partial \sigma_x^i(g)}{\sigma_x^i(g)} \right) \right\}. \quad (5)$$

In the formula for these "complete" sensitivity coefficients [16], the space variable has been omitted and *e.g.* $\sigma_x^i(g)$ is the cross section of nuclide i for reaction x in energy group g. The first expression on the right hand side corresponds to the standard definition ("explicit" term), with the additional summations ("implicit" effects) as an indirect term.

(2) For the reaction rates at core center relative to ^{235}U fission (F25), *i.e.*, F49/F25, F28/F25, F37/F25 and C28/F25, Generalized Perturbation Theory (GPT) [11] has been consistently used in the deterministic calculations for obtaining their sensitivity coefficients.

(3) Equivalent Generalized Perturbation Theory (EGPT) [17] has been employed for determining the sensitivity coefficients of the void reactivity effects in ZPPR-9 (Na void Step 3 and Na void Step 5) except for JAEA that used the standard formulation of GPT [11].

B. Analysis of Sensitivity Profiles

1. k_{eff}

The sensitivity coefficients of the actinides related to the two JEZEBEL bare spheres and to the sodium-cooled systems, *i.e.*, the two ZPR6-7 cores, ZPPR-9, and JOYO, show very good consistency among the participants, *e.g.* as seen in Fig. 1. The sensitivity coefficients are almost independent of the code (deterministic SAGEP, ERANOS, DANTSYS/SUSD3D and TSUNAMI-1D, stochastic TSUNAMI-3D) and basic nuclear data (JENDL-4.0, ENDF/B-VII.0 or JEFF-3.1) being used.

As far as the sensitivity coefficients for the structural materials, sodium, oxygen, and those for the scattering reactions of the actinides (see examples in Figs. 2–4), consistency is also shown for most cases.

In the case of the sensitivity coefficients for the FLATTOP core, some of the energy profiles are characterized by larger discrepancies. However, most of these discrepancies are well understood. Thus, for the JAEA solution,

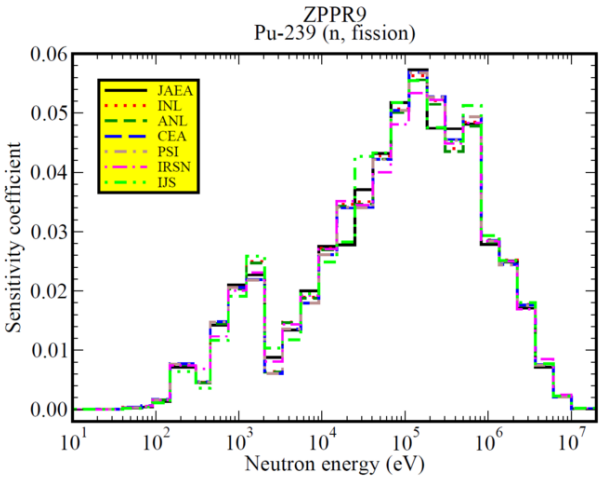

FIG. 1. Sensitivity profiles of ^{239}Pu fission cross section for ZPPR-9 k_{eff}.

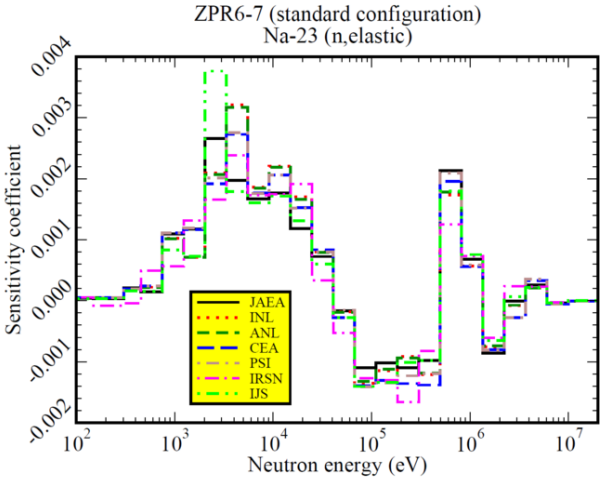

FIG. 2. Sensitivity profiles of ^{23}Na elastic cross section for ZPR6-7 k_{eff}.

it is largely attributed to the use of a 2D (r,z) model with diffusion theory instead of spherical geometry in conjunction with transport theory used by the other participants. This is causing much larger modeling effect for FLATTOP than for the other systems under investigation.

A further investigation was performed comparing Monte Carlo and deterministic methods. In particular, results for the sensitivities of the multiplication factor of the FLATTOP-Pu benchmark to perturbations of the ^{238}U elastic cross section were investigated. The results obtained by participants to the benchmark exercise are shown in Fig. 5 (top), including the JSI deterministic solution obtained by a refined P3 approximation for both the elastic as well as inelastic scattering cross sections. In addition, Fig. 5 (bottom) displays JSI Monte Carlo

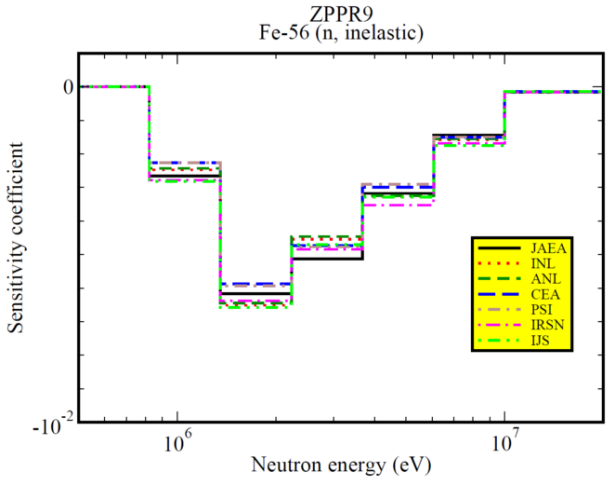

FIG. 3. Sensitivity profiles of ^{56}Fe inelastic cross section for ZPPR-9 $k_{\rm eff}$.

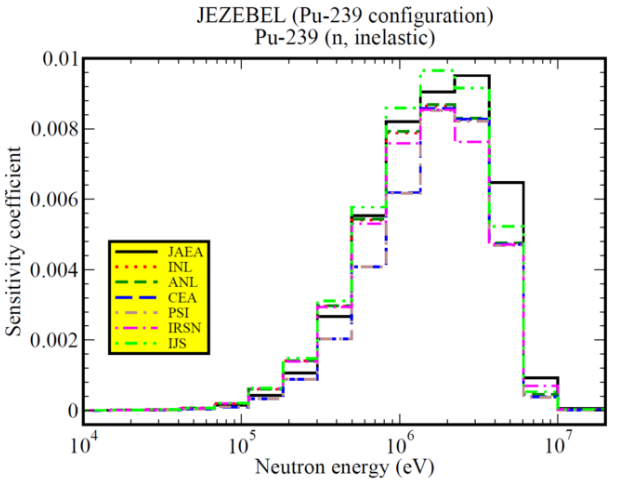

FIG. 4. Sensitivity profiles of ^{239}Pu inelastic cross section for JEZEBEL $k_{\rm eff}$.

results and data taken independently from the International Criticality Safety Benchmark Evaluation Project (ICSBEP) handbook. The results show the following features:

(a) The reference JSI deterministic values (P1 approximation) are the largest, especially above 0.3 MeV coinciding with groups 1-8, and peak at higher energy. Using the P3 approximation largely removes this difference and leads to agreement for energies up to about 1 MeV with the bulk of the other solutions.

(b) The continuous energy Monte Carlo solution also agrees, by bearing in mind that "small" sensitivity coefficients such as for those energies below 60 keV and above 5 MeV, are clearly difficult to calculate.

(c) The ORNL values provided in 238 groups are found

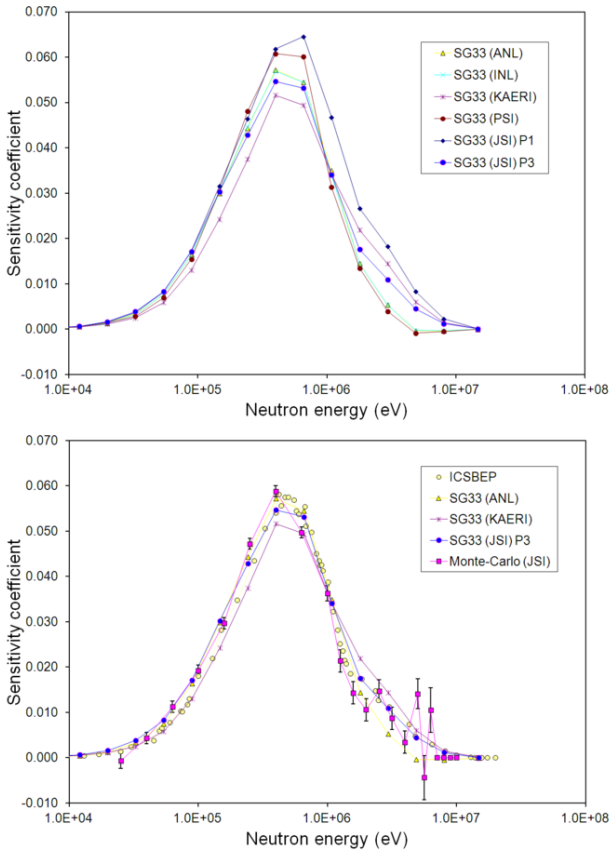

FIG. 5. Sensitivity profiles of ^{238}U elastic cross section for FLATTOP-Pu $k_{\rm eff}$(see text).

consistent with ICSBEP, which in turn appear consistent with the INL and ANL solutions for energies up to about 1.5 MeV, whereas the PSI values are higher near the peak around 0.5 MeV and the KAERI values are systematically lower for energies < 0.6 MeV.

2. *Spectral Indices F49/F25, F28/F25, F37/F25 and C28/F25*

The GPT was used by JAEA, INL, ANL, CEA, and PSI to calculate the sensitivity coefficients of spectral indices for JEZEBEL, ZPR6-7 and ZPPR-9 configurations. The results obtained by the participants are consistent, including those for the structural materials, oxygen and sodium in the case of ZPR6-7 and ZPPR-9. Some examples are given in Figs. 6–8.

3. *Reactivity Effects*

The Na void (Step 3) and Na void (Step 5) in the ZPPR-9 experiment have been studied.

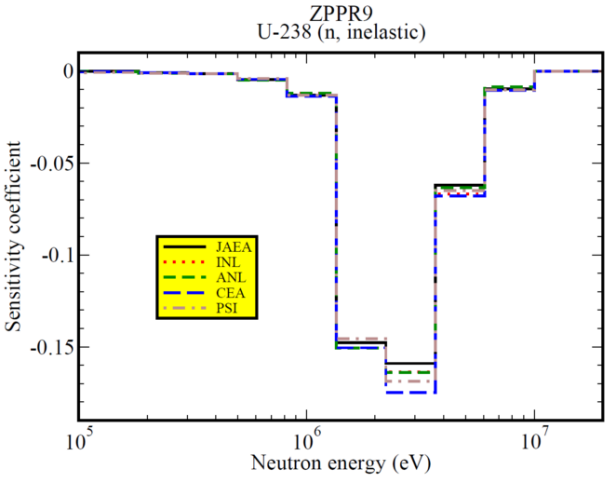

FIG. 6. Sensitivity profiles of ^{238}U inelastic cross section for ZPPR-9 F28/F25 spectral index.

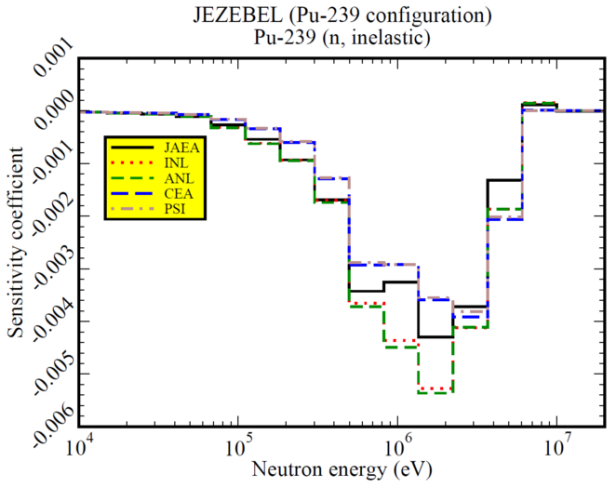

FIG. 7. Sensitivity profiles of ^{239}Pu inelastic cross section for JEZEBEL F37/F25 spectral index.

In general, good consistency is shown among the participants (JAEA, INL, ANL, CEA and PSI) providing for ZPPR-9 deterministic solutions based upon the EGPT methodology (see Fig. 9) except for JAEA (see above). However, some differences were observed in ^{240}Pu close to the threshold and for the sodium inelastic scattering cross section.

C. Summary of Major Recommendations

Calculation of sensitivity coefficients is now part of the standard calculation routes in many modern code systems. The agreement among results obtained by different methods is remarkable. However, a number of recommendations can be formulated on the basis of the comparisons described above:

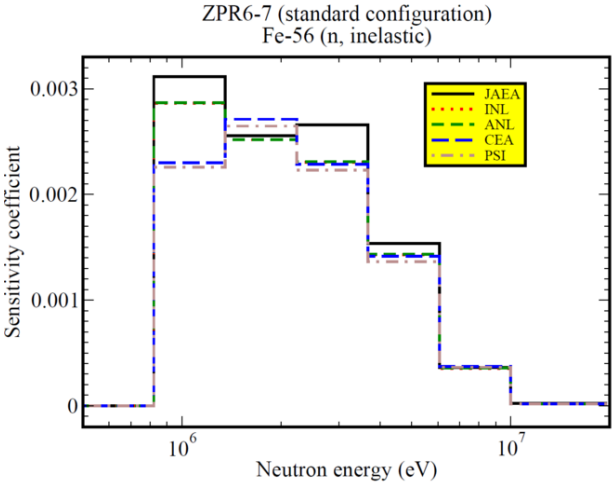

FIG. 8. Sensitivity profiles of ^{56}Fe inelastic cross section for ZPR6-7 C28/F25 spectral index.

- Sensitivity coefficients calculated, *e.g.* for the multiplication factor and reaction rate ratios with different deterministic methods and codes agree well among them, but one should be careful in specifying definitions and model approximations, such as *e.g.* the exact detector position and volume in the case of Generalized Perturbation Theory (GPT) for sensitivity coefficients of reaction rate ratios.
- "Small" sensitivity coefficient values are to be used with care, since in these cases errors can arise from numerical problems, such as those associated with the local convergence of the importance function.
- Resonance shielding effects, which appear not too important for the present exercise, should be considered with appropriate algorithms.
- Anisotropy of scattering should be accounted for at high energies when calculating sensitivity coefficients to elastic and probably also inelastic scattering cross sections.
- EGPT provides a powerful tool to calculate sensitivity coefficients for reactivity effects.
- Adjoint based and direct Monte Carlo techniques provide an interesting alternative to deterministic methods in particular for complex geometries. However, both methodologies are computationally very intensive. In addition, especially when using the direct method, care must be taken in carrying out the calculations with a sufficient precision. The sensitivity coefficients are computed by means of differences between two independent calculations,

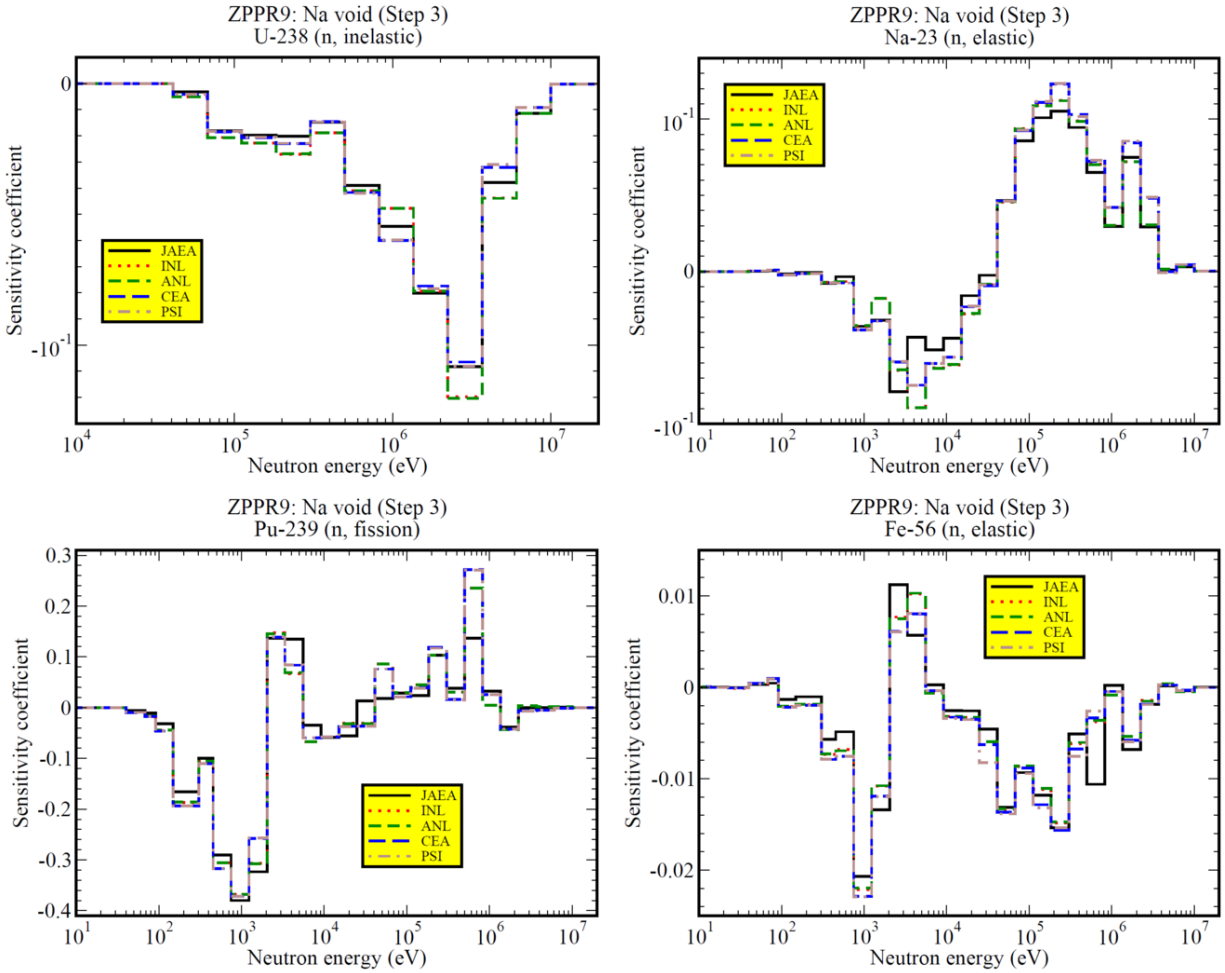

FIG. 9. Sensitivity profiles of various cross sections for ZPPR-9 Na voiding.

and sufficiently large perturbations of the cross sections must be introduced to ensure obtaining statistically significant differences of the results and at the same time avoiding non-linearity.

III. NUCLEAR DATA COVARIANCES

Nuclear data covariances are very important parameters in the cross section adjustment procedure. Generally, the covariance matrix of a scattered data set, x_i $(i = 1, \ldots, n)$ with the average value $m_{0i} = \langle x_i \rangle$, is defined as follows [18]:

Variance

$$\mu_{ii} = var(x_i) = \langle (x_i - m_{0i})^2 \rangle \text{ for } i = 1, \ldots, n, \quad (6)$$

Standard deviation (STD)

$$\sigma_i = std(x_i) = \sqrt{var(x_i)}, \quad (7)$$

Covariance

$$\mu_{ij} = cov(x_i, x_j) = \langle (x_i - m_{0i})(x_j - m_{0j}) \rangle,$$
$$\text{for } i, j = 1, \ldots, n \text{ with } i \neq j,$$

and correlation factor $(-1 \leq \rho_{ij} \leq 1)$

$$\rho_{ij} = \frac{\mu_{ij}}{\sqrt{\mu_{ii}\mu_{jj}}} = \frac{cov(x_i, x_j)}{std(x_i)std(x_j)}. \quad (8)$$

The covariance matrix must be symmetric and positive-definite. In this section, first the methodologies used to evaluate the nuclear data covariances are briefly reviewed. Next, some of the actual covariance data are illustrated. Comparisons are made among JENDL-4.0 (J-4.0 hereafter [19, 20]), and COMMARA-2.0 (C-2.0 hereafter [21]) which is to be used together with the ENDF/B-VII.0 central values [22], and the CEA COMAC [23]. More detailed comparisons can be found in Ref. [24].

A. Covariance Data Used in the Subgroup 33 Adjustment Exercise

Different covariance data have been developed in recent years and some of them have been used by the participants of Subgroup 33. For the evaluation of covariance data, different techniques have been used; in particular, a generalized least-squares method to combine large experimental data bases [25, 26] or the Kalman-filter method, see for example [27]. The basic idea of this method is to optimize the nuclear model parameters by the inclusion of the cross section measurement information with the Bayesian parameter estimation. Specific techniques have been used to assess covariance data in the resonance region [28–31]. Further discussion on the different methods can be found in the quoted references and in the final report of Subgroup 33 [24].

Increasing computing power has made it feasible to evaluate nuclear data and their associated covariances using Monte Carlo (MC) methodology [32, 33]. One of the advantages of the MC-based method is that it does not need the sensitivity of nuclear model parameters, which frees it from the assumption of linearity. The MC method does however require a fairly large amount of computing time to obtain sufficiently small statistical uncertainties, as well as the need of the prior model parameter uncertainty, shape and correlation for random sampling. These methods face the difficulty to take into account deficiencies in the nuclear reaction models, and the quality and quantity of the cross section measurements.

Table II summarizes the features of various covariance data treated in the Subgroup 33 exercise. In total, 5 covariance libraries were used.

B. Comparison of Covariance Data

Most of the covariance data (diagonal values and by and large also correlation coefficients) used in the different participants data sets, are comparable in magnitude. However, a closer examination points out differences, sometimes associated with covariance data evaluation methods. To give some examples we will first show some discrepancies among the CEA COMAC library, the COMMARA-2.0 and the JENDL-4.0 covariances for ^{239}Pu and ^{241}Pu fission and ^{238}U inelastic scattering.

Figs. 10–12 show the diagonal values of ^{239}Pu and ^{241}Pu fission and ^{238}U inelastic scattering cross section covariance matrices. The uncertainty on the ^{239}Pu fission cross section is small in all cases. However, there is approximately a factor of two difference between the COMAC values and the JENDL or COMMARA values. This difference is at the origin of very significant uncertainty value on most k_{eff} of Pu-fueled integral experiments (see section V). Also, in the case of the fission of ^{241}Pu, there are large differences between the COMAC values and the JENDL or COMMARA values in the energy region below ~10 keV. These differences in uncertainty do not play a very important role in the present exercise, but can have a much stronger impact on core design and fuel cycle parameters of large Fast Reactor cores with softer spectra. Finally, the difference observed in the ^{238}U inelastic scattering cross section uncertainties has a significant impact on many key integral parameters since it will affect the slowing down characteristics of most cores, according to core composition, conversion ratio values, *etc.*

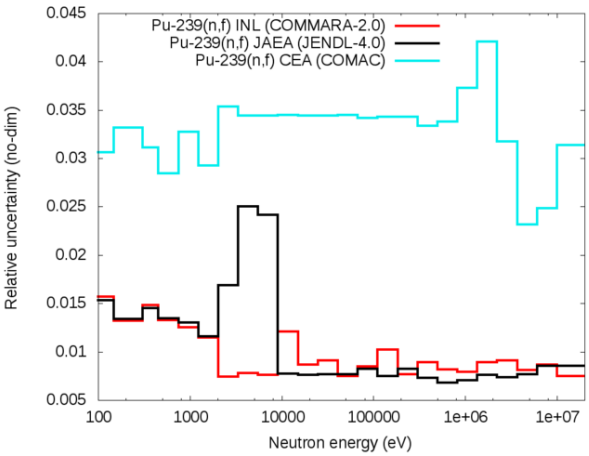

FIG. 10. Relative uncertainties of ^{239}Pu(n,f) cross sections.

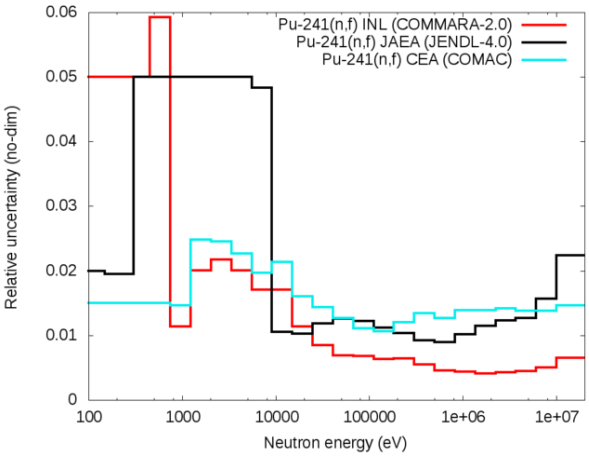

FIG. 11. Relative uncertainties of ^{241}Pu(n,f) cross sections.

C. Further Comparison of JENDL-4.0 and COMMARA-2.0 Covariance Libraries

One can say that in general, for the 11 isotopes treated in the Subgroup 33 exercise, that is, ^{10}B, ^{16}O, ^{23}Na, ^{56}Fe, ^{52}Cr, ^{58}Ni, ^{235}U, ^{238}U, ^{239}Pu, ^{240}Pu, and ^{241}Pu, their associated covariance data are found to be rather similar be-

TABLE II. Features of covariance data used in the Subgroup 33 adjustment exercise.

Covariance library	Evaluated Isotopes	Covariance data included	Methodology applied to evaluate covariance data	Other features
COMMARA-2.0 (BNL,LANL)	- 12 light nuclei (coolants and moderators) - 78 structural materials and fission products - 20 actinides	- Reaction cross sections + $\bar{\nu}$ for 20 actinides + PFNS of ^{238,239,240}Pu + $\bar{\mu}$ of ^{23}Na, ^{56}Fe	- Generalized least-squares method - Resonance R-matrix analysis - Kalman-filter method - Kernel approximation	- 33-energy group structure - To be used together with the ENDF/B-VII.0 central values - Released in October 2010 [21]
JENDL-4.0 (JAEA)	95 nuclides, including ^{10,11}B, ^{14,15}N, ^{16}O, ^{23}Na, ^{48}Ti, ^{52,53}Cr, ^{55}Mn, ^{56}Fe, ^{59}Co, ^{58,60}Ni, ^{90}Zr, ^{209}Bi, and all actinides	- Reaction cross sections + $\bar{\mu}$ for 16 light nuclei and structural materials - Reaction cross sections + $\bar{\nu}$ + PFNS + $\bar{\mu}$ for 79 actinides	- Generalized least-squares method - Resonance R-matrix analysis - Kalman-filter method	- ENDF standard format - File 33 is given for resonance energy region - Released in May 2010 [19, 20]
COMAC(CEA) + JENDL/ENDF for some isotopes	- 24 light and intermediate nuclei - 15 actinides	Reaction cross sections + $\bar{\nu}$ (from JENDL-4.0) + PFNS (from JENDL-4.0)	- Generalized least-squares - Resonance R-matrix and Optical Model analysis - Marginalization of systematic experimental uncertainties	33-energy group structure
TENDL (NRG)	^{235,238}U and ^{239}Pu	No covariance files but random ENDF files based on TENDL-2010 [34]	Monte Carlo-based method: TMC + selection based on distance minimization	Pointwise cross sections
SCALE 6.1 (ORNL)	- 2 isotopes in structural materials - 8 actinides (^{234,235,238}U, ^{237}Np, ^{239,240,241,242}Pu)	Reaction cross sections + $\bar{\nu}$ + PFNS	- Generalized least-squares method - Delta chi-square filter method	- Initially a 44-energy group structure, collapsed to a 33-group structure - Released in June 2011 [35]

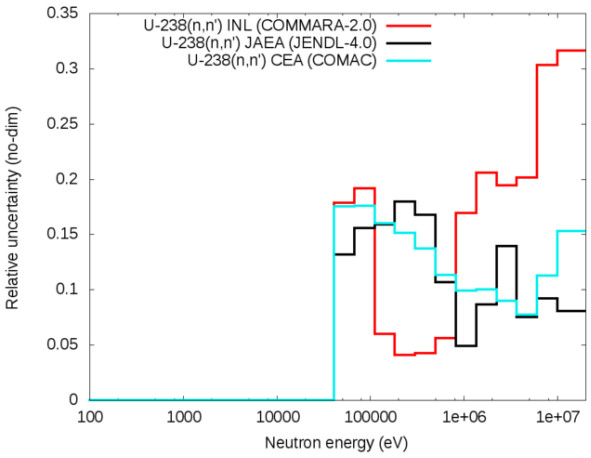

FIG. 12. Relative uncertainties of ^{238}U(n,n') cross sections.

tween the two libraries, probably due to the use of similar evaluation methodology such as the full or simplified R-matrix analysis, the Bayesian estimation connected with some theoretical nuclear model codes, or the simultaneous evaluation for fission data of major actinides, *etc.* Furthermore, experimental cross section data from the international library EXFOR are commonly used to fit nuclear reaction model parameters.

However, there are some isotope-reaction-energy regions where the covariance data of the two libraries are notably different. Three examples will be examined in detail.

1. ^{235}U Capture in 3-300 keV Energy Region

As seen in Fig. 13, the standard deviation (STD) of C-2.0 is exactly ±20%, while that of J-4.0 is very small around ±2-4%. Further, the correlations of C-2.0 are almost perfectly positive, but those of J-4.0 are only partially positive. The difference of the capture cross section center values between ENDF/B-VII.0 and J-4.0 is around -10 to +5% in this energy range. From Refs. [19–21], C-2.0 applied the Bayesian code KALMAN with the GNASH code for the covariance evaluation, on the other hand, JENDL-4.0 used the generalized least square code GMA. It seems unlikely that these two methods generate such a large difference, if both methods adopt the same experimental information. More analysis seems to be needed to assess the covariance in the fast energy re-

gion of ^{235}U capture reaction.

2. ^{23}*Na Elastic Scattering Data Around 2 keV*

At this energy, there appears a giant resonance peak which affects significantly the sodium-voiding reactivity in sodium-cooled fast reactor cores. As found in Fig. 14, the shape of the standard deviation is extremely different the between two libraries; that is, the minimum STD value occurs at the cross section peak energy in C-2.0, and on the contrary, the maximum appears there in J-4.0. With a simple consideration, the trend of C-2.0 seems more natural, since the larger cross sections would be more accurate due to the small statistical uncertainty in the measurement. The correlations are also quite different. In the C-2.0 covariance, the 2 keV peak has no correlations with other energy, while J-4.0 is partially positive everywhere above 100 eV. The covariance of C-2.0 is evaluated by the EMPIRE/KALMAN combination, where the prior resonance model parameter uncertainties are derived from Mughabghab [31]; on the other hand, J-4.0 applies the GMA code with some corrections to meet the measured cross sections with the evaluated ones of J-4.0 which is based on the multi-level Breit-Wigner formula with rather old resonance parameter values recommended by BNL in 1981. The cross section difference between ENDF/B-VII.0 and J-4.0 is -17 to +4% around 2 keV, therefore, the difference of STDs might be reasonable if we take into account the corrections given to J-4.0 covariance.

3. ^{56}*Fe Elastic Scattering in 0.3-25 keV Energy Range*

The central values of the ^{56}Fe elastic scattering cross section in the resonance region from 10^{-5} eV through 850 keV are almost identical for ENDF/B-VII.0 and JENDL-4.0, since the resonance parameters adopted in both libraries are based on a common evaluation around 1990. The covariance data of C-2.0 and J-4.0 were, however, independently evaluated. In the C-2.0 covariance, the resonance region of ^{56}Fe up to 850 keV was evaluated with the kernel approximation and data from Mughabghab [31]; on the other hand, the covariance data of J-4.0 were firstly estimated from the experimental data with the GMA code. Then the estimated variances were modified by considering the difference between the average of the experimental data and that of JENDL-4.0 [19]. The differences of the STD shapes and the correlations in Fig. 15 might stem from these utterly different methodologies of their covariance evaluations, though the energy-averaged STD values seem rather similar with each other, that is, ±5.6% in C-2.0 and ±4.5-11% in J-4.0.

IV. COVARIANCES OF EXPERIMENTAL INTEGRAL PARAMETERS

A. Experimental Covariance Matrix Definition

Experimental uncertainties of an integral parameter are usually given by the experimenters in the form of components. However, correlations between integral parameters are scarcely found in the experiment reports; therefore, we have to estimate them from the experimental information available. The method adopts the following three steps.

(1) Classification of Uncertainty Components to either Common or Independent (step 1). In this step one identifies all components of the experimental uncertainties for "Data A" and "Data B" for which quantitative values were reported, and each of them is put into a category "Common uncertainty (*i.e.*, the correlation factor is 1.0) between Data A and B", or into a category "Independent uncertainty (*i.e.*, the correlation factor is 0.0)". If an uncertainty component is judged as a mixture of common and independent uncertainties, that is, the correlation factor is not considered as either 1.0 or 0.0, then the uncertainty component must be divided into more detailed subcomponents until the uncertainty component becomes either common or independent uncertainty.

(2) Summing up of Common and Independent Uncertainties (step 2). The common and independent uncertainties respectively are summed-up statistically to obtain standard deviation, σ_{Total}, the diagonal term of matrix. The statistical treatment is justified by the assumption that all uncertainty components are already divided until there are no correlations between any uncertainty items in the measurement of an integral parameter. The total uncertainty of a data set A, $\sigma_{Total,A}$, *i.e.*, the diagonal term of uncertainty matrix V_e (see Eq. (1)), is given by the summation in quadrature of common and independent uncertainties

$$\sigma_{Total,A} = \sqrt{\sigma^2_{Common,A} + \sigma^2_{Independent,A}}, \qquad (9)$$

where σ_{Common} is the sum of all common uncertainty components and $\sigma_{Independent}$ is the sum of all independent uncertainty components.

(3) Evaluation of the Correlation Factor (step 3). The correlation factor, non-diagonal term, of data sets A and B, $\rho_{A,B}$, is derived as the ratio of common uncertainties to the total uncertainties as

$$\rho_{A,B} = \frac{\sum_i \sigma_{Common,A,i} \times \sigma_{Common,B,i}}{\sigma_{Total,A} \times \sigma_{Total,B}}, \qquad (10)$$

where suffix i is the common uncertainty components between data set A and set B. Steps 1 to 3 must be repeated for all matrix elements to generate a full experimental covariance matrix as the input of adjustment exercise. Note that, for example, the correlation factors among several sodium void reactivity measurements would be changed depending on the combination of void steps, even in the same experimental core.

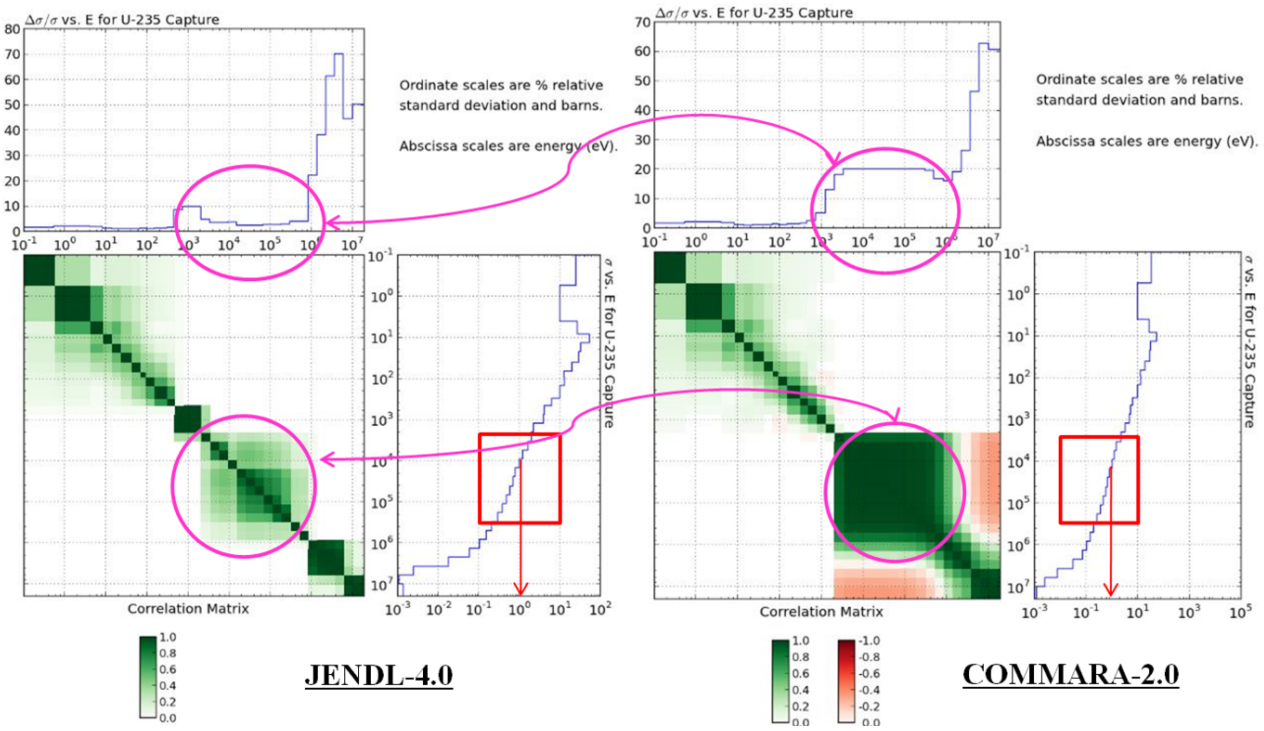

FIG. 13. Comparisons of JENDL-4.0 and COMMARA-2.0 covariance for ^{235}U neutron capture.

B. Full Experimental Covariance Matrix in Subgroup 33 Exercise

Applying the above-mentioned methodology, the full covariance matrix for the 20 experiments treated in the Subgroup 33 exercise is summarized in Table III. Additional comments are given below:

(1) The correlation factors of the Reaction Rate Ratios (RRRs) in JEZEBEL ^{239}Pu, FLATTOP and ZPR6-7 are borrowed from those of ZPPR-9, since the denominator of the RRRs, F25, is common in these experiments, and there is scarce information for the former three experiments to evaluate the common and independent components of the RRRs. The F37/F25 ratio is assumed to possess similar characteristics with F28/F25 which has a threshold feature versus neutron energy.

(2) From the fuel composition tables of [37, 38], the plutonium fuel plates used in ZPR6-7, ZPR6-7 High ^{240}Pu content and ZPPR-9 experiments were found to be the same. This means at least that the criticality of these three cores must be correlated through the composition uncertainties. In Table III, the evaluated correlation factors with the sensitivity coefficients of core compositions are added. The correlations among other parameters of these three cores are neglected here, since the effects of common core material to other parameters are usually small compared with that of criticality.

C. Modeling Covariance Matrix

The evaluation methodology of the modeling covariance, V_m (see Eq. (1)), depends on the method adopted to obtain the calculation value of an integral experiment. Here, we consider three kinds of methods: (1) Continuous-energy Monte Carlo method based on the as-built experimental geometry and compositions (MC method, hereafter), (2) Deterministic method based on the combination of the standard calculation and the corrections by the most-detailed models (Deterministic method), and (3) Combination of the deterministic calculation based on the simplified geometry and the correction by the Monte Carlo calculation with as-built geometry (Combined method). The resulting matrix for the selected experiments is given in Table IV. A full description can be found in [24].

V. COMPARISON OF INTEGRAL EXPERIMENT INITIAL C/E'S, UNCERTAINTIES AND TARGET SYSTEM UNCERTAINTIES

A. Introduction

In this section we will inspect the results provided by the benchmark participants regarding the initial $C/E's$, uncertainties associated to the integral experimental analysis (both experimental and calculation), as well

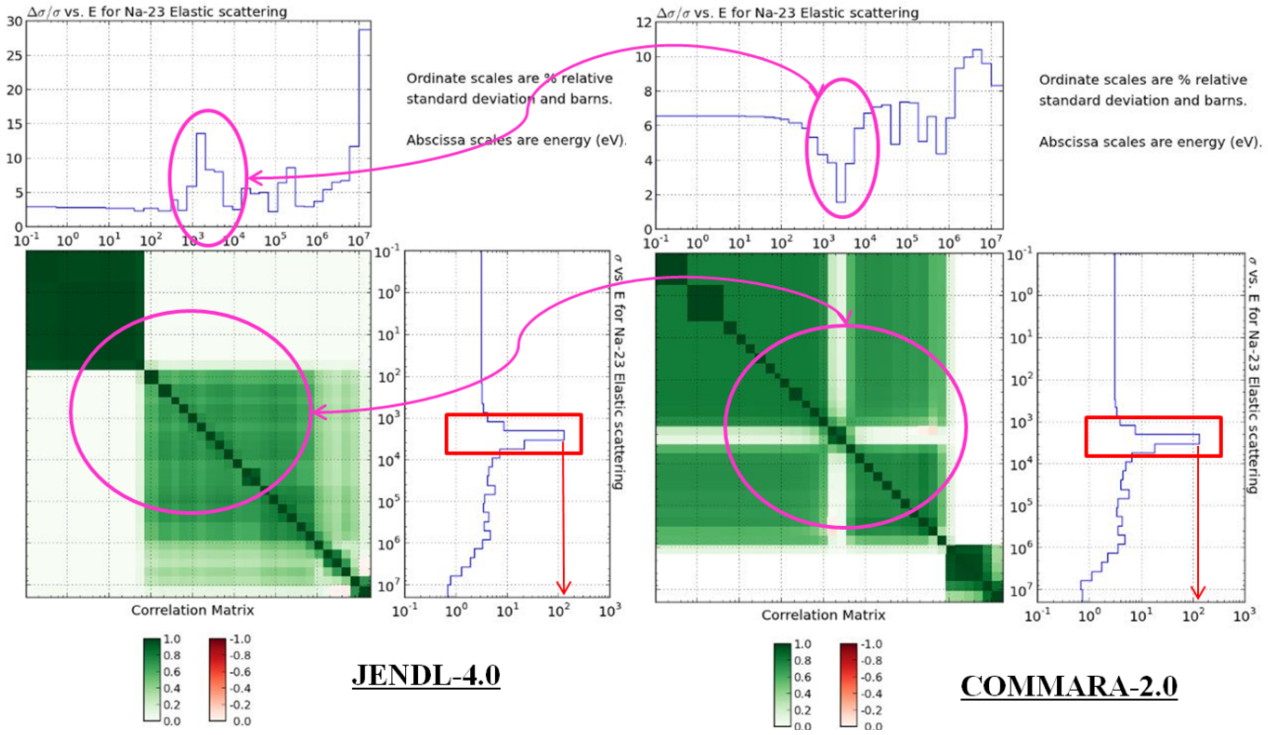

FIG. 14. Comparisons of JENDL-4.0 and COMMARA-2.0 covariance for ^{23}Na neutron elastic scattering.

those related to nuclear data, and target systems uncertainties (nuclear data related). The integral experimental analysis results have been provided by the following organizations:

- ANL: ENDF/B-VII.0 cross sections, MCNP5 for experiment analysis, and ERANOS system and COMMARA-2.0 covariance data for uncertainty analysis.
- CEA: JEFF-3.1.1 cross sections, ERANOS/PARIS (in conjunction with corrective factors) for experimental analysis, and ERANOS/PARIS and COMAC covariance data for uncertainty analysis.
- INL: ENDF/B-VII.0 cross sections, MCNP5 for experiment analysis, and SANDRA code and COMMARA-2.0 covariance data for uncertainty analysis.
- IRSN: ENDF/B-VII.0 cross sections, SCALE-6 for experiment analysis, and BERING code and COMMARA-2.0 covariance data for uncertainty analysis (only k_{eff} quantities provided).
- JAEA: JENDL-4.0 cross sections, MVP for experimental analysis, and SAGEP code and JENDL-4.0 covariance data for uncertainty analysis.
- JSI: ENDF/B-VII.0 cross sections, DANTSYS for experiment analysis, and SUSD3D system and COMMARA-2.0 covariance data for uncertainty analysis (only k_{eff} quantities were provided with the exclusion of JOYO MK-I). P1 and S4 with the built-in Gaussian quadrature constants were used in DANTSYS transport calculations.
- KAERI: ENDF/B-VII.0 cross sections, DANTSYS for experiment analysis, DANTSYS/SUSD3D system and COMMARA-2.0 covariance data for uncertainty analysis (only k_{eff} quantities provided for uncertainty evaluation).
- ORNL: ENDF/B-VII.0 cross sections, TSUNAMI-1D for experiment analysis, and TSURFER code and ORNL covariance data for uncertainty analysis (only 1D results analyzed).
- PSI: JEFF-3.1 cross sections, ERANOS (in conjunction with corrective factors) for experimental analysis, and ERANOS and COMMARA-2.0 covariance data for uncertainty analysis.

In the following sections inspection and analysis of the participants' results are provided.

B. C/E's

Table V compares the $(E-C)/C$ results provided by the participants expressed in %. For all k_{eff} values, with

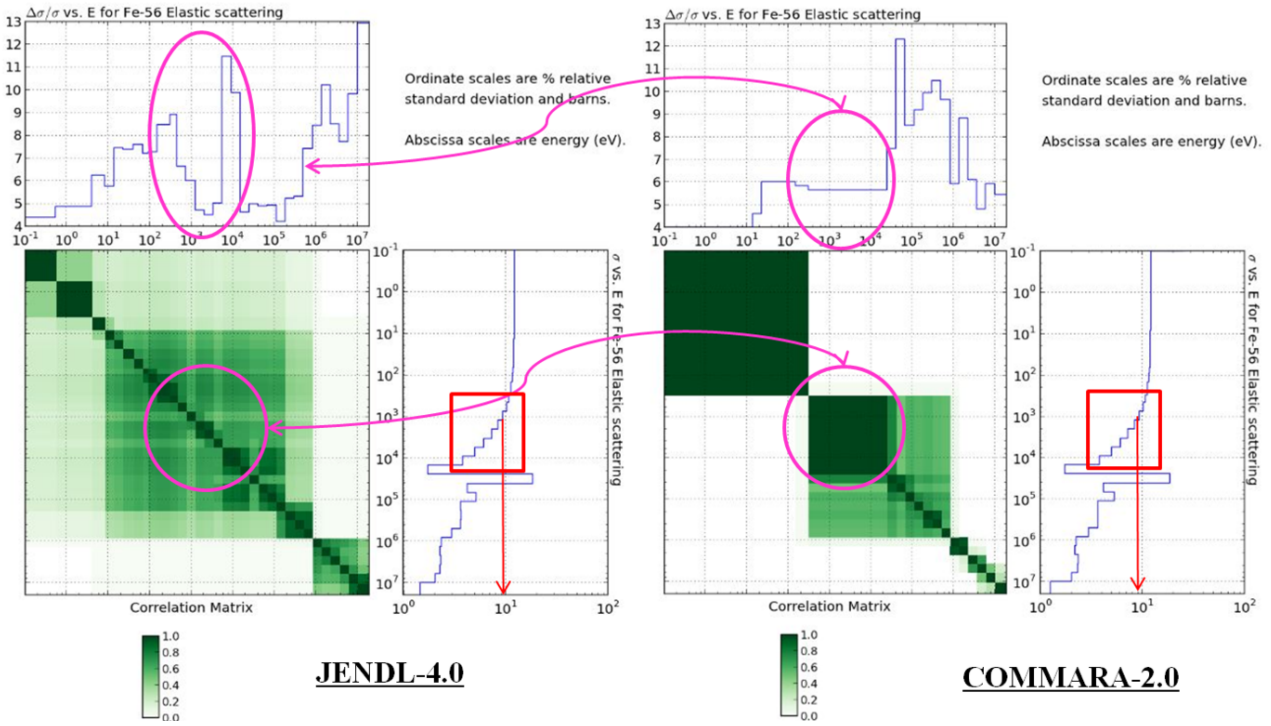

FIG. 15. Comparisons of JENDL-4.0 and COMMARA-2.0 covariance for ^{56}Fe neutron elastic scattering.

exception of KAERI, the discrepancies between experimental and calculation results lie in a quite narrow range of ∼250 pcm. This indicates that the current cross section libraries are in very good agreement for the set of experiments selected for the exercise, that are often used for the validation of these cross section data sets.

However, one has not to forget that k_{eff} is an integral quantity and therefore the agreement can be the result of cancellation of uncertainties. One exception is F28/F25 of ZPR6-7.

The spectral indices discrepancies are contained in a more widespread range of 4%. It is not clear why there is little agreement between CEA and PSI results, which both used the JEFF-3.1 cross sections. It could be due to differences during the cell calculations with the ECCO code. It is also interesting to note that the general tendency for all cross section sets is to underestimate the fission spectral indices results.

Finally, for sodium void results the discrepancy spread is within a ∼6% range. It is interesting to observe that both ENDF/B-VII.0 and JEFF-3.1 cross section sets have different sign between the spectral component experiment (Step 3) and the leakage component one (Step 5), while JENDL-4.0 overestimates in both cases.

C. Experimental and Calculation Uncertainties on C/E's

Table VI shows the (quadratic) combination of experimental and calculation uncertainty on the C/E as provided by the participants. All the participants, as indicated in the exercise, have adopted the same experimental uncertainties provided in the original documentation of the experiment benchmark models; therefore, the observed differences have to be attributed to the diverse assumptions the participants have taken on their calculation values. However, the following organizations have chosen not to apply any calculation uncertainties: CEA, JSI, and KAERI. IRSN has applied a constant 0.1% calculation uncertainty to seven k_{eff}, the only quantities they have considered for the exercise.

In general the uncertainties are relatively low and quite consistent among the different participants. There are a few exceptions. For the sodium void reactivity, participants that have adopted the Monte Carlo (instead of deterministic) codes which have quite high uncertainties (∼7%). This is due to the intrinsic (statistical) difficulty that stochastic methods encounter when confronted with small reactivity variations. It has to be kept in mind that for a reliable adjustment it is needed that both experimental and calculation uncertainties stay as low as possible.

Low experimental uncertainties provide good quality results, thus giving credibility to the adjustment pro-

TABLE III. Experimental covariance matrix of integral parameters V_e applied in the Subgroup 33 exercise. Diagonal values are 1σ uncertainties in %, non-diagonal values are correlation factors (between -1 and $+1$).

No.	Core	Parameter	1	2	3	4	5	6	7	8	9	10	11	12	13	14	15	16	17	18	19	20
1	Jezebel-Pu239	keff	0.2																			
2		F28/F25	0	1.1																		
3		F49/F25	0	0.23	0.9																	
4		F37/F25	0	0.23	0.32	1.4																
5	Jezebel-Pu240	keff	0	0	0	0	0.2															
6	Flattop	keff	0	0	0	0	0	0.3														
7		F28/F25	0	0	0	0	0	0	1.1													
8		F37/F25	0	0	0	0	0	0	0.23	1.4												
9	ZPR6-7	keff	0	0	0	0	0	0	0	0	0.23											
10		F28/F25	0	0	0	0	0	0	0	0	0	3.0										
11		F49/F25	0	0	0	0	0	0	0	0	0	0.23	2.1									
12		C28/F25	0	0	0	0	0	0	0	0	0	0.23	0.32	2.4								
13	ZPR6-7 Pu240	keff	0	0	0	0	0	0	0	0	0.13	0	0	0	0.22							
14	ZPPR-9	keff	0	0	0	0	0	0	0	0	0.31	0	0	0	0.30	0.117						
15		F28/F25	0	0	0	0	0	0	0	0	0	0	0	0	0	0	2.7					
16		F49/F25	0	0	0	0	0	0	0	0	0	0	0	0	0	0	0.23	2.0				
17		C28/F25	0	0	0	0	0	0	0	0	0	0	0	0	0	0	0.23	0.32	1.9			
18		Central Na void	0	0	0	0	0	0	0	0	0	0	0	0	0	0	0	0	0	1.9		
19		Large Na void	0	0	0	0	0	0	0	0	0	0	0	0	0	0	0	0	0	0.41	1.9	
20	Joyo	keff	0	0	0	0	0	0	0	0	0	0	0	0	0	0	0	0	0	0	0	0.18

cess. Low calculation uncertainties prevent the adjustment from compensating for shortcomings present in the calculation route. In other words, if the calculation uncertainties are high, there is the danger that the changes in the cross sections coming from the adjustment are not physical, but the result of an artificial compensation. However, the integral data which have large calculation uncertainty do not harm the adjusted results, since the weight of the data becomes small and gives less effects to the cross section changes. The risk is to underestimate the calculation uncertainty because, in such a case, the cross sections are not physically changed to force the adjusted C/E values to be 1.0.

D. Nuclear Data Uncertainties

Table VII illustrates the nuclear data uncertainties evaluated by the participants on the experimental quantities considered for the adjustment exercise. ORNL used ENDF/B-VII.0 covariance information that was collapsed to fit the 33-group format of the exercise. Six organizations (ANL, INL, IRSN, JSI, KAERI, and PSI) have used the same covariance data matrix, COMMARA-2.0. As one would expect there is good agreement among the results of these organizations with the exception of KAERI. The problem is likely related to the sensitivity coefficients (see related discussion in section II devoted to this subject).

In general JENDL-4.0 shows consistently lower uncertainty values than COMMARA-2.0. Exceptions are the spectral indices of ^{239}Pu fission and ^{238}U capture, indicating that for these two reactions JENDL-4.0 has larger variances than COMMARA-2.0. Uncertainties calculated by CEA using the COMAC covariance matrices are higher than corresponding results using COMMARA-2.0. The only exception is for ^{237}Np fission spectral indices. Quite remarkably, the $k_{\rm eff}$ uncertainty values span

TABLE IV. Modeling covariance matrix V_m used in the Subgroup 33 exercise (all calculations based on continuous-energy Monte Carlo method). Diagonal values are 1σ uncertainties in %, non-diagonal values are correlation factors (between -1 and $+1$).

No.	Core	Parameter	1	2	3	4	5	6	7	8	9	10	11	12	13	14	15	16	17	18	19	20
1	Jezebel-Pu239	keff	0.03																			
2		F28/F25	0	0.9																		
3		F49/F25	0	0.5	0.8																	
4		F37/F25	0	0.5	0.5	0.8																
5	Jezebel-Pu240	keff	0	0	0	0	0.03															
6	Flattop	keff	0	0	0	0	0	0.03														
7		F28/F25	0	0	0	0	0	0	0.8													
8		F37/F25	0	0	0	0	0	0	0.5	0.7												
9	ZPR6-7	keff	0	0	0	0	0	0	0	0	0.03											
10		F28/F25	0	0	0	0	0	0	0	0	0	2.2										
11		F49/F25	0	0	0	0	0	0	0	0	0	0.5	1.4									
12		C28/F25	0	0	0	0	0	0	0	0	0	0.5	0.5	1.2								
13	ZPR6-7 Pu240	keff	0	0	0	0	0	0	0	0	0	0	0	0	0.03							
14	ZPPR-9	keff	0	0	0	0	0	0	0	0	0	0	0	0	0	0.02						
15		F28/F25	0	0	0	0	0	0	0	0	0	0	0	0	0	0	2.1					
16		F49/F25	0	0	0	0	0	0	0	0	0	0	0	0	0	0	0.5	1.2				
17		C28/F25	0	0	0	0	0	0	0	0	0	0	0	0	0	0	0.5	0.5	1.4			
18		Central Na void	0	0	0	0	0	0	0	0	0	0	0	0	0	0	0	0	0	5.3		
19		Large Na void	0	0	0	0	0	0	0	0	0	0	0	0	0	0	0	0	0	0	5.0	
20	Joyo	keff	0	0	0	0	0	0	0	0	0	0	0	0	0	0	0	0	0	0	0	0.03

a range from ∼1500 to ∼2000 pcm. Relatively high values (up to more than 10%) are associated to the ^{238}U fission spectral indices.

Finally, concerning the uncertainties attached to the sodium reactivity coefficients, there is a fairly good agreement among all the participants. ZPPR-9 Step 3 results lie in the range between 6 and 7%, and Step 5 results between 7 and 10%.

E. Uncertainty Consistency for Adjustment

In this section we examine the consistency of the combined experimental, calculation, and nuclear data uncertainties with the observed discrepancies between experimental and calculated results. In order to establish this consistency, we define the adjustment margin AM

$$AM = U_{ND} + U_{C/E} - \left| \frac{E - C}{C} \right|, \qquad (11)$$

where $U_{ND} = \sqrt{SM_\sigma S^t}$ is the uncertainty associated to nuclear data, $U_{C/E} = \sqrt{V_e + V_m}$ is the quadratic combination of the experimental and calculation uncertainty, E is the experimental result and C the calculated result. The AM quantity establishes if in the adjustment there is enough room provided by the nuclear data uncertainty to accommodate the C/E discrepancy. Of course, the C/E discrepancy has to take into account its associated uncertainty. If the AM values are negative, this implies that there is not enough uncertainty for the adjustment in the one sigma range. This will be reflected afterwards in the χ^2 values. One could interpret the appearance of negative values as a sign of some inconsistency in the covariance matrix (usually due to too low uncertainties

TABLE V. (E-C)/C results provided by the participants expressed in %.

Core	Parameter	ANL	CEA	INL	IRSN	JAEA	JSI	KAERI	ORNL	PSI
JEZEBEL239	k_{eff}	0.014	0.187	0.014	0.051	0.130	-0.091	-0.296	-0.001	0.059
JEZEBEL239	F28/F25	2.351	0.026	2.354	-	3.242	-	1.630	2.232	1.791
JEZEBEL239	F49/F25	2.534	1.412	2.533	-	1.667	-	2.019	2.570	1.539
JEZEBEL239	F37/F25	1.319	1.526	1.317	-	2.103	-	2.680	1.244	-0.013
JEZEBEL240	k_{eff}	0.019	-0.255	0.019	0.051	0.160	-0.235	-0.267	-0.079	-0.373
FLATTOP-PU	k_{eff}	-0.100	0.020	-0.097	-0.112	0.140	-0.953[a]	-0.944	-0.255	0.071
FLATTOP-PU	F28/F25	1.811	1.034	1.812	-	2.323	-	1.278	3.030	1.386
FLATTOP-PU	F37/F25	0.446	1.535	0.442	-	0.756	-	1.469	0.989	-0.697
ZPR6-7	k_{eff}	-0.040	-0.270	-0.043	-0.216	-0.527	-0.188	-0.091	-	-0.144
ZPR6-7	F28/F25	-0.446	4.207	-0.448	-	-3.251	-	1.183	-	-0.441
ZPR6-7	F49/F25	3.761	3.752	3.756	-	2.145	-	-1.320	-	4.244
ZPR6-7	C28/F25	-0.973	-0.445	-0.970	-	-1.643	-	-2.387	-	-0.467
ZPR6-7 240	k_{eff}	0.060	-0.221	0.063	-0.099	-0.329	-0.171	-0.003	-	-0.091
ZPPR-9	k_{eff}	0.080	0.005	0.078	-0.133	-0.210	-0.160	-0.133	-	0.004
ZPPR-9	F28/F25	2.985	3.664	2.987	-	1.750	-	0.948	-	4.104
ZPPR-9	F49/F25	1.956	2.417	1.958	-	0.080	-	1.131	-	2.480
ZPPR-9	C28/F25	-0.918	-0.334	-0.921	-	-1.845	-	-2.586	-	-0.372
ZPPR-9	Na Void Step 3	-1.887	-3.401	-1.884	-	-6.385	-	-4.585	-	-2.804
ZPPR-9	Na Void Step 5	2.752	3.126	2.754	-	-4.970	-	-6.978	-	2.759
JOYO MK-I	k_{eff}	0.249	0.083	0.255	0.219	0.180	-	-0.504	-	0.056

[a] Results are very sensitive to $S_N P_N$ order ($S_6P_1 : -0.81$, $S_8P_1 : -0.48$, $S_{12}P_1 : -0.24$, $S_{16}P_1 : -0.15$, $S_{48}P_3 : -0.17$).

TABLE VI. Combination of experimental and calculation uncertainties on the $C/E's$ (%).

Core	Parameter	ANL	CEA	INL	IRSN	JAEA	JSI	KAERI	ORNL	PSI
JEZEBEL239	k_{eff}	0.201	0.200	0.201	0.224	0.202	0.200	0.200	0.200	0.224
JEZEBEL239	F28/F25	1.421	1.100	1.421	-	1.447	-	1.100	1.100	1.487
JEZEBEL239	F49/F25	0.949	1.400	0.949	-	1.172	-	0.900	0.900	1.345
JEZEBEL239	F37/F25	1.432	0.900	1.432	-	1.612	-	1.400	1.400	1.720
JEZEBEL240	k_{eff}	0.201	0.200	0.201	0.224	0.202	0.200	0.200	0.200	0.224
FLATTOP-PU	k_{eff}	0.303	0.300	0.302	0.316	0.302	0.300	0.300	0.300	0.316
FLATTOP-PU	F28/F25	1.860	1.100	1.860	-	1.384	-	1.100	1.100	1.487
FLATTOP-PU	F37/F25	1.432	1.402	1.432	-	1.561	-	1.400	1.400	1.720
ZPR6-7	k_{eff}	0.230	0.230	0.230	0.251	0.231	0.230	0.230	-	0.250
ZPR6-7	F28/F25	3.499	2.100	3.499	-	3.744	-	3.000	-	3.162
ZPR6-7	F49/F25	2.524	3.000	2.524	-	2.541	-	2.100	-	2.326
ZPR6-7	C28/F25	2.683	2.400	2.683	-	2.692	-	2.400	-	2.600
ZPR6-7 240	k_{eff}	0.221	0.220	0.221	0.242	0.222	0.220	0.220	-	0.241
ZPPR-9	k_{eff}	0.120	0.117	0.117	0.154	0.119	0.117	0.117	-	0.153
ZPPR-9	F28/F25	2.915	2.700	2.915	-	3.414	-	2.700	-	2.879
ZPPR-9	F49/F25	2.119	2.000	2.119	-	2.338	-	2.000	-	2.236
ZPPR-9	C28/F25	1.992	1.900	1.992	-	2.354	-	1.900	-	2.147
ZPPR-9	Na Void Step 3	7.737	1.900	7.737	-	5.593	-	1.900	-	4.225
ZPPR-9	Na Void Step 5	7.543	1.900	7.543	-	5.311	-	1.900	-	4.133
JOYO MK-I	k_{eff}	0.181	0.180	0.181	0.206	0.182	-	0.180	-	0.206

associated to specific cross sections).

The AM quantity is similar to the χ quantity used by JAEA as explained in [7]. The χ for every integral parameter is defined as

$$\chi = \frac{|E - C|}{\sqrt{U_{ND}^2 + U_{C/E}^2}} \tag{12}$$

and is used with a three sigma range criterion for deciding the elimination of an experiment from the adjustment.

Moreover, other methods can be suggested to verify the consistency of a set of integral experiments and parameter uncertainties. For example, the Cook's distance is used in statistics to estimate the influence of a data point when performing least squares analysis. Data points with large residuals (outliers) and/or high uncertainties may distort accuracy of the adjustment as well as its conclusions. Points with a large Cook's distance are to be carefully checked. Some results of this type of analysis can be found in [24] and in section VI D.

TABLE VII. Uncertainties due to nuclear data (%).

Core	Parameter	ANL	CEA	INL	IRSN	JAEA	JSI	KAERI	ORNL	PSI
JEZEBEL239	k_{eff}	0.640	2.072	0.636	0.611	0.693	0.658	0.117	1.186	0.511
JEZEBEL239	F28/F25	3.720	7.342	3.696	-	3.198	-	-	3.311	2.426
JEZEBEL239	F49/F25	0.830	2.811	0.823	-	0.625	-	-	0.809	0.719
JEZEBEL239	F37/F25	2.390	1.483	2.354	-	1.505	-	-	7.204	1.604
JEZEBEL240	k_{eff}	0.660	1.763	0.656	0.540	0.649	0.634	0.123	0.982	0.579
FLATTOP-PU	k_{eff}	0.760	1.913	0.764	0.519	1.257	0.719	0.123	1.128	0.829
FLATTOP-PU	F28/F25	3.120	7.885	3.093	-	2.936	-	-	2.616	1.948
FLATTOP-PU	F37/F25	2.050	1.585	2.034	-	1.444	-	-	7.076	1.421
ZPR6-7	k_{eff}	0.970	1.586	0.968	0.972	0.816	0.943	0.313	-	0.972
ZPR6-7	F28/F25	6.400	9.959	6.395	-	4.819	-	-	-	6.400
ZPR6-7	F49/F25	0.840	2.378	0.836	-	1.147	-	-	-	0.833
ZPR6-7	C28/F25	1.510	3.916	1.512	-	2.004	-	-	-	1.493
ZPR6-7 240	k_{eff}	0.970	1.559	0.971	0.970	0.812	0.948	0.311	-	0.973
ZPPR-9	k_{eff}	1.180	1.666	1.191	1.202	0.902	1.183	0.384	-	1.203
ZPPR-9	F28/F25	7.850	10.688	7.896	-	5.277	-	-	-	7.742
ZPPR-9	F49/F25	0.870	2.387	0.870	-	1.152	-	-	-	0.846
ZPPR-9	C28/F25	1.550	3.894	1.545	-	2.030	-	-	-	1.521
ZPPR-9	Na Void Step 3	7.670	6.493	7.563	-	5.950	-	-	-	7.228
ZPPR-9	Na Void Step 5	9.920	8.543	9.679	-	7.311	-	-	-	9.157
JOYO MK-I	k_{eff}	0.890	1.416	0.863	0.867	0.583	-	0.348	-	0.878

The present analysis has been performed using the rather simple and intuitive formulation of Eq. (11).

Table VIII reports the AM values for the different solutions provided by the participants.

There are only seven negative values (indicated in shaded cells). The KAERI FLATTOP k_{eff} would be challenging to adjust in view of the associated quite large negative AM (-521 pcm). This is the result of different contributions: a quite unusually large initial C/E discrepancy (almost 1000 pcm), no calculation uncertainty provided, and, finally, the sensitivity coefficient problem previously mentioned. PSI has a relative high negative AM for the ^{239}Pu fission spectral index in ZPR6-7, and one should expect some difficulty in adjusting this integral parameter, but this cannot be proven as PSI has not yet performed the adjustment.

The ANL and INL four negative values are relative to the ^{239}Pu fission spectral indices and are likely due to the low uncertainty given in COMMARA-2.0 to ^{239}Pu fission. The only negative value for CEA is associated to the fairly low uncertainty on ^{237}Np fission for COMAC previously observed in section V.4. For these entire five negative AM values one should expect, after adjustment, a difficulty for the C/E to reach the unity value even including the new evaluated associated uncertainty in the one sigma range. This is indeed the case if one inspects such quantities after adjustment (see related section). The impact on χ^2 is not expected to be large for two reasons. First the negative AM values are relatively low (<1% for spectral indices), and then, because the χ^2 is normalized to (divided by) the number of experiments (degrees of freedom). Having only one or two small inconsistencies will not show up in an adjustment with 20 experiments.

Let us continue our analysis observing that in Eq. (11), a not negligible role is played by the $U_{C/E}$ term. As indicated in section V.3, the desirable situation is to have this quantity as low as possible in order to provide a reliable adjustment. Let's define the experiment merit EM, where in Eq. (11) we suppress the term U_{ND}. What we want to spot now are positive values. Positive EM will indicate that the experiment is not providing enough useful information (*i.e.*, has not enough merit to be included in the adjustment) because there is too much uncertainty associated with respect to the observed C/E. In practice, these experiments could be excluded from the adjustment because they are not valuable either because of poor experimental quality and/or because the employed calculation analysis carries too much uncertainty, or kept in order to provide a constraint that should not be changed by the adjustment.

In total fairness, in terms of usefulness of an experiment, correlations in the experimental uncertainties should be established and one should look also at the case where only the experimental uncertainty is considered. In fact, the calculation uncertainty component depends on circumstances independent from the experiment. Besides, another criterion for retaining or discarding an experiment would be to look at their correlation through the cross product of sensitivities weighted with the covariance matrix (the so-called representativity factor). If the correlation factor is very close to 1, one of the two experiments should be discarded as it provides redundant information (unless the configurations are not experimentally correlated), and kept only for a–posteriori verification with the new adjusted cross sections and covariance matrix data.

On the other hand, because EM values neglect the uncertainty coming from the nuclear data U_{ND}, this could, in some circumstances, mislead in concluding about the usefulness of an experiment. In particular, let's con-

TABLE VIII. Adjustment Margin (AM) values expressed in %.

Core	Parameter	ANL	CEA	INL	IRSN	JAEA	JSI	KAERI	ORNL	PSI
JEZEBEL239	k_{eff}	0.827	2.085	0.823	0.784	0.764	0.767	0.021	1.385	0.676
JEZEBEL239	F28/F25	2.790	8.417	2.763	-	1.404	-	-	2.179	2.122
JEZEBEL239	F49/F25	-0.755	2.799	-0.761	-	0.129	-	-	-0.861	0.525
JEZEBEL239	F37/F25	2.503	0.857	2.469	-	1.014	-	-	7.360	3.311
JEZEBEL240	k_{eff}	0.842	1.708	0.83	0.726	0.691	0.598	0.056	1.103	0.430
FLATTOP-PU	k_{eff}	0.963	2.193	0.969	0.723	1.418	0.602	-0.521	1.173	1.075
FLATTOP-PU	F28/F25	3.169	7.950	3.141	-	1.997	-	-	0.686	2.048
FLATTOP-PU	F37/F25	3.036	1.452	3.024	-	2.249	-	-	7.487	2.444
ZPR6-7	k_{eff}	1.160	1.545	1.155	1.008	0.520	0.985	0.453	-	1.079
ZPR6-7	F28/F25	9.453	7.852	9.446	-	5.312	-	-	-	9.121
ZPR6-7	F49/F25	-0.397	1.626	-0.396	-	1.543	-	-	-	-1.085
ZPR6-7	C28/F25	3.220	5.871	3.225	-	3.053	-	-	-	3.6
ZPR6-7 240	k_{eff}	1.131	1.559	1.129	1.116	0.705	0.997	0.528	-	1.123
ZPPR-9	k_{eff}	1.220	1.778	1.230	1.224	0.811	0.957	0.368	-	1.352
ZPPR-9	F28/F25	7.780	9.724	7.825	-	6.941	-	-	-	6.516
ZPPR-9	F49/F25	1.033	1.970	1.031	-	3.410	-	-	-	0.602
ZPPR-9	C28/F25	2.625	5.460	2.616	-	2.539	-	-	-	3.296
ZPPR-9	Na Void Step 3	13.520	4.995	13.416	-	5.158	-	-	-	8.649
ZPPR-9	Na Void Step 5	14.711	7.317	14.468	-	7.653	-	-	-	10.531
JOYO MK-I	k_{eff}	0.822	1.513	0.789	0.854	0.585	-	0.024	-	1.029

sider the case where there is a very good agreement between calculation and experimental results so that the $(E-C)/C$ is almost zero, and therefore EM is positive. If the initial nuclear data uncertainties are greater than the $U_{C/E}$, still the resulting a–posteriori uncertainty will be reduced, after adjustment, for the experiment under consideration. Therefore, one has to be very careful in drawing conclusions, and, for sure, this subject of experimental selection deserves further investigations.

EM values corresponding to the benchmark solutions provided by participants are shown in Table IX. Inspection of this table provides the following conclusions regrouped by type of integral parameters:

- Critical Masses – For organizations using ENDF/B-VII.0 cross sections only the JOYO experiment provides a useful contribution to the adjustment. This can be readily seen looking at the column of IRSN that has considered only critical masses. The reason for this is the excellent performance of ENDF/B-VII.0 for Pu-fueled fast cores, while the significant amount of ^{235}U in JOYO requires an adjustment (in particular for the capture, as it will be seen in the section VI on adjustment). On the contrary, organizations using JEFF-3.1 (CEA, and PSI) and JENDL-4.0 (JAEA) perform well for JOYO. CEA will take advantage of adjustment associated to the discrepancies in k_{eff} of JEZEBEL ^{239}Pu (and strangely enough not ^{240}Pu), FLATTOP but not for the softer cores (ZPR6-7, ZPPR-9). Exactly the contrary is true for JAEA (good agreement for harder cores, adjustment needed for softer cores). It is not clear why for PSI, that uses JEFF-3.1, the Pu fuelled cores seem not to need any adjustment.
- Spectral Indices – ^{238}U capture spectral indices have positive EM values for everybody (with exception of KAERI), and therefore it doesn't seem to provide any contribution to the adjustment except as a constraint. For the fission spectral indices the situation is more complex. ^{238}U fission spectral indices require adjustments in harder cores practically for all participants, while JEFF-3.1 needs it also for softer cores. ^{239}Pu fission indices need adjustment in all cores. One exception is JAEA that has positive EM values for the ZPR6-7 and ZPPR-9 cores, indicating that the adjustment needed for the Pu fuelled softer cores k_{eff} do not concern the ^{239}Pu fission but some other reactions (or isotope). For ^{237}Np fission spectral indices the situation is mixed. These spectral indices are not important for the adjustment of ENDF/B-VII.0 users, while action is needed for CEA on both JEZEBEL and FLATTOP, and JAEA (but only for JEZEBEL). The fact that PSI has positive EM values for these indices indicates that probably is using a version of JEFF-3.1 with different ^{237}Np cross sections with respect to CEA.
- Sodium Void Reactivity Coefficients – ENDF/B-VII.0 does not benefit from these experiments, the main reason being the high uncertainties associated to the C/E's. JAEA will use the information from the experiment dominated by the central component, while CEA will also benefit from that dominated by the leakage component. There is no agreement on the EM values of CEA and PSI. This time the indication is that they are probably using different ^{23}Na cross sections.

Conversely to EM let's now define the Theoretical Adjustment Margin (TAM) where in Eq. (11) we suppress

TABLE IX. Experiment Merit (EM) values expressed in %.

Core	Parameter	ANL	CEA	INL	IRSN	JAEA	JSI	KAERI	ORNL	PSI
JEZEBEL239	k_{eff}	0.187	0.013	0.187	0.173	0.072	0.109	-0.096	0.199	0.165
JEZEBEL239	F28/F25	-0.930	1.074	-0.933	-	-1.795	-	-0.530	-1.132	-0.305
JEZEBEL239	F49/F25	-1.585	-0.012	-1.584	-	-0.496	-	-1.119	-1.670	-0.193
JEZEBEL239	F37/F25	0.113	-0.626	0.115	-	-0.491	-	-1.280	0.156	1.707
JEZEBEL240	k_{eff}	0.182	-0.055	0.182	0.186	0.042	-0.035	-0.067	0.121	-0.149
FLATTOP-PU	k_{eff}	0.203	0.280	0.205	0.204	0.162	0.188	-0.644	0.045	0.245
FLATTOP-PU	F28/F25	0.049	0.066	0.048	-	-0.939	-	-0.178	-1.930	0.100
FLATTOP-PU	F37/F25	0.986	-0.133	0.990	-	0.805	-	-0.069	0.411	1.023
ZPR6-7	k_{eff}	0.190	-0.040	0.187	0.035	-0.296	0.042	0.139	-	0.106
ZPR6-7	F28/F25	3.053	-2.107	3.051	-	0.493	-	1.817	-	2.721
ZPR6-7	F49/F25	-1.237	-0.752	-1.232	-	0.396	-	0.780	-	-1.918
ZPR6-7	C28/F25	1.710	1.955	1.713	-	1.050	-	0.013	-	2.133
ZPR6-7 240	k_{eff}	0.161	-0.001	0.158	0.143	-0.107	0.049	0.217	-	0.150
ZPPR-9	k_{eff}	0.040	0.112	0.039	0.021	-0.091	-0.226	-0.016	-	0.149
ZPPR-9	F28/F25	-0.070	-0.964	-0.071	-	1.664	-	1.752	-	-1.225
ZPPR-9	F49/F25	0.163	-0.417	0.161	-	2.257	-	0.869	-	-0.244
ZPPR-9	C28/F25	1.075	1.566	1.071	-	0.509	-	-0.686	-	1.775
ZPPR-9	Na Void Step 3	5.850	-1.501	5.853	-	-0.792	-	-2.685	-	1.421
ZPPR-9	Na Void Step 5	4.791	-1.226	4.789	-	0.341	-	-5.078	-	1.374
JOYO MK-I	k_{eff}	-0.068	0.097	-0.074	-0.013	0.002	-	-0.324	-	0.150

the $U_{C/E}$ term. This corresponds to the ideal situation where we have a perfectly measured experiment and perfect calculation tools with no error or uncertainty associated. Even though this is more an academic exercise, negative *TAM* values can provide stronger recommendations for the quality of the covariance data. Again, negative *TAM* will point out the inability of the covariance data to accommodate the adjustment, where now all the discrepancies have to be attributed to shortcomings in the nuclear data. Table X shows the *TAM* values for the solutions provided by the participants. As expected, there are more negative *TAM* values than *AM* ones. If one excludes the columns of KAERI and ORNL (very low or zero U_{ND} values for the reasons previously indicated), it is quite striking that the rows for the ^{239}Pu fission spectral indices have practically all negative *TAM* values. This indicates that all cross section files have overly optimistic uncertainties for ^{239}Pu fission cross sections.

Another good reason for looking at *TAM* values is the following consideration: if the method uncertainty is very large, the *AM* and χ, quoted above, would suggest that an experiment is still useful for the adjustment, despite the fact that the use of better methods (*e.g.*, with fewer approximations) would make clear that the specific experiment is not useful. In other words, why should one compensate weaknesses of the calculation methods with cross section modifications? This was an early criticism to any statistical adjustment method.

One should simply remember that the method uncertainty reduction is a necessary condition in order to provide unambiguous indications on the integral experiment selection. This is also consistent with the fact that in most cases what we call "method uncertainty" is in fact more a systematic uncertainty or even a bias, with rather limited "statistical" meaning. This is especially true when deterministic methods are used in the experiment analysis. When stochastic methods are used the uncertainty is more statistical in nature, provided that the Monte Carlo code employed in the analysis has no errors or computational approximations (such as the treatment of unresolved resonances in early versions of MCNP4).

VI. ANALYSIS OF THE ADJUSTMENTS

In this section the results of the adjustments are discussed. First the so-called Phase I (*i.e.*, all participants use their own initial cross sections, own nuclear data covariance, with integral experiment and method correlation) results are investigated with focus on specific cases of interest. A typical result of Phase II (*i.e.*, use of own initial cross sections, but a different nuclear data covariance matrix) is then discussed. The impact of adjustments and of a–posteriori correlations (Phase III) is successively analyzed.

Finally, the results of some "stress tests" performed in order to verify the robustness of the adjustment procedures, are also reported.

A. Use of Different Nuclear Data and Associated Covariances (Phase I)

1. General Comments

A few general comments can be made as discussed below.

In most results, no incoherent trends are found when compared to initial uncertainties. Fig. 16 illustrates this

TABLE X. Theoretical Adjustment Margin (*TAM*) values expressed in %.

Core	Parameter	ANL	CEA	INL	IRSN	JAEA	JSI	KAERI	ORNL	PSI
JEZEBEL239	k_{eff}	0.626	1.885	0.622	0.560	0.562	0.567	-0.179	1.185	0.453
JEZEBEL239	F28/F25	1.369	7.317	1.342	-	-0.043	-	-	1.079	0.635
JEZEBEL239	F49/F25	-1.704	1.399	-1.710	-	-1.042	-	-	-1.761	-0.820
JEZEBEL239	F37/F25	1.071	-0.043	1.037	-	-0.599	-	-	5.960	1.591
JEZEBEL240	k_{eff}	0.641	1.508	0.637	0.502	0.489	0.398	-0.144	0.903	0.207
FLATTOP-PU	k_{eff}	0.660	1.893	0.667	0.407	1.116	0.462	-0.821	0.873	0.759
FLATTOP-PU	F28/F25	1.309	6.850	1.281	-	0.613	-	-	-0.414	0.562
FLATTOP-PU	F37/F25	1.604	0.050	1.592	-	0.688	-	-	6.087	0.724
ZPR6-7	k_{eff}	0.930	1.315	0.925	0.757	0.289	0.755	0.223	-	0.828
ZPR6-7	F28/F25	5.954	5.752	5.947	-	1.568	-	-	-	5.958
ZPR6-7	F49/F25	-2.921	-1.374	-2.920	-	-0.998	-	-	-	-3.411
ZPR6-7	C28/F25	0.537	3.471	0.542	-	0.361	-	-	-	1.026
ZPR6-7 240	k_{eff}	0.910	1.339	0.908	0.871	0.483	0.777	0.308	-	0.882
ZPPR-9	k_{eff}	1.100	1.661	1.113	1.069	0.692	0.840	0.251	-	1.198
ZPPR-9	F28/F25	4.865	7.024	4.909	-	3.526	-	-	-	3.637
ZPPR-9	F49/F25	-1.086	-0.030	-1.088	-	1.072	-	-	-	-1.634
ZPPR-9	C28/F25	0.632	3.560	0.624	-	0.185	-	-	-	1.149
ZPPR-9	Na Void Step 3	5.783	3.095	5.679	-	-0.434	-	-	-	4.424
ZPPR-9	Na Void Step 5	7.168	5.417	6.925	-	2.341	-	-	-	6.398
JOYO MK-I	k_{eff}	0.641	1.333	0.608	0.648	0.402	-	-0.156	-	0.823

major effect for some typical examples.

One other important point is that variances are not that much reduced between prior and posterior cross sections uncertainties (except for CEA where initial uncertainties for some isotopes may be found pessimistic and some minor cross sections). It means that the final overall uncertainty reductions on benchmarks calculation or concept calculation are mainly due to correlations created by the adjustment. This point will be investigated in the next paragraph.

A final additional general comment on these results is the fact, that it appears that only a few (∼5) initial isotopes are involved in the adjustment procedure. ^{58}Ni, ^{52}Cr, ^{10}B do not contribute to the data adjustment.

2. *Specific Adjustment Analysis*

A first investigation of the adjustment results for some selected data as obtained by JAEA (using their own nuclear data and covariance data set J-4.0), INL (using their own nuclear data and covariance data set COMMARA-2.0) and CEA (using their own nuclear data and covariance data set COMAC) is given below:

(a) ^{239}Pu capture (Figs. 17–19)

- In the energy range ∼3-500 keV the uncertainties in the three covariance data sets (J-4.0, COMAC, COMMARA-2.0) are rather similar and the uncertainty is in the range ∼6-9% to 7-12%. As for the adjustments, they are consistently indicating an increase of the capture cross section by ∼1-2% up to a maximum of ∼10%.
- In the range ∼5-50 keV, the suggested increase of the capture cross sections in the three files are such that even the adjusted data look very consistent and still close to each other as before adjustment.

(b) ^{239}Pu inelastic scattering cross section and prompt fission neutron spectrum (Fig. 20).

- ^{239}Pu(n,n') is an important reaction (*i.e.*, large sensitivities) when ^{239}Pu is a major component of the core (*e.g.*, JEZEBEL and FLATTOP), in particular for k_{eff} and F28/F25.
- In general, some decrease of (n,n') is suggested for each file. For example, this trend allows to get a better agreement with F28/F25, which is underestimated for both JEZEBEL and FLATTOP by all groups, since negative sensitivity coefficients for the F28/F25 parameter to variations of the ^{239}Pu(n,n') are calculated as expected (even if not in perfect agreement) by all groups.
- However, the changes of the inelastic cross section are the highest for INL and the lowest for CEA.

Even if after adjustment a rather better agreement is found among the three data sets, a good understanding of the trends is obtained only if the ^{239}Pu inelastic cross section adjustments are considered together with the prompt fission neutron spectrum adjustments. In fact, only JAEA and CEA results show significant adjustments for that parameter while INL and ANL show very small adjustments. The lower adjustment (decrease) of (n,n') in the JAEA and CEA results is partly compensated by the decrease of the energy fission spectrum below ∼3.5 MeV suggested both in the JAEA and in the CEA results. When a smaller decrease of the inelastic cross section is suggested, this is associated with a

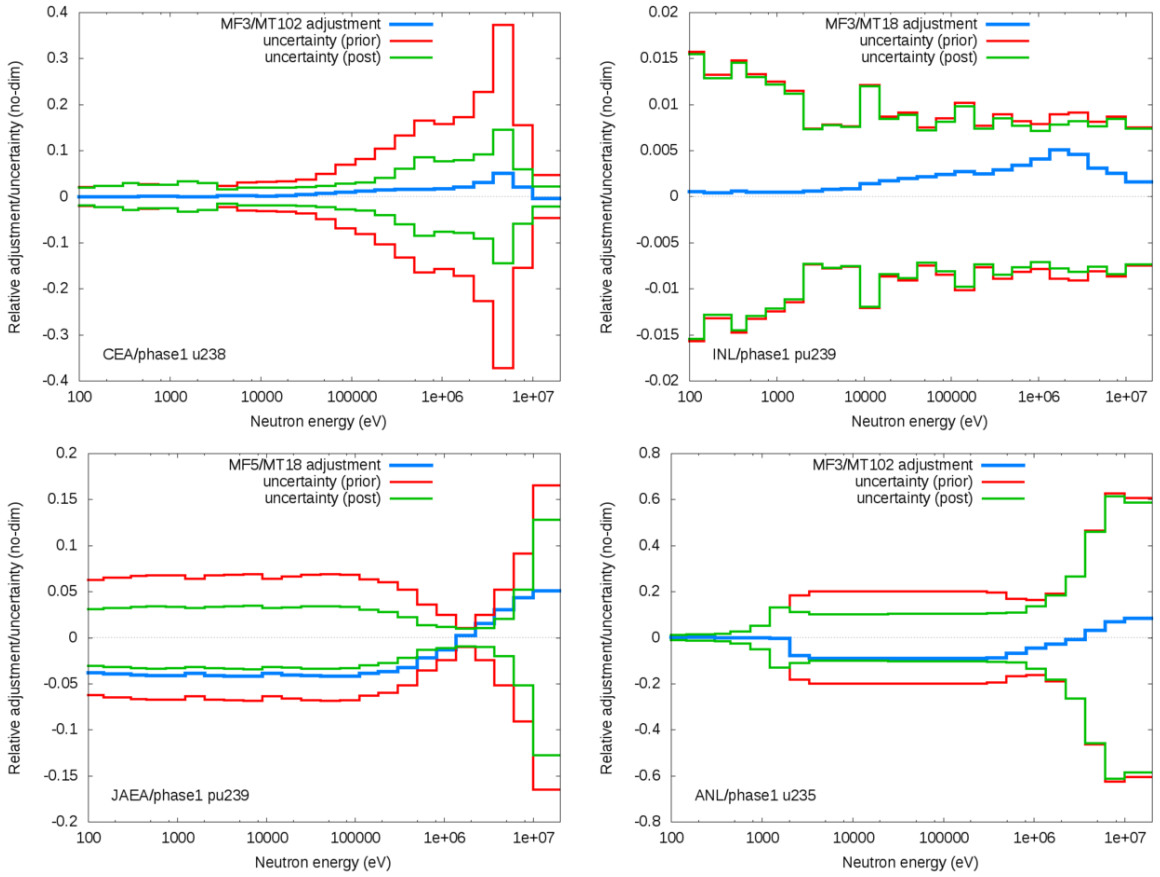

FIG. 16. Example of adjustment trends for major isotopes. The results are consistent with a priori and a–posteriori uncertainties.

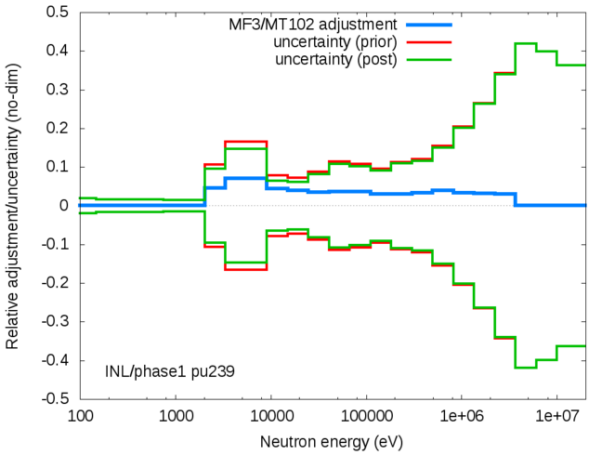

FIG. 17. INL ^{239}Pu neutron capture adjustments.

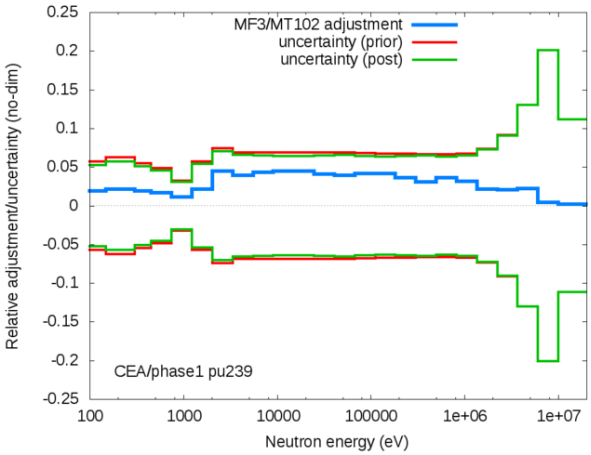

FIG. 18. CEA ^{239}Pu neutron capture adjustments.

higher reduction of the prompt fission neutron spectrum (see CEA with respect to JAEA adjustments of the two parameters). In fact a lower inelastic cross section at high energy allows fewer neutrons below, *e.g.* 1-2 MeV, and the same effect is produced by a lower amount of prompt fission neutrons in that energy range. In other words, since both adjustments of the JAEA and CEA results (*i.e.*, decrease of (n,n') and harder fission spectrum)

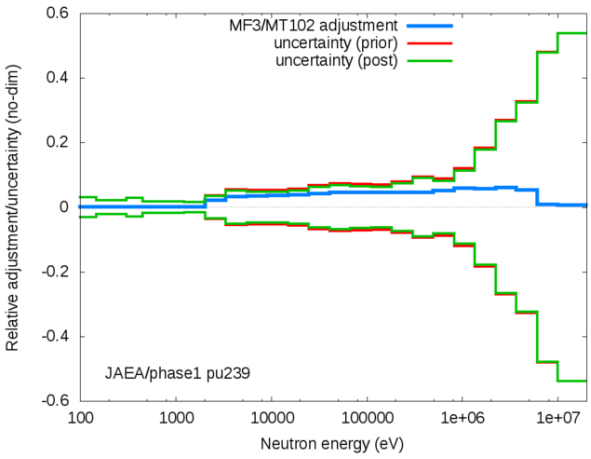

FIG. 19. JAEA ^{239}Pu neutron capture adjustments.

consistently harden the neutron spectrum and help to improve the C/E of F28/F25 in FLATTOP and JEZEBEL, in the INL adjustment a larger (n,n') decrease is needed since a smaller decrease (JAEA and CEA) is "compensated" by the fission spectrum hardening. In summary, the net result is better C/E values (*i.e.*, closer to 1) for the FLATTOP and JEZEBEL F28/F25 (and F37/F25) with the three adjustments (JAEA, CEA and INL). Finally, the suggested change of the prompt neutron fission spectrum both in the JAEA and in the CEA cases, are very consistent.

(c) ^{238}U inelastic scattering and fission cross sections (Figs. 21–23).

- The uncertainty values for the inelastic scattering cross section in the three files are rather different in magnitude and energy trend. For example, in the range 1-20 MeV the COMMARA-2.0 uncertainties are 2-3 times higher than in the J-4.0 (and in the CEA-COMAC) covariance dataset. Below ∼1 MeV that trend is reversed between the two files.

- The ^{238}U inelastic cross section adjustments of the present benchmark are in any case rather small and often much smaller than the uncertainties, and the a–posteriori cross sections are only marginally more consistent than the a priori values. Anyway, CEA and INL/ANL exhibit the need to reduce this reaction cross section.

- For CEA, there is an adjustment of the fission cross section of ^{238}U (a slight decrease of ∼1% in the energy range ∼400 keV - 1 MeV), while the INL adjustment shows a slight decrease of $\bar{\nu}$. The CEA variance is too pessimistic and the INL/CEA difference lies outside the scope INL/CEA relative difference.

(d) ^{235}U capture (Fig. 24).

The uncertainty values on this parameter are significantly different among the different covariance data files (see section III C).

The larger uncertainties in COMMARA-2.0 (and in CEA covariance data) allow a significant decrease of the cross section, essentially to improve the $k_{\rm eff}$ under prediction of INL. Finally, the JAEA adjustment is a decrease of the capture cross section only at very high energy where the J-4.0 uncertainties are higher. Elsewhere, the low uncertainty data in J-4.0 do not allow any significant decrease of the ^{235}U capture data.

It is worth noting that most teams (INL/ANL, CEA, IRSN and JAEA) point out the necessity of decreasing the ^{235}U capture cross section. An equivalent conclusion was given by WPEC Subgroup 29.

(e) For other data, *e.g.* ^{23}Na inelastic and elastic, ^{56}Fe inelastic scattering cross sections, the adjustments are rather small and it is rather difficult to extract clear common trends.

In summary, the analysis of these examples suggests that:

- Adjustment should include all significant parameters in order to provide meaningful indication (see case of inelastic scattering and prompt fission spectrum of ^{239}Pu), and a wide range of integral experiments with different sensitivity profiles.

- Very different covariance data give rise to different adjustments (case of ^{238}U(n,n') and ^{235}U capture). This point reinforces the need to produce very reliable covariance data and to understand the impact of very small variance data and of correlations (in energy, among reactions, *etc.*).

B. Impact of Replacing Covariance Data on the Adjustment (Phase II)

In principle, the central cross section values and the corresponding covariance data of a library must be consistent. However, here we intentionally replace the covariance data used in the adjustment procedure, though we use the same values of other adjustment parameters, especially the C/E values which completely depend on the central cross sections, to analyze the pure effects of the different covariance data to the adjusted results. Two adjustment cases are surveyed as follows:

- Case J (Phase I): This is the reference adjustment case. Cross sections and covariance data are both based on the JENDL-4.0 library (J-4.0, Refs. 19-20).

- Case B (Phase II): The covariance data are taken from C-2.0 and no J-4.0 covariance data are supplemented. The other adjustment parameters are identical with Case J.

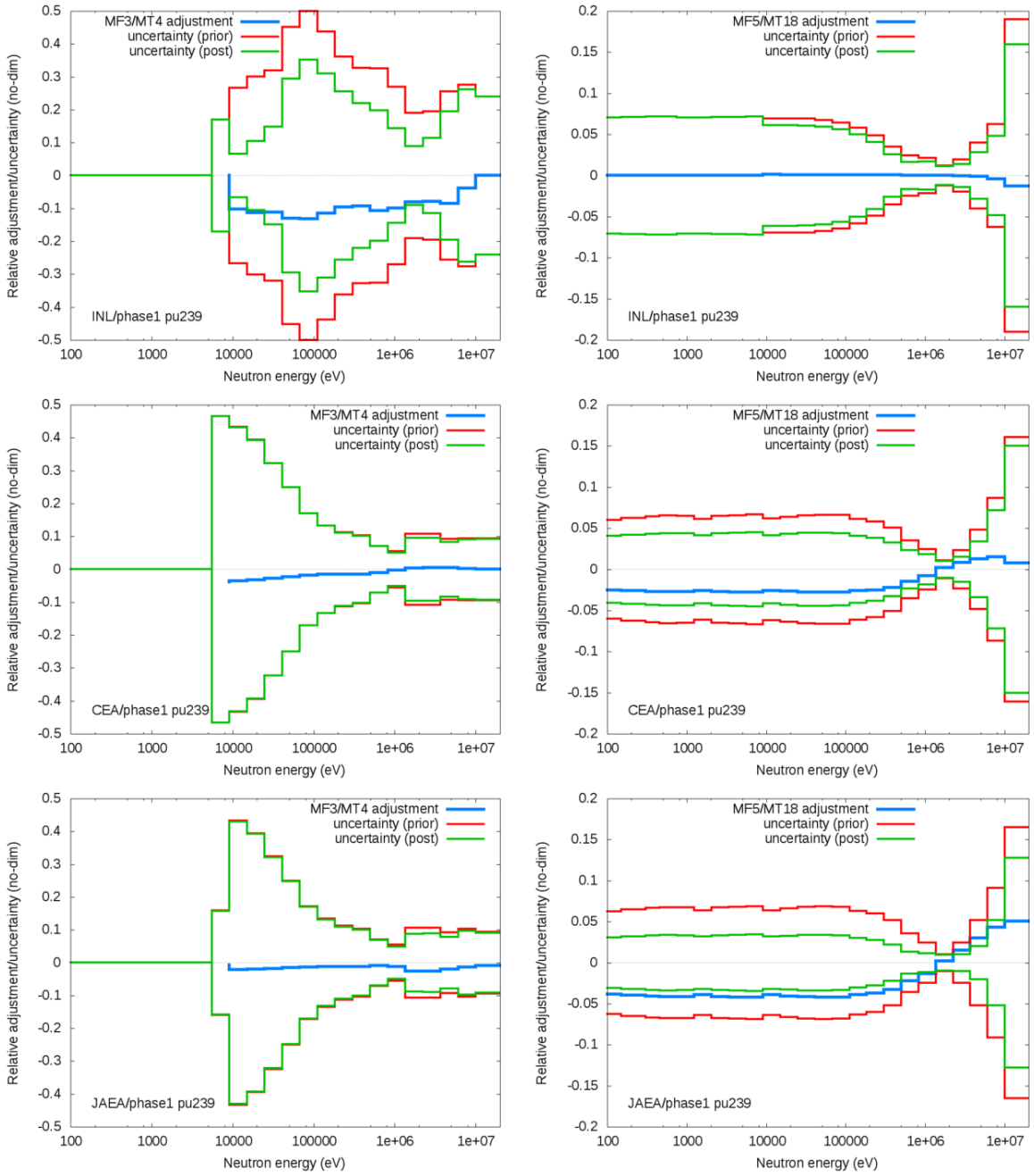

FIG. 20. ^{239}Pu(n,n') cross section and prompt fission spectrum adjustments.

To investigate the effect of different covariance data, the cases of criticality and the sodium void reactivity have been investigated. Here we will focus on the case of criticality ($k_{\rm eff}$).

Fig. 25 compares the $k_{\rm eff}$ C/E changes of the two cases due to the adjustment. It is found that the adjusted C/E values of the two cases are almost identical for $k_{\rm eff}$ of small through large cores. In detail, however, there are some differences between Case J and Case B for the $k_{\rm eff}$ of the JOYO MK-I core which contains ^{235}U fuel as well as plutonium, while the other cores do not include ^{235}U in fuel. The use of C-2.0 shows better improvement of JOYO C/E values than J-4.0.

The contribution of ^{235}U capture cross section adjustment in case B (Phase II) is significantly different by ∼400 pcm between the J-4.0 and C-2.0 covariance data,

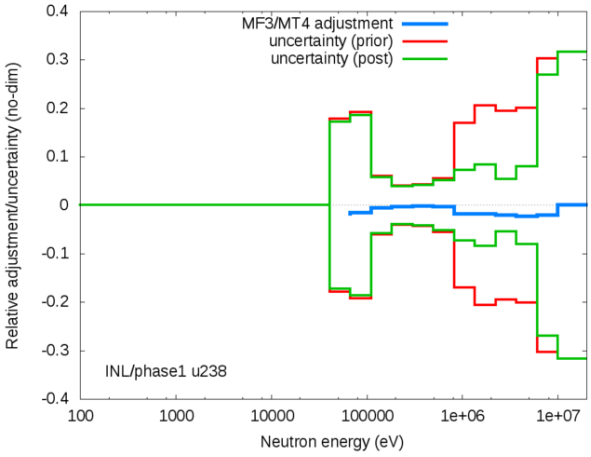

FIG. 21. INL ^{238}U inelastic scattering cross section adjustments.

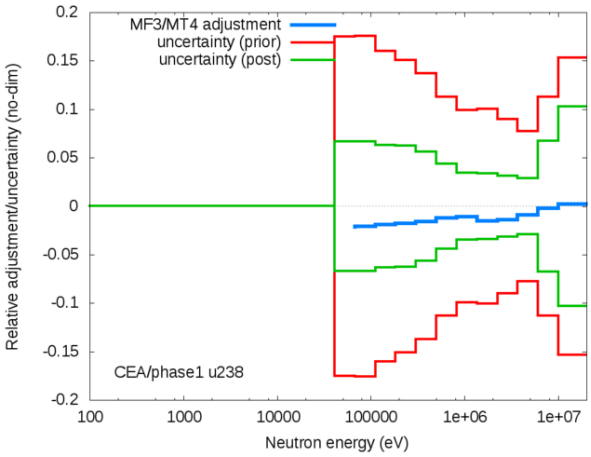

FIG. 22. CEA ^{238}U inelastic scattering cross section adjustments.

while those of ^{23}Na and ^{56}Fe elastic scattering are smaller (∼70 pcm each) but opposite in sign. The overall k_{eff} correction is of the order of ∼200 pcm and makes the C/E agreement much better.

As for the most important contribution, *i.e.*, ^{235}U capture, the difference of STDs between C-2.0 and J-4.0 significantly affected the changing rate of the cross section. The small STD of J-4.0 must constrain the alteration of the cross section by the adjustment. The large STD of C-2.0 allows the large changing rate of the ^{235}U capture cross sections to improve the C/E value of JOYO k_{eff} by the adjustment.

One can see in Fig. 25 that the initial a priori covariance data *do not seem to influence the final* C/E *values* as well as their uncertainties.

This final point is due to the form of generalized least square equations. Let us remind the form of the equation

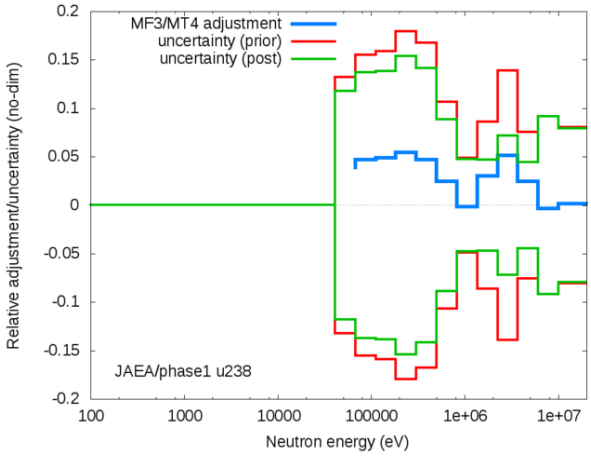

FIG. 23. JAEA ^{238}U inelastic scattering cross section adjustments.

for a–posteriori covariances

$$M'_\sigma = M_\sigma - M_\sigma S^t \left(M_E + S M_\sigma S^t\right)^{-1} S M_\sigma. \quad (13)$$

If $S M_\sigma S^t >> M_E = V_e + V_m$, then the a–posterior uncertainties on experiments due to the new cross section data, $S M'_\sigma S^t$, are almost equal to M_E. V_e stands for integral experiments covariances and V_m for modeling covariances.

C. Effect of Uncertainties and Correlations (Prior/Posterior) on "Target System" Uncertainties (Phase III)

In order to investigate the impact of adjustments and in particular of a–posteriori correlations, two "Target Systems" have been defined on which the effect of the adjustment is tested. This corresponds to what is expected to be done in practice: one wants to verify the impact of an adjustment in terms of reduction of uncertainties. Two target systems have been defined: the JAEA Fast Breeder Reactor (FBR) defined in Ref. [40] and the ANL Advanced Burner Reactor (ABR), described in Ref. [41]. For this last system, a metal and oxide core fuel versions have been considered, and for the oxide core, also a recycled fuel core version has been considered.

We evaluated the impact of correlations before and after adjustment on the target systems k_{eff} uncertainties. Only the COMAC-V0 covariance matrices were used. The following uncertainty propagation calculations were performed:

- Case 1: Full prior/posterior covariance matrix.
- Case 2: Remove from the previous case correlations between different isotopes (*e.g.*, no correlation between ^{235}U and ^{238}U).

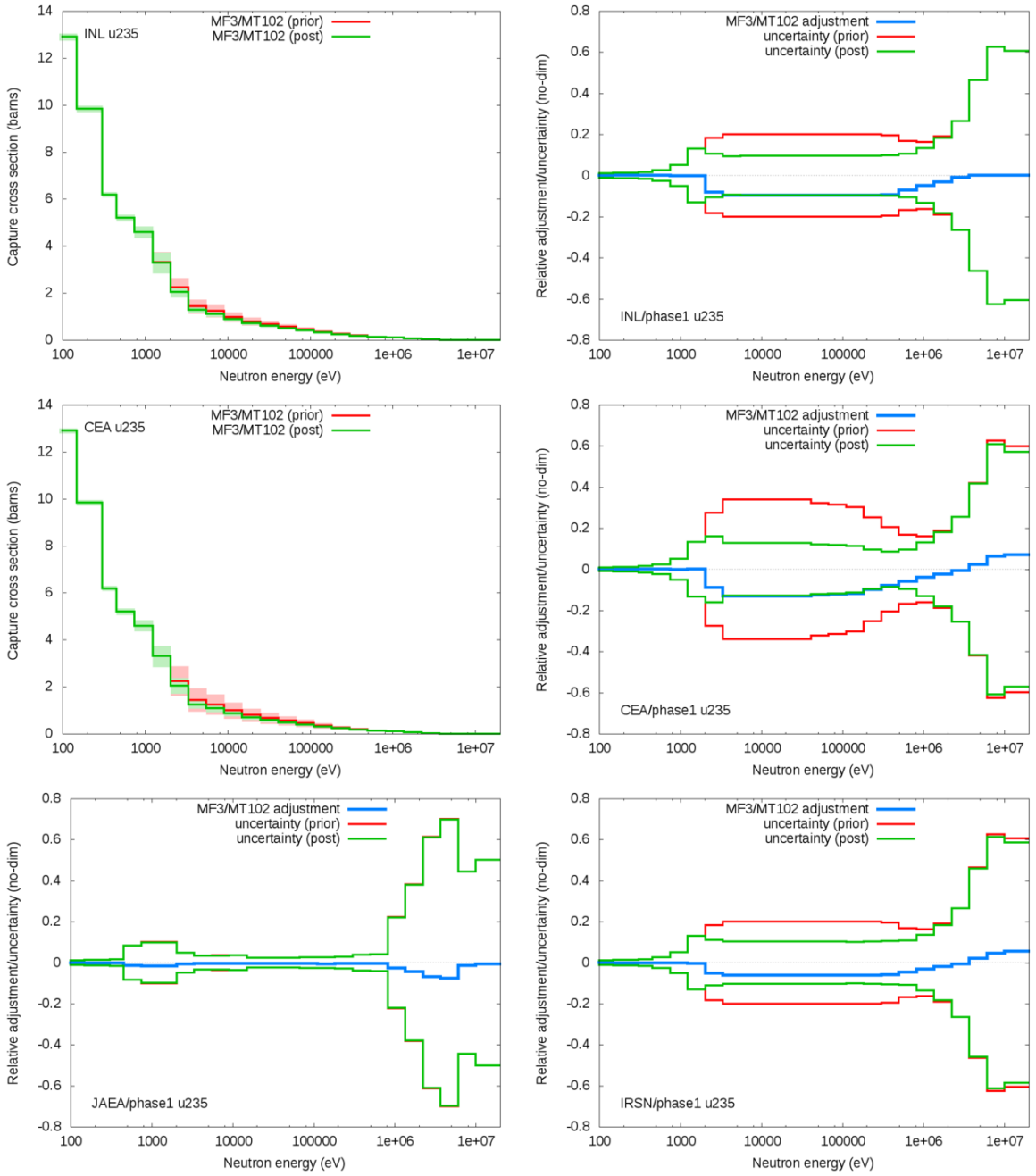

FIG. 24. Adjustment of ^{235}U neutron capture cross section obtained by INL (top), CEA (middle), JAEA and IRSN (bottom).

- Case 3: Remove from the previous case correlations on reactions for each isotope (*e.g.*, inelastic and elastic scattering for ^{238}U).
- Case 4: Keep only variances.

The results are shown in Table XI. For all target systems, the uncertainty using prior and posterior covariance matrices converge to rather similar values when correlations are deleted. Moreover, one can see that:

- Correlations among isotopes (after adjustment) are important and contribute to the uncertainty reduction by a factor 2-3 in terms of target system uncertainties.
- Correlations among reactions for each isotope are significant, as well as correlation between energy

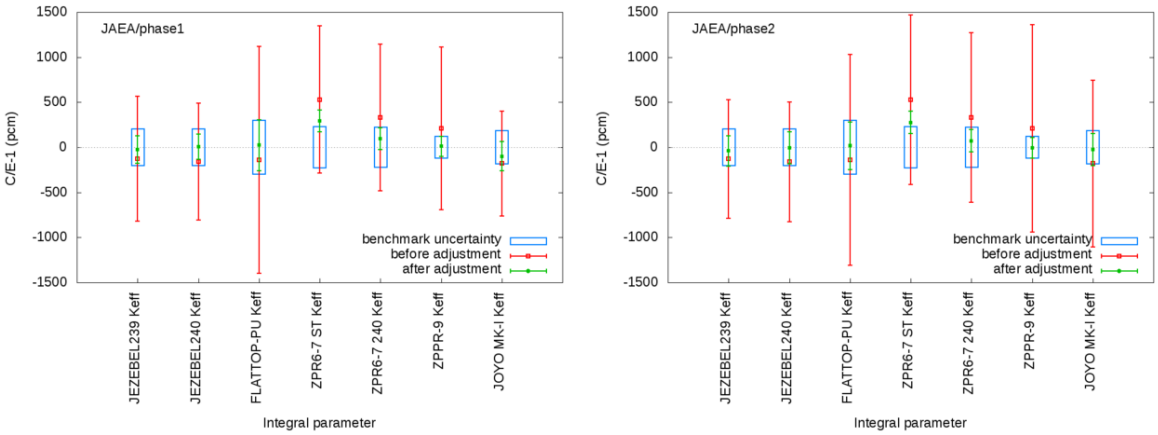

FIG. 25. Modifications of C/E of k_{eff} values due to adjustment.

TABLE XI. Impact of correlations on the k_{eff} uncertainty of the "Target Systems."

ABR Oxide	Prior covariances	Posterior covariances
Case 1	1550 pcm	170 pcm
Case 2	1550 pcm	510 pcm
Case 3	1720 pcm	680 pcm
Case 4	1200 pcm	820 pcm
JAEA FBR	Prior covariances	Posterior covariances
Case 1	1310 pcm	220 pcm
Case 2	1310 pcm	490 pcm
Case 3	1560 pcm	610 pcm
Case 4	1170 pcm	900 pcm
ABR Metal	Prior covariances	Posterior covariances
Case 1	1740 pcm	250 pcm
Case 2	1740 pcm	560 pcm
Case 3	2020 pcm	730 pcm
Case 4	1290 pcm	850 pcm
ABR Oxide Recycled	Prior covariances	Posterior covariances
Case 1	1250 pcm	260 pcm
Case 2	1250 pcm	490 pcm
Case 3	1400 pcm	590 pcm
Case 4	1080 pcm	820 pcm

groups for each reaction.

- As for the prior covariance matrix, taking into account cross-correlations (between reactions and energy groups) tends to give an overall uncertainty of the same order of magnitude (Case 4 → Case 1), except for the ABR Metal core. But, the effect of energy correlations is an increase of the uncertainty (Case 4 → Case 3) and the effect of constraint on reactions tends to lower this uncertainty (Case 3 → Case 2 = Case 1).
- As for the a–posterior covariance matrix, the introduction of correlations gives always a reduction of uncertainty Case 4 → Case 3 → Case 2 → Case 1.

More results related to the impact of the adjustments on the "Target Systems" can be found in [24]. These results do confirm the trends and the conclusions given above.

D. Calculation of Cook's Distance: Influence of Experiments

If the adjustment is done by discarding a chosen integral data point I, the results (adjusted cross sections) are noted as $\{\sigma_p^I\}$. The original adjustment is noted as $\{\sigma_p\}$. The Cook distance is calculated using

$$D_I = \left(\sigma_p^I - \sigma_p\right)^t \left(M'_\sigma\right)^{-1} \left(\sigma_p^I - \sigma_p\right). \qquad (14)$$

Low values of D show a negligible impact of the remote data points. High values of D indicate very influential experiments. This last point may be due to very low experimental uncertainties as well as very important influence on final multigroup cross sections.

The calculation of Cook distance was carried out using COMAC-V0 covariances. The results (blue bars) can be seen on Fig. 26. The influence of each experiment is detailed by type:

- k_{eff}: JOYO is an important experiment in the adjustment for two reasons: all isotopes have an impact on the reactivity of the core (^{235}U + ^{239}Pu fuel) and the experimental uncertainty is rather small (180 pcm). If we change manually this specific uncertainty, from 180 pcm to 500 pcm, we obtain the red bars on Fig. 26, where the weight of JOYO is reduced by almost a factor 10 ; JEZEBEL ^{240}Pu and ^{239}Pu are the second and third experiments with the most leverage mostly because of the low experimental uncertainty; FLATTOP is 4 times less important than JEZEBEL ^{239}Pu because of its large experimental uncertainty (300 pcm instead of 200 pcm); ZPPR-9 has the same influence

as JEZEBEL ^{239}Pu, thanks to its very small experimental uncertainty (118 pcm); ZPR6-7 and ZPR6-7 High ^{240}Pu content have a negligible impact, in comparison with ZPPR-9, mostly due to their experimental uncertainties (∼230 pcm).

- Sodium void reactivity: these experiments seem to be important (the same order of magnitude with JEZEBEL ^{240}Pu and JOYO). Structural material such as ^{23}Na and ^{56}Fe are more sensitive to this kind of experiment than to multiplication factor, which can explain the weight of sodium void in the adjustment. Also, the experimental uncertainties for ZPPR-9 Step 3 and Step 5 are quite low.

- Reaction rate ratios: for all cases, this type of integral experiment has a very limited impact in the adjustment because the sensitivities are mostly focused on only two reactions in the whole set of cross section parameters.

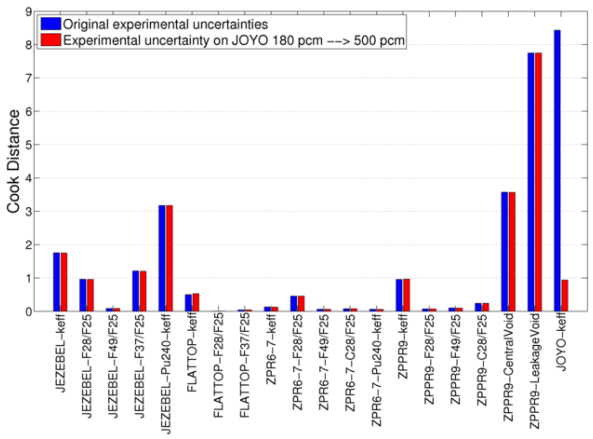

FIG. 26. Cook distance of experiments. The largest distances indicate the most influential integral parameters.

E. Stress Tests on the Adjustments

1. *Stress Test Specification*

In the previous paragraphs we have described the cross section adjustment exercise based on the selected 20 fast reactor experiment benchmarks as the reference case. As seen in the previous discussion, the adjusted results of the reference case are quite satisfactory from both viewpoints of the integral and differential data. The objective of this section is to study the impact on the adjusted results when an integral experiment with different nature from the standard 20 experiments set is added to the reference case. This exercise was characterized as the "Stress test", *i.e.*, one specific integral experiment was added with a C/E value very different from 1 to 20 reference integral experiments, to find what would be the feedback on the adjusted results.

A larger number of cases are described in detail in Ref. [24], however here we will summarize only a typical result. In particular, the following two adjustment cases have been analyzed:

1) Case J4: This is the reference adjustment case with the standard 20 integral data. Cross sections and covariance data are based on the JENDL-4.0 library (Refs. [19, 20]).

2) "Stress test": One integral experiment, *i.e.*, the $k_{\rm eff}$ of the ZPR-9/34 core [39], is added to the reference Case J4. The unique features of the ZPR-9/34 core are:

- The core region consists of 93% enriched-uranium and iron.

- The height and diameter of the core are 1.8m and 1.2m, respectively.

- The core is surrounded by stainless steel reflector.

The experimental $k_{\rm eff}$ value and associated uncertainty of the stress test experiment is based on the ICSBEP handbook [8]. The $k_{\rm eff}$ value is calculated by a continuous-energy Monte Carlo code with two-dimensional homogenized (r,z) benchmark models, and applied with the corrective factors between the simplified RZ model and the as-built three-dimensional heterogeneous model which are supplied in the ICSBEP handbook. The modeling uncertainty is based on the uncertainty estimation associated with the "Monte Carlo transformation of model" correction factors to convert the simplified (r,z) model values to the as-built model which is also supplied in the ICSBEP handbook [8]. The Monte Carlo statistical uncertainties of the simplified (r,z) model calculation are also added to the modeling uncertainties, though they are negligible compared with the model transformation uncertainties.

2. *Results of the Stress Test*

As for the initial results, it is interesting to note that the $k_{\rm eff}$ value of ZPR-9/34 is overestimated by +1420 pcm; on the other hand, $k_{\rm eff}$ values of six cores treated in Case J4, numbers 1, 5, 6, 9, 13 and 20, are within only ±530 pcm. The objective of the "Stress test" is to verify whether the adjustment operation could manage the C/E value of ZPR-9/34 very different from 1 without harmful influence to other integral data and/or cross sections adjustment performances.

The C/E value changes for all integral data in Case J4 and "Stress test" are summarized in Tables XII and XIII. The "Stress test" does not seem to give any critical harm to the standard 20 integral data of Case J4. In fact in the "Stress test" case, the adjusted results are practically as good as in Case J4. Even the C/E value of the extra ZPR-9/34 $k_{\rm eff}$ which is newly added to the adjustment, changes to almost 1.00.

In both cases the χ^2 test gives an excellent indication of reliability of the adjustment (0.53 and 0.63, respectively). Moreover, the analysis of the impact of newly added experiment can be analyzed in terms of Eqs. (11) and (12). As for the diagnostics using Eq. (12), the values associated to each experiment in the case of JAEA, here chosen as example, are given in the last column of Tables XII and XIII. The ZPR-9/34 $k_{\rm eff}$ experiment shows an acceptable value (*i.e.*, $\chi = 1.21$ which is below 3 sigma). If we use the parameters defined in section V and based on Eq. (11), one obtains for the adjustment margin, $AM = -0.005$, the experiment merit, $EM = -1.16$, and the theoretical adjustment margin, $TAM = -0.17$. These values can be interpreted as follows: the new experiment will marginally contribute to the overall adjustment (*i.e.*, $AM \sim 0$); however there is merit in the newly added information ($EM < 0$); but the negative value of TAM indicates that nuclear data, important for that specific experiment, have associated uncertainties that are probably underestimated.

Finally, it is needed to confirm that the adjustment does no harm not only in terms of integral data a–posteriori values, but also in terms of differential cross sections. For this purpose, the nuclide- and reaction-wise contributions to the total $k_{\rm eff}$ modifications were investigated, comparing the cases with and without stress test.

In the "Stress test" case, it is found that the large improvement of the C/E value, approximately -1300 pcm, is attained by the cross section changes of ^{56}Fe capture and elastic scattering reactions, which are considered to result in the negative reactivity of the absorption effect by the iron in the core region, and the neutron leakage enhancement by the stainless steel reflector. These two cross section adjustments are responsible for ∼700 and ∼600 pcm, respectively.

Fig. 27 shows the cross section modifications for the ^{56}Fe capture reaction. In the reference Case J4, there are small changes of the cross sections. However, quite large cross section alterations occur in the "Stress test". The order of magnitude is +11% below 100 keV, which is very close to the STD value, ±10%. Changes of this magnitude might be close to or exceed the limitation of allowance from the viewpoint of the nuclear data evaluation.

Fig. 28 illustrates the changes of the ^{56}Fe elastic scattering cross sections. In the Case J4, there are small alterations. On the other hand, in the "Stress test", the ^{56}Fe elastic cross sections are decreased to adjust $k_{\rm eff}$ values of the stainless steel or iron reflector core of ZPR-9/34. These cross section changes are quite large, but still within the STD values, which may be acceptable from the nuclear data viewpoint.

The fact that the required adjustments are so close to the STD values in the JAEA covariance matrix, can be associated to the negative, even if small value, of the TAM parameters, as discussed in the previous paragraph.

As far as the other cross sections, the stress test does not modify significantly the adjustment results obtained in the case J4. As an example, the adjustments of the ^{239}Pu capture cross sections are shown in Fig. 29. Both in Case J4 and in the "Stress test" case, the change is approximately +3-5%, which is within one standard deviation (STD) value of the JENDL-4.0 covariance, that is, ±6-9% in the dominant energy region.

In summary the example shown here and further stress tests reported in [24], tend to confirm the robustness of the adjustment procedures.

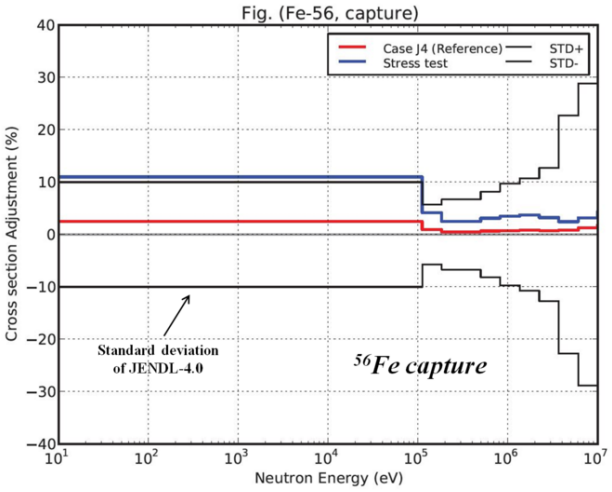

FIG. 27. Change of cross sections by adjustment: ^{56}Fe(n,γ).

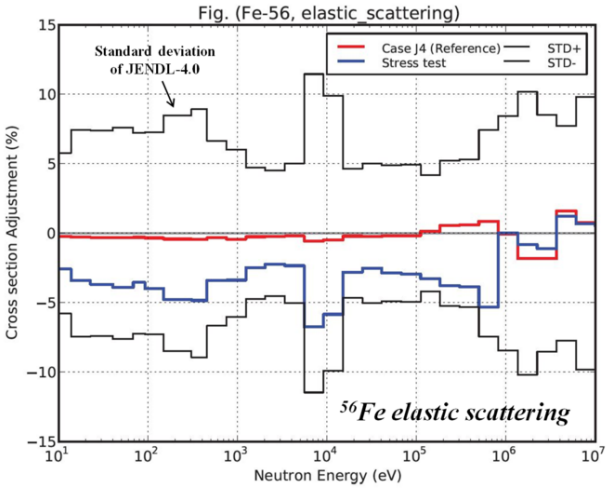

FIG. 28. Change of cross sections by adjustment: ^{56}Fe(n,n).

F. Conclusion of Adjustment Results

This first analysis indicates that:

- Adjustment should include all significant parameters in order to provide meaningful indications (see

TABLE XII. Results of the adjustment based on JENDL-4.0 (Case J4: Standard 20 integral data) – reduced $\chi^2 = 0.53$.

No.	Core	Integral parameter	C/E Value		Integral parameter uncertainty (%)		Nuclear-data-induced uncertainty (%)		Ratio of $\lvert C/E-1\rvert$ to prior total uncertainty[a]
			Before	After	Experiment ($\sqrt{V_e}$)	Modeling ($\sqrt{V_m}$)	Before ($\sqrt{SM_\sigma S^t}$)	After ($\sqrt{SM'_\sigma S^t}$)	
1	JEZEBEL239	k_{eff}	0.9987	0.9997	0.20	0.03	0.69	0.15	0.18
2	JEZEBEL239	F28/F25	0.969	0.990	1.1	0.94	3.20	1.02	0.89
3	JEZEBEL239	F49/F25	0.984	0.987	0.9	0.75	0.63	0.47	1.23
4	JEZEBEL239	F37/F25	0.979	0.989	1.4	0.80	1.50	0.67	0.93
5	JEZEBEL240	k_{eff}	0.9984	1.0001	0.20	0.03	0.65	0.14	0.24
6	FLATTOP-PU	k_{eff}	0.9986	1.0002	0.30	0.03	1.26	0.28	0.11
7	FLATTOP-PU	F28/F25	0.977	0.998	1.1	0.84	2.94	0.97	0.70
8	FLATTOP-PU	F37/F25	0.993	1.001	1.4	0.69	1.44	0.72	0.35
9	ZPR6-7	k_{eff}	1.0053	1.0029	0.23	0.03	0.82	0.12	0.62
10	ZPR6-7	F28/F25	1.034	1.029	3.0	2.24	4.82	1.85	0.55
11	ZPR6-7	F49/F25	0.979	0.976	2.1	1.43	1.15	0.83	0.75
12	ZPR6-7	C28/F25	1.017	1.011	2.4	1.22	2.00	1.12	0.50
13	ZPR6-7 240	k_{eff}	1.0033	1.0010	0.22	0.03	0.81	0.12	0.39
14	ZPPR-9	k_{eff}	1.0021	1.0001	0.117	0.02	0.90	0.11	0.23
15	ZPPR-9	F28/F25	0.983	0.977	2.7	2.09	5.28	2.02	0.27
16	ZPPR-9	F49/F25	0.999	0.996	2.0	1.21	1.15	0.83	0.03
17	ZPPR-9	C28/F25	1.019	1.013	1.9	1.39	2.03	1.12	0.60
18	ZPPR-9	Na Void Step 3	1.068	1.038	1.9	5.26	5.95	3.32	0.84
19	ZPPR-9	Na Void Step 5	1.052	1.014	1.9	4.96	7.31	4.04	0.58
20	JOYO MK-I	k_{eff}	0.9982	0.9990	0.18	0.03	0.58	0.16	0.29

[a] Ratio of $\lvert C/E-1\rvert$ to prior total-uncertainty: $\lvert C/E-1\rvert/\sqrt{SM_\sigma S^t + V_e + V_m}$.

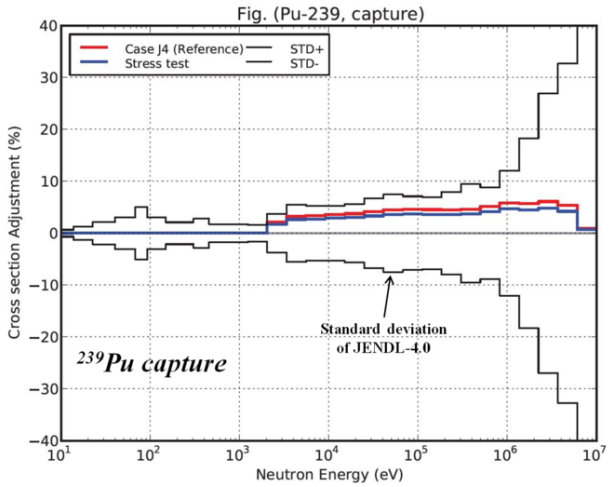

FIG. 29. Change of cross sections by adjustment: $^{239}\text{Pu}(n,\gamma)$.

case of inelastic scattering and chi of ^{239}Pu), and a wide range of integral experiments with different sensitivity profiles.

- Very different covariance data give rise to different adjustments (case of ^{238}U(n,n') and ^{235}U capture). This point reinforces the need to produce very reliable covariance data and to understand the impact of very small variance data and of correlations (in energy, among reactions, *etc.*).
- Initial C/E's are driving the path to adjustment in some cases (see example of CEA ^{238}U(n,n') trends depending on C/E's values in [24]).
- Experimental uncertainties have to be correctly quantified, because they drive the weight in the adjustment process (see Cook's distance). In other words, a misestimated experimental uncertainty can lead to biased trends on cross sections and overestimation of the uncertainty reduction.
- Final calculated uncertainties on benchmarks do not seem to depend on chosen a priori cross section covariance; uncertainty reduction through integral experiment is driven by integral experiment uncertainties.
- A–posteriori cross section covariances are only driven by the competition between a priori covariance matrix and initial experimental matrix with deterministic adjustments procedure.

VII. CONCLUSIONS

Subgroup 33 has succeeded in providing a deeper understanding of nuclear data adjustment methods and of their application.

The findings of the Subgroup 33 have pointed out that the statistical adjustments methodologies in use worldwide for different reactor analysis and design purposes

TABLE XIII. Results of the "stress test" adjustment with ZPR-9/34 added to the 20 integral data, (Case J4) – reduced $\chi^2 = 0.63$.

No.	Core	Integral parameter	C/E Value		Integral parameter uncertainty (%)		Nuclear-data-induced uncertainty (%)		Ratio of $\lvert C/E-1\rvert$ to prior total uncertainty[a]
			Before	After	Experiment ($\sqrt{V_e}$)	Modeling ($\sqrt{V_m}$)	Before ($\sqrt{SM_\sigma S^t}$)	After ($\sqrt{SM'_\sigma S^t}$)	
1	JEZEBEL239	k_{eff}	0.9987	0.9997	0.20	0.03	0.69	0.15	0.18
2	JEZEBEL239	F28/F25	0.969	0.989	1.1	0.94	3.20	1.02	0.89
3	JEZEBEL239	F49/F25	0.984	0.987	0.9	0.75	0.63	0.47	1.23
4	JEZEBEL239	F37/F25	0.979	0.989	1.4	0.80	1.50	0.67	0.93
5	JEZEBEL240	k_{eff}	0.9984	1.0000	0.20	0.03	0.65	0.14	0.24
6	FLATTOP-PU	k_{eff}	0.9986	1.0007	0.30	0.03	1.26	0.28	0.11
7	FLATTOP-PU	F28/F25	0.977	0.997	1.1	0.84	2.94	0.97	0.70
8	FLATTOP-PU	F37/F25	0.993	1.001	1.4	0.69	1.44	0.72	0.35
9	ZPR6-7	k_{eff}	1.0053	1.0028	0.23	0.03	0.82	0.12	0.62
10	ZPR6-7	F28/F25	1.034	1.033	3.0	2.24	4.82	1.84	0.55
11	ZPR6-7	F49/F25	0.979	0.979	2.1	1.43	1.15	0.81	0.75
12	ZPR6-7	C28/F25	1.017	1.011	2.4	1.22	2.00	1.12	0.50
13	ZPR6-7 240	k_{eff}	1.0033	1.0009	0.22	0.03	0.81	0.12	0.39
14	ZPPR-9	k_{eff}	1.0021	1.0002	0.117	0.02	0.90	0.11	0.23
15	ZPPR-9	F28/F25	0.983	0.979	2.7	2.09	5.28	2.01	0.27
16	ZPPR-9	F49/F25	0.999	0.999	2.0	1.21	1.15	0.82	0.03
17	ZPPR-9	C28/F25	1.019	1.013	1.9	1.39	2.03	1.12	0.60
18	ZPPR-9	Na Void Step 3	1.068	1.046	1.9	5.26	5.95	3.29	0.84
19	ZPPR-9	Na Void Step 5	1.052	1.019	1.9	4.96	7.31	4.03	0.58
20	JOYO MK-I	k_{eff}	0.9982	0.9984	0.18	0.03	0.58	0.16	0.29
21	ZPR-9/34	k_{eff}	1.0142	1.0012	0.11	0.24	1.15	0.25	1.21

[a] Ratio of $\lvert C/E-1\rvert$ to prior total-uncertainty: $\lvert C/E-1\rvert/\sqrt{SM_\sigma S^t + V_e + V_m}$.

are well understood and that they are essentially equivalent.

The results of the adjustments indicate, for some important data, common trends for modification even if starting from different basic nuclear data and different covariance matrices. The results obtained show also some degree of robustness in the sense that the observed trends can "survive" rather severe "stress tests".

In this respect, these methodologies can provide a powerful tool for nuclear data (and associated uncertainties) improvement if used in an appropriate manner. In fact, it has been indicated that the associated sensitivity analysis requires careful use of existing methods and that the choice of specific integral experiments of different types (critical masses but also reaction rates, reactivity coefficients and irradiation experiments) and sensitive to different energy neutron spectra, is of high relevance to avoid as much as possible compensating effects in the adjustments.

Finally, it has been pointed out the crucial role of the covariance data used, both those associated to the nuclear data and those associated to the integral experiments. The a–posteriori correlations are mainly responsible for the uncertainty reduction of parameters of reference design systems. Their physics meaning and appropriate utilization will need further study.

The deeper understanding of the methodologies and of their applications implies that the role for cross section adjustment is more and more perceived as that of providing useful feedback to evaluators and differential measurement experimentalists in order to improve the knowledge of neutron cross sections to be used in a wider range of applications.

This new role for cross section adjustment requires tackling and solving a new series of issues:

- Definition of criteria to assess the reliability and robustness of an adjustment.
- Requisites to assure the quantitative validity of the covariance data.
- Criteria to alert for inconsistency between differential and integral data.
- Definition of consistent approaches to use both adjusted data and a–posteriori covariance data to improve quantitatively nuclear data files.
- Provide methods and define conditions to generalize the results of an adjustment in order to evaluate the "extrapolability" of the results of an adjustment to a different range of applications (*e.g.*, different reactor systems) for which the adjustment was not initially intended.
- Suggest guidelines to enlarge the experimental data base in order to meet needs that were identified by the cross section adjustment.

Acknowledgements: The authors wish to express their sincere gratitude to the staff of the National Nuclear Data Center, especially S. Hoblit who took care of LaTeX corrections in the course of the review process. The work at INL is supported by the U.S. Department of Energy, Office of Nuclear Energy, under DOE Idaho Operations Office Contract DE-AC07-05ID14517. The work at BNL was sponsored by the Office of Nuclear Physics, Office of Science of the U.S. Department of Energy under Contract No. DE-AC02-98CH10886 with Brookhaven Science Associates, LLC.

[1] G. Aliberti *et al.*, Nucl. Sci. Eng. **46**, 13 (2004).
[2] G. Aliberti *et al.*, Ann. of Nucl. Energy **33**, 700 (2006).
[3] *Uncertainty and Target Accuracy Assessment for Innovative Systems Using Recent Covariance Data Evaluations*, Report **26**, NEA/WPEC-26, OECD/NEA, Paris (2008).
[4] G. Cecchini, U. Farinelli, A. Gandini and M. Salvatores, *Analysis of integral data for few-group parameter evaluation of fast reactors*, Proc. 3rd Int. Conf. Peaceful Uses Atomic Energy, Geneva, P/627, p. 388 (1964).
[5] H. Mitani and H. Kuroi, J. Nucl. Sci. and Tech. **9**, p. 383 and p. 642 (1972).
[6] J.P. Chaudat, J.Y. Barre and A. Khairallah, *Improvements of the Predicted Characteristics for Fast Power Reactor from Integral Experiments: Cadarache Version III Multigroup Cross Section Set*, Proc. of the Symp. Physics of Fast Reactor, Tokyo, Vol. 3, p. 1207 (1973).
[7] *Assessment of Existing Nuclear Data Adjustment Methodologies*, International Evaluation Co-operation, Intermediate Report of WPEC Subgroup 33, NEA/NSC/WPEC/DOC(2010)429, OECD/NEA, Paris, 2011.
[8] International Handbook of Evaluated Criticality Safety Benchmark Experiments, NEA/NSC/DOC(95)03, September 2007 Edition.
[9] International Handbook of Evaluated Reactor Physics Benchmark Experiments, NEA/NSC/DOC(2006)1, March 2007 Edition.
[10] L.G. LeSage, *An Overview of the Argonne National Laboratory Fast Critical Experiments, 1963-1990*, ANL-NT-175, April 2001.
[11] L.N. Usachev, Proc. Int. Conf. on Peaceful Uses of Nuclear Energy, Vol. 5, 503, Geneva (1955) and A. Gandini, J. Nucl. Energy **21**, p. 755 (1967).
[12] M. Ishikawa, *Recent application of nuclear data to fast reactor core analysis and design in Japan*, International Conference on Nuclear Data for Science and Technology, Santa Fe, Sept 26 - Oct 1, 2004, p. 1405 (2005).
[13] G. Rimpault *et al.*, *The ERANOS data and code system for fast reactor neutronic analyses*, Proceedings of the International Conference on the New Frontier of Nuclear Technology: Reactor Physics, Safety and High-Performance Computing (PHYSOR 2002), Seoul, Korea (2002).
[14] I. Kodeli, Nucl. Sci. Eng. **138**, 45 (2001).
[15] R.E. Alcouffe *et al.*, *DANTSYS: A Diffusion Accelerated Neutral Particle Transport Code System*, Los Alamos National Laboratory report, LA-12969-M (1995).
[16] *TSUNAMI-3D: Control module for three-dimensional cross-section sensitivity and uncertainty analysis for criticality* (SCALE, VOL I, Sect. C9), Technical Report ORNL/TM-2005/39, Oak Ridge National Laboratory (2009).
[17] A. Gandini, G. Palmiotti and M. Salvatores, Ann. Nucl. Energy **13**, 109 (1986).
[18] D.L. Smith, *Probability, Statistics, and Data Uncertainties in Nuclear Science and Technology*, An OECD Nuclear Energy Agency Nuclear Data Committee Series, Nuclear Physics and Nuclear Data in Science and Technology, Volume 4 (1991).
[19] K. Shibata *et al.*, J. Nucl. Sci. and Tech. **48**, 1 (2011), and JENDL-4.0 homepage, `http://wwwndc.jaea.go.jp/jendl/j40/j40.html`.
[20] O. Iwamoto, T. Nakagawa and S. Chiba, J. Kor. Phys. Soc. **59**, 1224 (2011).
[21] M. Herman *et al.*, *COMMARA-2.0 Neutron Cross Section Covariance Library*, BNL-94830-2011, U.S. Department of Energy (March 2011).
[22] M.B. Chadwick *et al.*, Nucl. Data Sheets **107**, 2931 (2006).
[23] C. De Saint Jean *et al.*, J. Kor. Phys. Soc. **59**, 1276 (2011).
[24] *Methods and issues for the combined use of integral experiments and covariance data*, International Evaluation Co-operation **33**, NEA/WPEC-33, OECD/NEA, Paris (2013).
[25] W.P. Poenitz, *Data Interpretation, Objective Evaluation Procedures and Mathematical Techniques for the Evaluation of Energy-dependent Ratio, Shape and Cross Section Data*, Proceedings of the Conference on Nuclear Data Evaluation Methods and Procedures, Brookhaven National Laboratory, New York, Sep. 22-25, 1980, BNL-NCS-51363, p. 249 (1981).
[26] D.W. Muir, *ZOTT99, Data Evaluation Using Partitioned Least-Squares*, Code package IAEA1371/01, NEA Computer Program Service (1999).
[27] T. Kawano and K. Shibata, *Covariance Evaluation System*, Japan Atomic Energy Research Institute, JAERI-Data/Code 97-037 (September 1997).
[28] M. Herman, J. Kor. Phys. Soc. **59**, 1034 (2011).
[29] P. Obložinský, Y.-S. Cho, C.M. Mattoon and S.F. Mughabghab, *Formalism for neutron cross section covariances in the resonance region using kernel approximation*, Brookhaven National Laboratory, BNL-91287-2010 (April 2010).
[30] R.C. Little *et al.*, Nuclear Data Sheets **109**, 2828 (2008).
[31] S.F. Mughabghab, *Atlas of Neutron Resonances, Resonance Parameters and Thermal Cross Sections, Z = 1-100*, 5th Edition, Elsevier, Amsterdam (2006).
[32] A.J. Koning, *New working methods for nuclear data evaluation: how to make a nuclear data library?*, Proceedings of International Conference on Nuclear Data for Science and Technology, ND2007, DOI: 10.1051/ndata:07683 (2007).
[33] D. Rochman *et al.*, J. Kor. Phys. Soc. **59**, 1236 (2011).

[34] A.J. Koning and D. Rochman, `http://www.talys.eu/tendl-2010` (2010).
[35] B.T. Rearden *et al.*, Nucl. Technol. **174**, 236 (2011).
[36] E. Dupont, A.J. Koning and N. Otuka, J. Kor. Phys. Soc. **59**, 1333 (2011).
[37] T. Ikegami, *ZPPR-9 Experiment: A 650 MWe-class Sodium-cooled MOX-fueled FBR Core Mock-up Critical Experiment with Clean Core of Two Homogeneous Zones*, International Handbook of Evaluated Reactor Physics Benchmark Experiments (IRPhE), ZPPR-LMFR-EXP-002, NEA/NSC/DOC(2006)1, OECD/NEA, 2011.
[38] R.M. Lell, J.A. Morman, R.W. Schaefer and R.D. McKnight, *ZPR-6 Assembly 7 Experiments: A Fast Reactor Core with Mixed (Pu,U)-Oxide Fuel and Sodium with a Thick Depleted Uranium Reflector*, International Handbook of Evaluated Reactor Physics Benchmark Experiments (IRPhE), ZPR-LMFR-EXP-001, NEA/NSC/DOC(2006)1, OECD/NEA, 2011.
[39] R.W. Schaefer, K.A. Bunde and P.J. Collins, *The Uranium/Iron Benchmark Assembly: A 235U(93%)/Iron Cylinder Reflected by Stainless Steel*, International Handbook of Evaluated Criticality Safety Benchmark Experiment (ICSBEP), Volume II, NEA/NSC/DOC(95)03, 2011.
[40] H. Hayashi *et al.*, *Progress Report of the Design Study on a Large Scale Reactor*, Power reactor and Nuclear fuel development Corporation, PNC TN9410 92 (1992).
[41] E.A. Hoffman, W.S. Yang, R.N. Hill, Trans. Am. Nucl. Soc. **96** (2007).

5 Le retour aux sources (de neutrons) – les travaux en cours

Après le détachement à l'AEN, le retour au CEA en 2014 correspond à un retour à des activités plus techniques, essentiellement liées à la mesure et la modélisation des données.

Les activités de recherche s'inscrivent dans le cadre de la Collaboration n_TOF [Gunsing 16]. Depuis 2014, la disponibilité d'une deuxième ligne de faisceau [Weiss 15] [Sabate 17] a doublé les capacités de l'installation n_TOF du CERN, en particulier pour la mesure de noyaux très radioactifs, de faibles sections efficaces, et d'échantillons de faibles masses. Les nouvelles données mesurées sont importantes pour les sciences appliquées et fondamentales, notamment pour l'amélioration des standards [Diakaki 16] [Amaducci 19], pour l'énergie nucléaire [Lerendegui 18] [Mastromarco 19], et pour la nucléosynthèse [Barbagallo 16] [Damone 18] [Lederer 19] [Gawlik 19].

Toutes les mesures réalisées auprès de l'installation n_TOF sont compilées dans la base EXFOR, qui est une composante essentielle du processus d'évaluation des données, afin qu'elles soient effectivement utilisées dans des domaines allant de l'énergie nucléaire à l'astrophysique. Depuis 2015, j'assure la coordination de la dissémination des données n_TOF en étroite collaboration avec l'AEN et l'AIEA [Dupont 17].

Dans le cadre des travaux de recherche les plus récents, deux thèses sont effectuées dans un contexte d'amélioration des bases de données évaluées et des codes de réaction nucléaire.

- Mesure et analyse de la section efficace de capture de l'uranium-233 (Thèse de M. Bacak, soutenue en octobre 2019)
- Étude de la fonction force radiative des actinides (Thèse de J. Moreno-Soto, soutenance prévue en 2020)

L'objectif final de ces travaux étant toujours de mieux simuler le comportement de systèmes neutroniques complexes, en particulier les réacteurs nucléaires.

5.1 Étude de la fonction force radiative des actinides

La thèse de J. Moreno-Soto est dédiée à l'étude de la « fonction force radiative » (PSF – Photon Strength Function) des actinides qui caractérise la capacité d'un noyau à absorber ou émettre des photons.

Pour les applications, il est important de connaître le flux et l'intensité des rayons gamma issus des réactions nucléaires afin de simuler l'échauffement des composants d'un blindage ou d'un réflecteur. Il existe peu de mesures différentielles et elles doivent être complétées par les résultats des modèles de réactions nucléaires.

Dans le cadre du modèle statistique, la désexcitation gamma d'un noyau dépend essentiellement de la densité de niveau et de la fonction force radiative. Cette dernière peut être étudiée en mesurant la cascade de désexcitation gamma du noyau avec un calorimètre tel que le Total Absorption Calorimeter (TAC) de la Collaboration n_TOF. Les mesures effectuées au CERN avec les cibles U-234, U-236 et U-238 fournissent ainsi des informations sur la multiplicité et l'énergie des gammas de capture qui peuvent être comparées aux simulations numériques. Ces dernières sont obtenues avec un code de transport Monte Carlo (GEANT4) utilisant des multiplicités et des spectres gamma calculés par le code de désexcitation DICEBOX.

Les simulations sont améliorées et validées grâce aux données mesurées avec le TAC. Cette approche permet de sélectionner les meilleurs modèles et un jeu de paramètres unique permettant de reproduire de manière cohérente les données des trois isotopes de

l'uranium. L'amélioration des codes de réaction nucléaire et des évaluations qui s'en suivra permettra de mettre à jour et de compléter les bibliothèques de données.

Les spectres des gammas de capture mesurés avec le TAC sont sensibles à la partie basse énergie (E_γ < S_n~5 MeV) de la PSF des modes dipolaires E1 et M1. La figure suivante représente différents modèles de PSF pour le mode dipolaire électrique E1 avec quelques mesures de réactions photonucléaires disponibles au-delà de 5 MeV.

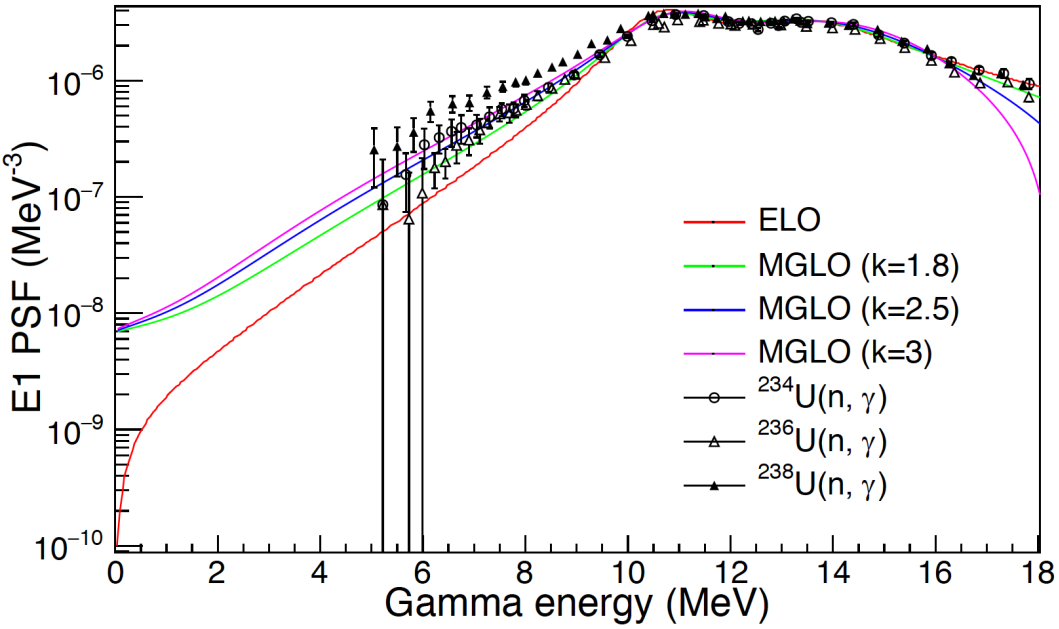

Modélisation de la fonction force radiative dipolaire électrique (E1) des isotopes de l'uranium

Les spectres mesurés avec le TAC permettent d'affiner la paramétrisation du mode dipolaire magnétique M1 qui est dominant à basse énergie pour E_γ < S_n~5 MeV (figure suivante).

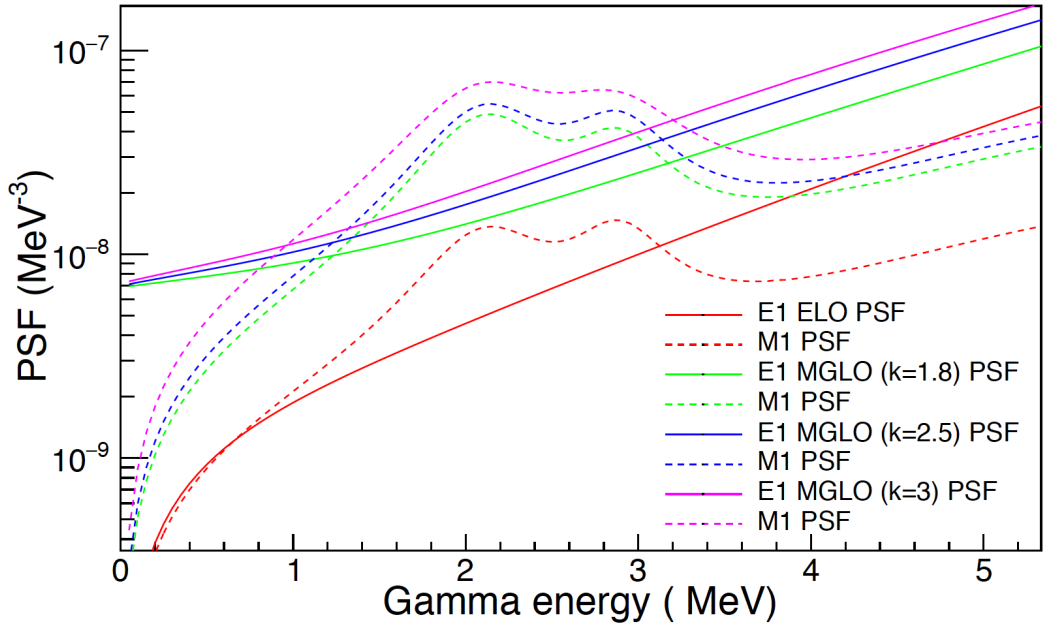

Modélisation des fonctions force radiative dipolaires E1 et M1 des isotopes de l'uranium

La publication [Moreno 19] qui suit présente les résultats expérimentaux et les calculs associés pour le système n + U-234.

[Moreno 19]

J. Moreno-Soto, et al. (E. Dupont), Study of the photon strength functions and level density in the gamma decay of the n + ^{234}U reaction, EPJ Conf. 211, 02002 (2019)

http://doi.org/10.1051/epjconf/201921102002

Study of the photon strength functions and level density in the gamma decay of the n + ^{234}U reaction

J. Moreno-Soto[1,*], E. Berthoumieux[1], E. Dupont[1], F. Gunsing[1], O. Serot[2], O. Litaize[2], M. Diakaki[2], A. Chebboubi[2], W. Dridi[3], S. Valenta[33], M. Krtička[33], O. Aberle[4], V. Alcayne[5], J. Andrzejewski[6], L. Audouin[7], V. Bécares[5], V. Babiano-Suarez[8], M. Bacak[4,9,1], M. Barbagallo[4,10], Th. Benedikt[11], S. Bennett[12], J. Billowes[12], D. Bosnar[13], A. Brown[14], M. Busso[10,15,16], M. Caamaño[17], L. Caballero-Ontanaya[8], F. Calviño[18], M. Calviani[4], D. Cano-Ott[5], A. Casanovas[18], F. Cerutti[4], E. Chiaveri[4,12], N. Colonna[10], G. Cortés[18], M. A. Cortés-Giraldo[19], L. Cosentino[20], S. Cristallo[10,15,21], L. A. Damone[10,22], P. J. Davies[12], M. Dietz[23], C. Domingo-Pardo[8], R. Dressler[24], Q. Ducasse[25], I. Durán[17], Z. Eleme[26], B. Fernández-Domínguez[17], A. Ferrari[4], P. Finocchiaro[20], V. Furman[27], K. Göbel[11], A. Gawlik[6], S. Gilardoni[4], I. F. Gonçalves[28], E. González-Romero[5], C. Guerrero[19], S. Heinitz[24], J. Heyse[29], D. G. Jenkins[14], A. Junghans[30], F. Käppeler[31], Y. Kadi[4], A. Kimura[32], I. Knapova[33], M. Kokkoris[34], Y. Kopatch[27], D. Kurtulgil[11], I. Ladarescu[8], C. Lederer-Woods[23], S. J. Lonsdale[23], D. Macina[4], A. Manna[35,36], T. Martínez[5], A. Masi[4], C. Massimi[35,36], P. Mastinu[37], M. Mastromarco[4], E. A. Maugeri[24], A. Mazzone[10,38], E. Mendoza[5], A. Mengoni[39], V. Michalopoulou[4,34], P. M. Milazzo[40], F. Mingrone[4], A. Musumarra[20,41], A. Negret[42], F. Ogállar[43], A. Oprea[42], N. Patronis[26], A. Pavlik[44], J. Perkowski[6], L. Persanti[10,15,21], C. Petrone[42], E. Pirovano[25], I. Porras[43], J. Praena[43], J. M. Quesada[19], D. Ramos-Doval[7], T. Rauscher[45,46], R. Reifarth[11], D. Rochman[24], M. Sabaté-Gilarte[19,4], A. Saxena[47], P. Schillebeeckx[29], D. Schumann[24], A. Sekhar[12], S. Simone[20], A. G. Smith[12], N. V. Sosnin[12], P. Sprung[24], A. Stamatopoulos[34], G. Tagliente[10], J. L. Tain[8], A. Tarifeño-Saldivia[18], L. Tassan-Got[4,34,7], A. Tsinganis[4], J. Ulrich[24], S. Urlass[30,4], G. Vannini[35,36], V. Variale[10], P. Vaz[28], A. Ventura[35], D. Vescovi[10,15], V. Vlachoudis[4], R. Vlastou[34], A. Wallner[48], P. J. Woods[23], T. Wright[12], P. Žugec[13], and the n_TOF Collaboration

[1]CEA Irfu, Université Paris-Saclay, F-91191 Gif-sur-Yvette, France
[2]CEA, DEN, DER, SPRC, Cadarache, F-13108 Saint-Paul-lez-Durance, France
[3]Laboratory on Energy and Matter for Nuclear Sciences Development (LR16CNSTN02), Technopark Sidi Thabet, 2020 Ariana, Tunisia
[4]European Organization for Nuclear Research (CERN), Switzerland
[5]Centro de Investigaciones Energéticas Medioambientales y Tecnológicas (CIEMAT), Spain
[6]University of Lodz, Poland
[7]Institut de Physique Nucléaire, CNRS-IN2P3, Univ. Paris-Sud, Université Paris-Saclay, F-91406 Orsay Cedex, France
[8]Instituto de Física Corpuscular, CSIC - Universidad de Valencia, Spain
[9]Technische Universität Wien, Austria
[10]Istituto Nazionale di Fisica Nucleare, Sezione di Bari, Italy
[11]Goethe University Frankfurt, Germany
[12]University of Manchester, United Kingdom
[13]Department of Physics, Faculty of Science, University of Zagreb, Zagreb, Croatia

[*]e-mail: javier.moreno-soto@cea.fr

[14]University of York, United Kingdom
[15]Istituto Nazionale di Fisica Nucleare, Sezione di Perugia, Italy
[16]Dipartimento di Fisica e Geologia, Università di Perugia, Italy
[17]University of Santiago de Compostela, Spain
[18]Universitat Politècnica de Catalunya, Spain
[19]Universidad de Sevilla, Spain
[20]INFN Laboratori Nazionali del Sud, Catania, Italy
[21]Istituto Nazionale di Astrofisica - Osservatorio Astronomico di Teramo, Italy
[22]Dipartimento di Fisica, Università degli Studi di Bari, Italy
[23]School of Physics and Astronomy, University of Edinburgh, United Kingdom
[24]Paul Scherrer Institut (PSI), Villingen, Switzerland
[25]Physikalisch-Technische Bundesanstalt (PTB), Bundesallee 100, 38116 Braunschweig, Germany
[26]University of Ioannina, Greece
[27]Joint Institute for Nuclear Research (JINR), Dubna, Russia
[28]Instituto Superior Técnico, Lisbon, Portugal
[29]European Commission, Joint Research Centre, Geel, Retieseweg 111, B-2440 Geel, Belgium
[30]Helmholtz-Zentrum Dresden-Rossendorf, Germany
[31]Karlsruhe Institute of Technology, Campus North, IKP, 76021 Karlsruhe, Germany
[32]Japan Atomic Energy Agency (JAEA), Tokai-mura, Japan
[33]Charles University, Prague, Czech Republic
[34]National Technical University of Athens, Greece
[35]Istituto Nazionale di Fisica Nucleare, Sezione di Bologna, Italy
[36]Dipartimento di Fisica e Astronomia, Università di Bologna, Italy
[37]Istituto Nazionale di Fisica Nucleare, Sezione di Legnaro, Italy
[38]Consiglio Nazionale delle Ricerche, Bari, Italy
[39]Agenzia nazionale per le nuove tecnologie (ENEA), Bologna, Italy
[40]Istituto Nazionale di Fisica Nucleare, Sezione di Trieste, Italy
[41]Dipartimento di Fisica e Astronomia, Università di Catania, Italy
[42]Horia Hulubei National Institute of Physics and Nuclear Engineering, Romania
[43]University of Granada, Spain
[44]University of Vienna, Faculty of Physics, Vienna, Austria
[45]Department of Physics, University of Basel, Switzerland
[46]Centre for Astrophysics Research, University of Hertfordshire, United Kingdom
[47]Bhabha Atomic Research Centre (BARC), India
[48]Australian National University, Canberra, Australia

Abstract. The accurate calculations of neutron-induced reaction cross sections are relevant for many nuclear applications. The photon strength functions and nuclear level densities are essential inputs for such calculations. These quantities for ^{235}U are studied using the measurement of the gamma de-excitation cascades in radiative capture on ^{234}U with the Total Absorption Calorimeter at n_TOF at CERN. This segmented 4π gamma calorimeter is designed to detect gamma rays emitted from the nucleus with high efficiency. This experiment provides information on gamma multiplicity and gamma spectra that can be compared with numerical simulations. The code DICEBOXC is used to simulate the gamma cascades while GEANT4 is used for the simulation of the interaction of these gammas with the TAC materials. Available models and their parameters are being tested using the present data. Some preliminary results of this ongoing study are presented and discussed.

1 Introduction

The aim of this work is to describe the γ-decay of excited nucleus following neutron capture. At low excitation energy, the number of levels per unit energy is rather small and levels can be experimentally resolved. However, as the excitation energy increases the level density is also increasing, so the statistical model is needed to describe the levels and transitions between them – the used quantities are nuclear level density (LD) and photon strength functions (PSFs). Their improved experimental and theoretical description is important for modeling of radiative capture reactions in nuclear astrophysics and nuclear technologies since the neutron capture cross sections above the resolved resonance region are usually calculated using the statistical model of Hauser-Feshbach [1] for which PSFs and LDs are essential inputs.

In this work, the Total Absorption Calorimeter (TAC) at n_TOF facility (CERN) [2–4] was used to measure ^{234}U(n,γ) reaction [5]. The TAC is a 4π detector segmented in 40 BaF_2 crystals with a very high efficiency (almost 100%) to detect the γ rays from the capture cascades. In Fig. 1 (left) one hemisphere of the TAC is shown. The ^{234}U sample is placed in the center and emits γ rays, which are detected by the BaF_2 detectors. Thanks to the segmentation of the detector it is possible to discriminate against the background by putting conditions on the multiplicity and the total deposited energy of events registered by the TAC.

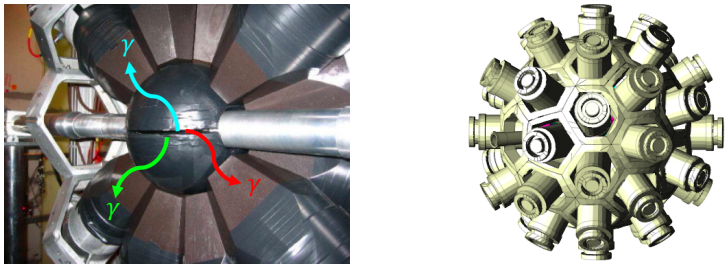

Figure 1. One hemisphere of the TAC consisting of the BaF_2 detectors, the neutron beam tube and the neutron absorber. A cascade event of three γ rays is depicted. If all γ rays are detected the crystal multiplicity is $m_{cr} = 3$ (left). The geometry of the full TAC as implemented in GEANT4 (right).

2 Experimental data

In a radiative capture reaction the compound nucleus decays through a cascade of γ rays. The measured cascade events are reconstructed by taking γ rays detected by the TAC in the BaF_2 detectors in a time coincidence window of 20 ns. A software threshold of 75 keV was set for all BaF_2 detectors to suppress the low energy background. The observables used for the analysis are:

- The neutron energy, E_n, calculated from the measured time of flight.
- The crystal multiplicity, m_{cr}, given by the number of hit crystals in each detected cascade event.
- The total deposited energy or sum energy E_{sum} in the detectors for each cascade event.
- The multi-step cascade spectra for each crystal multiplicity m_{cr}, which are the γ-ray energy spectra for fully detected cascades.

The ^{234}U(n,γ) time-of-flight spectrum is shown in the left panel of Fig. 2. Besides the uranium resonances, a structure due to capture reactions in the Ti canning is observed above a few keV [6].

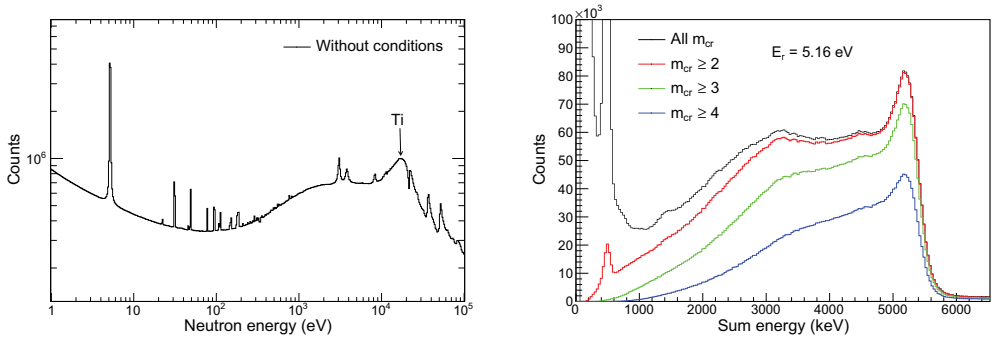

Figure 2. Time-of-flight spectrum converted to neutron energy (left). Total energy deposited for different sets of crystal multiplicities for ^{234}U(n,γ) in the resonance at 5.16 eV (right).

Fig. 2 (right) shows the sum-energy spectra in the resonance at 5.16 eV, corrected for background, for different multiplicity criteria [7]. All spectra clearly show the sum-peak at 5.3 MeV corresponding to the Q value of the reaction. There are differences between the spectra depending on the considered multiplicities. At low sum-energies (below 1 MeV) the spectrum for all m_{cr} is dominated by the remaining background. However, in the spectra for $m_{cr} \geq 2$ this background is completely absent. For the present study, only cascades with $m_{cr} \geq 2$ are considered to ensure that the background is correctly subtracted, furthermore the multistep cascade spectra are constructed using only the events with sum-energy in the interval $4.8 < E_{sum}$ (MeV) < 6.0.

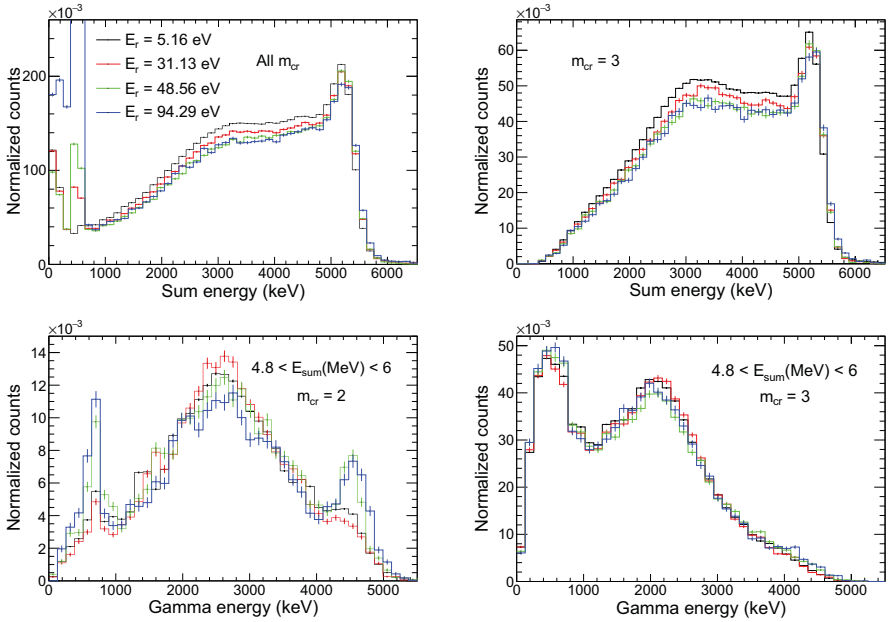

Figure 3. Sum-energy spectra of different resonances for all m_{cr} and $m_{cr} = 3$ (top). Multi-step γ-ray energy spectra of different resonances for $m_{cr} = 2, 3$ (bottom). The statistical uncertainties are small.

As can be seen in Fig. 3 (top), the sum-energy spectra for all m_{cr} of four s-wave resonances show significant differences at low energy only. These differences are due to the fact that the subtraction of the background is approximative – the remaining background induced by the scattered neutrons is most apparent in the resonance at $E_r = 94.29$ eV (blue) due to the

larger scattering width. However, these differences do not appear for $m_{cr} \geq 3$ because of the low multiplicity nature of the background. More importantly, the background subtraction gets more accurate with increasing sum-energy, hence all sum-energy spectra have similar behavior for $E_{sum} > 1$ MeV.

The multi-step γ-ray energy spectra, see Fig. 3 (bottom), show similar responses for the different resonances for $m_{cr} \geq 3$. The spectra for $m_{cr} = 2$ show significant differences depending on the considered resonance. These differences can be attributed to the Porter-Thomas fluctuations of primary transition intensities among the resonances, as expected the effects are mostly noticeable at the edges of the $m_{cr} = 2$ multi-step γ-ray energy spectra.

The normalization of all spectra was done by dividing the spectra by the number of counts in the sum-energy spectrum of $m_{cr} \geq 2$ between $E_{sum} = 4.8$ MeV and 6 MeV. The same normalization was applied to the simulations.

3 Simulations

The results presented in this work are based on the comparison of experimental data with statistical model simulations of γ decay. The in-house developed Monte Carlo code DICEBOXC, based on the same algorithm used by F. Bečvář [8] in his code DICEBOX, was used to simulate the gamma cascades while GEANT4 was used for the simulation of the interaction of these gammas with the complete TAC experimental assembly [2].

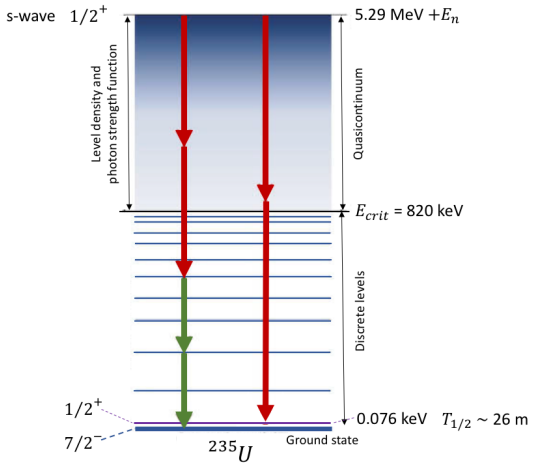

Figure 4. Schema of Monte Carlo cascades generation with DICEBOXC code. Red arrows depict the transitions generated in terms of LD and PSFs, green arows are the transitions among discrete levels taken from spectroscopic data.

DICEBOXC simulates sets of levels and their partial radiation widths known as nuclear realizations [8]. To describe the decay scheme, below a critical energy E_{crit} all the level energies, spins, parities and branching intensities of depopulating transitions are taken from existing experimental data. Above E_{crit}, the level scheme is generated by the code – the levels are obtained by a random discretization of an a priori known LD formula. Further, the PSFs are used to generate probabilities of transitions of type X (electric or magnetic) and multipolarity L. Fig. 4 shows a diagram of the operation of DICEBOXC.

The partial radiation width of an electromagnetic transition from level i to level f, $\Gamma_{i\gamma f}$, is selected from a Porter-Thomas distribution with the mean value $\left\langle \Gamma^{XL}_{i\gamma f} \right\rangle$ defined as

$$\left\langle \Gamma^{XL}_{i\gamma f} \right\rangle = \frac{f^{XL}(E_\gamma) \cdot E_\gamma^{2L+1}}{\rho(E_i, J_i, \pi_i)} \tag{1}$$

where ρ is the LD and $f^{XL}(E_\gamma)$ is the PSF. The γ-ray transition probabilities are corrected for internal conversion using tables from Ref. [9]. The levels and transitions below E_{crit} are taken from ENSDF database [10]. To ensure satisfactory statistics concerning the modelled quantities, 20 nuclear realizations with 10^5 γ-cascades per realization were simulated for each combination of LD and PSFs models.

To simulate the transport and detection of γ-rays, the toolkit GEANT4 is used [11]. The geometry and efficiency of TAC have been accurately modeled following CAD drawings of the engineering design and direct measurements [2, 12]. The modeled geometry is shown in the right panel of Fig. 1. Finally, an amplitude resolution of about 13-17%, depending on the detector, and a threshold of 75 keV for all crystals is assumed.

3.1 Level density models

The LD for given spin and parity is calculated as the product of three factors: the parity distribution $P(E,\pi)$, the spin distribution $R(E,J)$ and the LD $\rho(E)$. In this work, one assumes that both parities are equally probable $P(E,\pi) = 1/2$ at all E, while $R(E,J)$ is

$$R(E,J) = \exp\left(-\frac{J^2}{2\sigma_c^2}\right) - \exp\left(-\frac{(J+1)^2}{2\sigma_c^2}\right) \approx \frac{2J+1}{2\sigma_c^2}\exp\left[-\frac{\left(J+\frac{1}{2}\right)^2}{2\sigma_c^2}\right], \tag{2}$$

where σ_c is the spin cut-off factor. Different forms of spin cut-off factor could be used.

The DICEBOXC code includes various models for the LD $\rho(E)$. The Constant Temperature (CT) [13] model assumes that the number of levels varies according to the constant temperature law and LD is given by

$$\rho(E) = \frac{1}{T}\exp\left(\frac{E-E_0}{T}\right), \tag{3}$$

with parameters E_0 and a nuclear temperature T, which are usually fitted to experimental discrete levels, taken from Ref. [14]. In this work the spin cut-off parameter, which is constant for a given nucleus [15], was used.

The Back-shifted Fermi Gas (BSFG) [16] model assumes the nucleus as a gas of fermions creating pairs and single particle levels are equally spaced and non-degenerated with a LD given by

$$\rho(E) = \frac{\exp\left(2\sqrt{a(E-E_1)}\right)}{12\sqrt{2}\sigma_c a^{1/4}(E-E_1)^{5/4}}, \tag{4}$$

where E_1 is the energy backshift and a is the LD parameter. The energy-dependent spin cut-off factor for the BSFG model was taken from Ref. [15]. The parameters for BSFG model were taken from Ref. [14]. Variations of the BSFG model have been developed, as for example in ref. [17], which incorporates the thermodynamic temperature t. In this case, the spin cut-off is related to a fraction of the moment of inertia of the nucleus that is usually taken between 0.5 and 1. In addition, a BSFG model with energy-dependent LD parameter a and spin cut-off which accounts for the damping of the shell effects was introduced in RIPL-3 [18]. Finally, we used microscopic LD in the form of numerical interpolation tables calculated with the Hartree-Fock-Bogoliubov (HFB) method [19, 20].

3.2 Photon strength function

The statistical decay of compound nuclei from excitation energies above neutron separation energy is dominated by the $E1$ transitions due to the presence of the giant dipole electric

resonance (GDER). The shape of the $E1$ PSF for deformed nucleus is usually described by a sum of two standard Lorentzians [18, 21], as a consequence of vibration modes along and perpendicular to the symmetry axis. This description is known as Standard Lorentzian model (SLO):

$$f^{E1}_{SLO}(E_\gamma) = \frac{1}{3(\pi\hbar c)^2} \sum_{i=1}^{2} \frac{\sigma_{G_i} E_\gamma \Gamma^2_{G_i}}{\left(E^2_\gamma - E^2_{G_i}\right)^2 + E^2_\gamma \Gamma^2_{G_i}}, \tag{5}$$

where the parameters E_{G_i}, Γ_{G_i} and σ_{G_i} are the energy, width and cross section of the GDER.

Different variations were proposed to better describe the energy region below neutron separation energy. The model by Kadmenskii, Markushev and Furman (KMF) [22] aims only at this energy region while generalised Lorentzian models by Kopecky, Uhl and Chrien (GLO, ELO, EGLO) [23] and other models and calculations attempt to describe the $E1$ PSF in the whole energy region.

The KMF, GLO and ELO models use the damping width $\Gamma_T(E_\gamma, T_f)$ which depends on E_γ and the nuclear temperature T_f in form

$$\Gamma_T(E_\gamma, T_f) = \frac{\Gamma_G}{E^2_G}(E^2_\gamma + 4\pi^2 T^2_f). \tag{6}$$

Phenomenological modifications of this damping width in which is introduced a k parameter were proposed in the EGLO [23] and the MGLO [24] models. There are other models for $E1$ PSF, we refer the reader to the overview in RIPL-3 [18].

For the decay of levels below the neutron separation energy, $M1$ transitions play an important role. In this work the $M1$ PSF consists of the spin-flip (SF) resonance, which dominates the $M1$ PSF at relatively high energy typically around 7 MeV, and the scissor mode (SC), a concentration of $M1$ strength around 2-3 MeV in deformed nuclei. The SLO model was adopted to describe the $M1$ PSF. For further details see review [25] and references therein.

The electric quadrupole ($E2$) transitions, although playing a minor role with respect to dipole transitions, are also taken into account. The SLO model with a single Lorentzian was used to describe the $E2$ PSF as recommended in [18].

4 Comparison of simulations and measurements

Various combinations of LD and PSF models were checked and compared with the experimental data introduced in Sec. 2. The parameters were taken from RIPL-3 database [18] in which only one SLO term for the $M1$ PSF is recommended, or from original works, (i) the analysis of d- and ^{3}He-induced reactions on actinide targets performed at the Oslo Cyclotron Laboratory (OCL) [26] and (ii) the measurement of multi-step γ-ray energy spectra from resonant neutron capture on uranium samples with DANCE calorimeter [27]. In both a sum of SLO terms was adopted to describe the M1 PSF – one for the SF and two for the SC. The $E2$ transitions were included in the simulations by taking the parameters from [28]. The parameters use for the PSF in the different simulations are collected in Table. 1.

From the $E1$ PSF models introduced in Sec. 3.2 the SLO and KMF models do not reproduce the experimental data in combination with any LD model independently on the chosen parametrisation of the $M1$ PSF. Conversely, the ELO, GLO, EGLO and MGLO $E1$ PSF models, paired with a suitable LD model, allow, by tuning the parameters of the $M1$ PSF and the k parameter, a satisfactory description of the experimental data.

In Fig. 5 we compare experimental data with simulations using the PSFs parameters taken from (i) the RIPL-3 database [18] with GLO for $E1$ and SLO for $M1$ PSF, (ii) the DANCE

analysis [27] and (iii) the analysis of d- and ^{3}He-induced reactions at OCL [26]. The standard deviation due to different nuclear realizations is only calculated in the simulation for RIPL-3, for the other simulations the standard deviation shows similar behaviour and is not displayed for a better visualization. The statistical uncertainties are much smaller than the standard deviation. Overall, the introduction of the SC is mandatory for the improvement of the simulation and the increase of the SC strength in the DANCE analysis with respect to OCL improves the description of the experimental data. It may be possible that in order to match experimental data the SC strength has to be further increased and used in conjunction with steeper $E1$ PSF of generalised Lorentzian type.

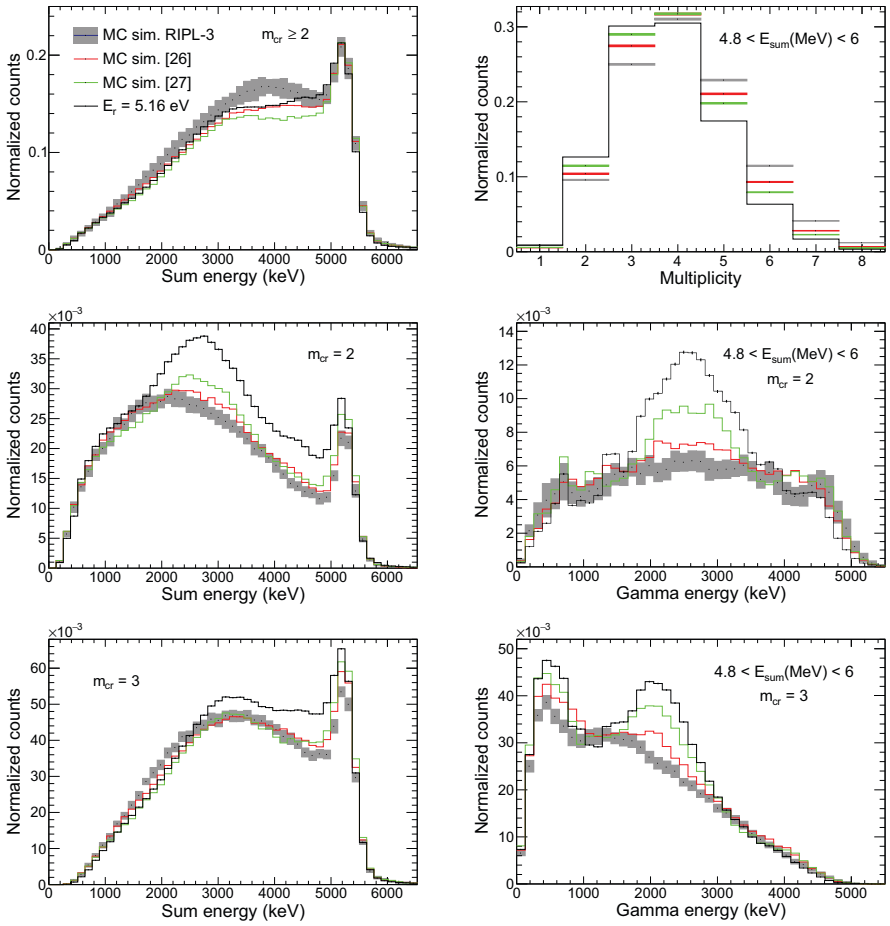

Figure 5. Comparison of experimental data to simulations using the LD and PSF models as recommended in RIPL-3 database [18] (grey filled), and as published in Refs. [26] (red line) and [27] (green line). The left column shows the total deposited energy spectra while on the right the multiplicity distribution and multi-step γ-ray energy spectra are shown. The resonance energy as well as the multiplicity and sum-energy conditions are specified in the figures.

5 Conclusion

The Total Absorption Calorimeter at the n_TOF facility (CERN) was used to measure the γ-ray cascades following the neutron capture in ^{234}U. Simulations of γ decay performed with DICEBOXC for various LD and PSFs combinations were compared with the experimental data. The inadequacy of the SLO and KMF models of $E1$ PSF as well as the necessity of scissors mode contribution to $M1$ PSF was shown. The simulations with model combinations proposed in OCL and DANCE analyses do not reproduce our data. This analysis will continue

with a detailed parameter search for analytical models and the use of tabulated PSFs from QRPA calculations [29], as well as the extension to other actinides.

Table 1. Parameters from RIPL-3 [18], OCL [26] and DANCE [27] for the PSFs.

Transition	E_1 (MeV)	Γ_1 (MeV)	σ_1 (mb)	E_2 (MeV)	Γ_2 (MeV)	σ_2 (mb)	E_3 (MeV)	Γ_3 (MeV)	σ_3 (mb)
E1 [18]	11.11	1.12	243.3	13.41	4.98	426	–	–	–
M1 [18]	–	–	–	–	–	–	6.61	4.00	2.35
E2 [28]	10.21	1.18	1.7	–	–	–	–	–	–
E1 [26]	11.40	4.20	572	14.40	4.20	1040	7.30	2.0	15.0
M1 [26]	2.15	0.80	0.45	2.90	0.60	0.40	6.61	4.00	7.00
E2 [28]	10.21	1.18	1.7	–	–	–	–	–	–
E1 [27]	11.28	2.48	325	13.73	4.25	384			
M1 [27]	2.15	0.80	0.60	2.90	0.60	0.53	6.61	4.00	1.50
E2 [28]	10.21	1.18	1.7	–	–	–	–	–	–

References

[1] W. Hauser, H. Feshbach, Phys. Rev. **87**, 366 (1952)
[2] C. Guerrero et al. (n_TOF), Nucl. Instrum. Meth. A **608**, 424 (2009)
[3] E. Chiaveri et al. (n_TOF), Nucl. Data Sheets **119**, 1 (2014)
[4] C. Guerrero et al. (n_TOF), Eur. Phys. J. A **49**, 27 (2013)
[5] W. Dridi, *PhD thesis* (Université d'Evry Val d'Essonne, 2006)
[6] C. Lampoudis et al. (n_TOF), in *Proceedings of the 2007 International Conference on Nuclear Data for Science and Technology* (2008), Vol. 1, pp. 595–598
[7] W. Dridi et al. (n_TOF), in *Conference Proceedings of the American Nuclear Society's Topical Meeting on Reactor Physics* (2006), Vol. C032, pp. 1–10
[8] F. Bečvář, Nucl. Instrum. Meth. A **417**, 434 (1998)
[9] R.S. Hager, E.C. Seltzer, Nucl. Data **A4**, 1 (1968)
[10] E. Browne, J. Tuli, Nucl. Data Sheets **122**, 205 (2014)
[11] S. Agostinelli et al. (GEANT4), Nucl. Instrum. Meth. A **506**, 250 (2003)
[12] C. Guerrero et al. (n_TOF), Nucl. Instrum. Meth. A **671**, 108 (2012)
[13] A. Gilbert, A.G.W. Cameron, Can. J. Phys. **43**, 1446 (1965)
[14] T. von Egidy, D. Bucurescu, Phys. Rev. C **72**, 044311 (2005)
[15] T. von Egidy, H.H. Schmidt, A.N. Behkami, Nucl. Phys. A **481**, 189 (1988)
[16] H.A. Bethe, Phys. Rev. **50**, 332 (1936)
[17] W. Dilg, W. Schantl, H. Vonach, M. Uhl, Nucl. Phys. A **217**, 269 (1973)
[18] R. Capote et al., Nucl. Data Sheets **110**, 3107 (2009)
[19] S. Goriely, S. Hilaire, A.J. Koning, Phys. Rev. C **78**, 064307 (2008)
[20] A.J. Koning, S. Hilaire, S. Goriely, Nucl. Phys. A **810**, 13 (2008)
[21] G.A. Bartholomew, Annual Review of Nuclear Science **11**, 259 (1961)
[22] S.G. Kadmenskii, V.P. Markushev, V.I. Furman, Sov. J. Nucl. Phys. **37**, 165 (1983)
[23] J. Kopecky, M. Uhl, R.E. Chrien, Phys. Rev. C **47**, 312 (1993)
[24] J. Kroll et al., Phys. Rev. C **88**, 034317 (2013)
[25] K. Heyde, P. von Neumann-Cosel, A. Richter, Rev. Mod. Phys. **82**, 2365 (2010)
[26] M. Guttormsen et al., Phys. Rev. C **89**, 014302 (2014)
[27] J.L. Ullmann et al., Phys. Rev. C **96**, 024627 (2017)
[28] *Handbook for Calculations of Nuclear Reaction Data Reference Input Parameter Library*, IAEA-TECDOC-1034 (Vienna, 1998)
[29] S. Goriely et al., Phys. Rev. C **98**, 014327 (2018)

5.2 Mesure et analyse de la section efficace de capture de l'uranium-233

La thèse de M. Bacak, soutenue en octobre 2019, concerne la mesure et l'analyse des sections efficaces de capture et de fission de l'uranium-233 auprès de l'installation n_TOF du CERN [Bacak 17] [Bacak 19] [Bacak 20a].

L'uranium-233 est l'isotope fissile principal du cycle Th/U. Une des particularités de ce noyau est d'être radioactif alpha ($T_{1/2}$ ~159 ky) et surtout d'avoir une section efficace de capture inférieure d'un ordre de grandeur à sa section efficace de fission. Cette caractéristique rend la mesure de la section de capture très difficile et seulement deux mesures ont été réalisées par le passé.

Pour réaliser cette nouvelle mesure, le calorimètre gamma (TAC) de la Collaboration n_TOF a été équipé d'une "cible active" d'uranium-233 sous la forme d'une chambre à fission multi-plateaux [Bacak 20b]. Cette dernière a été conçue pour être rapide (afin d'identifier les fragments de fission au milieu du bruit de fond alpha et limiter les empilements) et compacte (pour servir de cible active au centre du TAC). Le signal de la chambre à fission est utilisé pour identifier les rayons gamma prompts de fission détectés par le TAC, ce qui permet une discrimination efficace entre les réactions de capture et de fission.

La procédure d'analyse des données expérimentales permet d'estimer les sources de bruit de fond, les biais expérimentaux, et est complétée par des simulations pour calculer les corrections. Au final, on obtient le rapport alpha, c'est-à-dire le rapport des sections efficaces de capture et de fission, qui est un paramètre clé en neutronique.

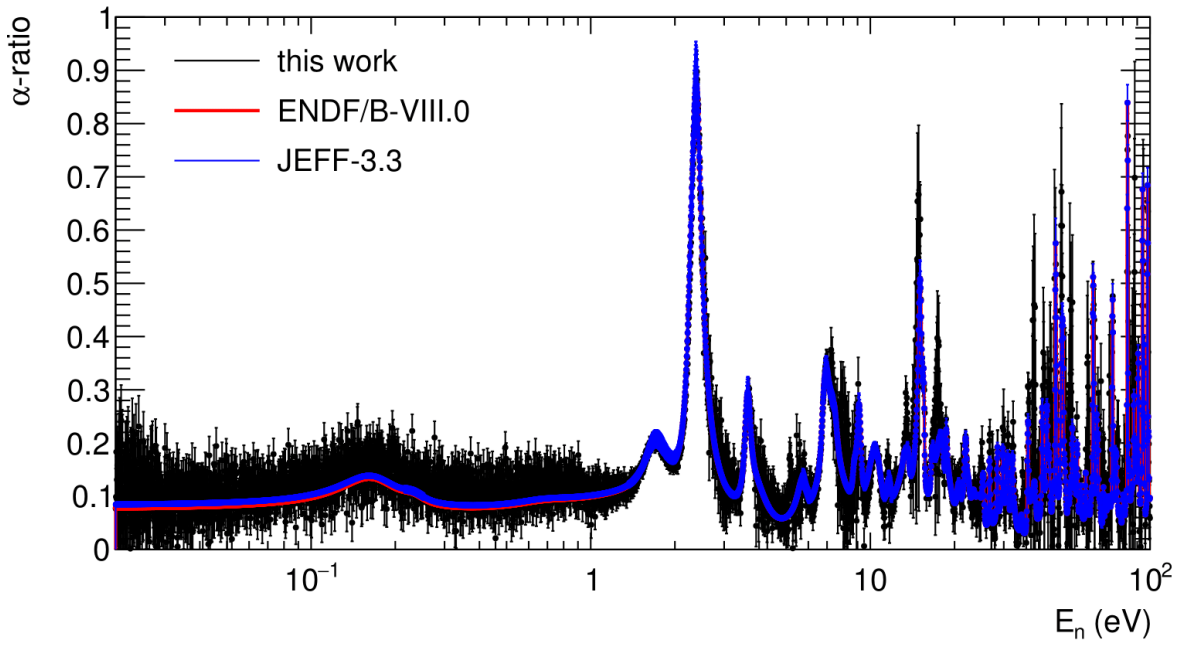

Comparaison des données mesurées et évaluées pour le rapport alpha
(rapport des sections efficaces de capture et de fission) de l'uranium-233

Les résultats de ce travail sont détaillés dans la publication [Bacak 20a] dans les pages suivantes.

[Bacak 20a]

M. Bacak, et al. (E. Dupont), Preliminary results on the ^{233}U alpha-ratio measurement at n_TOF, EPJ Conf. 239, 01043 (2020)

Preliminary results on the ^{233}U α-ratio measurement at n_TOF

M. Bacak[1,2,3,*], M. Aïche[4], G. Bélier[5], E. Berthoumieux[3], M. Diakaki[3,8], E. Dupont[3], F. Gunsing[3,1], J. Heyse[6], S. Kopecky[6], M. Krtička[7], B. Laurent[5], H. Leeb[2], L. Mathieu[4], P. Schillebeeckx[6], O. Serot[8], J. Taieb[5], S. Valenta[7], V. Vlachoudis[1], O. Aberle[1], J. Andrzejewski[9], L. Audouin[10], J. Balibrea[11], M. Barbagallo[12], F. Bečvář[7], J. Billowes[13], D. Bosnar[14], A. Brown[15], M. Caamaño[16], F. Calviño[17], M. Calviani[1], D. Cano-Ott[11], R. Cardella[1], A. Casanovas[17], F. Cerutti[1], Y. H. Chen[10], E. Chiaveri[1,13,18], N. Colonna[12], G. Cortés[17], M. A. Cortés-Giraldo[18], L. Cosentino[19], L. A. Damone[12,20], C. Domingo-Pardo[21], R. Dressler[22], I. Durán[16], B. Fernández-Domínguez[16], A. Ferrari[1], P. Ferreira[23], P. Finocchiaro[19], V. Furman[24], K. Göbel[25], A. R. García[11], A. Gawlik[9], S. Gilardoni[1], T. Glodariu†[26], I. F. Gonçalves[23], E. González-Romero[11], E. Griesmayer[2], C. Guerrero[18], H. Harada[27], S. Heinitz[22], D. G. Jenkins[15], E. Jericha[2], F. Käppeler[28], Y. Kadi[1], A. Kalamara[29], P. Kavrigin[2], A. Kimura[27], N. Kivel[22], I. Knapova[7], M. Kokkoris[29], D. Kurtulgil[25], E. Leal-Cidoncha[16], C. Lederer[30], J. Lerendegui-Marco[18], S. Lo Meo[31,32], S. J. Lonsdale[30], D. Macina[1], A. Manna[32,33], J. Marganiec[9,34], T. Martínez[11], A. Masi[1], C. Massimi[32,33], P. Mastinu[35], M. Mastromarco[12], E. A. Maugeri[22], A. Mazzone[12,36], E. Mendoza[11], A. Mengoni[31], P. M. Milazzo[37], F. Mingrone[1], A. Musumarra[19,38], A. Negret[26], R. Nolte[34], A. Oprea[26], N. Patronis[39], A. Pavlik[40], J. Perkowski[9], I. Porras[41], J. Praena[41], J. M. Quesada[18], D. Radeck[34], T. Rauscher[42,43], R. Reifarth[25], C. Rubbia[1], J. A. Ryan[13], M. Sabaté-Gilarte[1,18], A. Saxena[44], D. Schumann[22], P. Sedyshev[24], A. G. Smith[13], N. V. Sosnin[13], A. Stamatopoulos[29], G. Tagliente[12], J. L. Tain[21], A. Tarifeño-Saldivia[17], L. Tassan-Got[10], G. Vannini[32,33], V. Variale[12], P. Vaz[23], A. Ventura[32], R. Vlastou[29], A. Wallner[45], S. Warren[13], C. Weiss[2], P. J. Woods[30], T. Wright[13], P. Žugec[14,1], and the n_TOF Collaboration[1]

[1]European Organization for Nuclear Research (CERN), Switzerland
[2]Technische Universität Wien, Austria
[3]CEA Irfu, Université Paris-Saclay, F-91191 Gif-sur-Yvette, France
[4]CENBG, CNRS/IN2P3-Université de Bordeaux, Gradignan, France
[5]CEA, DAM, DIF, F-91297 Arpajon, France
[6]European Commission, Joint Research Centre, Geel, Retieseweg 111, B-2440 Geel, Belgium
[7]Charles University, Prague, Czech Republic
[8]CEA, DEN, Cadarache, France
[9]University of Lodz, Poland
[10]Institut de Physique Nucléaire, CNRS-IN2P3, Univ. Paris-Sud, Université Paris-Saclay, F-91406 Orsay Cedex, France
[11]Centro de Investigaciones Energéticas Medioambientales y Tecnológicas (CIEMAT), Spain
[12]Istituto Nazionale di Fisica Nucleare, Sezione di Bari, Italy
[13]University of Manchester, United Kingdom
[14]Department of Physics, Faculty of Science, University of Zagreb, Zagreb, Croatia
[15]University of York, United Kingdom
[16]University of Santiago de Compostela, Spain
[17]Universitat Politècnica de Catalunya, Spain
[18]Universidad de Sevilla, Spain
[19]INFN Laboratori Nazionali del Sud, Catania, Italy
[20]Dipartimento di Fisica, Università degli Studi di Bari, Italy
[21]Instituto de Física Corpuscular, CSIC - Universidad de Valencia, Spain
[22]Paul Scherrer Institut (PSI), Villingen, Switzerland
[23]Instituto Superior Técnico, Lisbon, Portugal
[24]Joint Institute for Nuclear Research (JINR), Dubna, Russia
[25]Goethe University Frankfurt, Germany
[26]Horia Hulubei National Institute of Physics and Nuclear Engineering, Romania
[27]Japan Atomic Energy Agency (JAEA), Tokai-mura, Japan
[28]Karlsruhe Institute of Technology, Campus North, IKP, 76021 Karlsruhe, Germany
[29]National Technical University of Athens, Greece
[30]School of Physics and Astronomy, University of Edinburgh, United Kingdom
[31]Agenzia nazionale per le nuove tecnologie (ENEA), Bologna, Italy
[32]Istituto Nazionale di Fisica Nucleare, Sezione di Bologna, Italy
[33]Dipartimento di Fisica e Astronomia, Università di Bologna, Italy
[34]Physikalisch-Technische Bundesanstalt (PTB), Bundesallee 100, 38116 Braunschweig, Germany

[35]Istituto Nazionale di Fisica Nucleare, Sezione di Legnaro, Italy
[36]Consiglio Nazionale delle Ricerche, Bari, Italy
[37]Istituto Nazionale di Fisica Nucleare, Sezione di Trieste, Italy
[38]Dipartimento di Fisica e Astronomia, Università di Catania, Italy
[39]University of Ioannina, Greece
[40]University of Vienna, Faculty of Physics, Vienna, Austria
[41]University of Granada, Spain
[42]Department of Physics, University of Basel, Switzerland
[43]Centre for Astrophysics Research, University of Hertfordshire, United Kingdom
[44]Bhabha Atomic Research Centre (BARC), India
[45]Australian National University, Canberra, Australia

Abstract. ^{233}U is the fissile nuclei in the Th-U fuel cycle with a particularily small neutron capture cross setion which is on average about one order of magnitude lower than its fission cross section. Hence, the measurement of the ^{233}U(n,γ) cross section relies on a method to accurately distinguish between capture and fission γ-rays. A measurement of the ^{233}U α-ratio has been performed at the n_TOF facility at CERN using a so-called fission tagging setup, coupling n_TOF 's Total Absorption Calorimeter with a novel fission chamber to tag the fission γ-rays. The experimental setup is described and essential parts of the analysis are discussed. Finally, a preliminary ^{233}U α-ratio is presented.

1 Introduction

The Th-U fuel cycle [1, 2] poses an alternative to the U-Pu fuel cycle for nuclear power, thus its relevant cross-sections have to be accurately known. The α-ratio is defined as the ratio between the capture and fission cross section of an isotope. The fission cross section of ^{233}U is well known but the available data for the ^{233}U(n,γ) cross section are scarce [3]. The reason is that the ^{233}U(n,f) cross section is on average one order of magnitude larger, as shown in Figure 1. Therefore, the measurement of the ^{233}U(n,γ) cross section relies on an efficient discrimination of the fission γ-rays from the capture events. Coupling a γ-ray detector with a fission detector allows to tag the γ-rays from fission and efficiently subtract them from the total measured spectra. A similar technique was used in several experiments [4–8].

2 Experimental Setup

2.1 The n_TOF facility

The neutron Time-Of-Flight facility n_TOF at CERN was proposed [9] and offers two beam lines for neutron cross-section measurements. The measurement of the ^{233}U α-ratio was performed in the first experimental area (EAR1) [10] of n_TOF with a flight path length of 185 m. At n_TOF neutrons are produced by spallation reactions induced by a 20 GeV/c pulsed proton beam from the CERN Proton Synchrotron on a water-cooled lead target. The fast neutrons created in the spallation process are moderated in a 4 cm layer of borated light water, eventually covering neutron energies from thermal up to few GeV.

*e-mail: michael.bacak@cern.ch

2.2 The Total Absorption Calorimeter

The γ-ray cascades emitted in the capture reaction are detected by n_TOF 's Total Absorption Calorimeter *TAC* [11]. The TAC is a segmented 4π scintillator array consisting of 40 individual BaF_2 crystals. The detectors are mounted in a honeycomb structure which holds the full spherical detector shell. The shell has a 20 cm and 50 cm inner and outer diameter respectively, covering 95 % of the total solid angle. In order to minimize the neutron sensitivity of the TAC, a combination of neutron moderator and absorber material is used to surround the sample. The so-called neutron absorber is made of polyethylene loaded with 7.56 w% natural lithium with a total density of 1.06 g/cm^3 and is shown in Figure 2.
The data acquisition system is based on digitizers and the waveforms are analyzed offline, grouped together using a coincidence window of 12 ns. Each of those TAC events is characterized by its time-of-flight

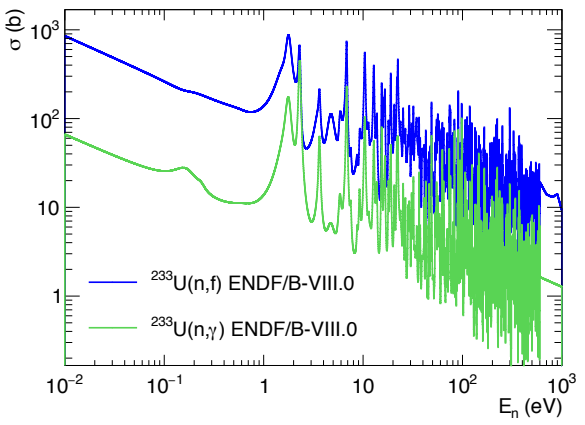

Figure 1. Comparison of fission and capture cross section from the ^{233}U evaluation of ENDF/B-VIII.0

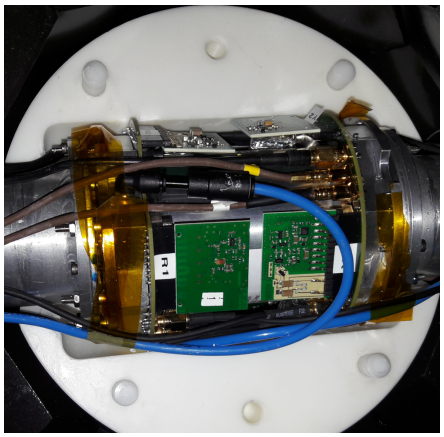

Figure 2. FICH fully connected and integrated into the absorber of the TAC.

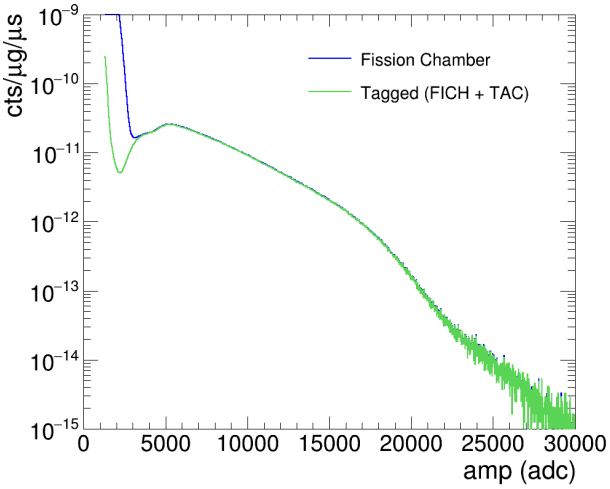

Figure 3. Comparison of the amplitude spectrum of the FICH and tagged signals.

TOF, determining the neutron energy E_n, the total deposited energy in the TAC E_{Sum}, and the number of hit crystals m_{cr}. The main advantage of the TAC is the use of those quantities to discriminate between different types of reactions, for example ambient background and γ-ray cascades from the (n,γ) process.

2.3 The compact fission chamber

In order to properly tag and remove the main source of γ-background, namely the prompt γ-ray cascades of the ^{233}U(n,f) reaction from the total measured spectra, a fission chamber (*FICH*) [12] has been developed. The detector is designed as a multi-plate ionization chamber containing two stacks of axial ionization cells. Figure 2 shows a picture of the FICH fully assembled and mounted in the neutron absorber. With a total length of 120 mm and a diameter of 90 mm the chamber hosts 14 ionization cells. Each cell has an inter-electrode gap of 3 mm which is not sufficient to stop fission fragments exiting perpendicular from the sample, but allows better timing performance. The detector is operated with high-purity CF_4 at a pressure of 1100 mbar controlled by a dedicated gas regulation system. Pre-amplifier and shaper modules [13] are directly mounted on the motherboards of each stack to reduce signal attenuation and to improve the signal to noise ratio.
Fourteen uranium oxide layers have been deposited at JRC-Geel on 10 µm thick aluminium foils by molecular plating. The base material was 99.936 % enriched in ^{233}U with the largest contaminant being 0.0496 % ^{234}U. The diameter of the mask used for the preparation of the ^{233}U samples was 40.00 ± 0.02 mm which also defines the active area of the samples. The activity of each sample has been determined by well-defined solid angle α-particle counting and amounts to an average α-activity of about 1.16 MBq per sample translating to an average areal mass density of 264.5 µg/cm^2.

3 Experimental response to ^{233}U + n events

The event reconstruction of fission tagged events was performed by setting a constant coincidence window of 14 ns between TAC and FICH events. The amplitude spectra of the events from the fission chamber and from tagged events is shown in Figure 3. The reduction of the α-particle background from the natural decay of ^{233}U is clearly visible, allowing for a cleaner α-FF separation.

3.1 FICH Efficiency

A critical part in the analysis concerns the calculation of the detection efficiency of the fission chamber ε_{FICH} which is based on the assumption that a fission event is detected independently by the TAC and the FICH. In this case, the fission chamber efficiency ε_{FICH} can be calculated solely from the experimental data. For fission events with amplitudes larger than 3000 adc channels the efficiency has a value of 0.867 ± 0.002. A more detailed description can be found in [14].

3.2 Background subtraction

In order to obtain the shape of the TAC response to ^{233}U(n,γ) events from the total measured sum energy spectra all background components have to be carefully subtracted. Dedicated measurements have been carried out to determine the contributions of the fission chamber without the ^{233}U layers (*Dummy*), the ambient background and the background induced by the natural α-activity of the radioactive isotopes in the samples. The *prompt fission γ-ray* spectrum is obtained by fission tagging and has to be corrected for the detection efficiency of the fission chamber ε_{FICH}. The sum energy spectra of the different contributions

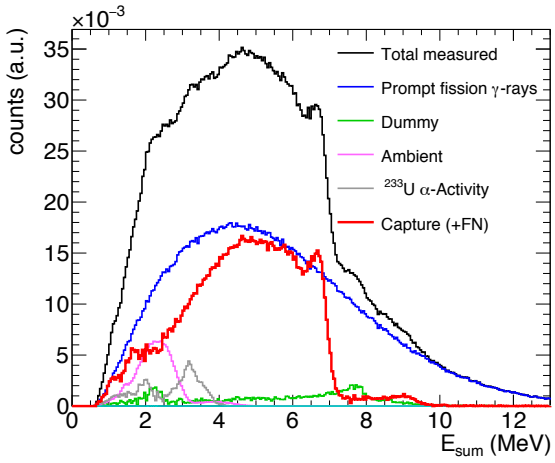

Figure 4. Components of the total measured deposited energy spectrum for a neutron energy range of $2.2\,\text{eV} < E_n < 2.4\,\text{eV}$ and $m_{cr} \geq 3$.

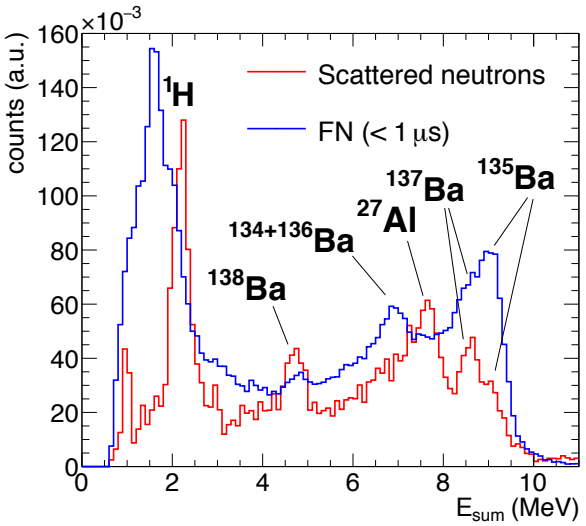

Figure 5. Comparison of the fission neutron and neutron scattering spectrum for a neutron energy range of $2.2\,\text{eV} < E_n < 2.4\,\text{eV}$. The sum energy peaks are labeled with nucleus X corresponding to the neutron separation energy of the nucleus after capture $X + n$.

are compared to the total measured spectrum in Figure 4 in the strongest capture resonance corresponding to a neutron energy range of $2.2\,\text{eV} < E_n < 2.4\,\text{eV}$ and for events with $m_{cr} \geq 3$ in order to clean the low crystal multiplicity background which would otherwise dominate the region for $E_{Sum} < 1.5\,\text{MeV}$.
After subtraction of the various background contributions the shape of the TAC response to ^{233}U(n,γ) events becomes visible. A sum peak appears at $E_{Sum} \approx 6.85\,\text{MeV}$ corresponding to the neutron separation energy of ^{234}U. The shape of the remaining background in the *Capture* component above $E_{Sum} = 7.5\,\text{MeV}$ does not match any other background component, leading to the conclusion that there is some other source of background not accounted for. The most probable explanation is related to the prompt fission neutrons (FN) being moderated and captured in the experimental setup. This shape is peculiar to the TAC as it shows the sum energy peaks at the separation energy of the main barium isotopes due to fission neutrons captured in the barium nuclei of the BaF_2 crystals within the first few microseconds after emission. Gating, for example, on the first micro second after a fission event allows to determine the shape of this FN background component. In Figure 5 the shape of the background induced by fission neutrons is compared to the background induced by neutron scattering in the range of $2.2\,\text{eV} < E_n < 2.4\,\text{eV}$, measured with a carbon sample. The two spectra show similar capture reactions characterized by the different sum energy peaks but with different intensities resulting in completely different shapes. Specifically the neutron separation energy of ^{135}Ba+n corresponding to the sum energy peak at $E_{Sum} = 9.1\,\text{MeV}$ is strongly suppressed in the scattered neutron spectra compared to the FN spectrum. Therefore, the scattered neutron spectrum cannot explain the remaining background in the Capture component in Figure 4 above $E_{Sum} = 7.5\,\text{MeV}$. However, the FN background component matches the shape of the remaining background above $E_{Sum} = 7.5\,\text{MeV}$ as shown in Figure 6, indicating that this background is related to fission neutrons. The FN component scales with the fission cross section allowing for an accurate correction and its contribution to the remaining capture response is shown in Figure 6.

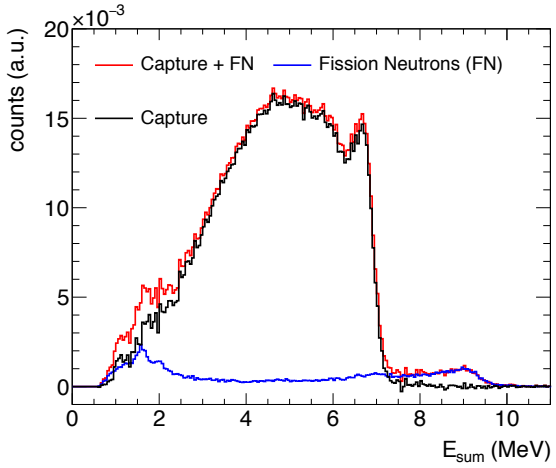

Figure 6. Subtraction of the contribution from fission neutrons in the neutron energy range of $2.2\,\text{eV} < E_n < 2.4\,\text{eV}$.

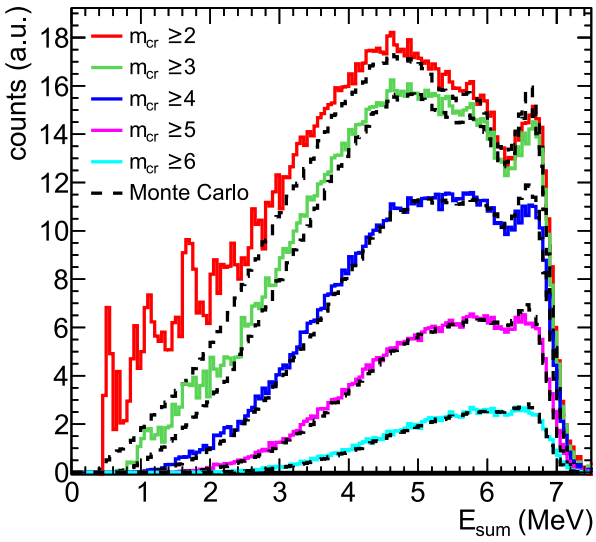

Figure 7. Comparison of the experimental and simulated response to ^{233}U(n,γ) events.

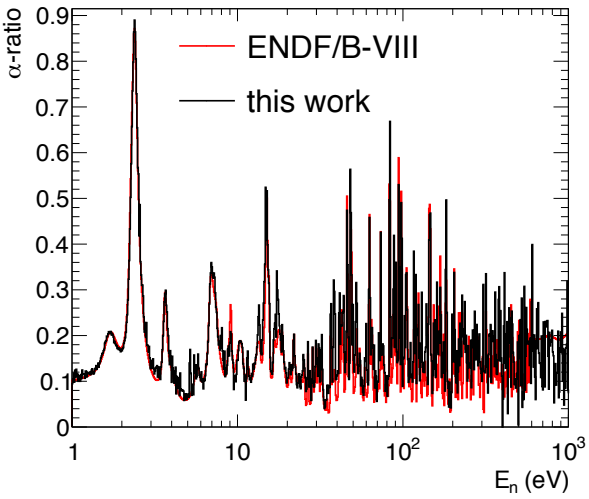

Figure 8. Preliminary ^{233}U α-ratio for 1 eV $< E_n <$ 1 keV compared to ENDF/B-VIII.0.

4 Determination of the ^{233}U α-ratio

Following the background subtraction, the efficiency of detecting the γ-ray cascades with the TAC has been calculated using the Monte Carlo simulation toolkit Geant4 [15]. The whole experimental setup, including the TAC, FICH, absorber and beam pipes has been modelled in Geant4.

The cascades emitted in the ^{233}U(n,γ) process were simulated with DICEBOX [16] and a comparison between the experimental and simulated response to ^{233}U(n,γ) events can be seen in Figure 7. The overall agreement for crystal multiplicities $m_{cr} \geq 3$ is good and allows to calculate the capture efficiency for a given analysis cut. The contribution of the isomeric states in the fission products (absent in the simulations) is important for events with $m_{cr} \geq 2$ and $E_{Sum} < 2.5$ MeV. With an estimation of the detection efficiency of 76.2 ± 2.2 % for $m_{cr} \geq 3$ and 2.5 MeV $< E_{Sum} <$ 7 MeV the ^{233}U α-ratio can be calculated from the response of the FICH and the TAC. In Figure 8 the preliminary result of the ^{233}U α-ratio measurement is compared to the ^{233}U α-ratio of the ENDF/B-VIII database. Overall, the ratios are in good agreement and local deviations are under investigation.

5 Summary

A fission tagging experiment to determine the ^{233}U α-ratio has been performed at n_TOF EAR1 yielding promising results for neutrons from thermal energies to several keV. The experimental setup and the key elements from the analysis have been described and a preliminary ^{233}U α-ratio has been presented. A detailed analysis of the extracted ^{233}U α-ratio is currently being performed and will be published in a forthcoming paper.

This work was partially supported by the French NEEDS/NACRE Project and by the European Commission within HORIZON2020 via the EURATOM Project EUFRAT. The authors would like to acknowledge more specifically JRC Geel for targets preparation and for providing full support for a first test measurement of the fission chamber at GELINA.

References

[1] V.G. Pronyaev, IAEA Report INDC (NDS) **408**, (1999)
[2] The Generation IV International Forum, http://www.gen-4.org/ (2013)
[3] L. W. Weston et al., Nuc. Sc. Eng. **34**:1, 1-12 (1968)
[4] C. Guerrero, E. Berthoumieux et al., Eur. Phys. J. A **48**, 29 (2012)
[5] J. Balibrea-Correa et al., EPJ Web of Conf. **146**, 11021 (2017)
[6] J. Balibrea-Correa, *Measurement of the neutron capture cross section of ^{235}U at the n_TOF facility*, PhD thesis, Madrid (2017)
[7] M. Jandel et al., Phys. Rev. Lett. **109**, 202506 (2012)
[8] S. Mosby et al., Phys. Rev. C **89**, 034610 (2014)
[9] C. Rubbia et al., CERN/LHC/98-02; CERN: Geneva, Switzerland (1998)
[10] C. Guerrero et al., Eur. Phys. J. A **49**, 27 (2013)
[11] C. Guerrero et al., Nucl. Instr. Meth. A **608**, 424 (2009)
[12] M. Bacak et al., EPJ Web Conf. **146**, 03027 (2017)

[13] J. Taieb et al., Nucl. Instr. Meth. A **833**, 1 (2016)
[14] M. Bacak et al., EPJ Web Conf. **211**, 03007 (2019)
[15] S. Agostinelli et al., Nucl. Instr. Meth. A **506**:250–303 (2003)
[16] F. Bečvář, Nucl. Instr. Meth. A **417**, 434 (1998)

6 Conclusions et perspectives

Cette synthèse de mes travaux de recherche a permis de présenter les différentes facettes du domaine des données nucléaires de base pour la simulation : besoin, mesure, modélisation, évaluation et validation.

- Le besoin d'amélioration des données et de leur incertitude ne va pas de soi après des décennies de recherche et il est donc souhaitable de le quantifier avant de mettre en place des programmes expérimentaux longs et couteux. Ce travail doit être fait dans une approche pluridisciplinaire en collaboration avec les utilisateurs des données. C'est par exemple ce qui est réalisé dans le cadre de la HPRL [Dupont 20] et des groupes de travail internationaux associés à l'AEN et à l'AIEA. A titre d'exemple, le travail sur les méthodes de recherche de tendance [Salvatores 14] réalisé par le sous-groupe 33 du WPEC a été présenté.
- Malgré des avancées notables dans le développement de modèles *ab initio* en physique nucléaire, la mesure reste la base des données évaluées indispensables à la majorité des applications. On peut citer les nombreuses mesures réalisées à JRC-Geel en Belgique [Sirakov 13] [Massimi 14] et plus récemment celles de la Collaboration n_TOF au CERN [Gunsing 16]. A titre d'exemple, la récente mesure du rapport alpha (capture/fission) de l'uranium-233 a été présentée [Bacak 20a].
- Les modèles de réaction nucléaires constituent l'ossature des évaluations en garantissant le respect des lois de la physique et en permettant d'interpoler (voire extrapoler) les données qui n'ont pas pu être mesurées. A titre d'exemple le cas de la modélisation des réactions photonucléaires des actinides [Dupont 07] a été présenté ainsi que l'étude de la fonction force radiative à partir des données de capture [Moreno 19].
- L'évaluation des données permet la synthèse entre les informations expérimentales et théoriques en combinant toutes les données mesurées avec les modèles de réactions nucléaires pour extraire les valeurs recommandées. Le fichier évalué doit être cohérent et complet (au sens du format ENDF) afin de couvrir l'ensemble des données caractérisant l'interaction d'un neutron avec un noyau. A titre d'exemple le cas de l'évaluation du rhodium-103 [Dupont 05a] a été présenté.
- La validation intégrale est l'étape finale permettant de vérifier que les données évaluées et leurs incertitudes répondent au besoin de l'application en termes de prédiction et de précision. Cette étape nécessite de disposer de mesures intégrales fiables et précises (des benchmarks) qui sont comparées aux résultats des simulations utilisant les données à valider. La validation peut concerner une seule réaction (cf. PROFIL [Tommasi 06]), une évaluation complète ou une bibliothèque entière (cf. JEFF-3.0 [Dupont 03] et SG33 [Salvatores 14]). Bien entendu, de nouveaux besoins d'amélioration des données peuvent être identifiés à l'issue de cette validation.

Le domaine des données nucléaires, à l'interface entre la physique nucléaire et ses applications, se caractérise par sa pluridisciplinarité et permet de travailler dans différents environnements professionnels (DEN, DSM-DRF, AEN) tout en restant focalisé sur une même thématique de recherche.

Dans la lignée des travaux antérieurs, les projets en cours et à venir permettront d'améliorer la connaissance en physique nucléaire de basse énergie pour les besoins des applications. D'une part en réalisant les mesures nécessaires auprès des principales sources de neutrons européennes et en collaborant avec les experts des autres disciplines (WPEC SG46 et SG-C/HPRL) pour définir les besoins, et d'autre part en participant à la coordination nationale (projet NACRE) et internationale (projet SANDA) des activités d'évaluation et de validation des données nucléaires. Dans le cadre de ces projets, les efforts de la DRF seront

essentiellement axés sur les activités de mesures et de modélisation des réactions nucléaires. Les programmes brièvement décrits ci-dessous pourront être réalisés auprès de différentes installations en Europe, en fonction du domaine d'énergie étudié, des caractéristiques des faisceaux, et de l'infrastructure technique disponible (DAQ, autres détecteurs…) au CERN (n_TOF), à GANIL/SPIRAL2 (NFS), et à JRC-Geel (GELINA).

Sections efficaces des actinides fissiles en anti-coïncidence avec la fission

A court terme, le programme de mesure et d'analyse des sections efficaces des actinides fissiles se poursuit. Ces mesures nécessitent une cible active permettant d'identifier les réactions de fission dans un bruit de fond radioactif important et de les distinguer des autres réactions mesurées simultanément, par exemple avec le calorimètre TAC pour la capture.

Suite au développements réalisés pour la mesure du rapport alpha de U-233 à n_TOF, il s'agit de poursuivre la collaboration avec CEA/DAM pour concevoir une nouvelle chambre à fission adaptée à la mesure des sections efficaces des actinides fissiles les plus radioactifs tels que Pu-239 et Pu-241, respectivement près de 7 fois et 11000 fois plus actifs que U-233. Ce détecteur pourra être utilisé comme cible active pour la mesure des sections efficaces (n,xn) à NFS et (n,γ) à n_TOF le cas échéant.

Différentes pistes de R&D devront être explorées auparavant pour maîtriser le taux de comptage très élevé et s'affranchir du bruit de fond radioactif : segmentation des anodes et discrimination de forme des signaux par exemple.

Développement d'un détecteur MGAS-TPC pour les mesures de temps de vol

En parallèle, un prototype MGAS-TPC de détecteur Micromegas de type TPC (Time Projection Chamber) adapté aux mesures en temps de vol sera développé. En plus de l'énergie déposée, ce détecteur permettra de mesurer les distributions angulaires des produits de la réaction (fragments de fission ou particules chargées légères telles que α, He-3, t, d, voire p).

Ces informations supplémentaires permettront d'une part, d'améliorer le rapport signal/bruit grâce à la connaissance complète de la cinématique de réaction, et d'autre part de réduire les incertitudes systématiques sur le calcul de l'intégrale de la section efficace dans 4π. Ce détecteur permettrait de mesurer les sections efficaces d'activation et de production de gaz (He, H, T) dans la gamme d'énergie de quelques centaines de keV (pour les réacteurs rapides) jusqu'à 14 MeV (pour les réacteurs à fusion), voire plus (pour les systèmes basés sur des accélérateurs, tels que IFMIF, DONES ou MYRRHA).

La connaissance des distributions angulaires permettra également d'étudier les mécanismes de réactions nucléaires en fonction du moment angulaire. Le cas de la fission dans le domaine des résonances et aux seuils de fission est particulièrement intéressant. De nouvelles mesures de sections efficaces de fission à haute résolution, incluant des informations sur l'anisotropie des fragments de fission, apporteraient un éclairage nouveau sur les structures de classe II des actinides super déformés.

La dernière génération de Micromegas 2D [Diakaki 18] dispose déjà des capacités de reconstruction de trajectoire des particules ionisantes, et peut donc servir de base pour le développement du prototype MGAS-TPC. Toutefois la R&D associée est ambitieuse, en particulier pour la partie électronique, et nécessitera certainement plusieurs années avant d'arriver à maturité.

L'identification de la trace des protons dans le détecteur MGAS-TPC est un objectif à plus long terme, ambitieux mais nécessaire pour exploiter le recul des protons lors de diffusions n-p. Cette identification rendra possible la mesure très précise des sections efficaces de fission par rapport à la réaction H(n,n), qui est un standard international connu avec une précision inférieure à 1% dans une large gamme d'énergie.

7 Annexe – Curriculum vitae

M. DUPONT Emmeric, né le 04/01/1972

Affiliation : IRFU/DPhN, CEA Paris-Saclay, Gif-sur-Yvette, France

Parcours professionnel

1995-1998 – Doctorant à l'Institut des Matériaux et Mesures de Référence à Geel en Belgique sous la direction de M. Salvatores. Titre de la thèse : Mesures à haute résolution et étude de la réaction de diffusion inélastique de neutrons sur le Fe-56 [Dupont 98].

1998-2005 – Ingénieur-chercheur à la Direction de l'Energie Nucléaire du CEA Cadarache, spécialisé dans l'évaluation, le traitement, et la validation intégrale des données nucléaires utilisées dans les codes de simulation.

2005-2009 – Ingénieur-chercheur à la Direction des Sciences de la Matière du CEA Saclay, spécialisé dans la mesure, la modélisation, et l'évaluation des données nucléaires.

2009-2014 – Administrateur scientifique de la Banque de données de l'Agence de l'OCDE pour l'Énergie Nucléaire (AEN) en charge de la coordination du développement, de l'amélioration, et de la validation intégrale des données nucléaires pour les applications.

Depuis 2014 – Ingénieur-chercheur à la Direction de la Recherche Fondamentale (ex DSM) du CEA Saclay, spécialisé dans la mesure et la modélisation des données de réaction nucléaire pour différents domaines fondamentaux et appliqués, allant des technologies nucléaires à l'astrophysique nucléaire.

Expérience d'encadrement

L'encadrement d'étudiants est un exercice limité dans le temps qui impose de bien définir le cadre de travail et des objectifs réalistes. Il est important que l'étudiant puisse identifier ses responsabilités et contributions afin de développer son autonomie et ses compétences. Dans tous les cas il est essentiel d'instaurer un dialogue avec l'encadrant et avec le reste de l'équipe afin de pouvoir guider et aider l'étudiant.

Ces principes de base ont été mis en œuvre lors de stages de longue durée permettant la réalisation de projets significatifs.

- Stage de M2 de R. Torre [Torre 05] effectué de mars à juillet 2005 et portant sur l'étude des paramètres de résonance et la modélisation des sections efficaces du samarium-148. Ce travail a été réalisé dans le cadre de la réévaluation des données nucléaires des produits de fission de la bibliothèque JEFF.
- Stage de M1 de W. Monange [Monange 06] effectué de juin à août 2006 et portant sur la simulation neutronique du réacteur à haut flux de l'Institut Laue-Langevin. Ce travail a été réalisé dans le cadre des mesures de sections efficaces réalisées auprès de ce réacteur.
- Stage de M1 de E. Benguigui [Benguigui 09] effectué de mai à août 2009 et portant sur l'étude de l'absorption de photons dans la résonance dipolaire géante des noyaux. Ce travail a été réalisé dans le cadre de la modélisation des réactions photo-nucléaires des actinides.

L'encadrement de doctorants nécessite des techniques de management similaires à celui des stagiaires, avec toutefois des critères plus élevés concernant les exigences scientifiques, l'autonomie et l'acquisition des compétences. Un objectif supplémentaire est d'aider le doctorant à valoriser son travail de thèse et à préparer la suite de sa carrière.

- Thèse de O. Bringer [Bringer 08] soutenue en octobre 2007 portant sur la mesure des sections efficaces de capture et de fission des actinides mineurs ainsi que sur leur

potentiel d'incinération. Ce travail a été réalisé dans le cadre des problématiques de gestion des déchets nucléaires.

- Thèse de M. Bacak, soutenue en octobre 2019, portant sur la mesure et l'analyse des sections efficaces de capture et de fission de l'uranium-233 auprès de la source de neutrons n_TOF (CERN). Ce travail est réalisé dans le cadre de l'amélioration des données nucléaires du cycle Th/U pour les réacteurs innovants [Bacak 20a].
- Thèse de J. Moreno-Soto, débutée en novembre 2017, portant sur l'étude de la « fonction force radiative » des actinides, c'est à dire leur capacité à absorber ou émettre des photons. Ce travail s'effectue dans le cadre de l'amélioration des modèles de réactions nucléaires [Moreno 19].

L'encadrement de post-doctorants relève plus de la relation entre pairs sur le plan scientifique mais avec des responsabilités de pilotage et de cadrage.

- Post-doctorat de I. Raskinyte en 2006 portant sur la modélisation des réactions photonucléaires [Raskinyte 06].

Expérience de coordination

La coordination des activités au sein d'une équipe, d'un groupe de travail ou d'une collaboration est une autre facette du métier de chercheur. Sans lien hiérarchique, la coordination doit être basée sur la discussion et le bon sens en privilégiant la recherche de consensus et le bénéfice mutuel entre les parties.

Les cinq années passées à l'Agence de l'OCDE pour l'Énergie Nucléaire ont été l'occasion de coordonner des activités scientifiques à une échelle internationale en tant que responsable de la coordination des activités des pays membres liées à la mesure, l'évaluation et la validation des données nucléaires.

- Secrétaire scientifique du Groupe de travail sur la coopération internationale en matière d'évaluation des données nucléaires (WPEC), et organisation des workshops associés.
- Responsable de la compilation des données dans la base de données internationale des réactions nucléaires (EXFOR).
- Coordination du développement du logiciel JANIS pour la visualisation des données nucléaires.
- Participation au projet de bibliothèque de données évaluées JEFF (Joint Evaluated Fission and Fusion library) et aux sous-groupes de travail WPEC sur l'évaluation des données nucléaires :
  - SG30 - *Improvement of accessibility and quality of the EXFOR database*
  - SG31 - *Meeting nuclear data needs for advanced reactor systems*
  - SG33 - *Methods and issues for the combined use of integral experiments and covariance data*
  - SG38 - *Beyond the ENDF format: a modern nuclear database structure*
  - SG39 - *Methods and approaches to provide feedback from nuclear and covariance data* adjustment for improvement of nuclear data files
  - SG40 - *Collaborative International Evaluated Library Organisation (CIELO) pilot project*

Ces compétences sont aujourd'hui valorisées auprès de la Collaboration n_TOF en coordonnant la dissémination des données expérimentales en étroite collaboration avec l'AEN et l'AIEA [Dupont 17], et plus généralement auprès des membres de la communauté des sciences nucléaires en présidant le Groupe d'experts en charge des demandes d'amélioration des données nucléaires via la « High Priority Request List » (HPRL) de l'AEN [Dupont 20].

Production scientifique

25 publications dans des revues avec comité de lecture

46 publications dans des actes de congrès avec comité de lecture

La liste complète des publications et rapports est consultable sur les sites suivants :

- Scopus : http://www.scopus.com/authid/detail.uri?&authorId=7101929776
- ResearchGate : http://www.researchgate.net/profile/Emmeric_Dupont
- Google Scholar : http://scholar.google.fr/citations?user=Bk7R8HYAAAAJ

8 Annexe – Liste des publications et rapports cités dans le manuscrit

[Agelou 09] M. Agelou, et al. (E. Dupont), *Detecting special nuclear materials inside cargo containers using photofission*, IEEE Nuclear Science Symposium, Orlando (FL), USA, p.936 (2009). http://doi.org/10.1109/NSSMIC.2009.5401567

[Amaducci 19] S. Amaducci, et al. (E. Dupont), *High accuracy, high resolution measurement of the ^{235}U(n,f) cross section at n_TOF from thermal to 170 keV neutron energy range*, European Physical Journal A 55, 120 (2019). http://doi.org/10.1140/epja/i2019-12802-7

[Antonov 11] A.N. Antonov, et al. (E. Dupont), *The electron-ion scattering experiment ELISe at the international Facility for Antiproton and Ion Research (FAIR) - a conceptual design study*, Nuclear Instruments and Methods A 637, 60 (2011). http://doi.org/10.1016/j.nima.2010.12.246

[Bacak 17] M. Bacak, et al. (E. Dupont), *A compact multi-plate fission chamber for the simultaneous measurement of ^{233}U capture and fission cross-sections*, EPJ Conf. 146, 03027 (2017). http://doi.org/10.1051/epjconf/201714603027

[Bacak 19] M. Bacak, et al. (E. Dupont), Preliminary results on the ^{233}U capture cross section and alpha ratio measured at n_TOF (CERN) with the fission tagging technique, EPJ Conf. 211, 03007 (2019). http://doi.org/10.1051/epjconf/201921103007

[Bacak 20a] M. Bacak, et al. (E. Dupont), *Preliminary results on the ^{233}U alpha-ratio measurement at n_TOF*, EPJ Conf. 239, 01043 (2020). http://doi.org/10.1051/epjconf/202023901043

[Bacak 20b] M. Bacak, et al. (E. Dupont), *A compact and fast fission detector for fission-tagging neutron capture experiments with radioactive fissile isotopes*, Nuclear Instruments and Methods A 969, 163981 (2020). http://doi.org/10.1016/j.nima.2020.163981

[Barbagallo 16] M. Barbagallo, et al. (E. Dupont), *^{7}Be(n,α)^{4}He reaction and the Cosmological Lithium Problem: measurement of the cross section in a wide energy range at n_TOF at CERN*, Physical Review Letters 117, 152701 (2016). http://doi.org/10.1103/PhysRevLett.117.152701

[Barbagallo 18] M. Barbagallo, et al. (E. Dupont), *Experimental setup and procedure for the measurement of the ^{7}Be(n,p)^{7}Li reaction at n_TOF*, Nuclear Instruments and Methods A 887, 27 (2018). http://doi.org/10.1016/j.nima.2017.12.025

[Benguigui 09] E. Benguigui et E. Dupont, Etude de l'absorption de photons dans la résonance dipolaire géante des noyaux atomiques, Rapport de stage de M1, Université Pierre et Marie-Curie, 2009.

[Bringer 07] O. Bringer, et al. (E. Dupont), *Measurements of thermal fission and capture cross sections of minor actinides within the Mini-INCA project*, Int. Conf. on Nuclear Data for Science and Technology, Nice, France, p.619 (2007). http://doi.org/10.1051/ndata:07612

[Bringer 08] O. Bringer, A. Letourneau and E. Dupont, *Impact of nuclear data uncertainties on the incineration of ^{237}Np and ^{241}Am targets*, Annals of Nuclear Energy 35, 1535 (2008). http://doi.org/10.1016/j.anucene.2008.01.002

[Chadwick 14] M.B. Chadwick, E. Dupont, et al., *The CIELO Collaboration: neutron reactions on ^{1}H, ^{16}O, ^{56}Fe, $^{235,238}U$, and ^{239}Pu*, Nuclear Data Sheets 118, 1 (2014). http://doi.org/10.1016/j.nds.2014.04.002

[Chadwick 18] M.B. Chadwick, et al. (E. Dupont), *CIELO Collaboration Summary Results: International Evaluations of Neutron Reactions on Uranium, Plutonium, Iron, Oxygen and Hydrogen*, Nuclear Data Sheets 148, 189 (2018). http://doi.org/10.1016/j.nds.2018.02.003

[Cosentino 16] L. Cosentino, et al. (E. Dupont), *Experimental setup and procedure for the measurement of the $^{7}Be(n,\alpha)\alpha$ reaction at n_TOF*, Nuclear Instruments and Methods A 830, 197 (2016). http://doi.org/10.1016/j.nima.2016.05.089

[Damone 18] L. Damone, et al. (E. Dupont), *$^{7}Be(n,p)^{7}Li$ Reaction and the Cosmological Lithium Problem: Measurement of the cross section in a wide energy range at n_TOF at CERN*, Physical Review Letters 121, 042701 (2018). http://doi.org/10.1103/PhysRevLett.121.042701

[Diakaki 16] M. Diakaki, et al. (E. Dupont), *Towards the high-accuracy determination of the ^{238}U fission cross section at the threshold region at CERN – n_TOF*, EPJ Conf. 111, 02002 (2016). http://doi.org/10.1051/epjconf/201611102002

[Diakaki 18] M. Diakaki, et al. (E. Dupont), *Development of a novel segmented mesh MicroMegas detector for neutron beam profiling*, Nuclear Instruments and Methods A 903, 46 (2018). http://doi.org/10.1016/j.nima.2018.06.019

[Dupont 98] E. Dupont, Mesures à haute résolution et étude de la réaction de diffusion inélastique de neutrons sur le ^{56}Fe, Thèse de Doctorat, Université de Provence, 1998. http://tel.archives-ouvertes.fr/tel-01145543

[Dupont 02a] E. Dupont and E. Fort, *AMERATEST – a contribution to the JEFF-3 file testing and initial benchmarking*, Journal of Nuclear Science and Technology 39, 924 (2002). http://doi.org/10.1080/00223131.2002.10875250

[Dupont 02b] E. Dupont, J. Tommasi, A. Nouri, Derivation of JEFF-3 trends from the PROFIL fast spectrum experiments, Rapport CEA NT-SPRC/LEPH-02/218, 2002.

[Dupont 03] E. Dupont, Preliminary Analysis of JEFF-3.0/GP Trends in Fast Spectrum Experiments, JEFF internal report JEF/DOC-956 (2003).

[Dupont 05a] E. Dupont, E. Bauge, S. Hilaire, A. Koning, J-C. Sublet, *Neutron data evaluation and validation of rhodium-103*, AIP Conference Proceedings 769, 95 (2005). http://doi.org/10.1063/1.1944965

[Dupont 05b] E. Dupont, E. Bauge and G. Noguère, Medium-Energy Evaluation of Iodine-127 & Iodine-129 for JEFF-3.1, JEFF internal report JEF/DOC-1076 (2005).

[Dupont 05c] E. Dupont, J. Tommasi, G. Noguere, Contribution à l'analyse des besoins d'évaluation des produits de fission en spectre rapide, Rapport CEA NT-SPRC/LEPH-05/203, 2005.

[Dupont 07] E. Dupont, I. Raskinyte, A.J. Koning, D. Ridikas, *Photonuclear data evaluations of actinides up to 130 MeV*, Int. Conf. on Nuclear Data for Science and Technology, Nice, France, p.685 (2007). http://doi.org/10.1051/ndata:07497

[Dupont 11a] E. Dupont, J. Galan, J. Gulliford, C. Nordborg, Y. Rugama, *Overview of the OECD NEA data bank activities*, Journal of the Korean Physical Society 59, 1309 (2011). http://doi.org/10.3938/jkps.59.1309

[Dupont 11b] E. Dupont, A.J. Koning and N. Otuka, *Exploratory data analysis of the EXFOR database*, Journal of the Korean Physical Society 59, 1333 (2011). http://doi.org/10.3938/jkps.59.1333

[Dupont 11c] E. Dupont, B. Beauzamy, H. Bickert, M. Bossant, C. Rodriguez, N. Soppera, *Statistical methods for the verification of databases*, NEA News 29(1), 32 (2011). http://www.oecd-nea.org/nea-news

[Dupont 14] E. Dupont, et al., *Working Party on International Nuclear Data Evaluation Cooperation (WPEC)*, Nuclear Data Sheets 120, 264 (2014). http://doi.org/10.1016/j.nds.2014.07.063

[Dupont 17] E. Dupont, et al., *Dissemination of data measured at the CERN n_TOF facility*, EPJ Conf. 146, 07002 (2017). http://doi.org/10.1051/epjconf/201714607002

[Dupont 20] E. Dupont, et al., *HPRL – International cooperation to identify and monitor priority nuclear data needs for nuclear applications*, EPJ Conf. 239, 15005 (2020). http://doi.org/10.1051/epjconf/202023915005

[Fischer 11] U. Fischer, et al. (E. Dupont), *The European effort on the evaluation and validation of nuclear data for fusion technology applications*, Journal of the Korean Physical Society 59, 1369 (2011). http://doi.org/10.3938/jkps.59.1369

[Fischer 14] U. Fischer, et al. (E. Dupont), *The activities of the European consortium on nuclear data development and analysis for fusion*, Nuclear Data Sheets 120, 226 (2014). http://doi.org/10.1016/j.nds.2014.07.053

[Fort 03] E. Fort, et al. (E. Dupont), *Improved performances of the fast reactor calculational system ERANOS-ERALIB1 due to improved a priori nuclear data and consideration of additional specific integral data*, Annals of Nuclear Energy 30, 1879 (2003). http://doi.org/10.1016/S0306-4549(03)00161-0

[Gawlik 19] A. Gawlik, et al. (E. Dupont), *Measurement of the $^{70}Ge(n,\gamma)$ cross section up to 300 keV at n_TOF CERN*, Physical Review C 100, 045804 (2019). http://doi.org/10.1103/PhysRevC.100.045804

[Gourgiotis 11] A. Gourgiotis, et al. (E. Dupont), *Accurate determination of Curium and Californium isotopic ratios by inductively coupled plasma quadrupole mass spectrometry (ICP-QMS) in ^{248}Cm samples for transmutation studies*, International Journal of Mass Spectrometry 291, 101 (2011). http://doi.org/10.1016/j.ijms.2010.02.002

[Gourgiotis 13] A. Gourgiotis, et al. (E. Dupont), *Bk and Cf chromatographic separation and Bk-249/Cm-248 and Cf-249/Cm-248 elemental ratios determination by inductively coupled plasma quadrupole mass spectrometry*, Talanta 106, 39 (2013). http://doi.org/10.1016/j.talanta.2012.11.056

[Gunsing 16] F. Gunsing, et al. (E. Dupont), *Nuclear data activities at the n_TOF facility at CERN*, European Physical Journal Plus 131, 371 (2016). http://doi.org/10.1140/epjp/i2016-16371-4

[Koning 07] A.J. Koning, et al. (E. Dupont), *The JEFF evaluated nuclear data project*, Int. Conf. on Nuclear Data for Science and Technology, Nice, France, p.721 (2007). http://doi.org/10.1051/ndata:07476

[Koning 11] A.J. Koning, et al. (E. Dupont), *Status of the JEFF nuclear data library*, Journal of the Korean Physical Society 59, 1057 (2011). http://doi.org/10.3938/jkps.59.1057

[Lederer 19] C. Lederer-Woods, et al. (E. Dupont), *Measurement of ^{73}Ge(n,γ) cross sections and implications for stellar nucleosynthesis*, Physics Letters B 790, 458 (2019). http://doi.org/10.1016/j.physletb.2019.01.045

[Lerendegui 18] J. Lerendegui, et al. (E. Dupont), *Radiative neutron capture on ^{242}Pu in the resonance region at n_TOF-EAR1*, Physical Review C 97, 024605 (2018). http://doi.org/10.1103/PhysRevC.97.024605

[Letourneau 11] A. Letourneau, et al. (E. Dupont), *Recent developments on micrometric fission chambers dedicated for high neutron fluxes*, IEEE Transactions on Nuclear Science 58, 1913 (2011). http://doi.org/10.1109/TNS.2011.2155670

[Massimi 14] C. Massimi, et al. (E. Dupont), *Neutron capture cross section measurements for ^{197}Au from 3.5 to 84 keV at GELINA*, European Physical Journal A 50, 124 (2014). http://doi.org/10.1140/epja/i2014-14124-8

[Mastromarco 19] M. Mastromarco, et al. (E. Dupont), *Cross section measurements of ^{155,157}Gd(n,γ) induced by thermal and epithermal neutrons*, European Physical Journal A 55, 9 (2019). http://doi.org/10.1140/epja/i2019-12692-7

[Monange 06] W. Monange, E. Dupont et A. Letourneau, Etude dynamique du réacteur à haut flux de l'Institut Laue-Langevin, Rapport DAPNIA-06-317, 2006.

[Moreno 19] J. Moreno-Soto, et al. (E. Dupont), *Study of the photon strength functions and level density in the gamma decay of the n + ^{234}U reaction*, EPJ Conf. 211, 02002 (2019). http://doi.org/10.1051/epjconf/201921102002

[Otuka 11] N. Otuka, S. Dunaeva, E. Dupont, O. Schwerer, A. Blokhin, *The role of the nuclear reaction data centres in experimental nuclear data knowledge sharing*, Journal of the Korean Physical Society 59, 1292 (2011). http://doi.org/10.3938/jkps.59.1292

[Otuka 14] N. Otuka, E. Dupont, et al., *Towards a more complete and accurate Experimental nuclear reaction data library (EXFOR): international collaboration between Nuclear Reaction Data Centres (NRDC)*, Nuclear Data Sheets 120, 272 (2014). http://doi.org/10.1016/j.nds.2014.07.065

[Raskinyte 06] I. Raskinyte, E. Dupont, B. Morillon, D. Ridikas, *Photonuclear data evaluation of actinides*, Int. Conf. on Nuclear Reaction Mechanisms, Varenna, Italy, June 2006.

[Romain 02] P. Romain, P. Dos-Santos Uzarralde, C. Le Luel, S. Hilaire, J-P. Delaroche, J-C. Sublet, E. Dupont, *The n + ^{239}Pu system – new data evaluation and validation methods*, Journal of Nuclear Science and Technology 39, 164 (2002). http://doi.org/10.1080/00223131.2002.10875066

[Sabate 17] M. Sabaté-Gilarte, et al. (E. Dupont), *High-accuracy determination of the neutron flux in the new experimental area n_TOF-EAR2 at CERN*, European Physical Journal A 53, 210 (2017). http://doi.org/10.1140/epja/i2017-12392-4

[Salvatores 14] M. Salvatores, et al. (E. Dupont), *Methods and issues for the combined use of integral experiments and covariance data: results of a NEA international collaborative study*, Nuclear Data Sheets 118, 38 (2014). http://doi.org/10.1016/j.nds.2014.04.005

[Sirakov 13] I. Sirakov, B. Becker, R. Capote, E. Dupont, S. Kopecky, C. Massimi, P. Schillebeeckx, *Results of total cross section measurements for ^{197}Au in the neutron energy region from 4 to 108 keV at GELINA*, European Physical Journal A 49 (2013). http://doi.org/10.1140/epja/i2013-13144-2

[Soppera 05] N. Soppera, H. Henriksson, A. Nouri, P. Nagel, E. Dupont, *JANIS-2: an improved version of the NEA Java-based Nuclear Data Information System*, AIP Conference Proceedings 769, 557 (2005). http://doi.org/10.1063/1.1945070

[Soppera 11] N. Soppera, M. Bossant, E. Dupont, H. Henriksson, Y. Rugama, *Recent upgrades to the nuclear data tool JANIS*, Journal of the Korean Physical Society 59, 1329 (2011). http://doi.org/10.3938/jkps.59.1329

[Soppera 12] N. Soppera, E. Dupont, M. Bossant, *JANIS Book of neutron-induced cross-sections*, OECD Nuclear Energy Agency (2012). http://www.oecd-nea.org/janis/book

[Soppera 14] N. Soppera, M. Bossant and E. Dupont, *JANIS 4: an improved version of the NEA Java-based nuclear data information system*, Nuclear Data Sheets 120, 294 (2014). http://doi.org/10.1016/j.nds.2014.07.071

[Taieb 09] J. Taieb, et al. (E. Dupont), *ELISe: a new facility for unprecedented experimental nuclear fission studies*, International Journal of Modern Physics E 18, 767 (2009). http://doi.org/10.1142/S0218301309012859

[Tommasi 06] J. Tommasi, E. Dupont and P. Marimbeau, *Analysis of sample irradiation experiments in Phenix for JEFF-3.0 nuclear data validation*, Nuclear Science and Engineering 154, 119 (2006). http://doi.org/10.13182/NSE154-119

[Torre 05] R. Torre, E. Dupont et G. Noguère, Etude des paramètres de résonance et modélisation des sections efficaces de 148Sm, Rapport CEA NT-SPRC/LEPH-05/205, 2005.

[Weiss 15] C. Weiss, et al. (E. Dupont), *The new vertical neutron beam line at the CERN n_TOF facility design and outlook on the performance*, Nuclear Instruments and Methods A 799, 90 (2015). http://doi.org/10.1016/j.nima.2015.07.027

[Zeydina 14] O. Zeydina, A.J. Koning, N. Soppera, D. Raffanel, M. Bossant, E. Dupont, B. Beauzamy, *Cross-checking of large evaluated and experimental nuclear reaction databases*, Nuclear Data Sheets 120, 277 (2014). http://doi.org/10.1016/j.nds.2014.07.066